AIR MATERIEL COMMAND
CAMBRIDGE FIELD STATION
230 ALBANY STREET
CAMBRIDGE 39, MASSACHUSETTS

UPPER AIR RESEARCH PROGRAM

REPORT NO. 2
BY

F. V. SCHULTZ
N.W. SPENCER
A. REIFMAN

ENGINEERING RESEARCH INSTITUTE
UNIVERSITY OF MICHIGAN

APPROVED BY:

Gunnar Hok

GUNNAR HOK

W G Dow

W. G. DOW

JULY 1, 1948

Contract No: W-33-038 ac - 14050

TABLE OF CONTENTS

Appendixes

LIST OF ILLUSTRATIONS

LIST OF ILLUSTRATIONS

SUMMARY

The results contained in this report have been obtained by the Electrical Engineering Department of the University of Michigan under Contract No. W33-038ac-14050 (15719) with the Air Materiel Command, United States Air Force. This project was initiated early in 1946. Technical cognizance has been the responsibility of the Air Materiel Command Cambridge Field Station, Cambridge, Massachusetts and, more specifically, of Dr. Marcus D. O'Day of the Cambridge Field Station.

The present report covers all phases of the upper atmosphere pressure and temperature measurements made by the University of Michigan, under the above mentioned contract, prior to June 1, 1948.

The pressure measurements have been made at altitudes between about 40 and 110 kilometers by means of University of Michigan instruments mounted on the following German V-2 rockets fired at the White Sands Proving Ground:

Rocket No. 11 fired August 22, 1946 (rocket failed)
Rocket No. 15 fired November 21, 1946
Rocket No. 20 fired February 20, 1947
Rocket No. 28 fired December 8, 1947

Pirani gauges have been used to measure the pressures at altitudes from about 40 to 75 kilometers and ionization gauges for altitudes from about 75 to 110 kilometers, which is approximately the highest altitude attained by any of the above listed rockets.

The readings of the pressure gauges are transmitted from the rocket to the ground, and recorded, by Naval Research Laboratory telemetering equipment. These records are read and the data reduced to pressure versus altitude information at the University of Michigan. The resulting composite pressure curves are shown in Figure i-1* of this report. It will be observed that the Michigan pressure measurements and those of the Naval Research Laboratory, which are plotted in this figure for purposes of comparison, are in general agreement. The tentative pressure estimates contained in Technical Note No. 1200 (1947)[1] of the National Advisory Committee for Aeronautics have also been plotted in Figure i-1 for comparison purposes. It will be observed that at all altitudes above about 55 kilometers the University of Michigan pressure values lie consistently below those predicted by the NACA. The pressure values obtained on the rocket flight of November 21, 1946, are appreciably lower than the values obtained on the other two successful rockets. These data may not be too reliable, because this was the first successful firing involving University of Michigan equipment and consequently more or less an experimental flight from the standpoint of instrumentation. It was found desirable to make rather extensive changes in the instrumentation for the succeeding rocket and, while nothing serious is known to have been wrong with the November instruments, it is possible that the results obtained on that flight are not as accurate as those obtained later. From the analysis contained in Appendix D of the present report it is concluded that the ambient atmospheric pressure should not exceed the pressure readings obtained by the University of Michigan, and probably is not less than one-half the measured pressure. The question of random errors is discussed in Appendix F and curves of probable random error as a function of pressure are shown in Figures F-10, F-11 and F-12.

The atmospheric temperature values shown in Figure i-2 were computed from the University of Michigan pressure curves of Figure i-1 by using the barometric equation, as discussed in Section D-9 of Appendix D. In view of the appreciable uncertainties in the pressure values it must be realized that these temperature values are subject to even greater uncertainties.

*Throughout this report the figures contained in a section or appendix are grouped at the end of that section or appendix.

1. In general, superscripts refer to publications listed in the Bibliography, at the end of this report. Occasionally a superscript will refer to a foot-note.

FIG. NO. I-1

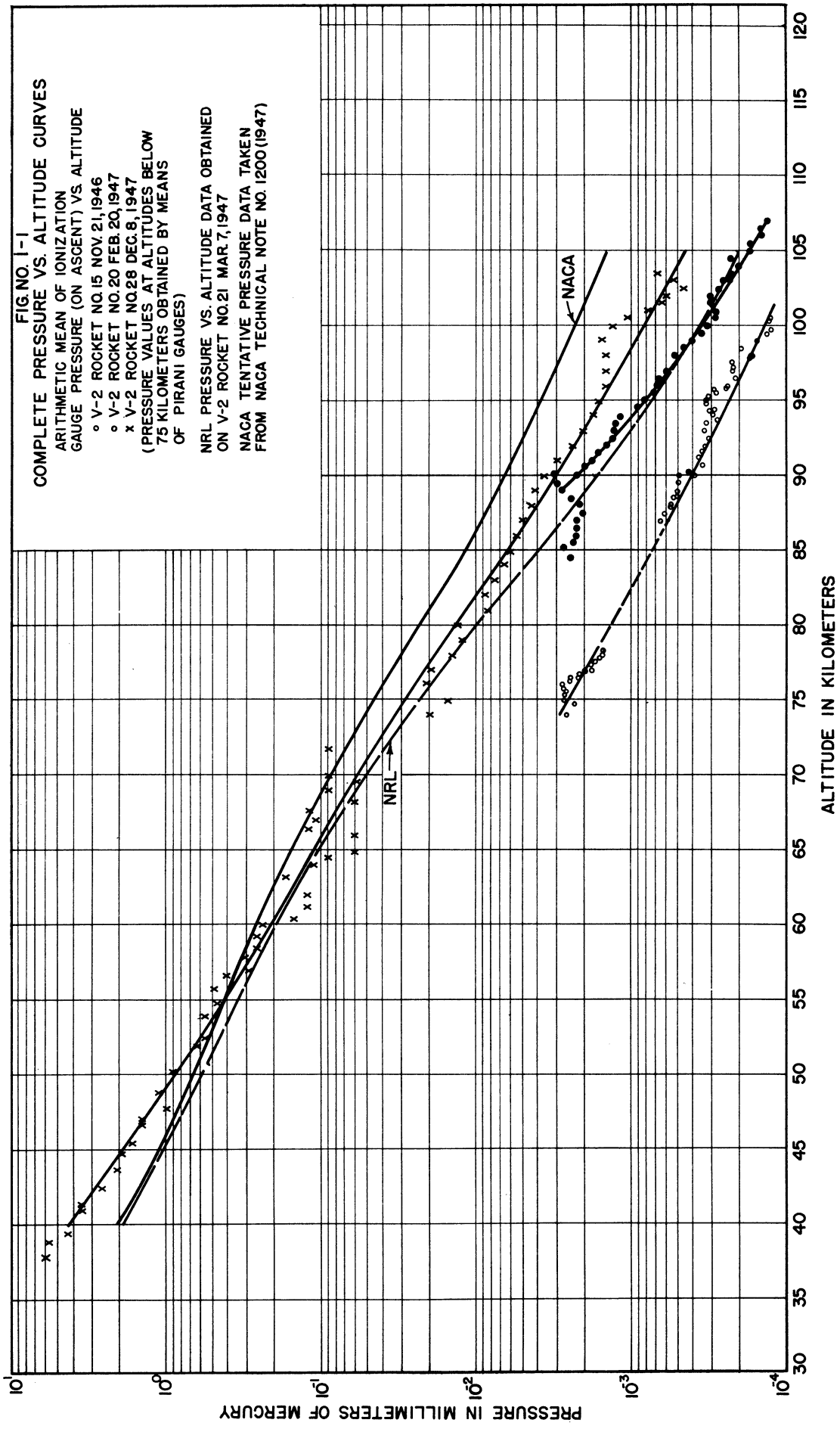
FIG. NO. I-1
COMPLETE PRESSURE VS. ALTITUDE CURVES
ARITHMETIC MEAN OF IONIZATION GAUGE PRESSURE (ON ASCENT) VS. ALTITUDE
∘ V-2 ROCKET NO. 15 NOV. 21, 1946
∘ V-2 ROCKET NO. 20 FEB. 20, 1947
x V-2 ROCKET NO. 28 DEC. 8, 1947
(PRESSURE VALUES AT ALTITUDES BELOW 75 KILOMETERS OBTAINED BY MEANS OF PIRANI GAUGES)
NRL PRESSURE VS. ALTITUDE DATA OBTAINED ON V-2 ROCKET NO. 21 MAR. 7, 1947
NACA TENTATIVE PRESSURE DATA TAKEN FROM NACA TECHNICAL NOTE NO. 1200 (1947)
NACA
NRL
PRESSURE IN MILLIMETERS OF MERCURY
10^{-1}
10^{0}
10^{-1}
10^{-2}
10^{-3}
10^{-4}
ALTITUDE IN KILOMETERS
30
35
40
45
50
55
60
65
70
75
80
85
90
95
100
105
110
115
120

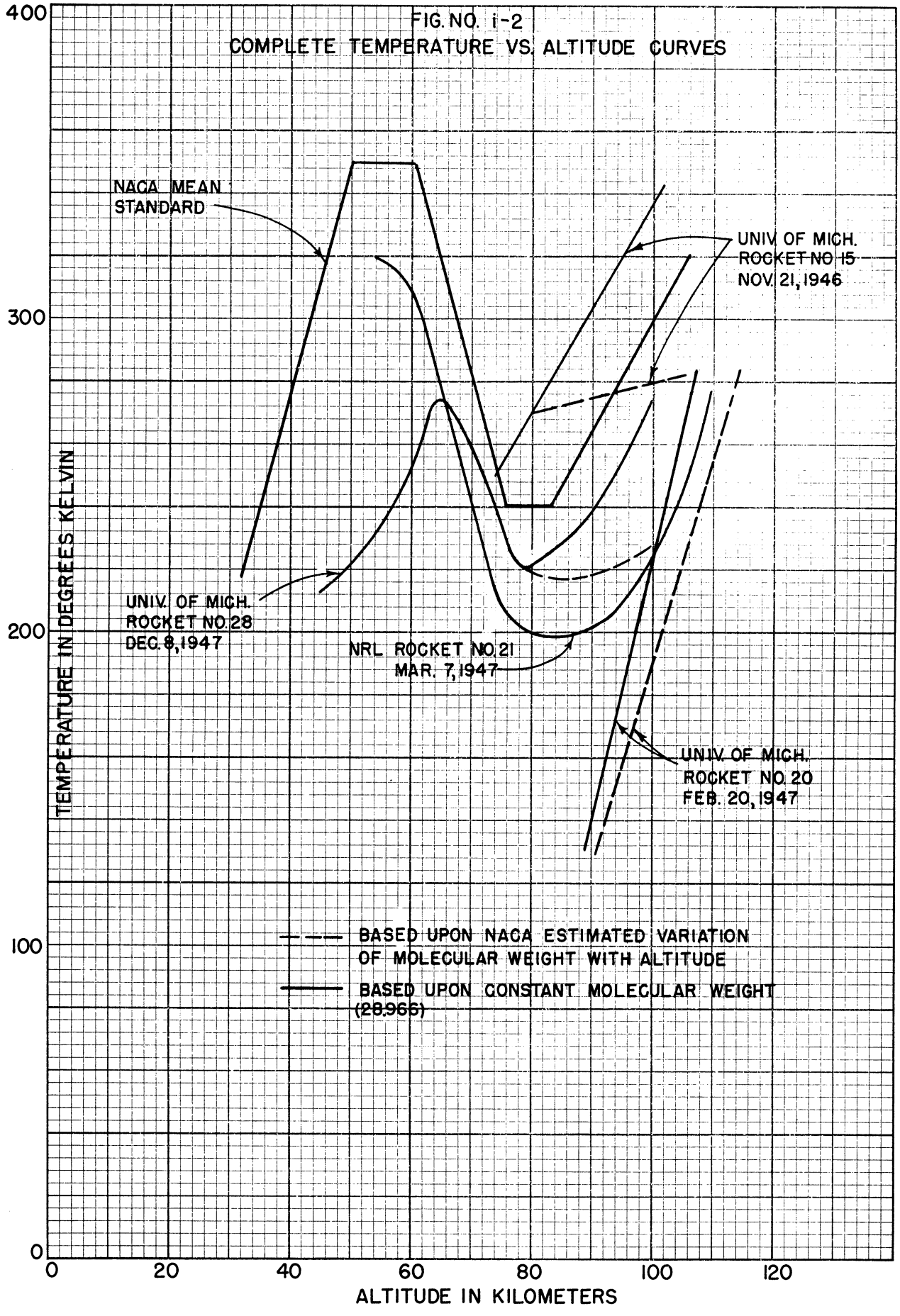
FIG. NO. i-2
COMPLETE TEMPERATURE VS. ALTITUDE CURVES
NACA MEAN STANDARD
UNIV. OF MICH. ROCKET NO 15 NOV. 21, 1946
UNIV. OF MICH. ROCKET NO 28 DEC. 8, 1947
NRL ROCKET NO 21 MAR. 7, 1947
UNIV. OF MICH. ROCKET NO 20 FEB. 20, 1947
BASED UPON NACA ESTIMATED VARIATION OF MOLECULAR WEIGHT WITH ALTITUDE
BASED UPON CONSTANT MOLECULAR WEIGHT (28.966)
TEMPERATURE IN DEGREES KELVIN
ALTITUDE IN KILOMETERS
0
100
200
300
400
0
20
40
60
80
100
120

ATMOSPHERIC PRESSURE AND TEMPERATURE MEASUREMENTS BETWEEN THE ALTITUDES OF 40 and 110 KILOMETERS

I. INTRODUCTION

I-1. Nature of the Investigation.

The Electrical Engineering Department of the University of Michigan, under contract with the Air Materiel Command, U. S. Air Force, has been engaged since early 1946 in experiments directed toward measuring the pressure and temperature of the upper atmosphere, and toward determining ion and electron concentrations and electron mean energies in the lower ionospheric regions of the upper atmosphere. Measuring instruments used in making the experimental determinations are carried to high altitudes by German V-2 rockets launched at the White Sands Proving Ground, New Mexico.

Technical cognizance of the work carried out under the contract rests with the Air Materiel Command Cambridge Field Station, Cambridge, Massachusetts. The University of Michigan has been guided by Dr. Marcus D. O'Day of the Cambridge Field Station in its choice of objectives and in its coordination with the work of other agencies contributing to the program of the Upper Atmosphere Rocket Research Panel.

At the time of preparation of this report, emphasis under the contract is being placed on measurements of atmospheric pressure and temperature. During the past eighteen months reasonably firm information has been obtained relative to pressure in the 40 to 110 kilometer range of altitudes, and less firm evidence as to temperature within the same altitude range. This information is based on data secured from V-2 rocket firings on November 21, 1946, February 20, 1947 and December 8, 1947. Measuring apparatus also was installed in a rocket fired August 22, 1946. However, this rocket was a failure and no experimental data were obtained from it.

When this contract for V-2 measurements was originally undertaken early in 1946, the primary stated objective was the measurement of electron and ion densities in the ionospheric "E" layer. A secondary objective was the measurement of atmospheric pressure and temperature in the neighborhood of the ionospheric "E" layer, that is, from about 80 kilometers upward to the V-2 rocket ceiling. Thus, high-altitude rather than low-altitude instrumentation was selected; the devices used for air pressure and temperature measurement functioned only above about 65 kilometers. The upper limit of measurements obtained was to be determined by the heights attained by the rockets fired.

In late 1947 it became desirable to broaden the scope of the University's future attention to pressure and temperature measurements to include coverage of all altitudes from the ground to rocket ceiling. Instrumentation was developed to accomplish this objective, the first design of which was carried on the rocket fired December 8, 1947.

In regard to the original primary objective, the decision was reached at the University of Michigan early in 1946 that a dependable method of measuring electron and ion concentration in the ionosphere is the measurement of the time delay experienced in transit through the ionosphere by a radio-frequency pulse having a frequency slightly above the "E" layer critical frequency. This method, suggested by Dr. M. H. Nichols of the University of Michigan, has proved to be successful.

The ionospheric pulse delay measurements involved very substantial ground as well as airborne installations. In order to strengthen this phase of the program a cooperative organization was set up to handle this work, involving members of the technical staffs of the Aircraft Radiation Laboratory at Wright Field, the Cambridge Field Station and the University of Michigan.

Because of the extensive background of radar beacon experience possessed by the Cambridge Field Station group, and because of the broadening interest in air pressure and temperature measurements, it has proven advantageous for the C.F.S. group to take over primary responsibility for the ionospheric pulse delay measurements, and for the University of Michigan to point its major efforts under the

contract toward the air pressure and temperature measurements. During late 1946 and 1947 the chief attention of the University to the pulse delay measurements was in the building and field operation of a frequency-scanning type of low frequency ground-based pulse transmitter.

As an alternate method of determining the concentrations of electrons and ions, and mean electron energies in the atmosphere, a variable-voltage probe experiment was designed. Equipment for making these measurements was carried on the V-2 rockets fired at White Sands on August 22, 1946, November 21, 1946, February 20, 1947 and December 8, 1947. The results of these experiments will be included in a subsequent report.

I-2. Content of this Report.

This report contains a discussion of various technical problems connected with the atmospheric pressure and temperature investigations and a description of experiments conducted in past firings, together with a review of the reasons for choice of experiments and methods. It also presents the data obtained from the V-2 rocket firings of November 21, 1946, February 20, 1947 and December 8, 1947, and relates these measurements to the ambient pressure and temperature of the atmosphere.

The report is divided into two main parts. The first part, which is the body of the report, consists of five sections which outline the measurement problem and present the data obtained, together with some discussion of the significance of these data. The second part consists of six appendixes. These discuss in more detail various aspects of the problem.

II. PRIOR KNOWLEDGE CONCERNING PROPERTIES OF THE UPPER ATMOSPHERE

On July 25, 1946 a University of Michigan report was issued,[2] entitled "The Measurement of Temperature and Pressure in the Ionosphere," by W. G. Dow and A. Reifman. The chief purpose of that report was to formalize the experimental problem being undertaken and to describe in detail a specific approach to the measurement of temperature at high altitudes. It included a brief, and not-too-critical, review of the state of knowledge as to atmospheric air density and temperature, together with a bibliography of important source material. In addition, the report presented certain estimates, chiefly due to Dr. Fred Whipple of the Harvard College Observatory,[3] of the variations of air pressure and temperature with altitude. Those estimates made it possible to set up the requirements for rocket instrumentation during the 1946-1947 period.

During the summer of 1946 the National Advisory Committee for Aeronautics sponsored a thorough, critical review of existing knowledge of the upper atmosphere pressure and temperature, as a result of which the NACA issued a bulletin[1] tabulating estimated values of the properties of the atmosphere at altitudes from 20 kilometers to 120 kilometers. This was to serve as a tentative extension to the NACA low-altitude standard atmosphere tables.

In the present report there are included curves illustrating the expected values of atmospheric pressure, temperature, density, etc., based on the NACA predictions. The curves shown here are based on the assumption that the change of the acceleration due to gravity is negligible over the range of altitudes considered. Also, they are based on the NACA mean temperature curve and do not show the effects resulting from changes in temperature.

Figures II-1 and II-2 show graphs of the NACA 1947 tentative standard atmosphere data for air density and pressure, respectively, versus altitude. Figure II-3 is a graph of their tentative standard of temperature versus altitude. Figure II-4 shows the corresponding estimates of mean free path versus altitude, and Figure II-5 shows estimates of gas particles per cubic centimeter versus altitude. The NACA data are based on the assumption that the mean molecular weight of the atmosphere varies as shown in Figure II-6.

In Figure II-7 is plotted the velocity of sound versus altitude, according to NACA predictions. These data are valuable for the computation of Mach number at various altitudes. Of course, at very high altitudes, where the mean free path becomes many meters in length, the velocity of sound is not a very definite quantity.

These curves of tentative standard atmosphere data will be referred to frequently in this report.

The NACA tentative standard atmosphere predictions were made to only 120 kilometers altitude. The experiments, described in the present report, were designed to explore the atmosphere as far as the ceiling of the V-2 rocket flights, expected to be of the order of 160 to 180 kilometers. It was believed important to have as much advance-estimate information as possible in interpreting the results of the early firings and in planning instrumentation for future firings; therefore, extrapolations of the NACA tentative standard data were made, and appear, as indicated, in Figures II-1 through II-7. These extensions were based on straight-line extrapolations from 120 to 160 kilometers of the NACA curves of temperature and mean molecular weight versus altitude. The values for the other curves were then computed using these values of temperature and of mean molecular weight in the equation of state. This was an arbitrary procedure, but at least it gave a first approximation to the values of atmospheric pressure, density, mean free path, etc., to be expected at altitudes between 120 and 160 kilometers.

The curve of kinematic viscosity versus altitude (shown in Figure II-8) is plotted only to an altitude of 120 kilometers. The reasons for this are evident from the following quotation concerning these data, taken from the NACA Technical Note No. 1200 (Page 16):

"The Sutherland formula (for the variation of the coefficient of viscosity with temperature) is strictly applicable only to a gas of constant composition and to pressures which are not too small, and

consequently the tabulated values for the coefficient of viscosity and for the kinematic viscosity are obviously not entirely reliable at the higher altitudes. However, the lack of data on the viscosity of oxygen in the atomic form does not permit at this time an estimation of the correction that is needed to allow for the specified dissociation. Furthermore, because of the fact that the effective value of the viscosity of a gas at very low pressure flowing over a body depends on the size and shape of the body, it is not practical to give a correction that will be applicable to more than one specific size and shape of a body. The values for viscosity at the higher altitudes should therefore be used with caution."

It is desirable to note that the NACA estimate of temperature (see Figure II-3) is limited to the statement of values at a few specific altitudes, straight-line interpolation being used between these specific points on the graph. This manner of presentation of their estimates emphasizes the lack of firmness of the then existing knowledge of upper atmosphere temperature.

For altitudes below 30 kilometers, the properties of the atmosphere have been well established by means of radio-sonde balloons, so for that lower region Figures II-1 to II-8 present information known to be correct. The evidence for the NACA estimates of properties of the atmosphere above 30 kilometers is, of necessity, indirect. Sources of this evidence included the following:

(1) Gunsound reflection data (30 to 60 kilometers).
(2) Spectrum of the night sky.
(3) Spectrum of the day sky.
(4) Study of meteor trails.
(5) Infrared study of the night sky.
(6) Ionospheric properties of the atmosphere, as determined by critical frequency and virtual height measurements.
(7) Observations on the aurora borealis.
(8) Laws governing equilibrium relationships involving dissociation of diatomic molecules in a radiation field.
(9) The various well-known physical laws relating density, pressure and temperature of gases in a gravitational field.

Experimental data obtained during the winter months of 1946-47 and of 1947-48 by the Naval Research Laboratory and by the University of Michigan indicate that the true air pressure in the 100 kilometer range of altitudes is less than the mean values estimated by the NACA by a factor of 10, or less. The temperature trend is of the same form as the NACA estimates, the measured temperatures being, in general, however, lower than the estimates. A detailed discussion of these indications appears in the Summary of this report.

In comparing the pressure and temperature data contained in this report with the values predicted by the NACA, one must keep in mind the following facts:

1. The NACA values shown in this report are mean values, and do not show the variations which likely occur from season to season and from one geographical location to another.

2. All the V-2 measurements have been made at a single geographical location.

3. All the data presented herein were obtained on V-2 flights made during the winter months.

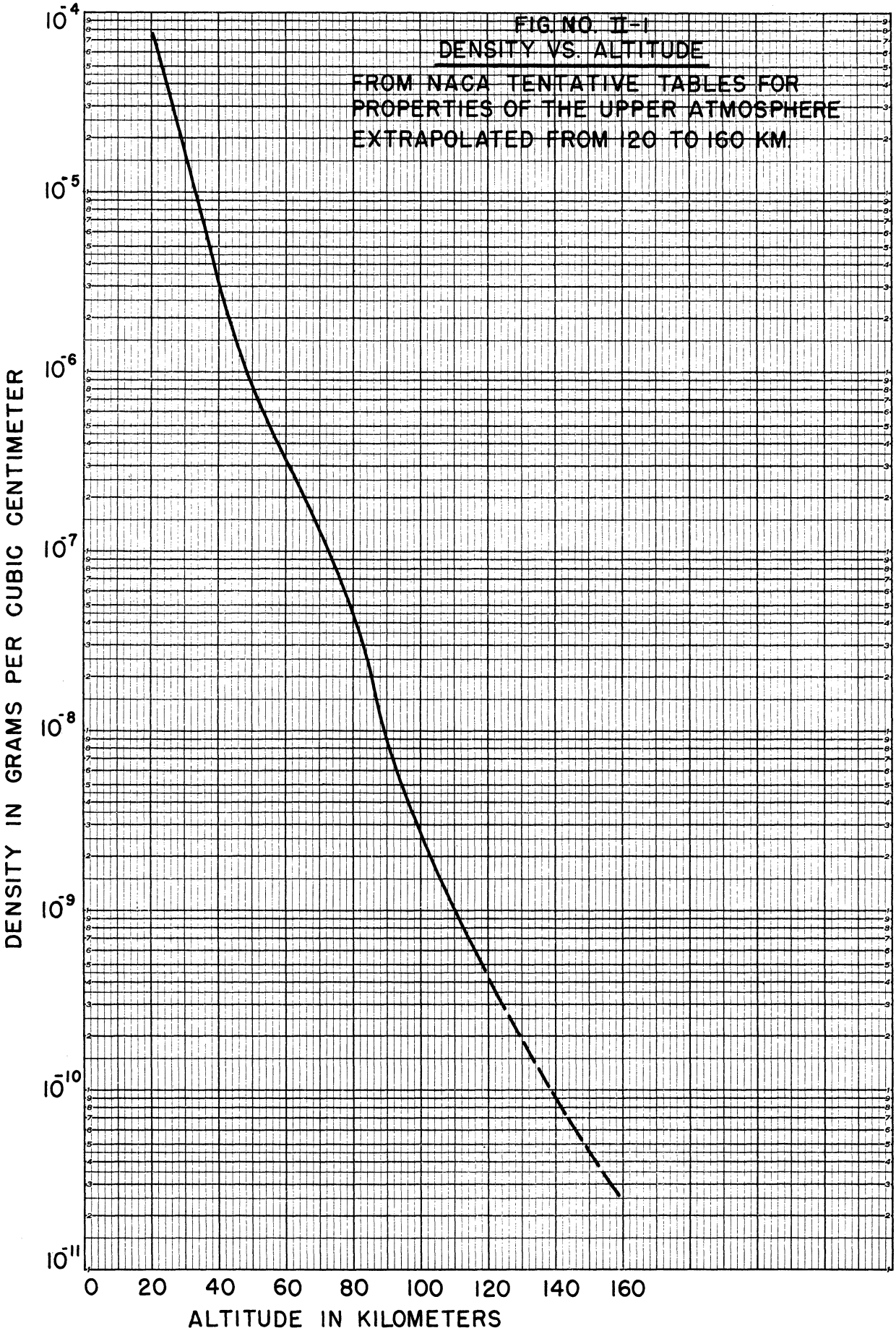
FIG. NO. II-1
DENSITY VS. ALTITUDE
FROM NACA TENTATIVE TABLES FOR
PROPERTIES OF THE UPPER ATMOSPHERE
EXTRAPOLATED FROM 120 TO 160 KM.
DENSITY IN GRAMS PER CUBIC CENTIMETER
10^{-4}
10^{-5}
10^{-6}
10^{-7}
10^{-8}
10^{-9}
10^{-10}
10^{-11}
0 20 40 60 80 100 120 140 160
ALTITUDE IN KILOMETERS

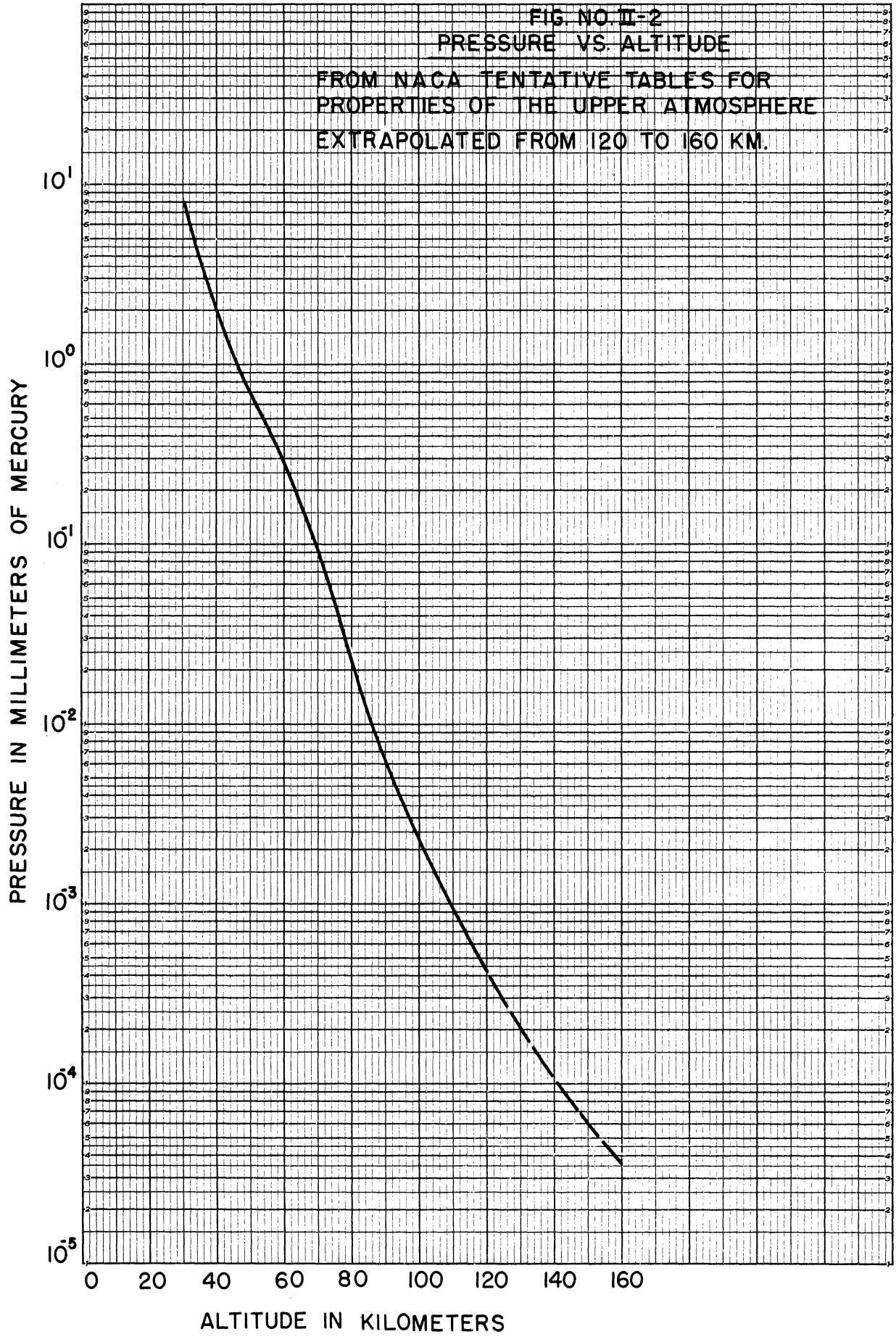
FIG. NO. II-2
PRESSURE VS. ALTITUDE
FROM NACA TENTATIVE TABLES FOR
PROPERTIES OF THE UPPER ATMOSPHERE
EXTRAPOLATED FROM 120 TO 160 KM.
PRESSURE IN MILLIMETERS OF MERCURY
10^{1}
10^{0}
10^{-1}
10^{-2}
10^{-3}
10^{-4}
10^{-5}
0
20
40
60
80
100
120
140
160
ALTITUDE IN KILOMETERS

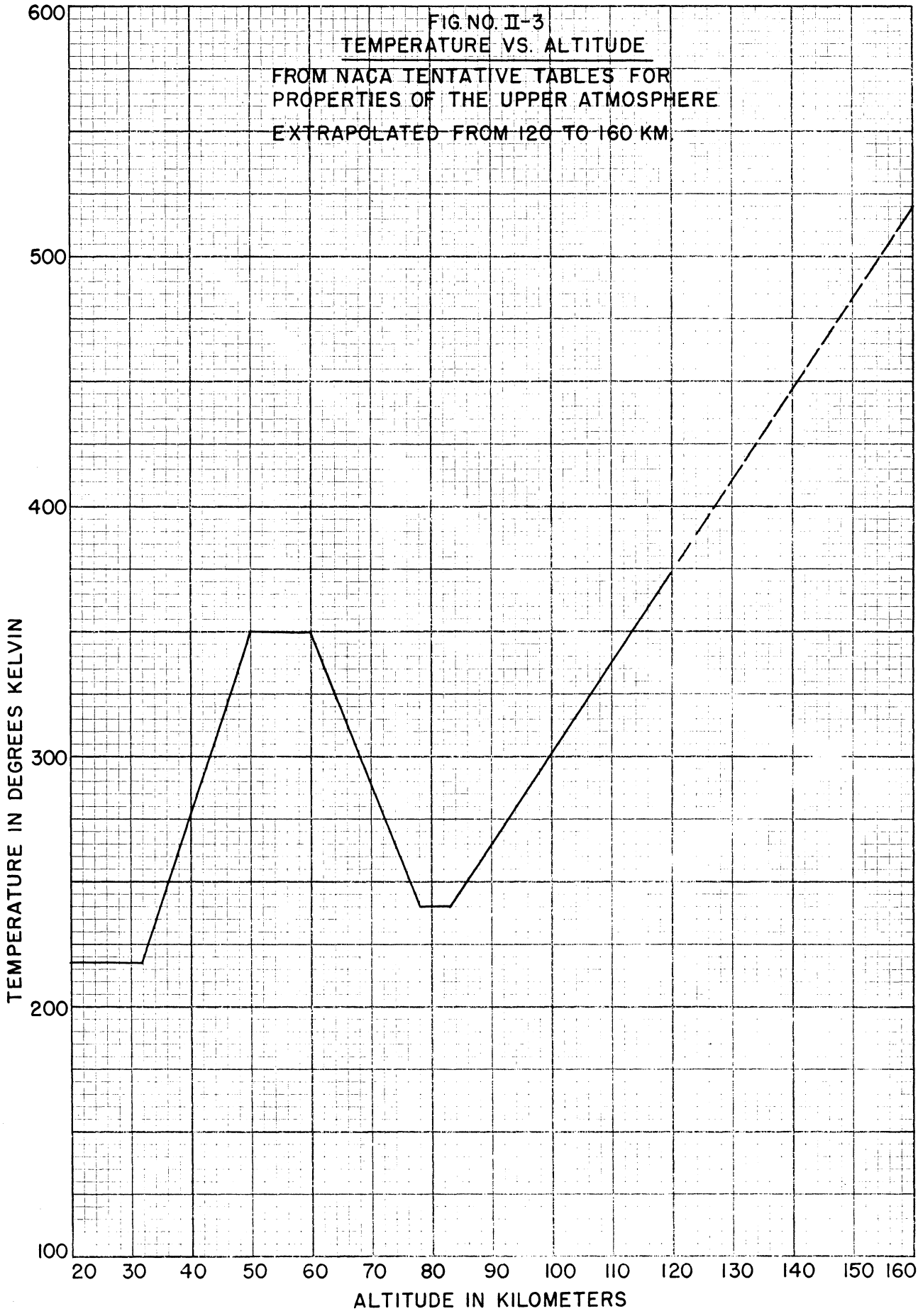
FIG. NO. II-3
TEMPERATURE VS. ALTITUDE
FROM NACA TENTATIVE TABLES FOR
PROPERTIES OF THE UPPER ATMOSPHERE
EXTRAPOLATED FROM 120 TO 160 KM
600
500
400
300
200
100
TEMPERATURE IN DEGREES KELVIN
20 30 40 50 60 70 80 90 100 110 120 130 140 150 160
ALTITUDE IN KILOMETERS

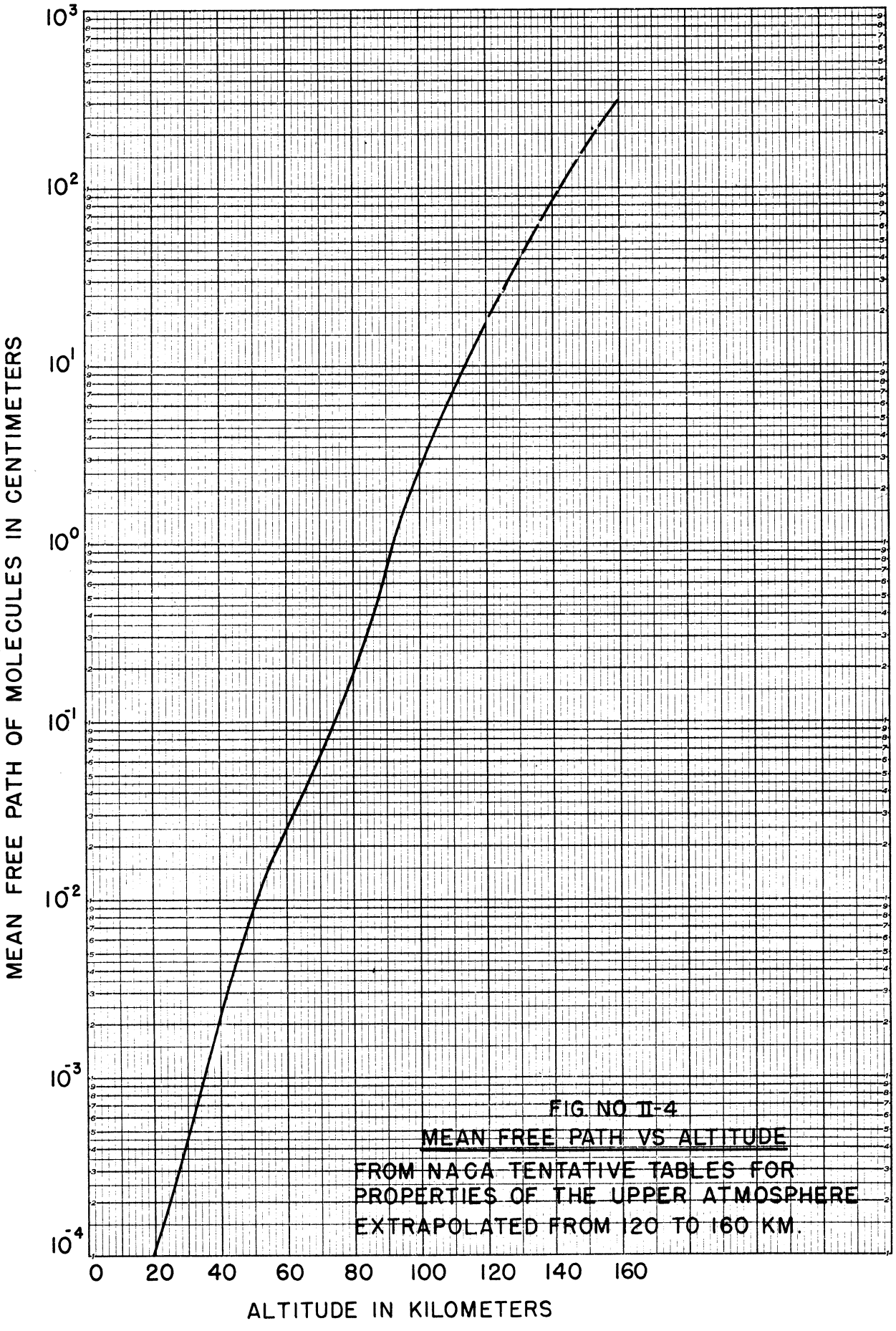

FIG. NO II-4

MEAN FREE PATH VS ALTITUDE

FROM NACA TENTATIVE TABLES FOR PROPERTIES OF THE UPPER ATMOSPHERE EXTRAPOLATED FROM 120 TO 160 KM.

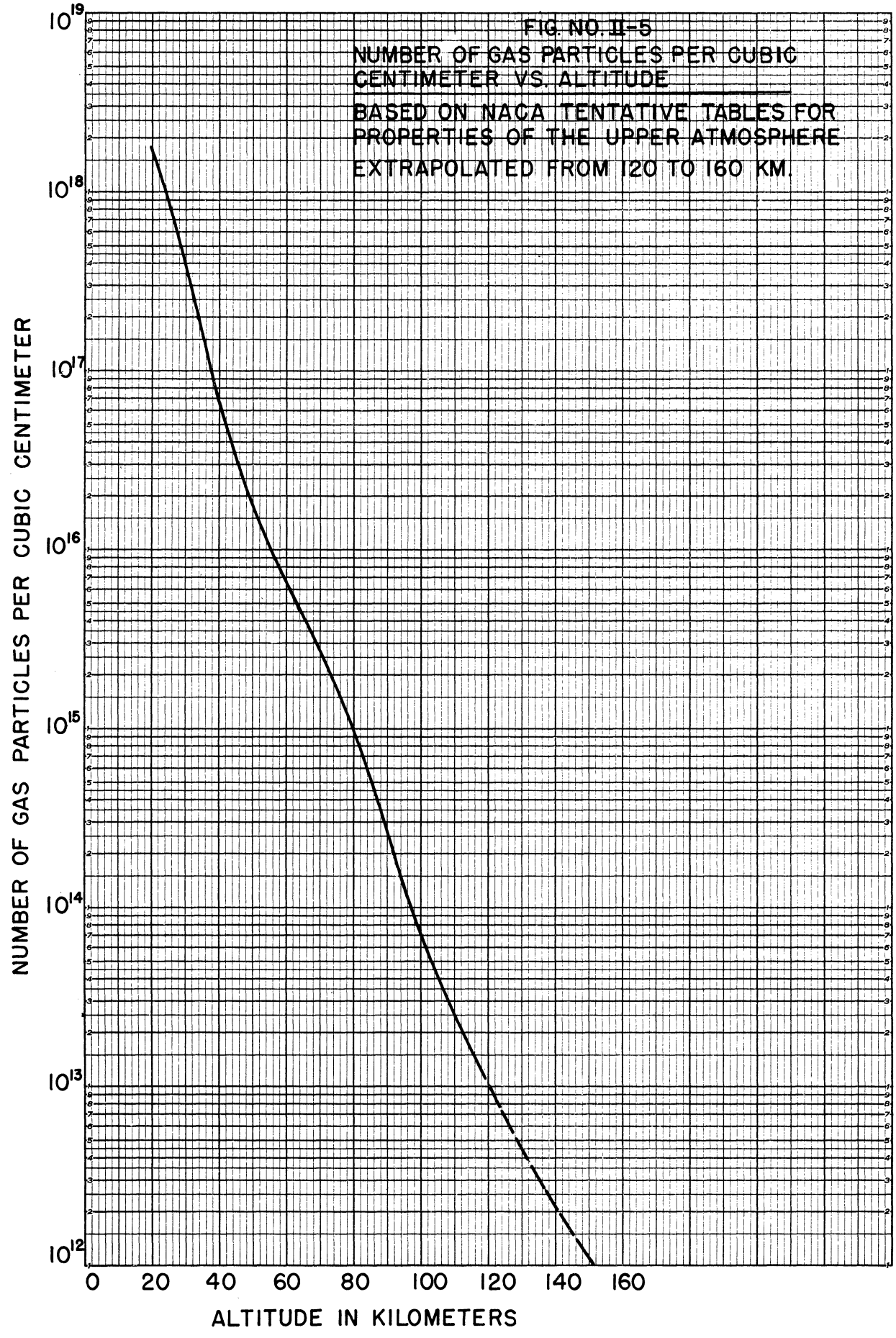
FIG. NO. II-5
NUMBER OF GAS PARTICLES PER CUBIC CENTIMETER VS. ALTITUDE
BASED ON NACA TENTATIVE TABLES FOR PROPERTIES OF THE UPPER ATMOSPHERE EXTRAPOLATED FROM 120 TO 160 KM.
NUMBER OF GAS PARTICLES PER CUBIC CENTIMETER
10^{19}
10^{18}
10^{17}
10^{16}
10^{15}
10^{14}
10^{13}
10^{12}
0 20 40 60 80 100 120 140 160
ALTITUDE IN KILOMETERS

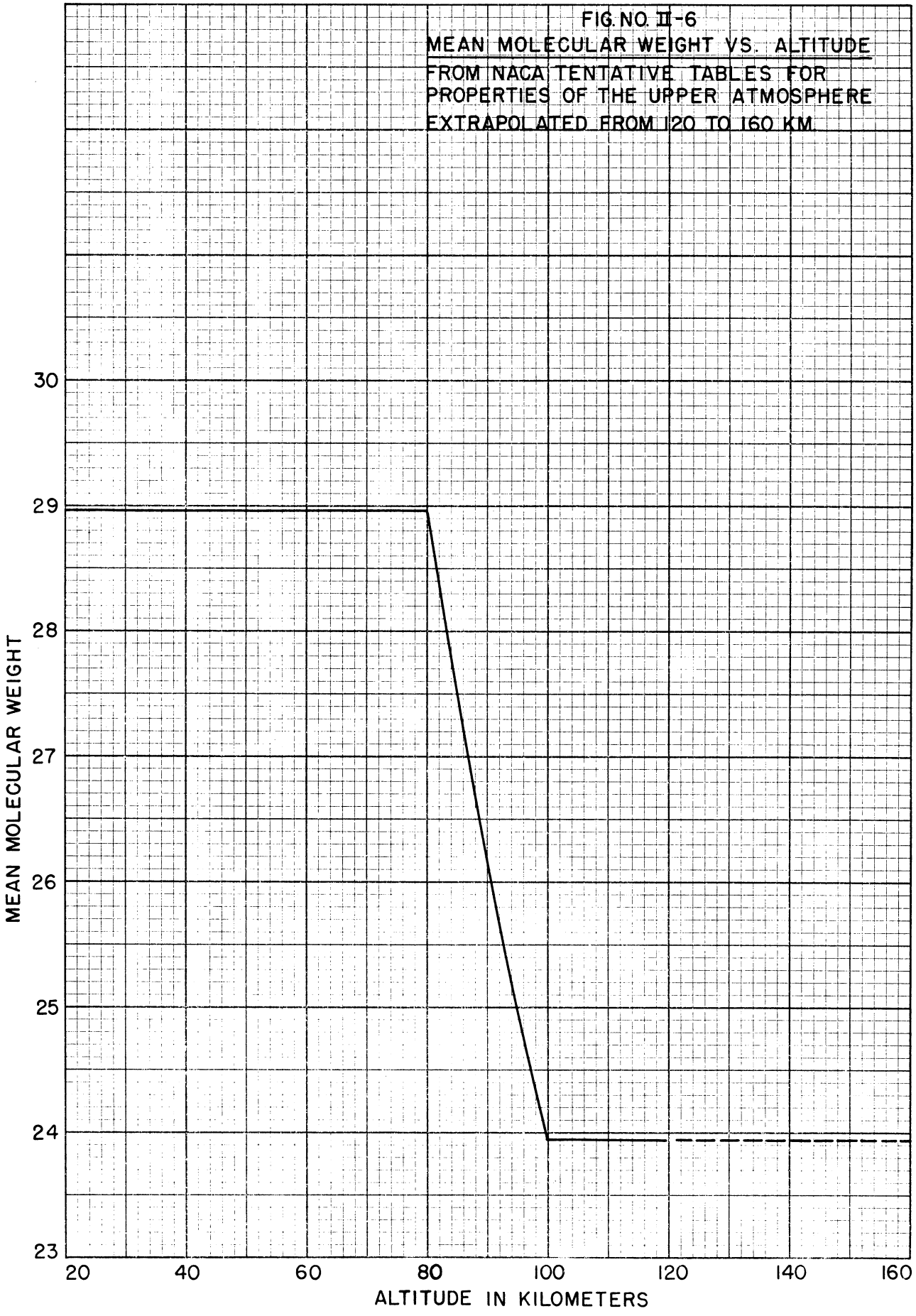
FIG. NO. II-6
MEAN MOLECULAR WEIGHT VS. ALTITUDE
FROM NACA TENTATIVE TABLES FOR
PROPERTIES OF THE UPPER ATMOSPHERE
EXTRAPOLATED FROM 120 TO 160 KM.
MEAN MOLECULAR WEIGHT
30
29
28
27
26
25
24
23
20
40
60
80
100
120
140
160
ALTITUDE IN KILOMETERS

FIG. NO. II-7

VELOCITY OF SOUND VS. ALTITUDE

FROM NACA TENTATIVE TABLES FOR PROPERTIES OF THE UPPER ATMOSPHERE EXTRAPOLATED FROM 120 TO 160 KM.

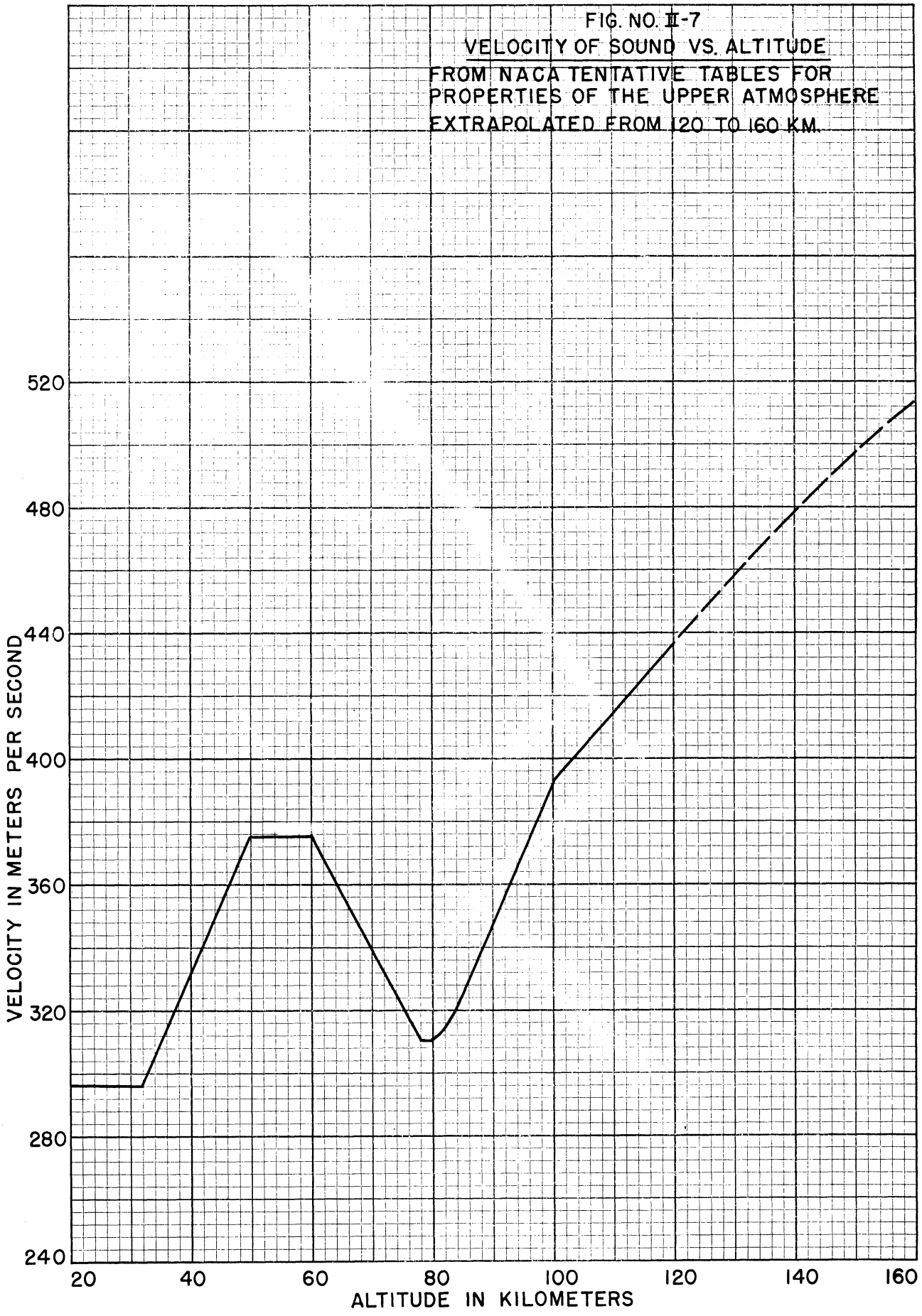

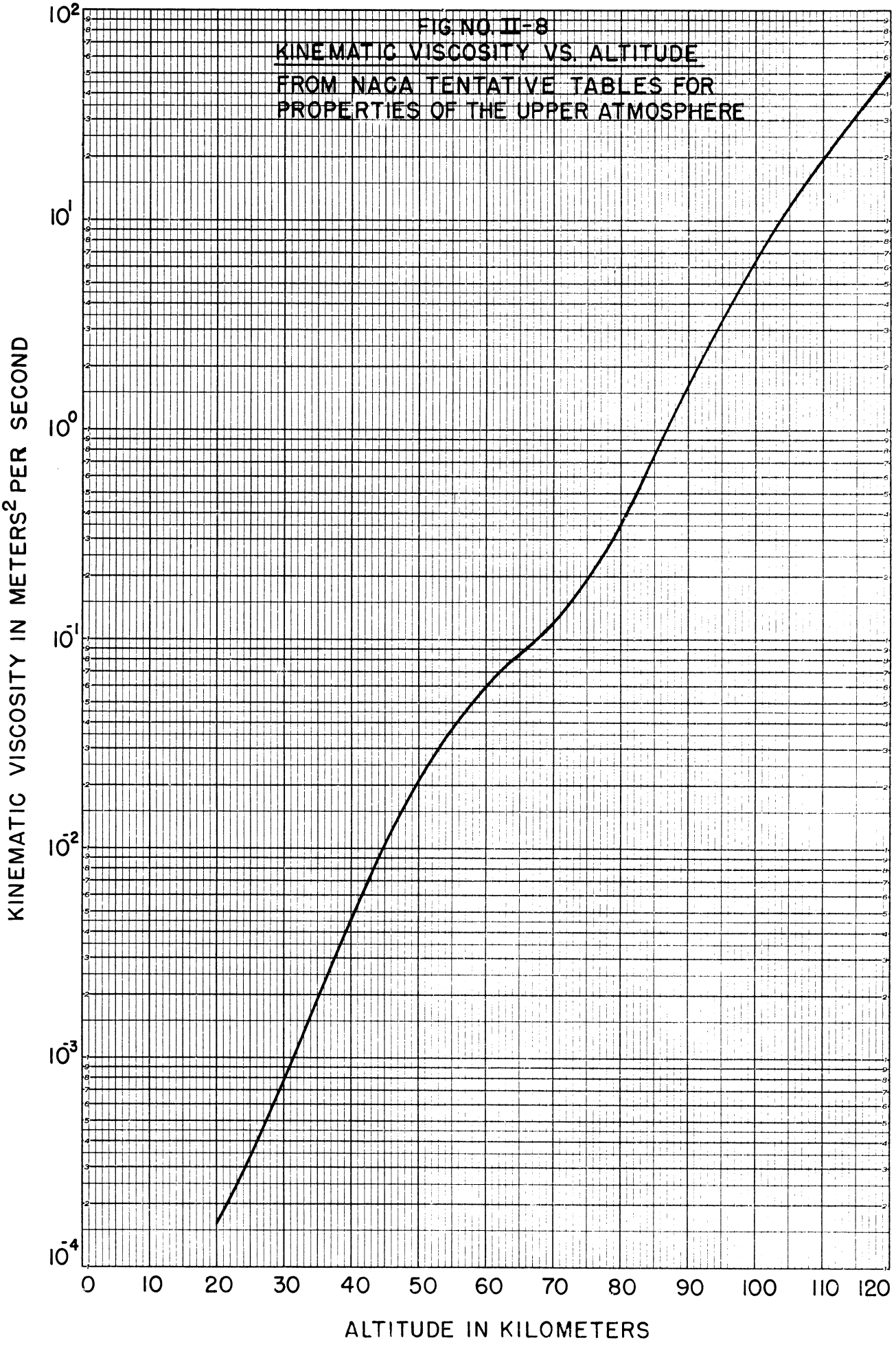
FIG. NO. II-8
KINEMATIC VISCOSITY VS. ALTITUDE
FROM NACA TENTATIVE TABLES FOR
PROPERTIES OF THE UPPER ATMOSPHERE
KINEMATIC VISCOSITY IN METERS² PER SECOND
10²
10¹
10⁰
10⁻¹
10⁻²
10⁻³
10⁻⁴
0
10
20
30
40
50
60
70
80
90
100
110
120
ALTITUDE IN KILOMETERS

III. THE MEASUREMENT PROBLEM

As mentioned in the Introduction of this report, the measurement of air pressure and temperature under the University of Michigan contract was originally a secondary objective, incidental to ionospheric electron density determinations. Therefore, in making pressure and temperature measurements, attention was first directed toward making these measurements in the neighborhood of the ionosphoric "E" layer; that is, from an altitude of about 80 kilometers up to the ceiling reasonably attainable by the V-2 rockets, approximately 160 kilometers. In this high range of altitudes, instrumentation can be (and was) so designed that the mean free path was long relative to the instrument dimensions.

In the fall of 1947 it was agreed that the responsibility for air pressure and temperature measurement coverage under the contract would be extended to include the entire range of altitudes from mean ground level to rocket ceiling, and instrumentation has been extended accordingly. However, prior to June 1, 1948, only preliminary efforts had been made toward determining the pressure and temperature at the lower altitudes.

The approximate ranges of atmospheric quantities of interest in the measurements are indicated, on the basis of the NACA tentative standard, by Table III-1 for the region from sea level to an altitude of 80 kilometers; also from 80 kilometers to approximate V-2 rocket ceiling. It should be noted that measurements to date indicate that the Table III-1 pressure and density values at 80 kilometers (probably also at 160 kilometers) may be higher than true values by a factor possibly as large as 10, and that the true temperatures at 80 kilometers, and above, are somewhat lower than shown by Table III-1.

TABLE III-1

SPOT DATA GIVEN BY AND EXTRAPOLATED FROM NACA TENTATIVE STANDARD ATMOSPHERE TABLES

1. Altitude in Km.	Sea Level	80 Km.	160 Km.
2. Pressure, mm. of Mercury	760	2.39×10^{-2}	3.5×10^{-5}
3. Air Density, gms./cu. cm.	8.82×10^{-5}	4.6×10^{-8}	2×10^{-11}
4. Temperature, $^{\circ}K$	$288^{\circ}K$	$240^{\circ}K$	$522^{\circ}K$
5. Mean free path, cm.	7.37×10^{-6}	1.95×10^{-1}	4×10^{2}
6. No. gas particles/cu. cm.	1.83×10^{18}	9.6×10^{14}	4.2×10^{11}

From such information as is available, it seems likely that the mean mass per particle is constant from ground level to an altitude of 80 kilometers, at a value of 4.81×10^{-23} grams per particle. Above 80 kilometers this figure may be expected to decline slightly, because of the dissociation of the oxygen (see Figure II-6).

From an instrumentation standpoint the most interesting figures in Table III-1 are those of mean free path. Considering the probability that at 80 kilometers true pressures are lower, by perhaps a factor of 10, than those shown in the table, it appears likely that the actual mean free path at 80 kilometers is of the order of 2 centimeters.

Roughly speaking, one can say that pressure, density, and mean free path change by a factor of two for a change in altitude of six or seven kilometers.

University of Michigan measurements on November 21, 1946 and February 20, 1947, were made mostly at altitudes between 70 and 110 kilometers. In this region the mean free path was short compared with the major dimensions of the rocket, so that considerations of shock wave formation, pressure variation along the rocket surfaces, etc., must be on the basis of compressible fluid theory. On the other hand, the mean free path for this range of altitudes is for the most part of the same order of magnitude as the dimensions of the ionization gauges used for measurement, and their readings must be evaluated accordingly.

Measurements made on the rocket fired December 8, 1947, started at an altitude of about 40 kilometers and continued to the crest of the trajectory (103 kilometers). Over the lower part of this range the mean free path of the gas particles was short compared to dimensions of both the rocket and the effective pressure gauges (Pirani gauges) so the analysis of the results over this lower range of altitudes must be on the basis of compressible fluid theory.

The problem of data analysis is considered in detail in Appendix D.

IV. CONSIDERATIONS OF INSTRUMENTATION

Early in the life of the contract, a study was made of the merits of various methods of measuring high vacua for the present purposes. As a result of this study, the decision was reached to use standard ionization gauges, primarily because they are the only devices presently available which will, in compact form, measure vacua down to pressures of the order of 10^{-6} millimeter of mercury, as needed for ceiling-height flights. Also, they are reasonably rugged. In addition, the pressure existing in an ionization gauge is determined by measuring the grid current and plate current of the gauge. The magnitudes of these quantities are easily converted into voltages that may be telemetered from rocket to ground. The telemetering service at White Sands is provided by the Naval Research Laboratory.

It was also decided, for various reasons, to use several gauges on each flight. These reasons included the very important one of having some insurance against failure of an individual device, and the fact that an average of the results of several instruments should be more dependable than the results from a single instrument. Furthermore, in the case of rocket flights to rocket ceiling, the mean free path becomes long enough to make useful the general method of temperature determination described in the University of Michigan report[2] "The Measurement of Temperature and Pressure in the Ionosphere," issued July 25, 1946. This method called for the placement of several gauges in the nose region, oriented differently relative to the direction of motion of the rocket.

In order to measure atmospheric pressures at altitudes below about 70 kilometers, some means other than the ionization gauge is required. The ionization gauge can be used only to measure pressures of less than about 10^{-2} millimeter of mercury. The Pirani gauge was chosen to measure these higher pressures for the following reasons:

(1) It measures over the correct range (about 10^{-2} to 1.0 millimeter of mercury).
(2) It is mobile.
(3) The output of the gauge is easily converted for use by the telemetering system.
(4) It is inexpensive.
(5) Pirani gauges are easily obtained.

As a result of these, and other considerations, including correlation with the variable-voltage probe experiment, the instrument design described in Appendix B was decided on and employed with only minor deviations to equip the August 22, 1946; November 21, 1946; February 20, 1947; and December 8, 1947 rockets.

V. PRESSURE DATA OBTAINED

V-1. Introduction.

In this section there are presented the pressure data obtained on the three successful rocket flights on which University of Michigan apparatus was flown. The curves included here show the unsmoothed data obtained by each of the pressure gauges. The noteworthy features of the information are pointed out and an attempt is made to interpret these features, in the light of existing knowledge.

In Appendix D of this report there is included a discussion of the systematic errors which it is believed exist in the method of measurement. It is shown in Section D-7 of that appendix that the ambient atmospheric pressure does not exceed the mean values of the pressure gauge readings on the ascent portion of the rocket flight and probably is not less than about one-half of these mean values.

In the last part of Appendix F the random errors occurring in the measurement process are discussed. Figures F-10 to F-14, inclusive, illustrate the resultant curves of probable error versus readings of the pressure gauges for the various rocket flights.

No detailed aspect data are available for the first two successful rockets carrying University of Michigan equipment but it is known that both rockets had substantial angular motions. Therefore, in the following pages it is possible only to conjecture as to the reasons for the various ionization gauges responding as they did. Aspect data are available for the third successful rocket (December 8, 1947) but these data have not yet been completely correlated with the readings of the pressure gauges.

It is not possible to take into account any effect which high velocity winds in the ionosphere might have had, since no data are available concerning such winds. However, it is possible that a high velocity, nearly vertical, wind may have been present during the November 21, 1946 and February 20, 1947 firings and that this caused the nose gauge (No. 5) to read no higher than the other gauges on these two rocket flights.

V-2. Presentation of Ionization Gauge Data from November 21, 1946 Firing.

The rocket fired at White Sands on November 21, 1946 carried five Type VG-1A* ionization gauges mounted in the nosepiece in the manner described in Appendix B. Figure V-1 illustrates diagrammatically the placement of the five numbered gauges in the nosepiece.

A commutator sampled the plate current and grid current values of each gauge 100 times per minute, so that the maximum fineness of resolution obtainable in the data was an observation every 0.6 second. Modifications incorporated in the measuring circuitry used on later rockets provided substantial improvement in the fineness of resolution on the pressure scale. Some improvement in this direction has also been achieved by bettering the techniques used in the interpretation of the telemetering records.

A discussion of the significance of the pressure readings of the ionization gauges is included in Appendix D of this report.

In Figures V-2, V-3, V-4, V-5 and V-6 the pressures determined by each gauge are plotted against time, measured from the moment of rocket launching. For purposes of comparison, a curve of the pressures given in the NACA Technical Note No. 1200[1] is plotted on each of these figures. Also, the pressure readings of gauges Nos. 1, 3 and 4 have been plotted against altitude in Figures V-7, V-8 and V-9. The following aspects of these figures are worthy of note:

1. The pressures reported by gauges No. 2 and No. 5 leveled off at practically constant values during most of the flight. This was represented on the telemetering indications by a failure of the plate currents of these gauges to drop below a fixed minimum value. In view of the sharp contrast between

*Manufactured by Distillation Products, Inc., Rochester, N.Y.

this behavior and that of the other three gauges, it is believed that possibly a plate current leakage path existed, permitting passage of a minimum current between plate and cathode regardless of pressure in the gauge. Therefore, the indications of gauges No. 2 and No. 5 are considered as being of little significance.

2. The head opened, exposing the gauges to the atmosphere, when the cone-tip pressure was very nearly 10^{-2} millimeter of mercury. This is a higher pressure than the ionization gauges are expected to record dependably, and this fact may be associated with the failure of gauges No. 2 and No. 5. The timing motor was set to open the head at about 100 seconds in the hope that the rocket would be heading toward a 150 kilometer crest, in which case the cone pressure at 100 seconds would have been well below 10^{-3} millimeter of mercury, so entirely suitable for registration by ionization gauges.

3. The pressure readings of all gauges, and more significantly of gauges No. 1, No. 3, and No. 4, are less than the NACA tentative standard figures by a factor of between 10 and 20 at the areas of closest agreement.

4. Readings of the three significant gauges show a much slower increase in pressure on initial descent from the crest of the trajectory than they show decrease on ascent. These pressure curves approach symmetry about some moment substantially later than the crest moment. This is believed due to the gauges on the ascent being located in a region of maximum pressure on the advancing nose of the rocket, whereas, during descent, they were in a low-pressure region. The rocket presumably nosed over in pitch only slightly during the first 270 seconds of flight, so that on the initial descent it was falling essentially tail down (as illustrated in Figure V-34), the nose thus being in the region where the pressure was substantially less than ambient pressure. It is not believed that this shift of the point of symmetry of the pressure curves is any evidence of lag in response of the gauges, because of the reason stated in 5 immediately below.

5. All gauges responded, upon exposure to the atmosphere at 98 seconds, so rapidly that the time resolution of the data is insufficient to indicate how quickly they did respond. The entire head-opening pressure indication change took place, on each gauge, between two successive samplings of the pressure. A theoretical analysis of the response time of the ionization gauges is included in Appendix D, and indicates that this response time should be of the order of 5 to 10 milliseconds.

6. Beyond about 270 seconds no significance is to be attached to any of the pressure readings. It is believed that the declining plate currents of the gauges beyond 270 seconds were due to failure of the gauges, because of the relatively high pressure existing at the lower altitudes. It is conceivable, however, that the pressures recorded by gauges No. 1, No. 3, and No. 4 are essentially correct out to 300 seconds.

7. The readings of gauges No. 3 and No. 4 show a decided periodicity during descent. The cyclic period is between 28 and 30 seconds. The approximate 90 degree phase relation of periodicity (No. 3 lagging) between these two gauges strongly suggests that the periodicity was due to spin of the rocket. Unfortunately, no information of value concerning the angular motion of the rocket during flight is available. Thus, no exact interpretation of the variations in gauge readings is possible.

8. Gauge No. 5, in the flat face of the truncated nose, shows definite evidence of a 30-second periodicity. The magnitude of the periodic varying is presumably masked by the leakage current mentioned earlier in the section, but the phase position is definitely discernible. The fact that the periodicity appears at all, in the face of the masking effect, suggests that the actual periodic pressure variations may have been comparable in magnitude to those of gauges No. 3 and No. 4. If the rocket were spinning exactly around its longitudinal axis, and if its motion had no nutational component, gauge No. 5 would experience no change of pressure at the period of spin. Therefore, the definite evidence of spin periodicity in gauge No. 5 indicates that either the axis of least moment of inertia did not coincide with the axis of figure of the rocket, or that there was a substantial nutational component of motion.

9. Gauge No. 1 shows very little, if any, 30-second periodic variation. Knowing that such a periodicity should be expected, one might locate maxima at perhaps 240 and 270 seconds, but the variation is definitely not comparable in magnitude to that of gauge No. 3 on the opposite side of the truncated cone. One is tempted to assay these variations in strength of the periodic variations on the basis of faults in gauge performance, or calibration, but the essential agreement between the gauge readings on the ascent rules out such an approach. The failure of gauge No. 1 to respond strongly to the rotary

motion while the other significant gauges do so respond could, perhaps, be explained on the basis of spin motion about an axis not coincident with the axis of figure, probably also on the basis of the existence of a substantial nutational motion.

10. The absence of periodicity during the ascent is, of course, explainable on the basis that any departure from the simply rolling-cone motion, discussed in Appendix E, would be relatively slight on the ascent, and with the axis of spin approximately tangent to the trajectory, little periodic pressure variation would appear in the readings of the gauges.

Study of the data, and of various facts regarding rocket motion and aerodynamic properties of the V-2 rocket, has indicated that the most useful portion of the data for determining upper atmosphere pressure and temperature are the ionization gauge readings during the ascending trajectory. Therefore, Figure V-10 has been prepared in which the pressure values for gauges Nos. 1, 3 and 4 during ascent have been superposed.

V-3. Presentation of Ionization Gauge Data from February 20, 1947 Firing.

The instrumentation for measurement of atmospheric pressure, carried in the rocket fired February 20, 1947, was essentially identical to that carried in the previous Air Materiel Command rocket fired November 21, 1946. This instrumentation is discussed in Section V-2 and in Appendix B of this report.

Figures V-11, V-12, V-13, V-14 and V-15 show the variation with time of the ionization gauge pressure readings from the February 20 firing, and Figures V-16, V-17, V-18 and V-19 contain the same pressure data plotted against altitude rather than time. Figure V-20 shows the superimposed readings, on ascent, of the four significant ionization gauges, plotted with altitude as the abscissa.

These records, when carefully studied, give certain indications of considerable general interest, as follows:

1. Gauge No. 4 appears to have been affected, as were two gauges on the November flight, by a leakage current in the plate circuit which seems to invalidate its readings.

2. The readings of all the significant gauges lie below the pressure values predicted by the NACA.

3. Gauge Nos. 1, 2, 3 and 5 give firm evidence, during rocket descent, of a cyclic motion, presumably spin about the longitudinal axis of the rocket, having approximately a seven-second period. This is of interest in connection with the fact that, prior to fuel burn-out, periodic interruptions in the telemetering transmission, due to rocket motor exhaust, occurred at about a two-second periodicity. Thus the indications are that possibly at either fuel burn-out or upon the ejection of a secondary test vehicle the spin rate was substantially reduced. Also, it is possible that atmospheric damping caused this decrease in the rate of spin. Again, no aspect data were available so it is possible only to conjecture concerning the angular motions of the rocket during flight.

It is in accordance with expectation that this periodicity is indicated only on the descent, not during ascent. During ascent the rocket is, to a first approximation, pointed in the direction of its flight, so that spin about the axis of figure should not produce appreciable periodic variation in the readings of any of the gauges. However, during descent the rocket is falling, presumably, at a pitch of the general nature indicated in Figure V-34. Therefore, on descent the entire nose region is in a receding position relative to the air stream, and the pressure, during descent, for all gauges should be less than during ascent, and presumably less than the static pressure. That this actually occurred is indicated clearly in Figures V-16 to V-19. It is fairly evident that the pressure on the down-side cone face, as at point 3. in Figure V-34, will be greater than on the up-side cone face, as at point 1. Therefore, as the rocket spins, each cone-side gauge should experience periodic pressure variations, as they did.

4. Gauge No. 5, located on the tip exposure (position 5 in Figure V-34), showed the same periodicity in reading as did the other gauges. If the seven-second periodic motion were true spin about the axis of figure of the rocket, there should be no cyclic variation in the readings of the No. 5 gauge at this spin period. The fact that gauge No. 5 did show the periodic variations is sufficient evidence that the seven-second cyclic motion was not pure spin about the axis of figure of the rocket.

5. There is reasonably firm evidence that this seven-second periodic motion was of the general nature of rotation about the longitudinal axis of the rocket; the important items of evidence being:

(a) The phase relationship between the gauge variations is in accord with cyclic rotation, in order (5), 1, 2, 3.
(b) If the periodic motion were due to tumbling, or to anything other than essentially a spin- type of motion, it would have affected the readings during the ascent as well as during the descent.

6. The combinations of items of evidence just stated suggests that the rocket weight distribution was not symmetrical about its axis of figure, so that one might suspect that either or both of the following circumstances existed:

(a) The rocket may have possessed a maximum as well as a minimum moment of inertia, therefore the ellipsoid rolling on the tangent plane (see Figure E-3) was not an ellipsoid of revolution; hence the overall motion included nutation. The periodicity of nutational motion is commensurate with that of the simultaneously occurring spin, as both result from rolling of the ellipsoid on the tangent plane. Therefore, nutation would have the practical effect of altering the pitch angle at a period proportional to that of the spin, causing a variation in the angle made by the rocket with the receding air stream and a resulting variation in the reading of gauge No. 5.
(b) The axis of least moment of inertia of the rocket may not have passed quite through the center of the nose cone. This would have the same effect on the readings of the ionization gauges as would a periodic change in pitch angle and would result in a periodic variation in the reading of gauge No. 5, at the same frequency as the variations of the readings of all the other gauges. Thus the fact that No. 5 gauge showed a periodicity the same as that of the other gauges suggests that the axis of least moment of inertia was substantially off-center at rocket tip. This hypothesis is in accord with the observation during ascent that gauge No. 2 read consistently higher than the nose gauge. This No. 2 gauge was presumably the one nearest the axis of spin. Also, the fact that the cyclic variations in the readings of gauge No. 2 were 180 degrees out-of-phase with those of gauge No. 5 indicates that the axis of spin pierced the side of the nose of the rocket at a point between gauges No. 2 and No. 5.

In this connection, it should be noted that the No. 5 gauge in the November flight, although insensitive due to leakage, gave indication of only a very slight periodicity during descent. This suggests that during the November flight the axis of spin coincided more nearly with the axis of figure than was the case in February.

7. At 173 seconds after rocket launching, gauges Nos. 1, 2 and 5 show an abrupt drop in pressure occurring in a time interval of less than one second. At this moment the rocket was approaching the crest of its trajectory. Its velocity was upward at an angle of 57 degrees with the horizontal, at a velocity of 626 kilometers per hour. Thus in one second, the rocket travelled about 500 feet.

At this 173-second moment, gauge No. 3 showed a much less abrupt but, nevertheless, a very definite increase in pressure.

Also, at this same moment, there occurred an abrupt and unmistakeable change in the nature of the volt-ampere curve reported by the variable-voltage probe. This change persisted throughout the remainder of the flight.

Very careful, but unsuccessful, studies have been made of the circuit in an effort to discover some possible fault that might have caused these changes. For example, the grid power for two of the five gauges came from one source, that for the other three from a second source, but the variation between rise and fall of gauge readings did not divide in accordance with the power source division.

It should be pointed out that, in general, a reduction in ionization gauge pressure results in a simultaneous increase in grid current and a decrease in plate current. The increase in grid current occurs because of the decrease of the cooling effect of the air on the gauge filament, thus permitting its temperature to rise and its emission to increase. Of course, a very slight change in filament temperature results in a substantial change in emission. At 173 seconds, in those gauges in which the pressure indication dropped, the grid currents rose as the plate currents fell, in about the expected amount in relation to the pressure change indicated. No imaginable single circuit fault would produce these two

opposite effects in the correct ratio, and at the same time affect the probe circuitry in the way indicated.

The only tenable conclusion is, therefore, that at 173 seconds the pressures measured by the gauges changed abruptly in the manner recorded, and that at the same time the nature of the atmospheric electrical content changed as indicated by the variable-voltage probe.

It should be pointed out that at the time of this firing the virtual height of the ionosphere was 120 kilometers. At 173 seconds after launching the rocket was at an altitude of 107.3 kilometers, which is not far, one way or the other, from the lower edge of the ionosphere.

So far no completely plausible explanation has been found for the above-discussed phenomena.

V-4. Presentation of Pressure Gauge Data from December 8, 1947 Firing.

The pressure-measurement instrumentation for this rocket was very similar to that carried on the November 21, 1946 and February 20, 1947 rockets, except that two Pirani gauges were carried in addition to the five ionization gauges. The five ionization gauges were mounted on a nosepiece identical to that used on the previous rockets, which nosepiece is shown diagrammatically in Figure V-1. One of the Pirani gauges was mounted on the aft part of this nosepiece (thus only about two feet from the nose of the rocket) and the other was placed a few inches forward of the No. 1 fin of the rocket (thus near the tail of the rocket). According to data obtained from German wind tunnel tests, this latter Pirani gauge was so located as to record values of pressure practically equal to ambient pressure. The Pirani gauges were included on the rocket in order to measure pressures at altitudes lower than those at which the ionization gauges are useful. The details of the instrumentation are discussed in Appendix B of this report.

V-4.1. Ionization Gauge Pressure Data Obtained from December 8, 1947 Firing.

Figures V-21, V-22, V-23, V-24, and V-25 show the variation with time of the ionization gauge pressure readings obtained on this flight. The same pressure data plotted versus altitude are shown in Figures V-26, V-27, V-28 and V-29. Gauge No. 2 appears to have been defective, and no further consideration will be given to its indications.

The outer cone of the nosepiece was thrown off at an altitude of about 45 kilometers and, of course, the ionization gauges also were opened to the outside pressure at this altitude. The ionization gauge, as used here, is not capable of measuring pressures as high as those which exist at this altitude, and the readings of the gauges are considered to be of no significance below an altitude of about 75 kilometers. Therefore, the pressure values are plotted only for altitudes in excess of 70 kilometers.

Aspect cameras were carried on this rocket and data were obtained from them which appear to be very useful for the purposes of analyzing the pressure data obtained by the ionization gauges. This aspect information was received at the University of Michigan late in March 1948. Therefore, due to the magnitude of the job of correlating the aspect information and the pressure data, it is not possible to include a complete analysis of the pressure data in this report. A separate report will be issued within a few months, which will present this analysis.

It is known that the rocket ascended to about 90 kilometers with the pitch and yaw angles nearly zero, and that there was a very slow roll, or spin, about the longitudinal axis of the V-2. Above this altitude the pitch and yaw angles increased considerably. Therefore, the pressure readings of the ionization gauges from about 75 to 90, or 95, kilometers, on the ascent portion of the trajectory, are the most reliable readings.

In Figure V-30 are plotted the superimposed pressure readings of the four significant ionization gauges on the ascent portion of the flight. From this figure it will be noted that between the altitudes of about 75 to 90 kilometers the readings of gauges No. 1, No. 3 and No. 4 lie very close together, whereas that of gauge No. 5 (the nose gauge) lies above the other three by a factor of a little less than two. These are just the results that one would naively expect to obtain from a rocket moving with its longitudinal axis very nearly parallel to its trajectory.

V-4.2. Pirani Gauge Pressure Data Obtained from December 8, 1947 Firing.

The pressure data obtained from the Pirani gauges carried on this rocket are presented in Figures V-31, V-32 and V-33. The curve of pressure versus time-of-flight for the gauge mounted near the tail of the rocket is shown in Figure V-31. German wind tunnel tests showed that a gauge located in this position would read values of pressure practically identical to ambient pressure. Figure V-32 shows the curve of pressure versus time-of-flight for the Pirani gauge mounted near the nose of the rocket. In Figure V-33 the pressure data from both gauges have been plotted against altitude, for the ascent portion of the trajectory. The exact location of these two Pirani gauges is described in Appendix B of this report.

In connection with these curves, three facts are worthy of note:

1. The wild gyrations in pressure readings which occur on the ascent portion of the trajectory are due to operation of the gauges near the limits of their useful range, where the calibration curves are very flat. Thus, small random variations in output voltage would be interpreted as large changes in pressure. Therefore, these highly doubtful points have been omitted from Figure V-33.

2. Due to space limitations, it was necessary to use a special Pirani gauge in the nose. This gauge had a limited operating range and this accounts for the fact that data were obtained over only a narrow range of pressures.

3. The WL-762 Pirani gauge had a time lag in response of three seconds and the special Pirani gauge had a time lag of 4-1/2 seconds. These time delays were not taken into account in plotting the pressure values shown in Figures V-31, V-32, and V-33 but they were considered in using the Pirani gauge data in Figure i-1.

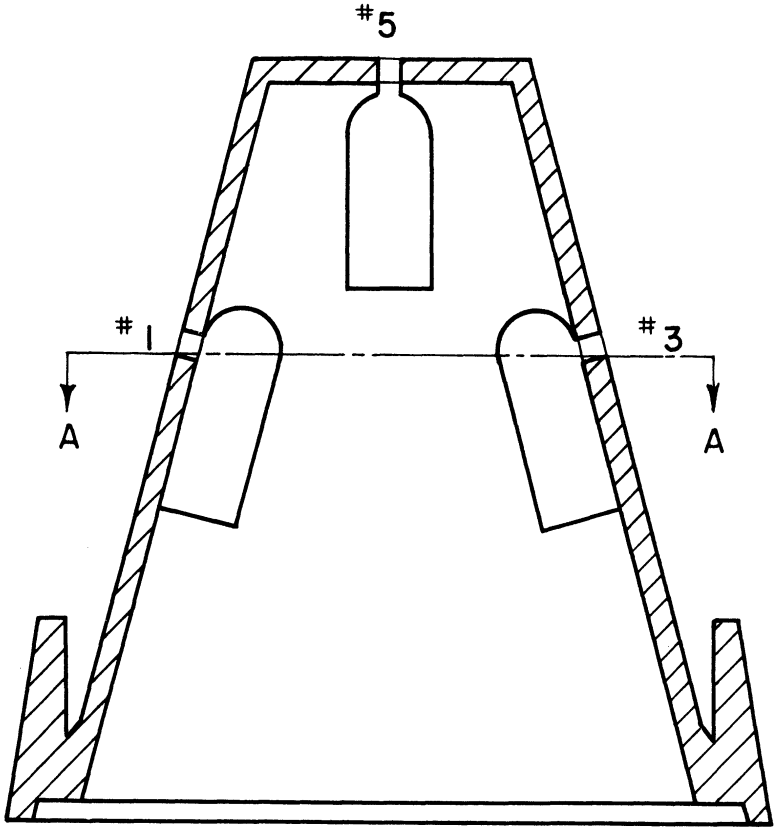

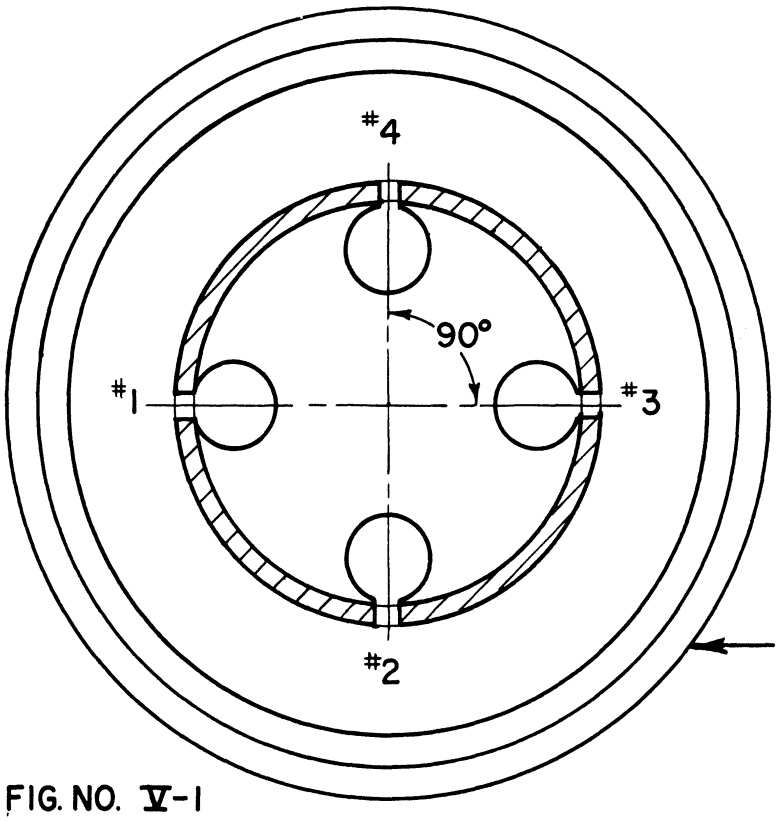

FIG. NO. V-1

DIAGRAM OF V-2 NOSE-PIECE SHOWING PLACEMENT OF FIVE IONIZATION GAUGES.

FIG. NO. V-2

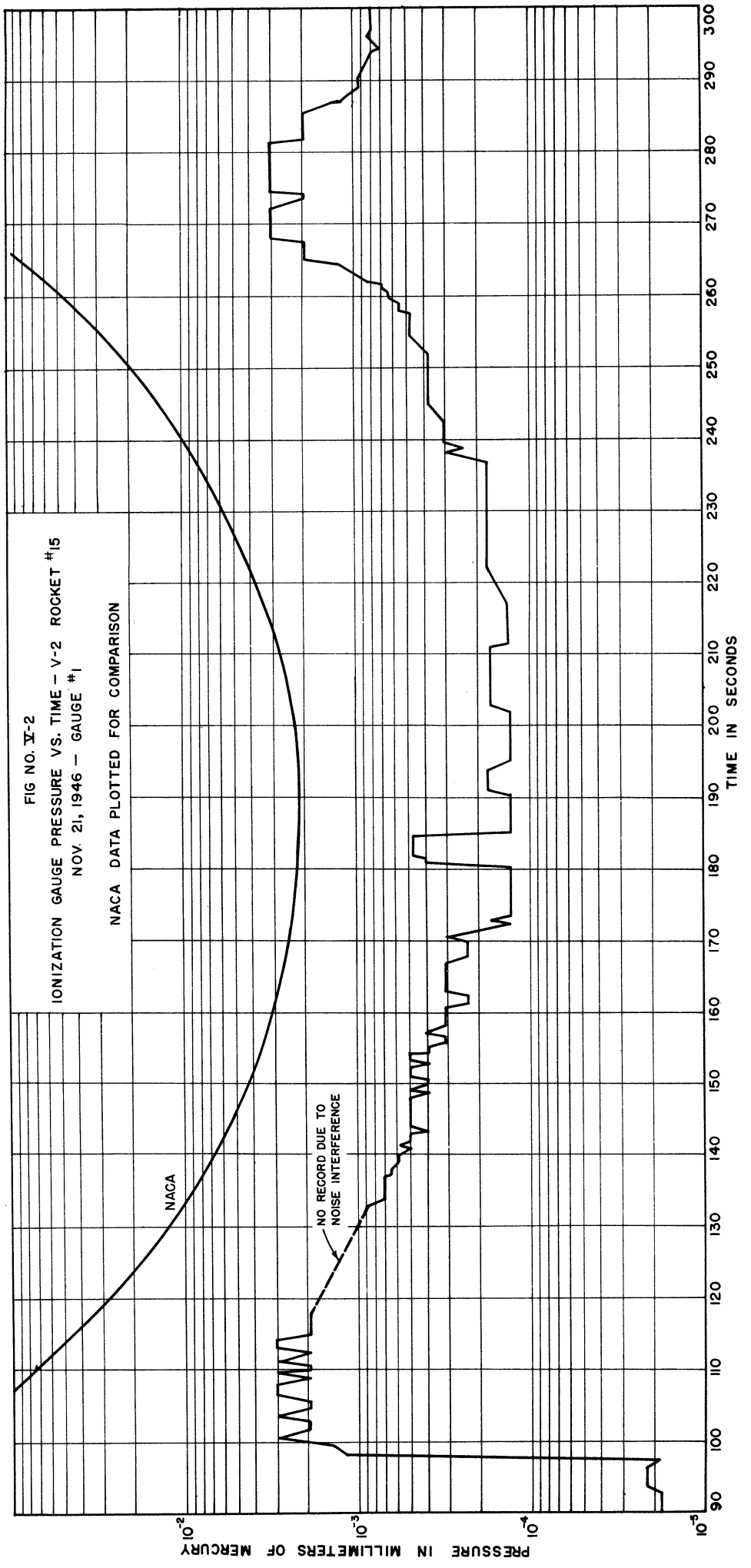
FIG NO. V-2
IONIZATION GAUGE PRESSURE VS. TIME – V-2 ROCKET #15
NOV. 21, 1946 – GAUGE #1
NACA DATA PLOTTED FOR COMPARISON
NACA
NO RECORD DUE TO NOISE INTERFERENCE
PRESSURE IN MILLIMETERS OF MERCURY
10^{-2}
10^{-3}
10^{-4}
10^{-5}
TIME IN SECONDS
90
100
110
120
130
140
150
160
170
180
190
200
210
220
230
240
250
260
270
280
290
300

FIG. NO. V-3

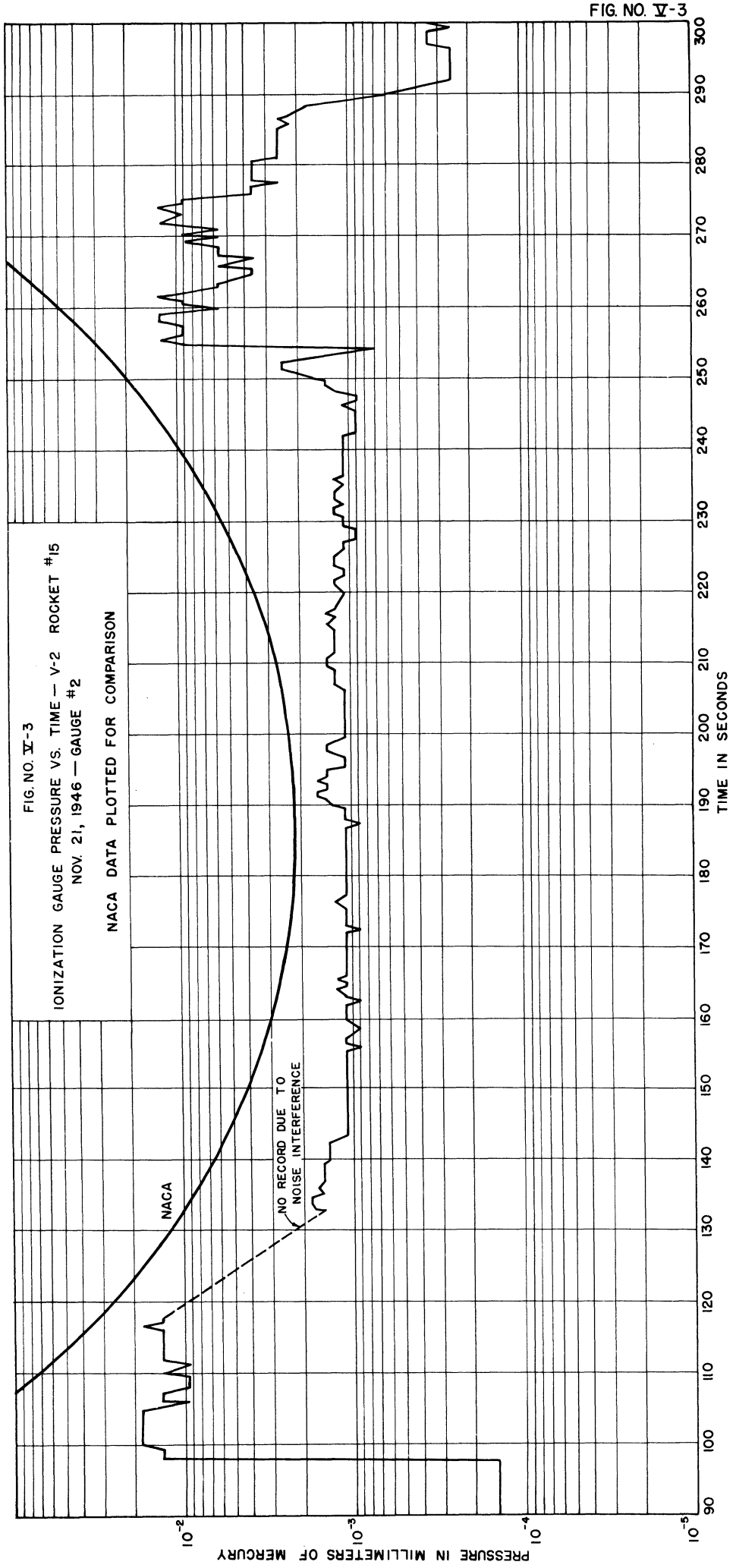
FIG. NO. V-3
IONIZATION GAUGE PRESSURE VS. TIME — V-2 ROCKET #15
NOV. 21, 1946 — GAUGE #2
NACA DATA PLOTTED FOR COMPARISON
NACA
NO RECORD DUE TO NOISE INTERFERENCE
PRESSURE IN MILLIMETERS OF MERCURY
10^{-2}
10^{-3}
10^{-4}
10^{-5}
90
100
110
120
130
140
150
160
170
180
190
200
210
220
230
240
250
260
270
280
290
300
TIME IN SECONDS

FIG. NO. V-4

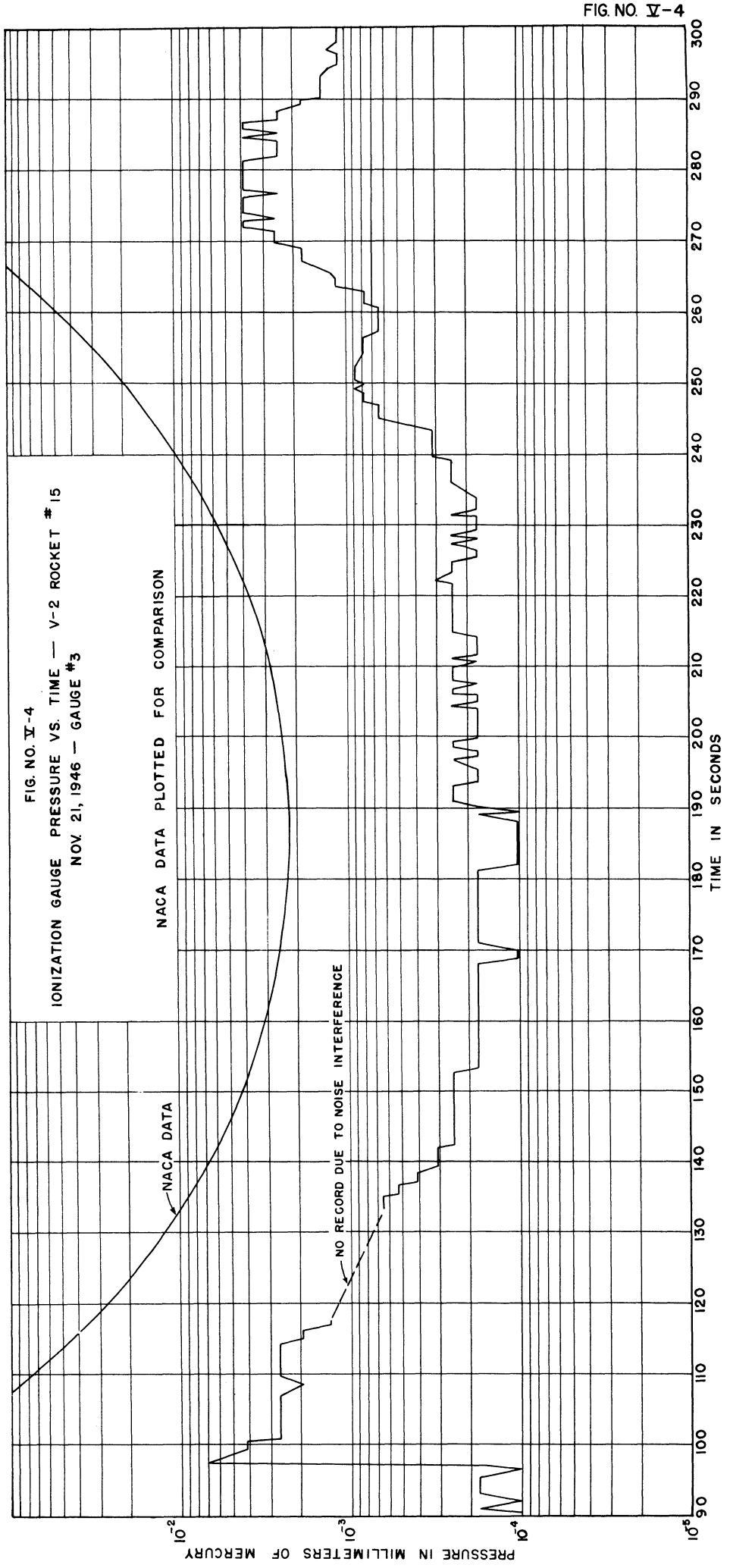
FIG. NO. V-4
IONIZATION GAUGE PRESSURE VS. TIME — V-2 ROCKET #15
NOV. 21, 1946 — GAUGE #3
NACA DATA PLOTTED FOR COMPARISON
NACA DATA
NO RECORD DUE TO NOISE INTERFERENCE
PRESSURE IN MILLIMETERS OF MERCURY
10^{-2}
10^{-3}
10^{-4}
10^{-5}
TIME IN SECONDS
90
100
110
120
130
140
150
160
170
180
190
200
210
220
230
240
250
260
270
280
290
300

FIG. NO. V-5

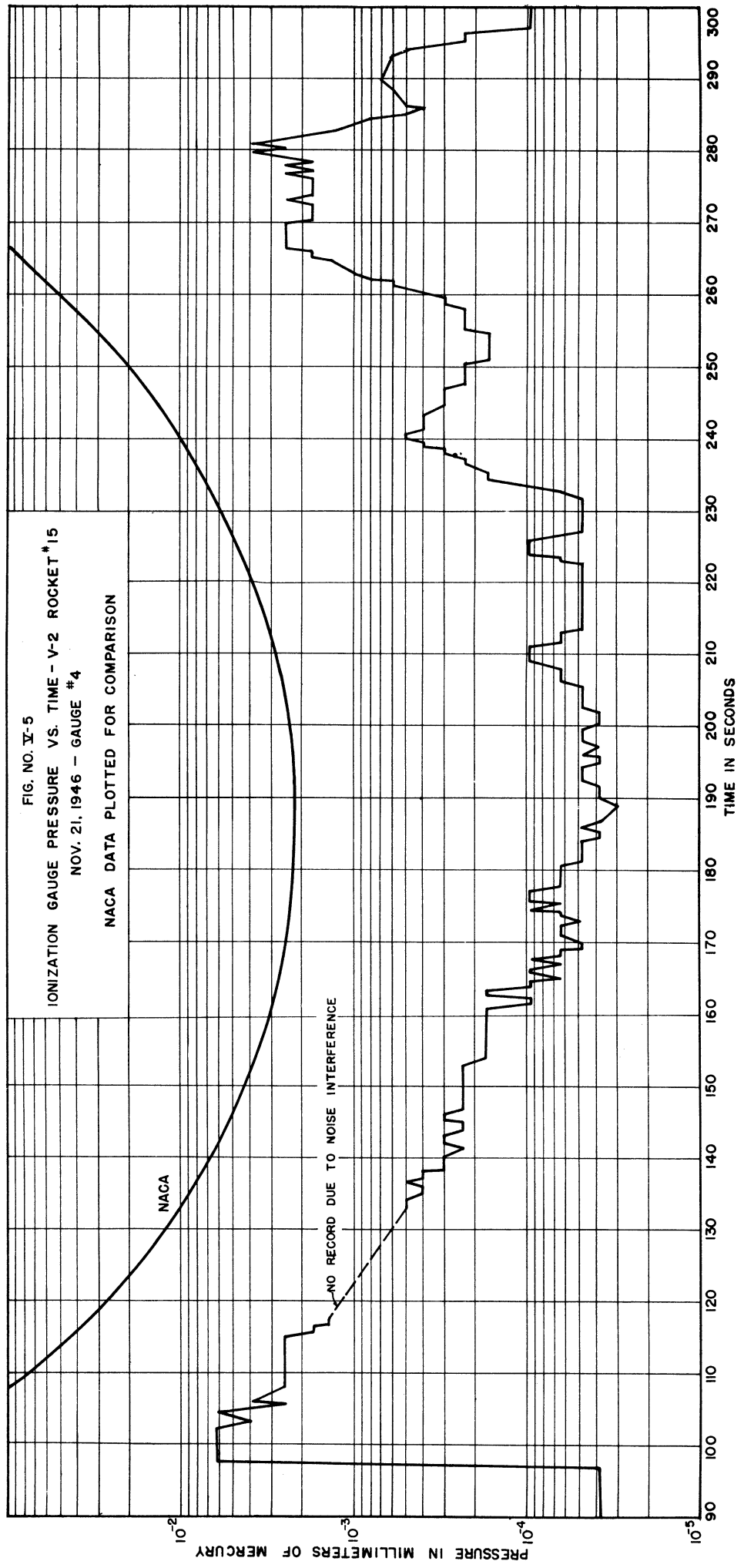
FIG. NO. V-5
IONIZATION GAUGE PRESSURE VS. TIME - V-2 ROCKET #15
NOV. 21, 1946 - GAUGE #4
NACA DATA PLOTTED FOR COMPARISON
NACA
NO RECORD DUE TO NOISE INTERFERENCE
PRESSURE IN MILLIMETERS OF MERCURY
10^{-2}
10^{-3}
10^{-4}
10^{-5}
TIME IN SECONDS
90
100
110
120
130
140
150
160
170
180
190
200
210
220
230
240
250
260
270
280
290
300

FIG. NO. V-6

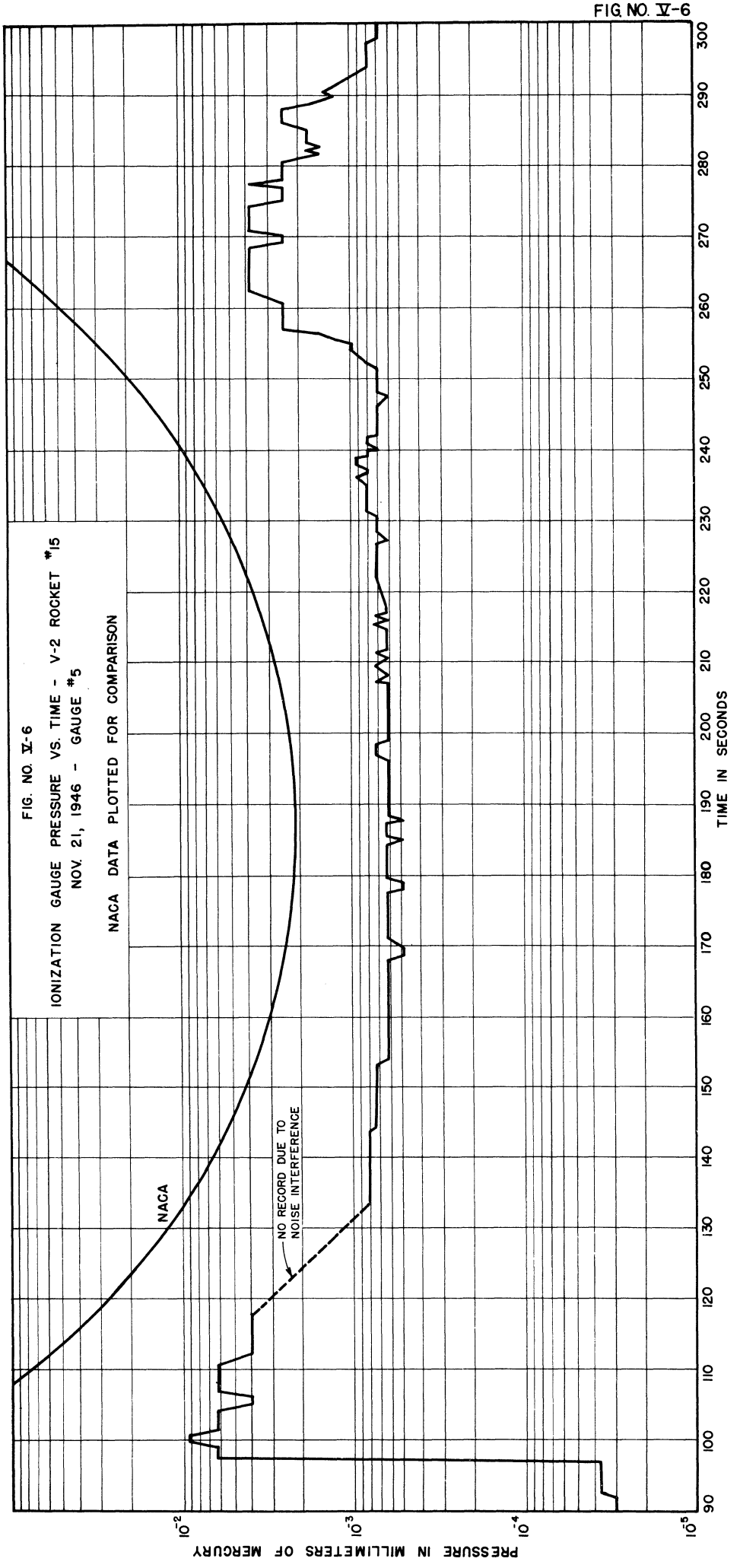
FIG. NO. V-6
IONIZATION GAUGE PRESSURE VS. TIME - V-2 ROCKET #15
NOV. 21, 1946 - GAUGE #5
NACA DATA PLOTTED FOR COMPARISON
NACA
NO RECORD DUE TO NOISE INTERFERENCE
PRESSURE IN MILLIMETERS OF MERCURY
10^{-2}
10^{-3}
10^{-4}
10^{-5}
TIME IN SECONDS
90
100
110
120
130
140
150
160
170
180
190
200
210
220
230
240
250
260
270
280
290
300

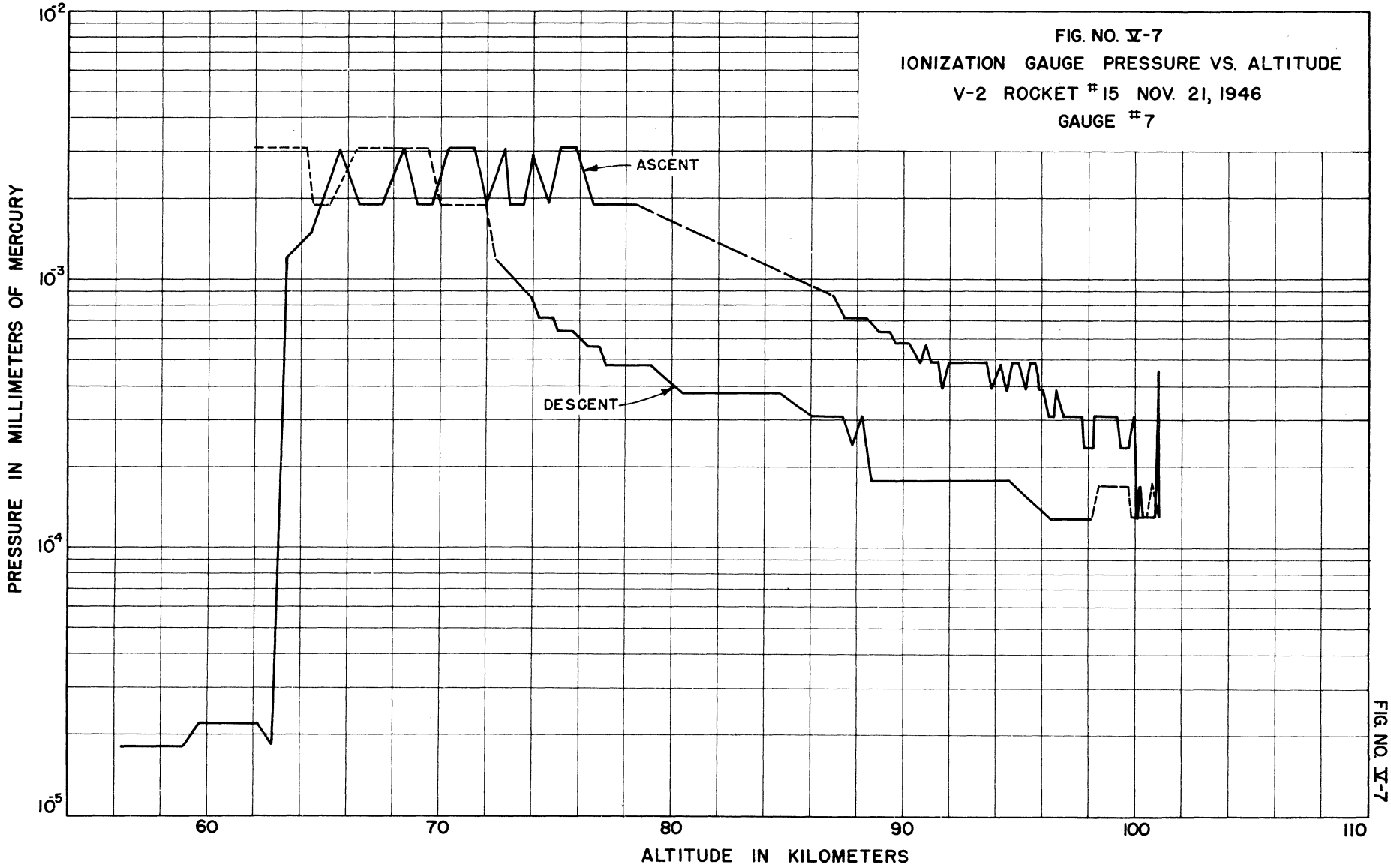
FIG. NO. V-7
IONIZATION GAUGE PRESSURE VS. ALTITUDE
V-2 ROCKET # 15 NOV. 21, 1946
GAUGE # 7
ASCENT
DESCENT
PRESSURE IN MILLIMETERS OF MERCURY
10^{-2}
10^{-3}
10^{-4}
10^{-5}
60
70
80
90
100
110
ALTITUDE IN KILOMETERS

FIG NO. V-7

FIG. NO. V-8

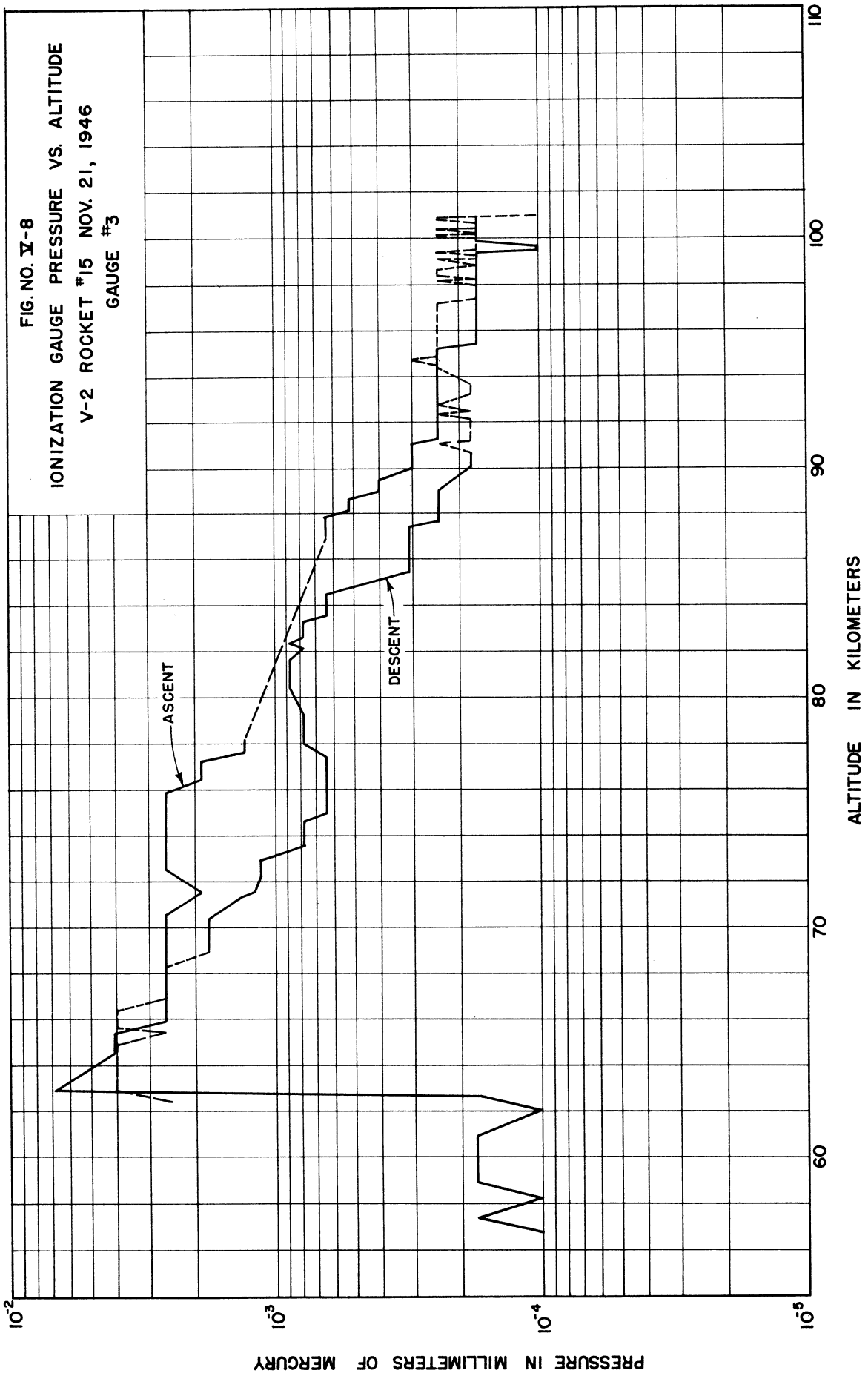
FIG. NO. V-8
IONIZATION GAUGE PRESSURE VS. ALTITUDE
V-2 ROCKET #15 NOV. 21, 1946
GAUGE #3
ASCENT
DESCENT
10^{-2}
10^{-3}
10^{-4}
10^{-5}
PRESSURE IN MILLIMETERS OF MERCURY
60
70
80
90
100
110
ALTITUDE IN KILOMETERS

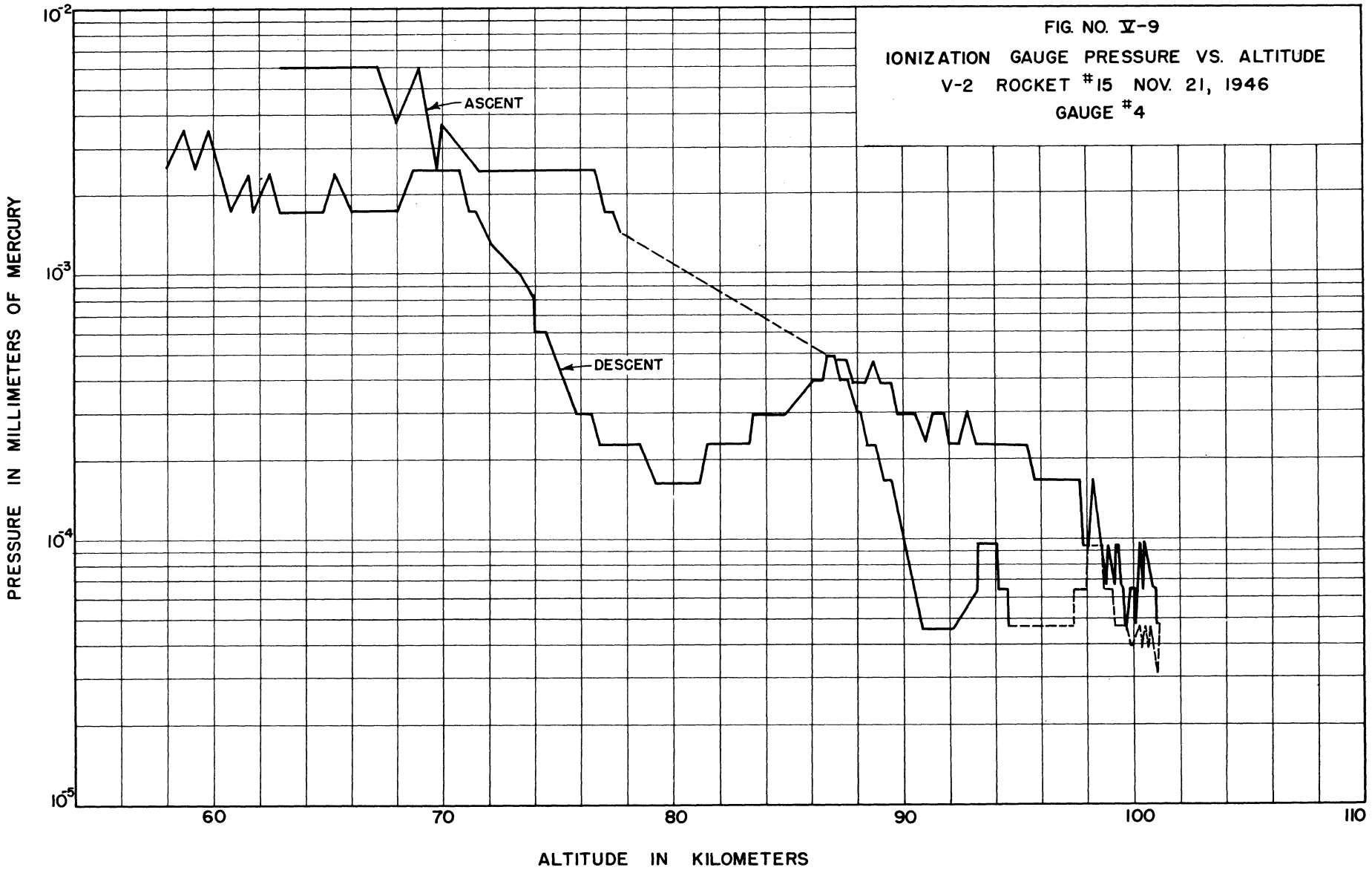
FIG. NO. V-9
IONIZATION GAUGE PRESSURE VS. ALTITUDE
V-2 ROCKET #15 NOV. 21, 1946
GAUGE #4
ASCENT
DESCENT
10^{-2}
10^{-3}
10^{-4}
10^{-5}
60
70
80
90
100
110
PRESSURE IN MILLIMETERS OF MERCURY
ALTITUDE IN KILOMETERS
FIG. NO. V-9

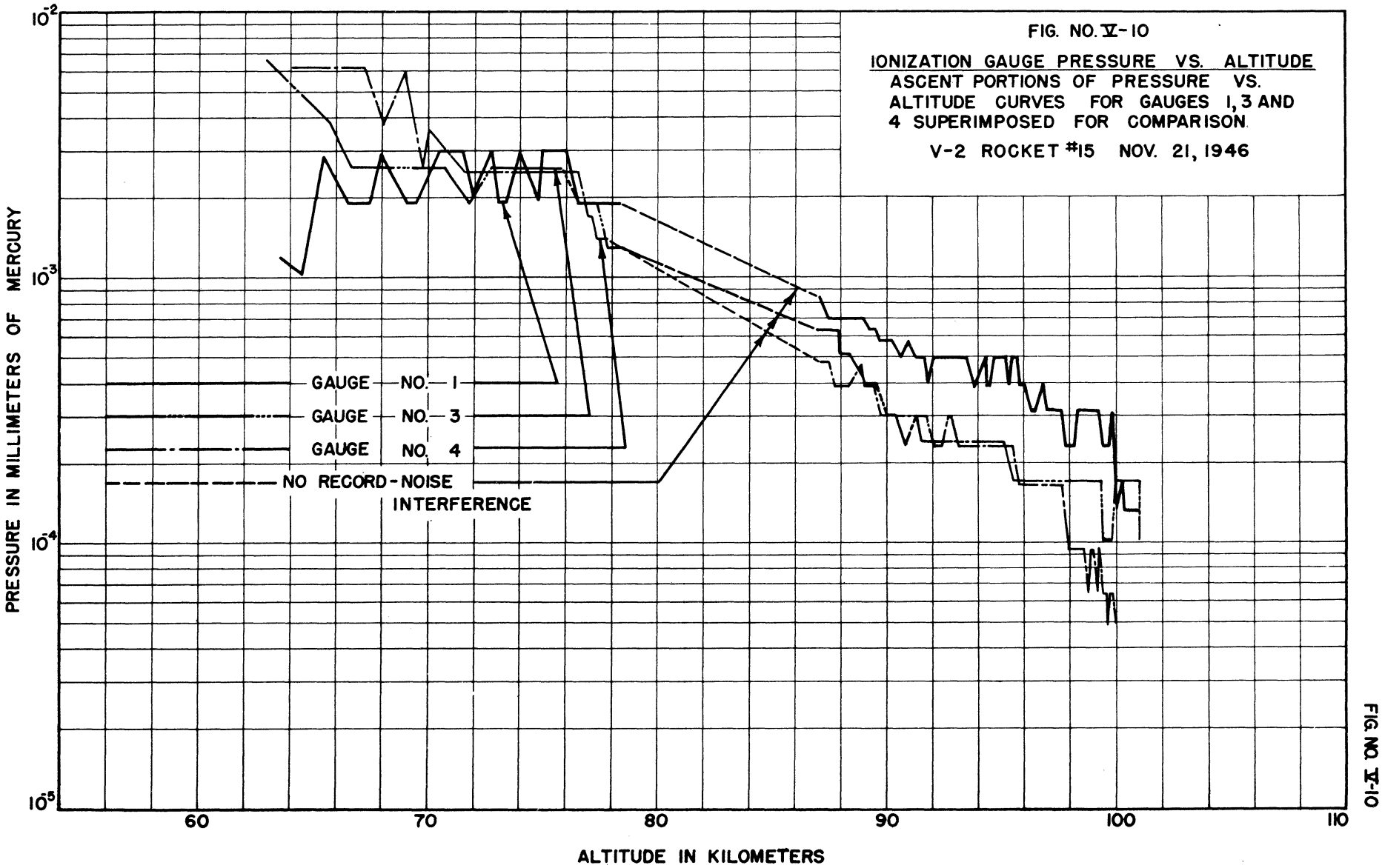
FIG. NO. V-10
IONIZATION GAUGE PRESSURE VS. ALTITUDE
ASCENT PORTIONS OF PRESSURE VS. ALTITUDE CURVES FOR GAUGES 1, 3 AND 4 SUPERIMPOSED FOR COMPARISON.
V-2 ROCKET #15 NOV. 21, 1946
GAUGE NO. 1
GAUGE NO. 3
GAUGE NO. 4
NO RECORD - NOISE INTERFERENCE
PRESSURE IN MILLIMETERS OF MERCURY
10^{-2}
10^{-3}
10^{-4}
10^{-5}
60
70
80
90
100
110
ALTITUDE IN KILOMETERS

FIG. NO. V-10

FIG. NO. V-11

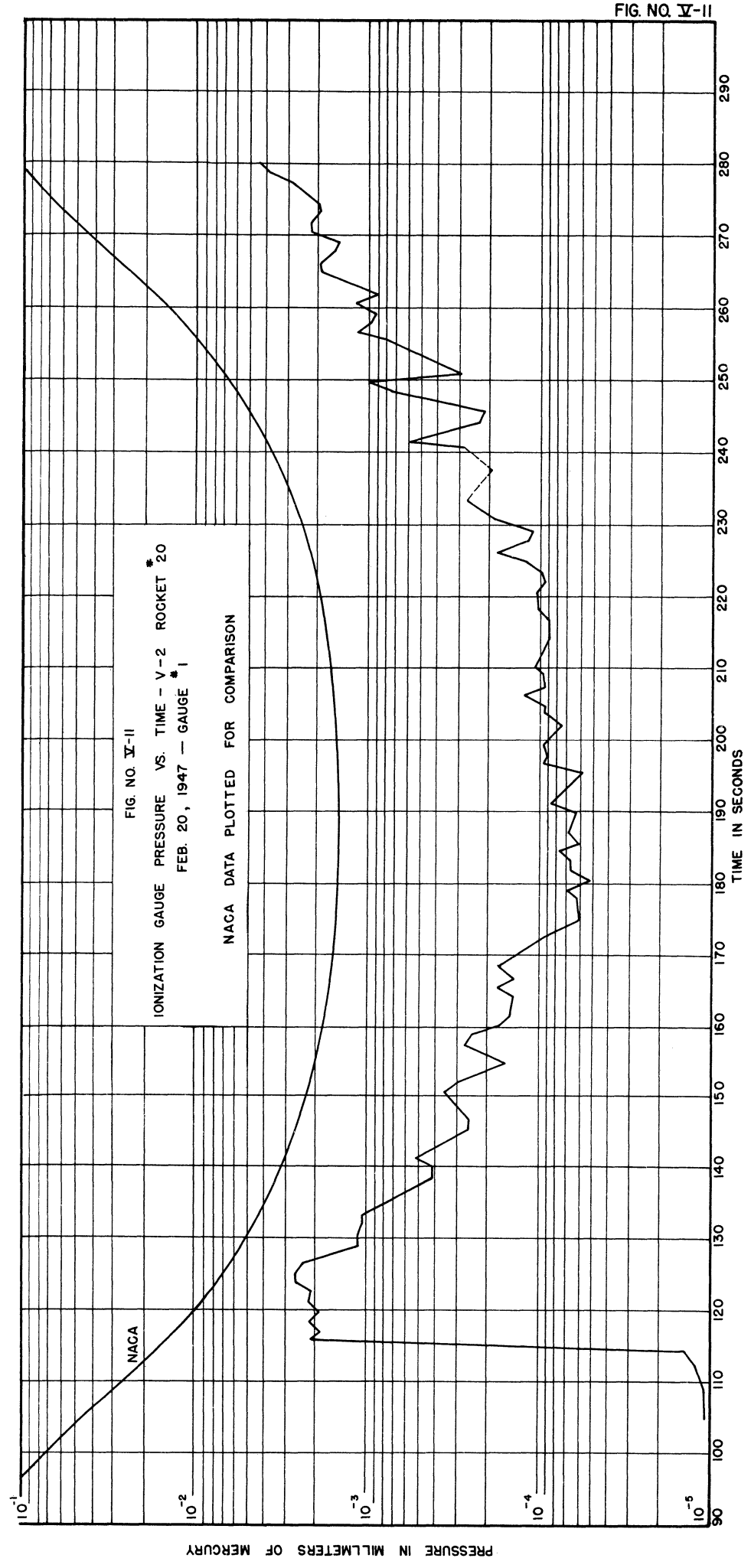
FIG. NO. V-11
IONIZATION GAUGE PRESSURE VS. TIME - V-2 ROCKET #20
FEB. 20, 1947 — GAUGE #1
NACA DATA PLOTTED FOR COMPARISON
NACA
PRESSURE IN MILLIMETERS OF MERCURY
10^{-1}
10^{-2}
10^{-3}
10^{-4}
10^{-5}
90
100
110
120
130
140
150
160
170
180
190
200
210
220
230
240
250
260
270
280
290
TIME IN SECONDS

FIG. NO. V-12

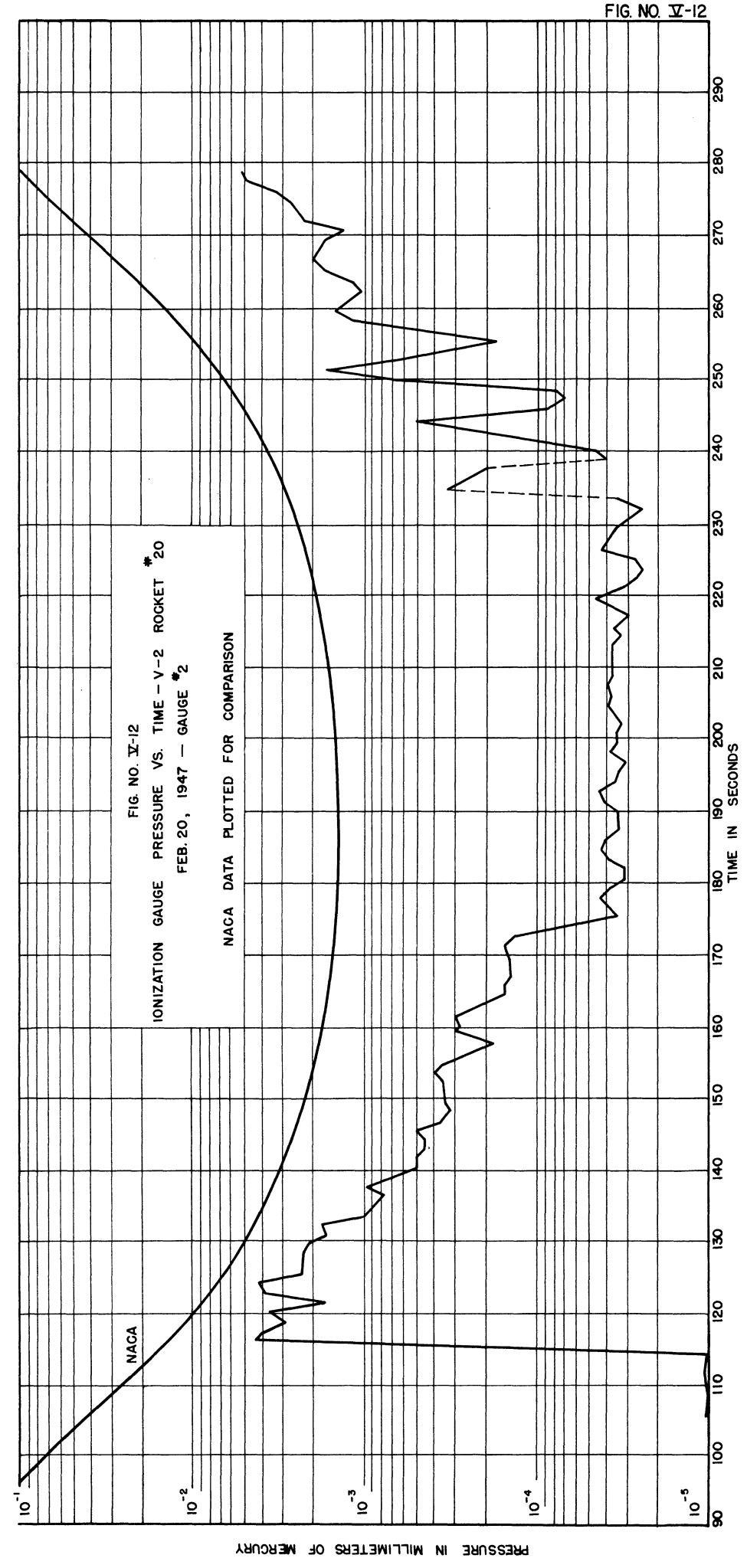
FIG. NO. V-12
IONIZATION GAUGE PRESSURE VS. TIME - V-2 ROCKET #20
FEB. 20, 1947 — GAUGE #2
NACA DATA PLOTTED FOR COMPARISON
NACA
PRESSURE IN MILLIMETERS OF MERCURY
10^{-1}
10^{-2}
10^{-3}
10^{-4}
10^{-5}
90
100
110
120
130
140
150
160
170
180
190
200
210
220
230
240
250
260
270
280
290
TIME IN SECONDS

FIG. NO. V-13

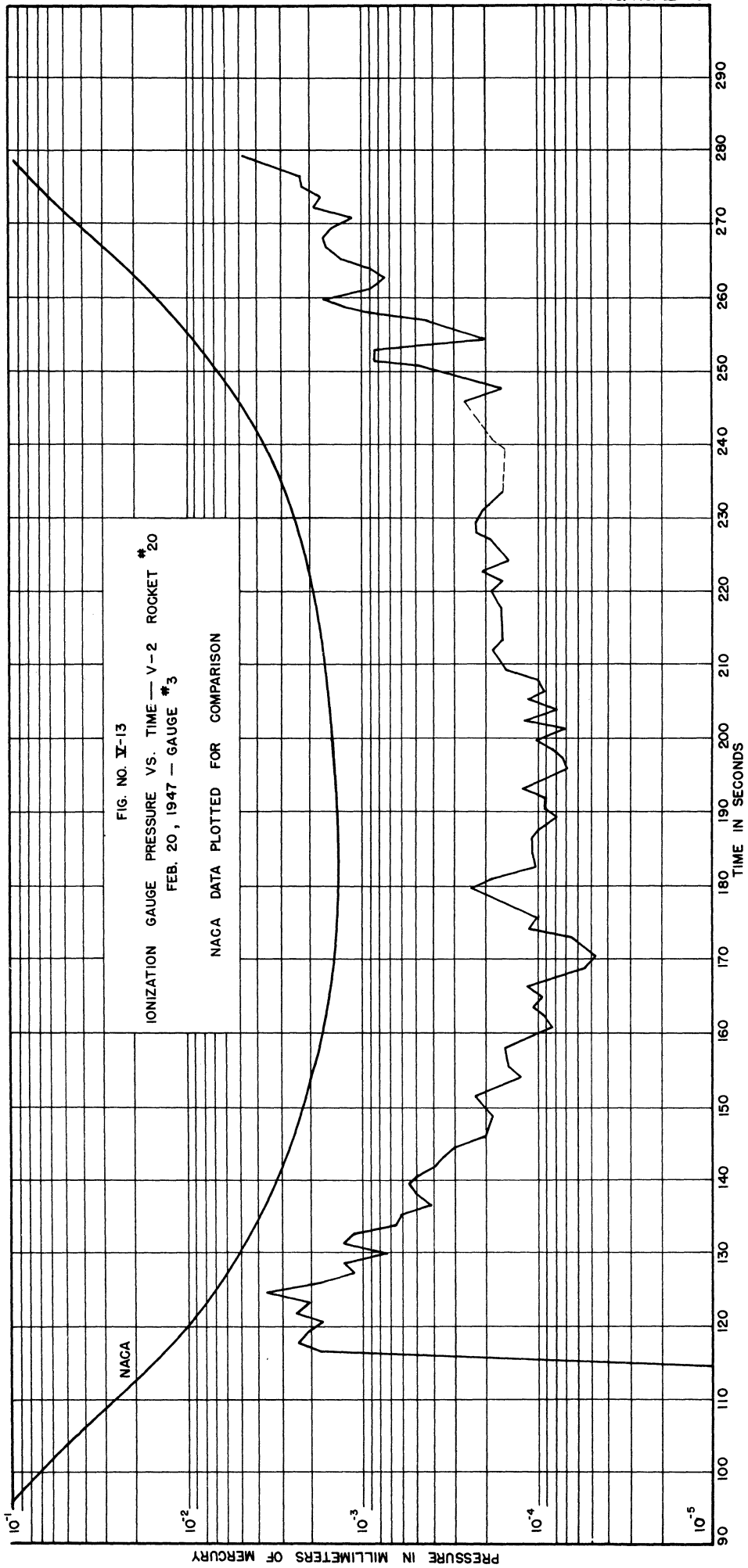
FIG. NO. V-13
IONIZATION GAUGE PRESSURE VS. TIME — V-2 ROCKET #20
FEB. 20, 1947 — GAUGE #3
NACA DATA PLOTTED FOR COMPARISON
NACA
PRESSURE IN MILLIMETERS OF MERCURY
10^{-1}
10^{-2}
10^{-3}
10^{-4}
10^{-5}
TIME IN SECONDS
90
100
110
120
130
140
150
160
170
180
190
200
210
220
230
240
250
260
270
280
290

FIG. NO. V-14

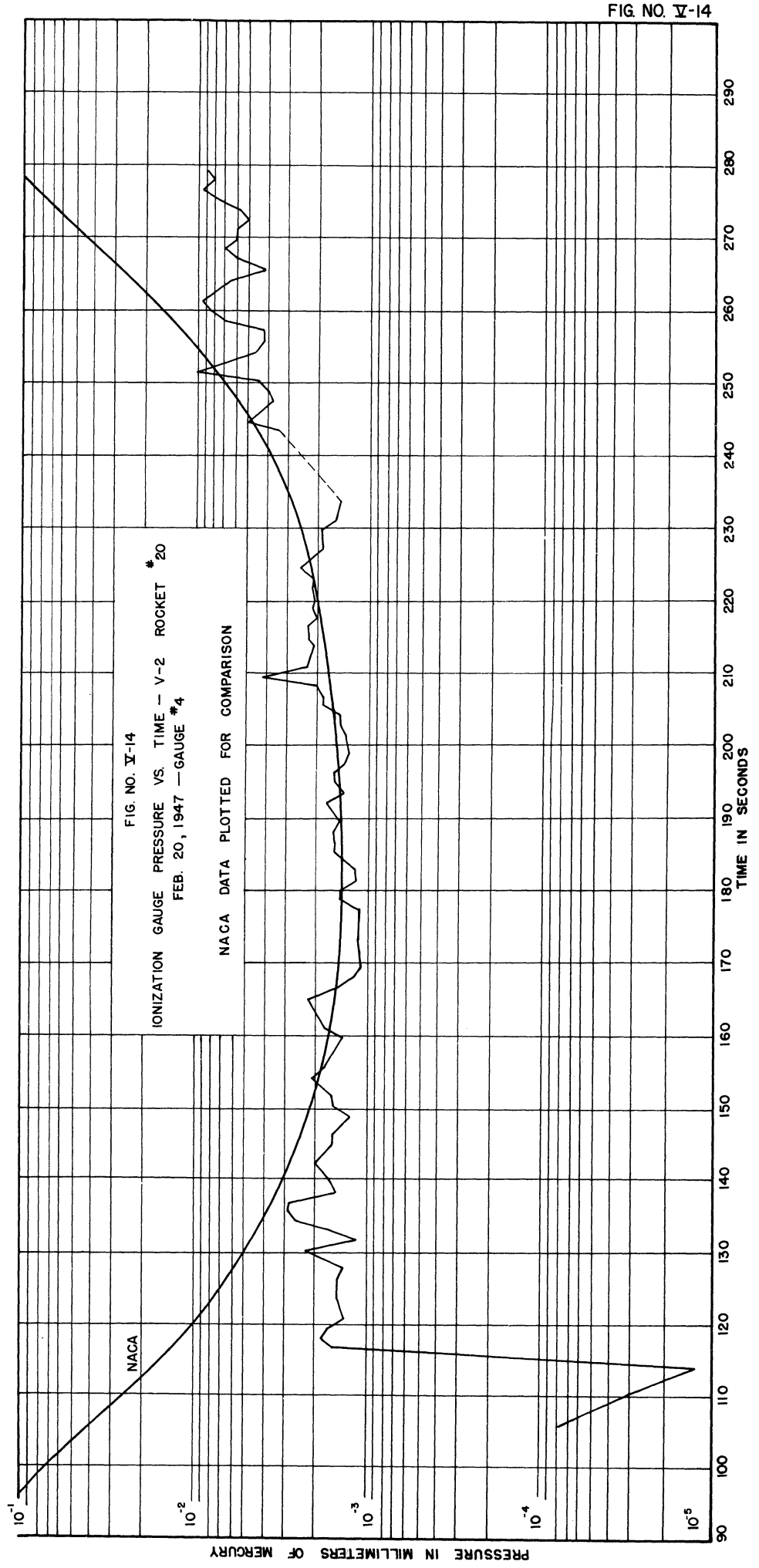
FIG. NO. V-14
IONIZATION GAUGE PRESSURE VS. TIME — V-2 ROCKET #20
FEB. 20, 1947 — GAUGE #4
NACA DATA PLOTTED FOR COMPARISON
NACA
PRESSURE IN MILLIMETERS OF MERCURY
TIME IN SECONDS
10^{-1}
10^{-2}
10^{-3}
10^{-4}
10^{-5}
90
100
110
120
130
140
150
160
170
180
190
200
210
220
230
240
250
260
270
280
290

FIG. NO. V-15

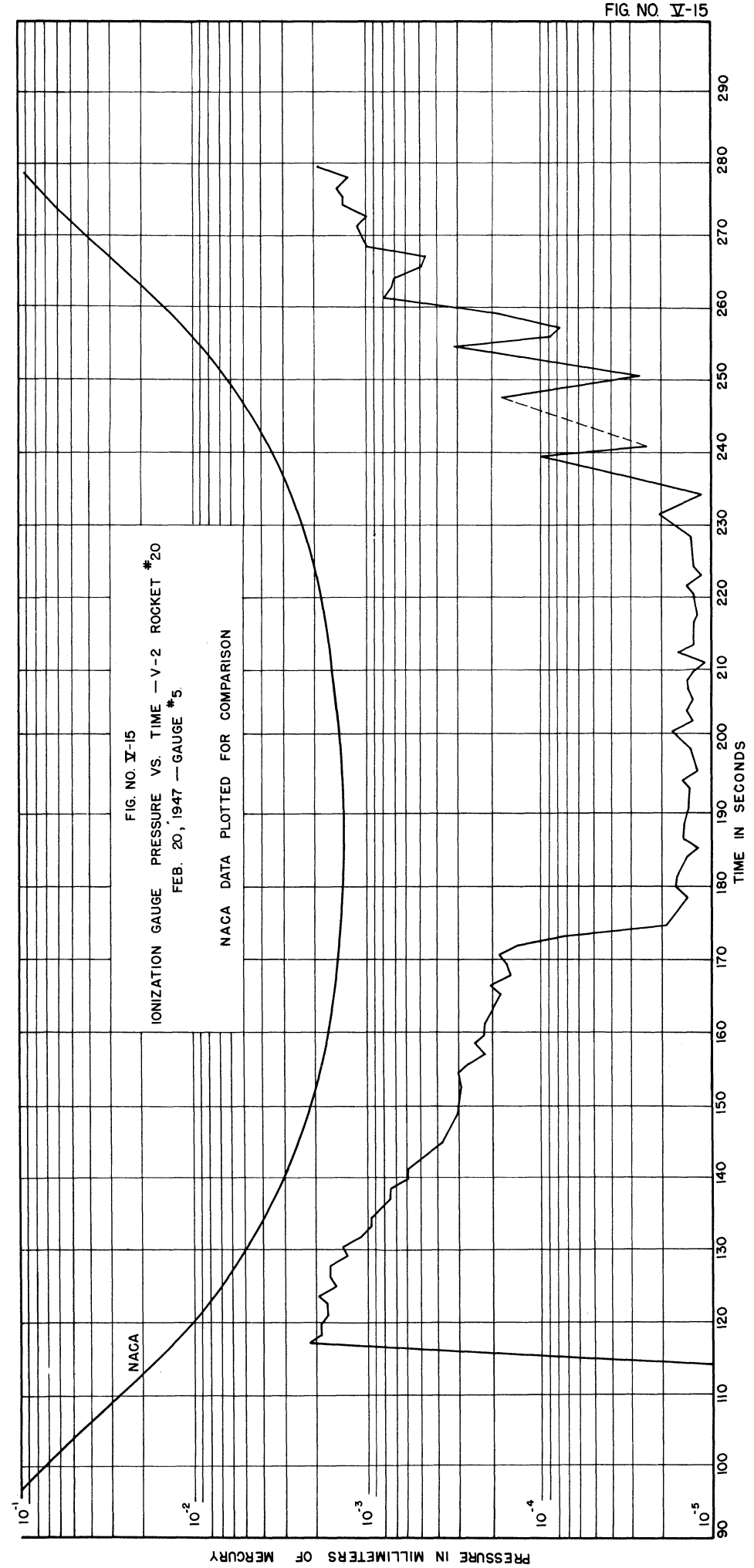
FIG. NO. V-15
IONIZATION GAUGE PRESSURE VS. TIME — V-2 ROCKET #20
FEB. 20, 1947 — GAUGE #5
NACA DATA PLOTTED FOR COMPARISON
NACA
PRESSURE IN MILLIMETERS OF MERCURY
10^{-1}
10^{-2}
10^{-3}
10^{-4}
10^{-5}
90
100
110
120
130
140
150
160
170
180
190
200
210
220
230
240
250
260
270
280
290
TIME IN SECONDS

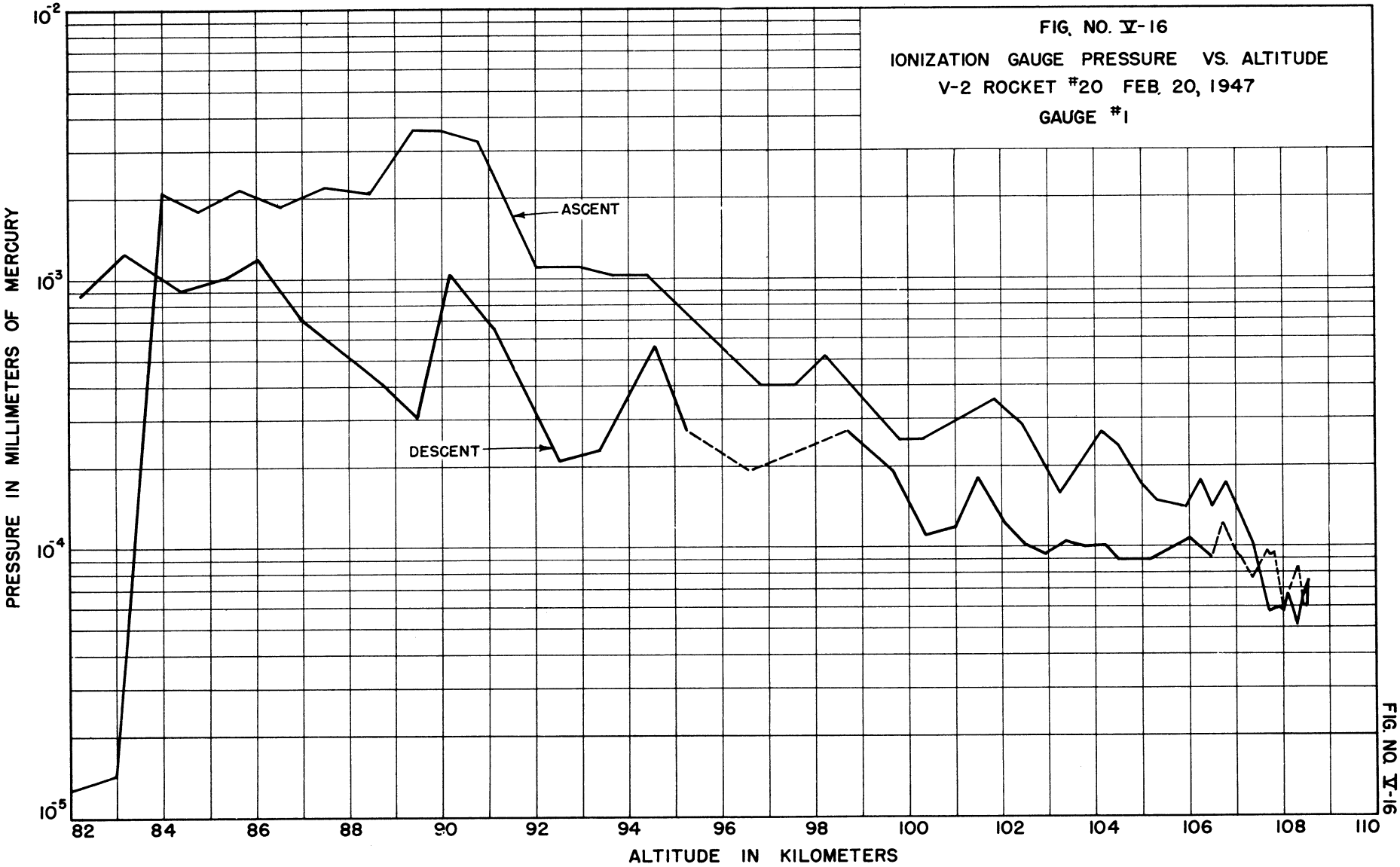
FIG. NO. V-16
IONIZATION GAUGE PRESSURE VS. ALTITUDE
V-2 ROCKET #20 FEB. 20, 1947
GAUGE #1
ASCENT
DESCENT
PRESSURE IN MILLIMETERS OF MERCURY
10^{-2}
10^{-3}
10^{-4}
10^{-5}
82
84
86
88
90
92
94
96
98
100
102
104
106
108
110
ALTITUDE IN KILOMETERS
FIG. NO. V-16

FIG. NO. V-17

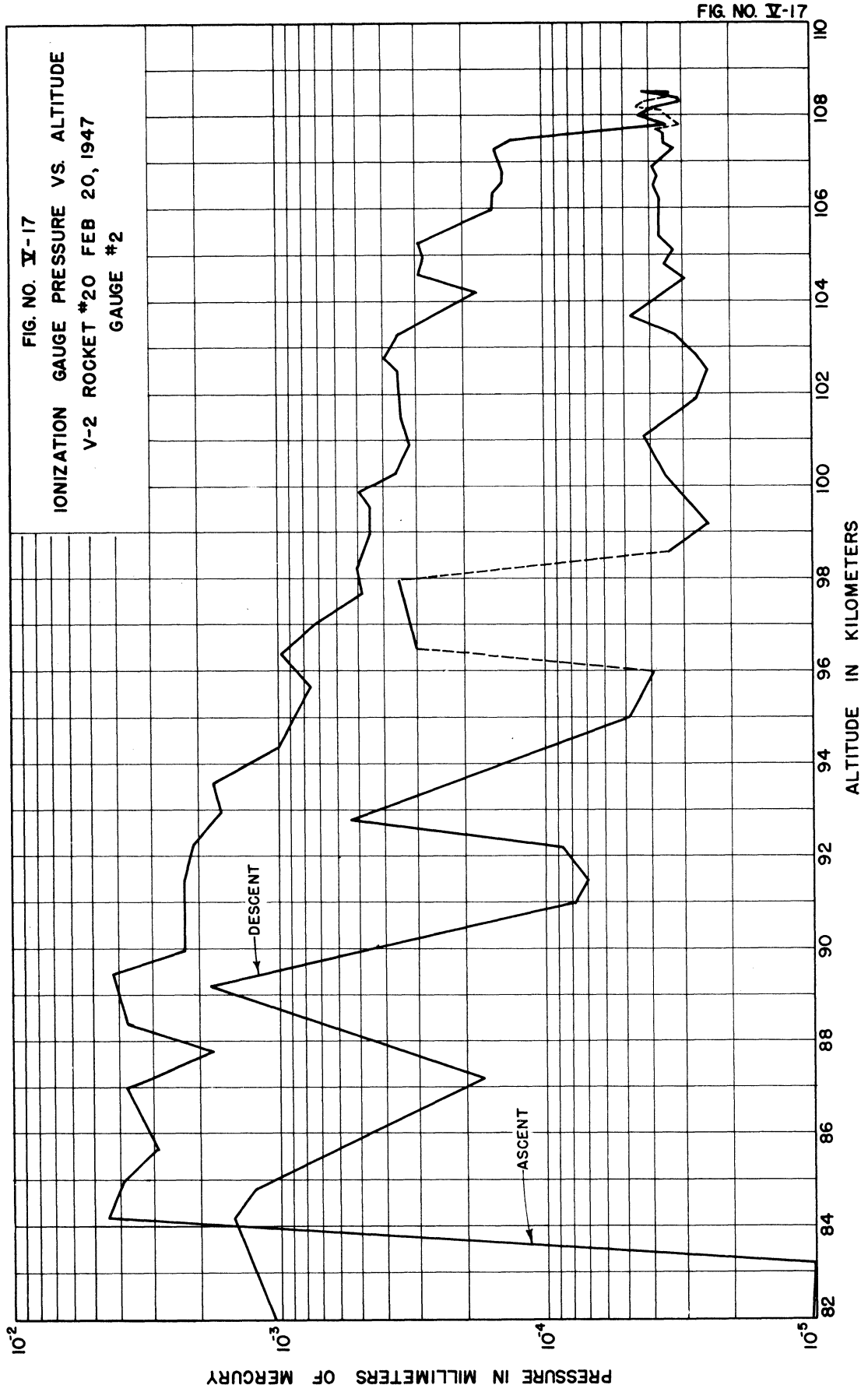
FIG. NO. V-17
IONIZATION GAUGE PRESSURE VS. ALTITUDE
V-2 ROCKET #20 FEB 20, 1947
GAUGE #2
DESCENT
ASCENT
PRESSURE IN MILLIMETERS OF MERCURY
10^{-2}
10^{-3}
10^{-4}
10^{-5}
82
84
86
88
90
92
94
96
98
100
102
104
106
108
110
ALTITUDE IN KILOMETERS

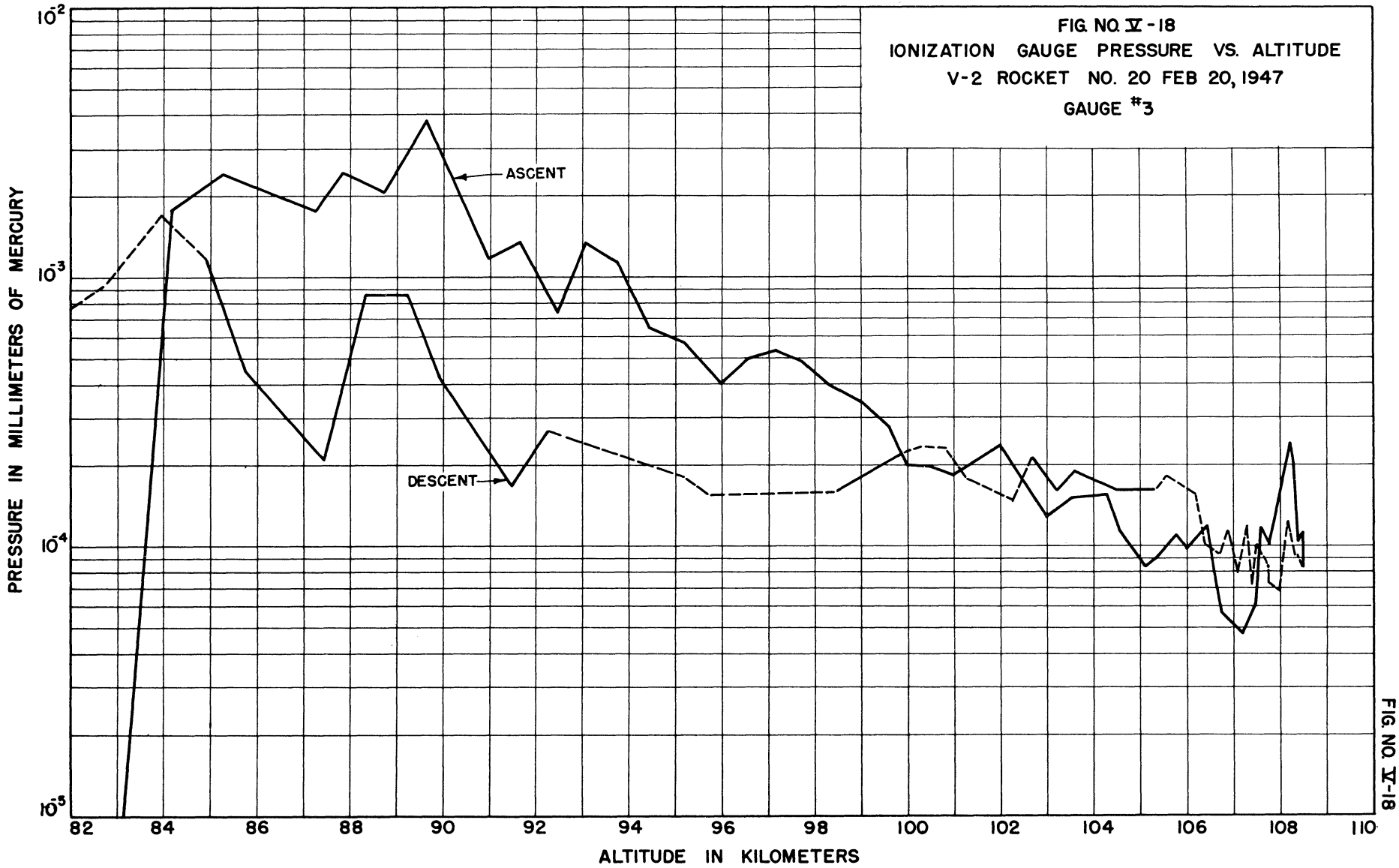
FIG. NO. V-18
IONIZATION GAUGE PRESSURE VS. ALTITUDE
V-2 ROCKET NO. 20 FEB 20, 1947
GAUGE #3
ASCENT
DESCENT
PRESSURE IN MILLIMETERS OF MERCURY
10^{-2}
10^{-3}
10^{-4}
10^{-5}
82
84
86
88
90
92
94
96
98
100
102
104
106
108
110
ALTITUDE IN KILOMETERS

FIG. NO. V-18

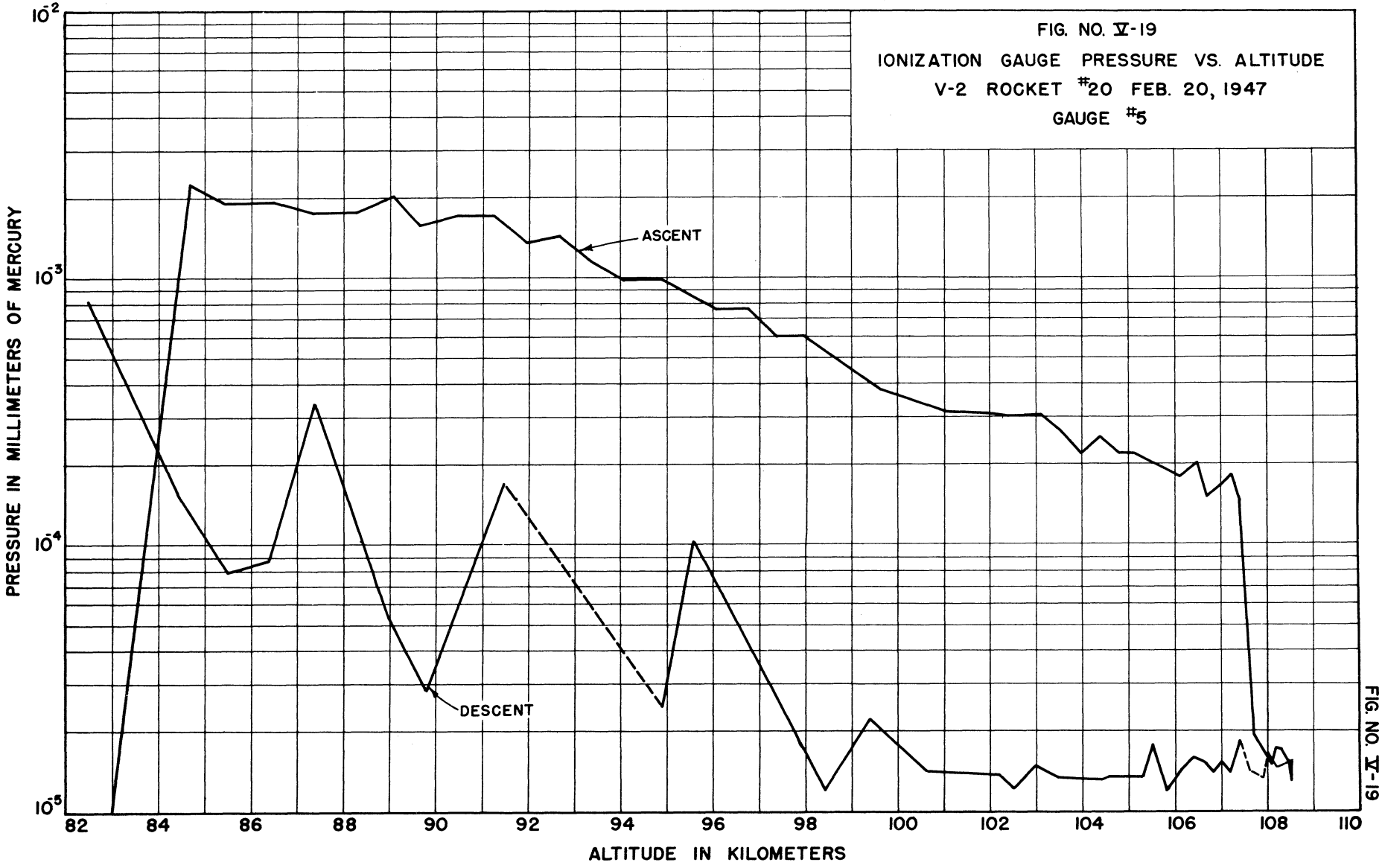
FIG. NO. V-19
IONIZATION GAUGE PRESSURE VS. ALTITUDE
V-2 ROCKET #20 FEB. 20, 1947
GAUGE #5
PRESSURE IN MILLIMETERS OF MERCURY
10^{-2}
10^{-3}
10^{-4}
10^{-5}
ASCENT
DESCENT
82
84
86
88
90
92
94
96
98
100
102
104
106
108
110
ALTITUDE IN KILOMETERS

FIG. NO. V-19

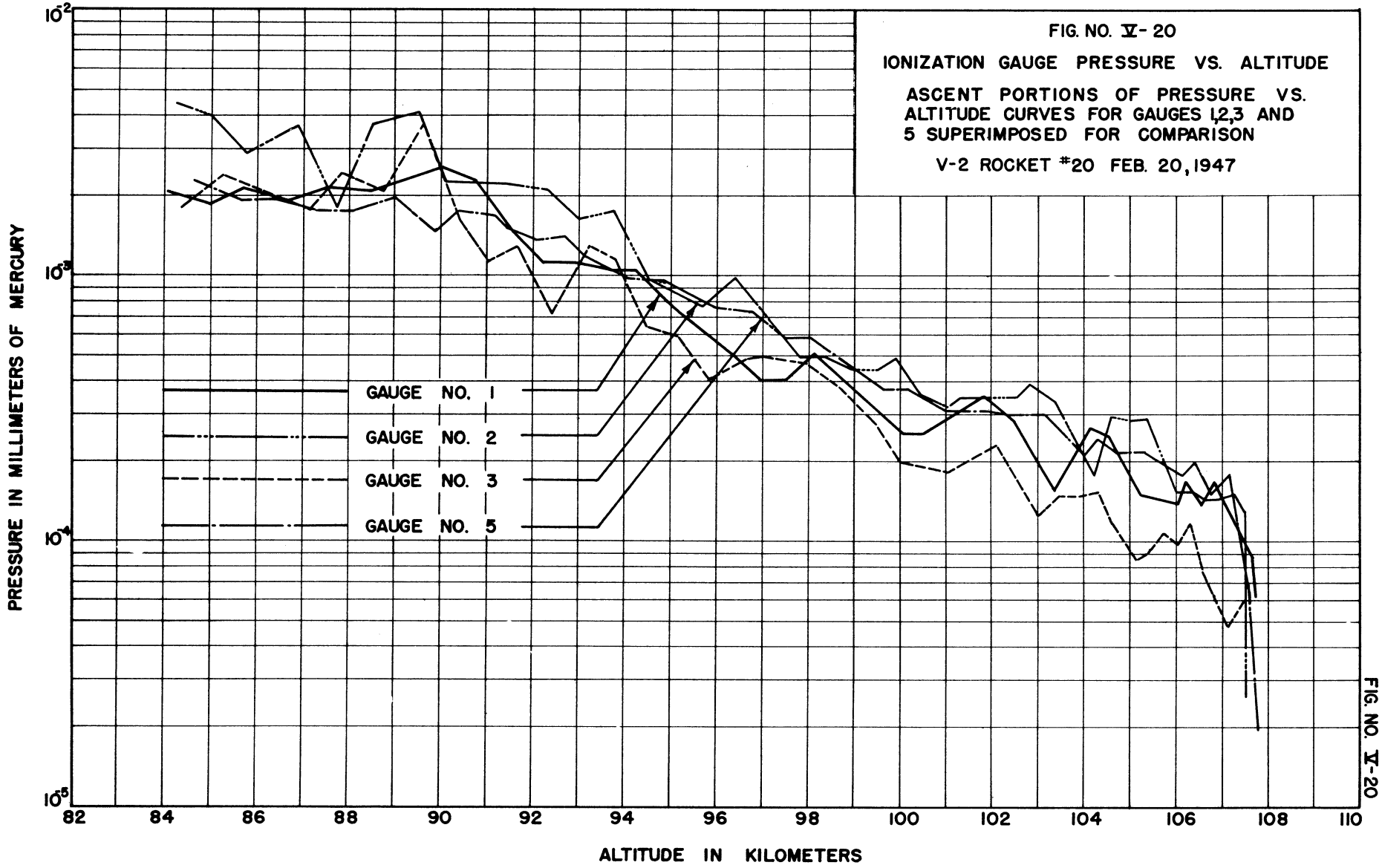
FIG. NO. V-20
IONIZATION GAUGE PRESSURE VS. ALTITUDE
ASCENT PORTIONS OF PRESSURE VS. ALTITUDE CURVES FOR GAUGES 1,2,3 AND 5 SUPERIMPOSED FOR COMPARISON
V-2 ROCKET #20 FEB. 20, 1947
GAUGE NO. 1
GAUGE NO. 2
GAUGE NO. 3
GAUGE NO. 5
PRESSURE IN MILLIMETERS OF MERCURY
10^{-2}
10^{-3}
10^{-4}
10^{-5}
82
84
86
88
90
92
94
96
98
100
102
104
106
108
110
ALTITUDE IN KILOMETERS
FIG. NO. V-20

FIG. NO. V-21

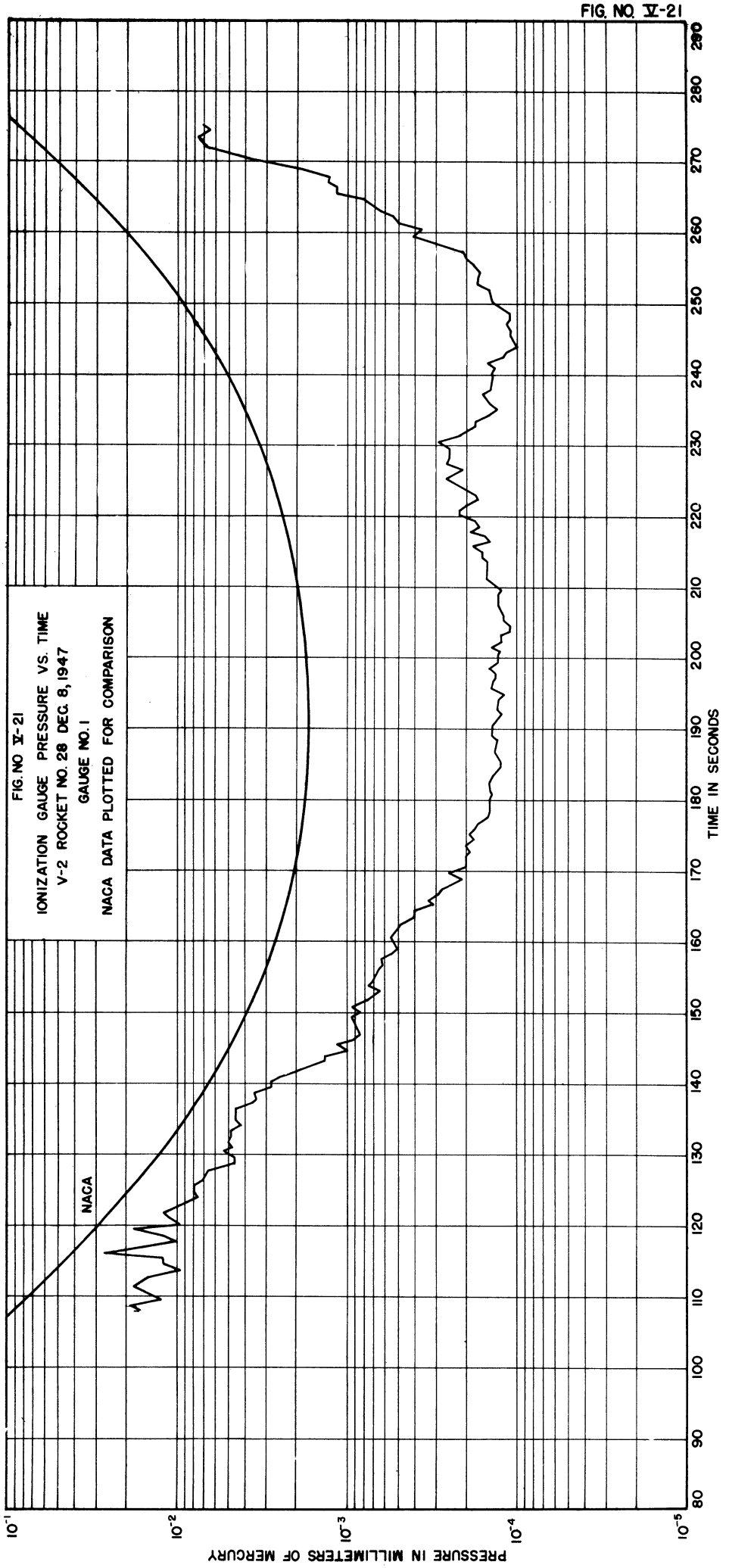
FIG. NO V-21
IONIZATION GAUGE PRESSURE VS. TIME
V-2 ROCKET NO. 28 DEC. 8, 1947
GAUGE NO. 1
NACA DATA PLOTTED FOR COMPARISON
NACA
PRESSURE IN MILLIMETERS OF MERCURY
10^{-1}
10^{-2}
10^{-3}
10^{-4}
10^{-5}
TIME IN SECONDS
80
90
100
110
120
130
140
150
160
170
180
190
200
210
220
230
240
250
260
270
280
290

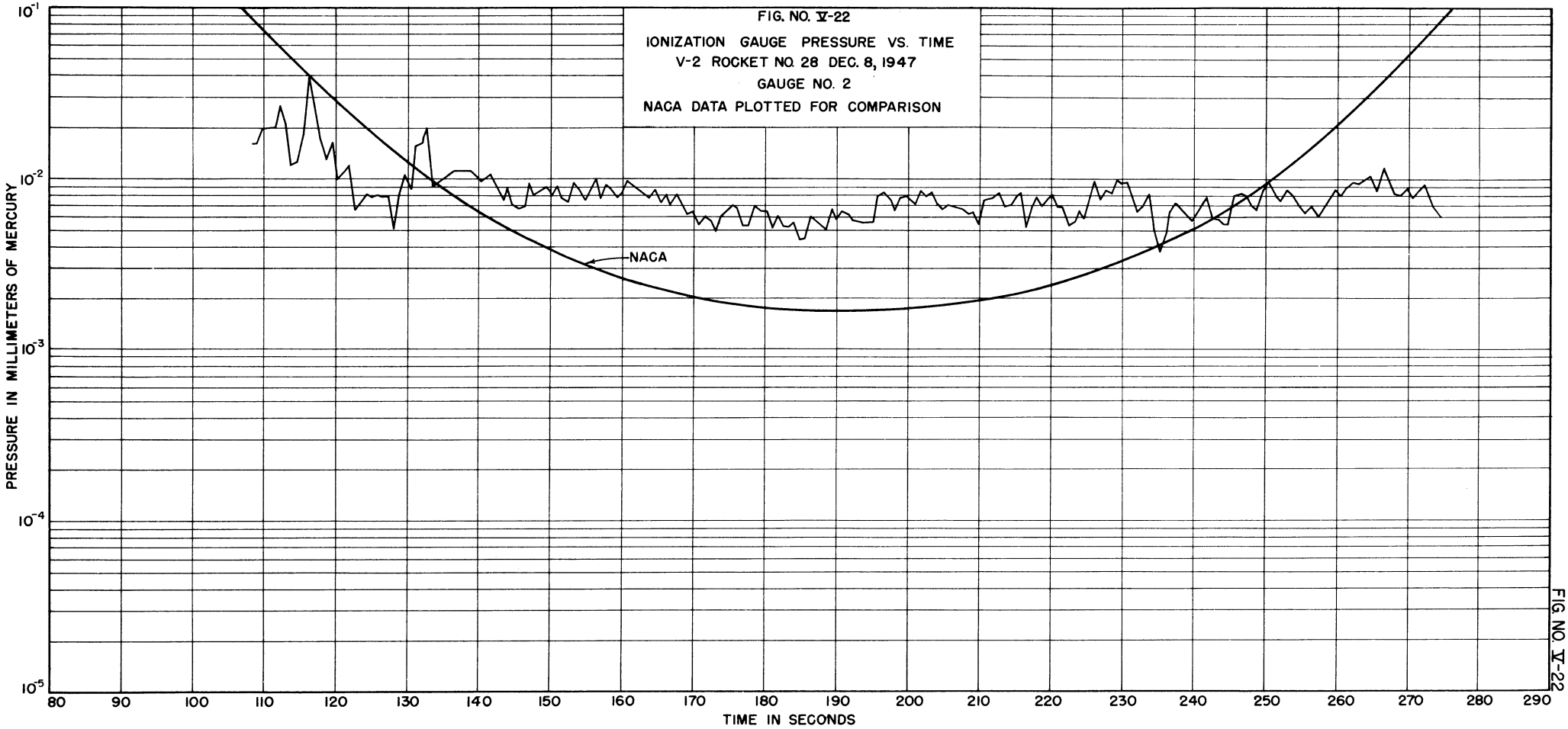
FIG. NO. V-22
IONIZATION GAUGE PRESSURE VS. TIME
V-2 ROCKET NO. 28 DEC. 8, 1947
GAUGE NO. 2
NACA DATA PLOTTED FOR COMPARISON
NACA
PRESSURE IN MILLIMETERS OF MERCURY
10^{-1}
10^{-2}
10^{-3}
10^{-4}
10^{-5}
80 90 100 110 120 130 140 150 160 170 180 190 200 210 220 230 240 250 260 270 280 290
TIME IN SECONDS

FIG. NO. V-22

FIG. NO. V-23

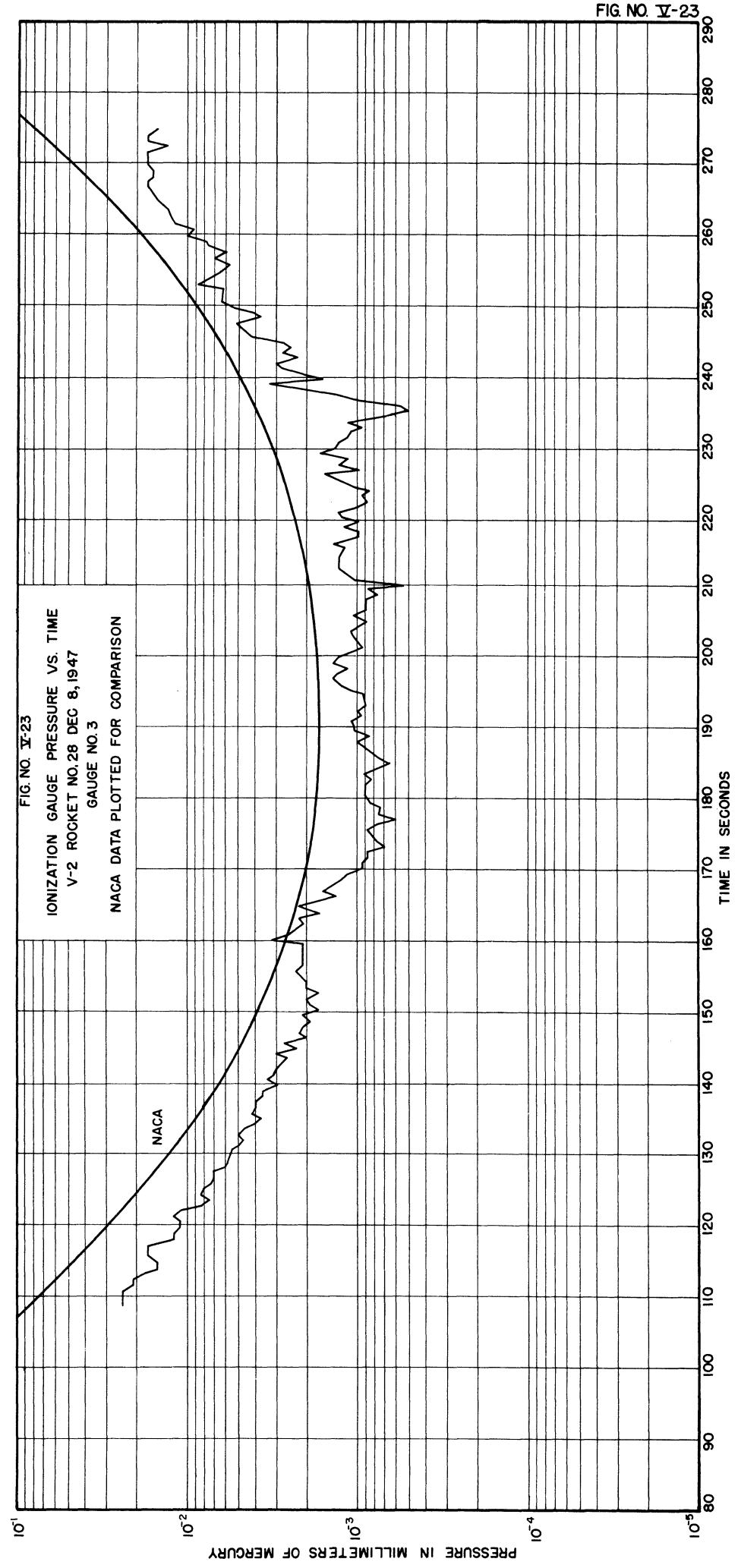
FIG. NO. V-23
IONIZATION GAUGE PRESSURE VS. TIME
V-2 ROCKET NO. 28 DEC 8, 1947
GAUGE NO. 3
NACA DATA PLOTTED FOR COMPARISON
NACA
PRESSURE IN MILLIMETERS OF MERCURY
10^{-1}
10^{-2}
10^{-3}
10^{-4}
10^{-5}
TIME IN SECONDS
80
90
100
110
120
130
140
150
160
170
180
190
200
210
220
230
240
250
260
270
280
290

FIG. NO. V-24

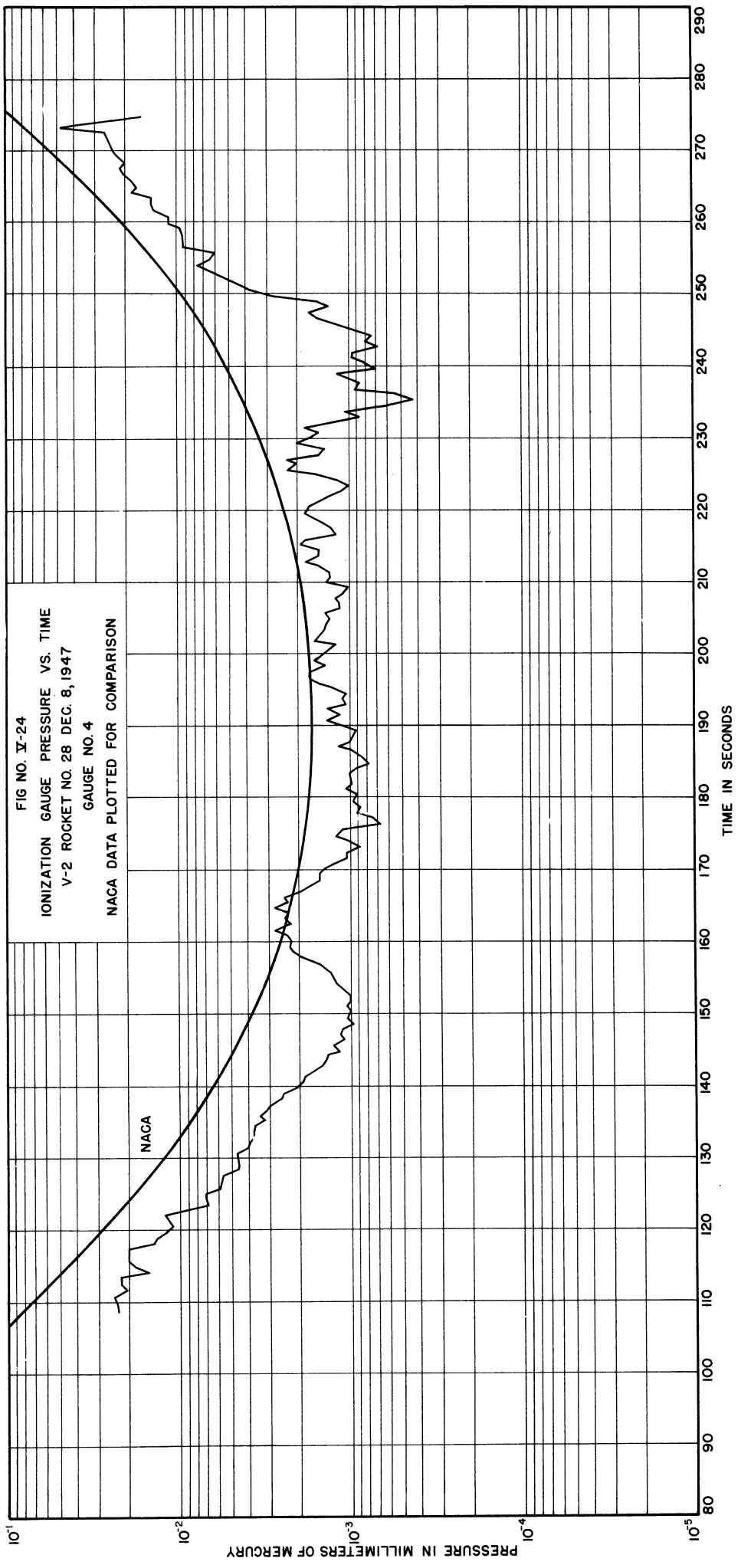
FIG NO. V-24
IONIZATION GAUGE PRESSURE VS. TIME
V-2 ROCKET NO. 28 DEC. 8, 1947
GAUGE NO. 4
NACA DATA PLOTTED FOR COMPARISON
NACA
PRESSURE IN MILLIMETERS OF MERCURY
10^{-1}
10^{-2}
10^{-3}
10^{-4}
10^{-5}
TIME IN SECONDS
80
90
100
110
120
130
140
150
160
170
180
190
200
210
220
230
240
250
260
270
280
290

FIG. NO. V-25

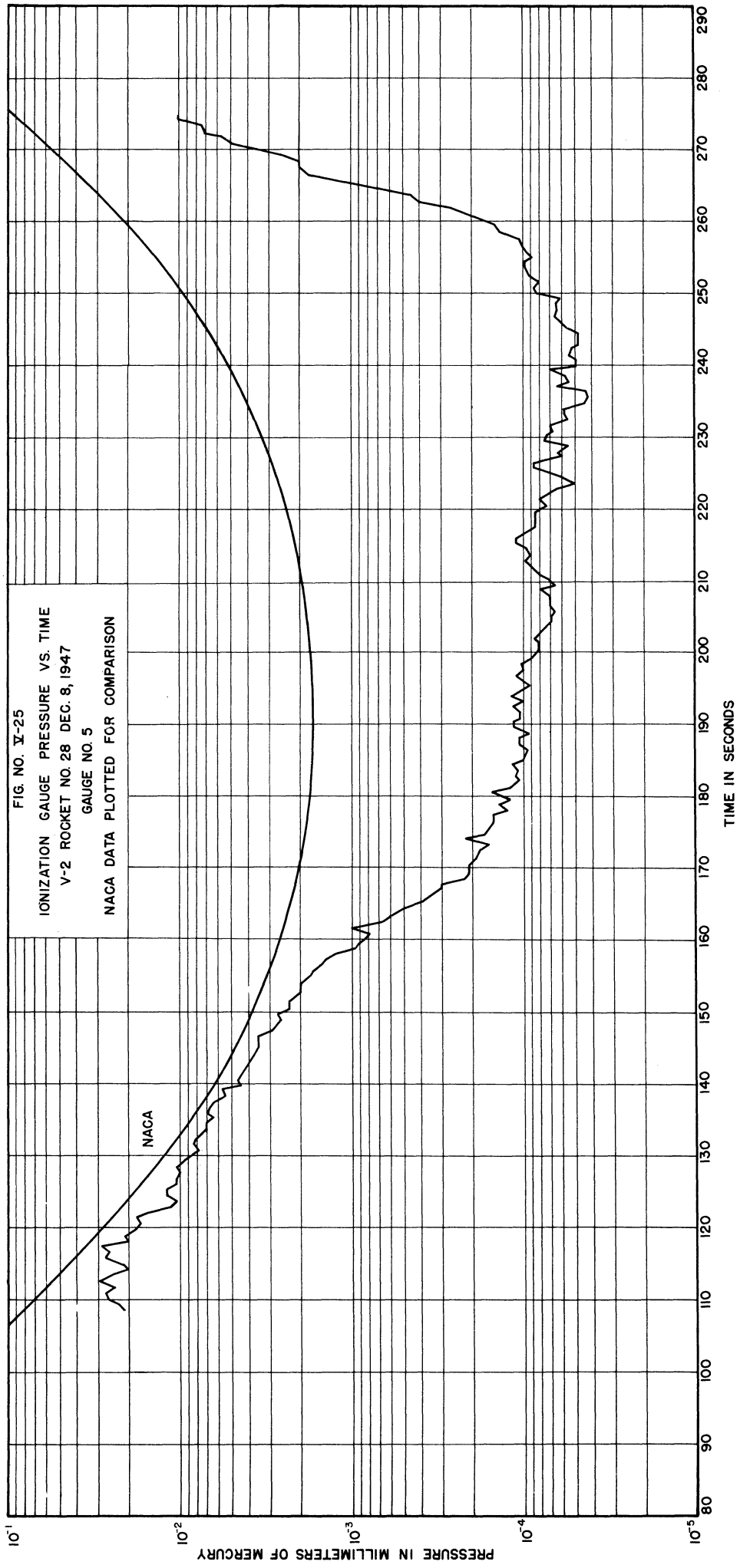
FIG. NO. V-25
IONIZATION GAUGE PRESSURE VS. TIME
V-2 ROCKET NO. 28 DEC. 8, 1947
GAUGE NO. 5
NACA DATA PLOTTED FOR COMPARISON
NACA
PRESSURE IN MILLIMETERS OF MERCURY
10^{-1}
10^{-2}
10^{-3}
10^{-4}
10^{-5}
TIME IN SECONDS
80
90
100
110
120
130
140
150
160
170
180
190
200
210
220
230
240
250
260
270
280
290

FIG. NO. V-26

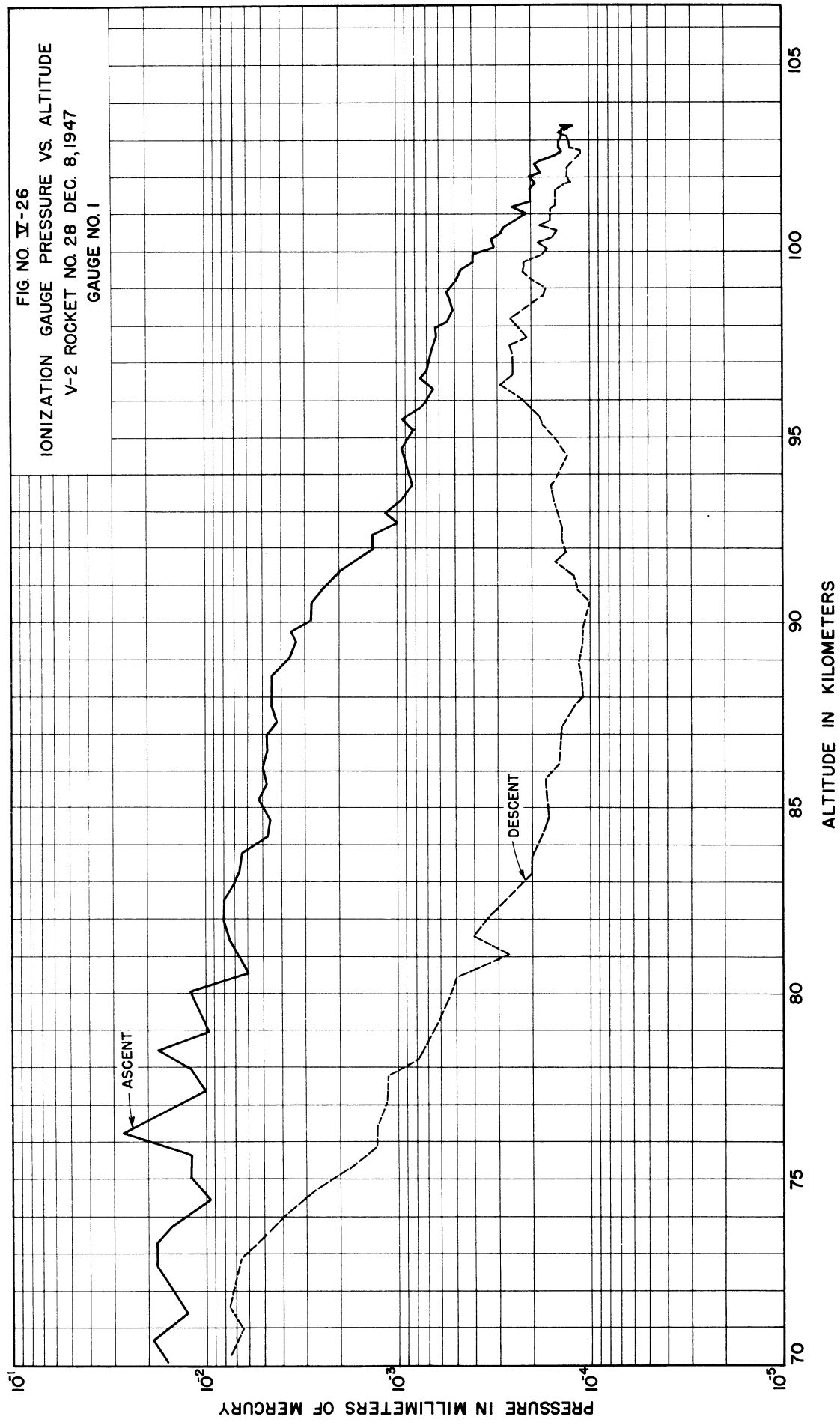
FIG. NO. V-26
IONIZATION GAUGE PRESSURE VS. ALTITUDE
V-2 ROCKET NO. 28 DEC. 8, 1947
GAUGE NO. 1
ASCENT
DESCENT
PRESSURE IN MILLIMETERS OF MERCURY
10^{-1}
10^{-2}
10^{-3}
10^{-4}
10^{-5}
70
75
80
85
90
95
100
105
ALTITUDE IN KILOMETERS

FIG. NO. V-27

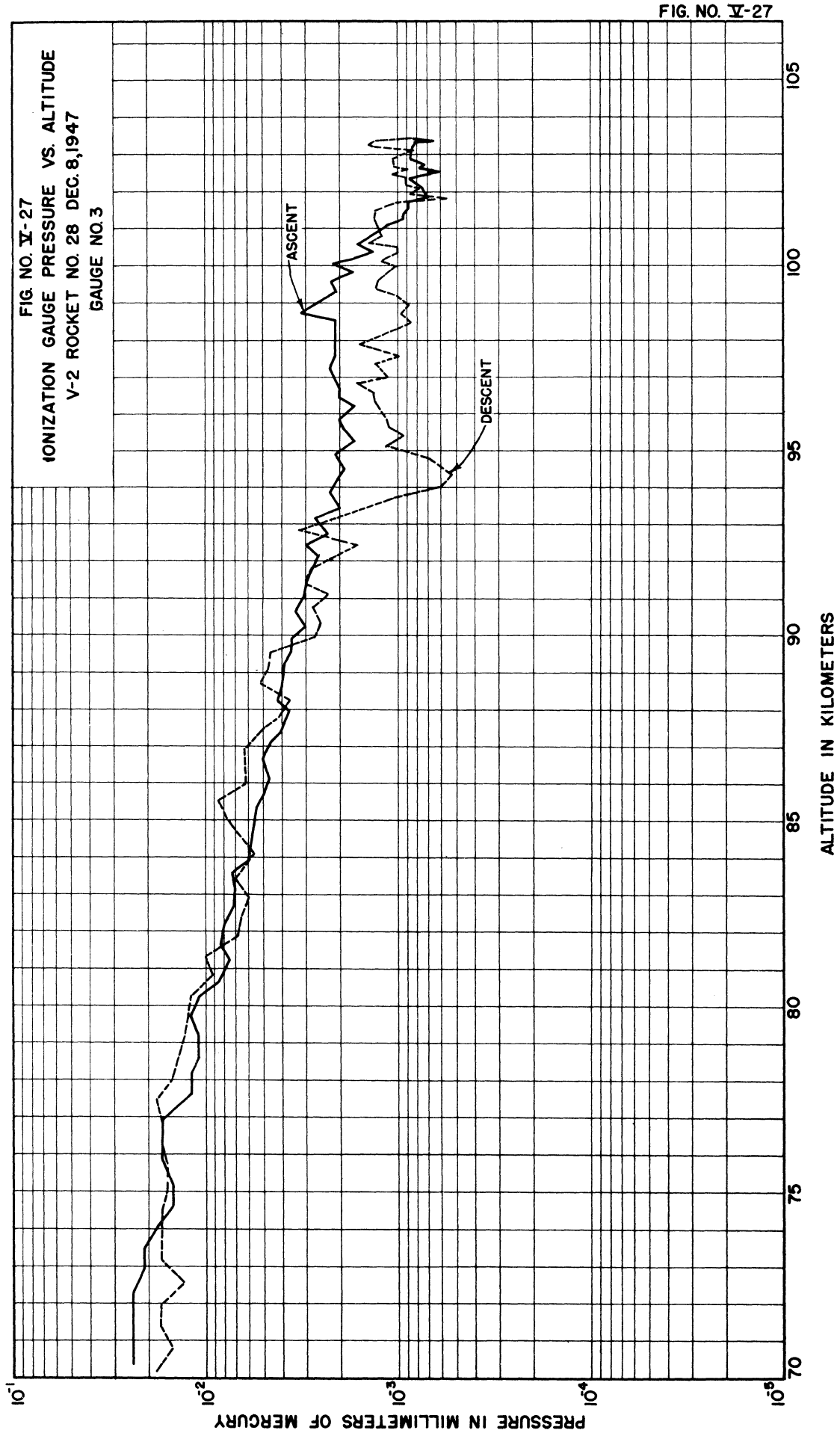
FIG. NO. V-27
IONIZATION GAUGE PRESSURE VS. ALTITUDE
V-2 ROCKET NO. 28 DEC. 8, 1947
GAUGE NO. 3
ASCENT
DESCENT
PRESSURE IN MILLIMETERS OF MERCURY
10^{-1}
10^{-2}
10^{-3}
10^{-4}
10^{-5}
ALTITUDE IN KILOMETERS
70
75
80
85
90
95
100
105

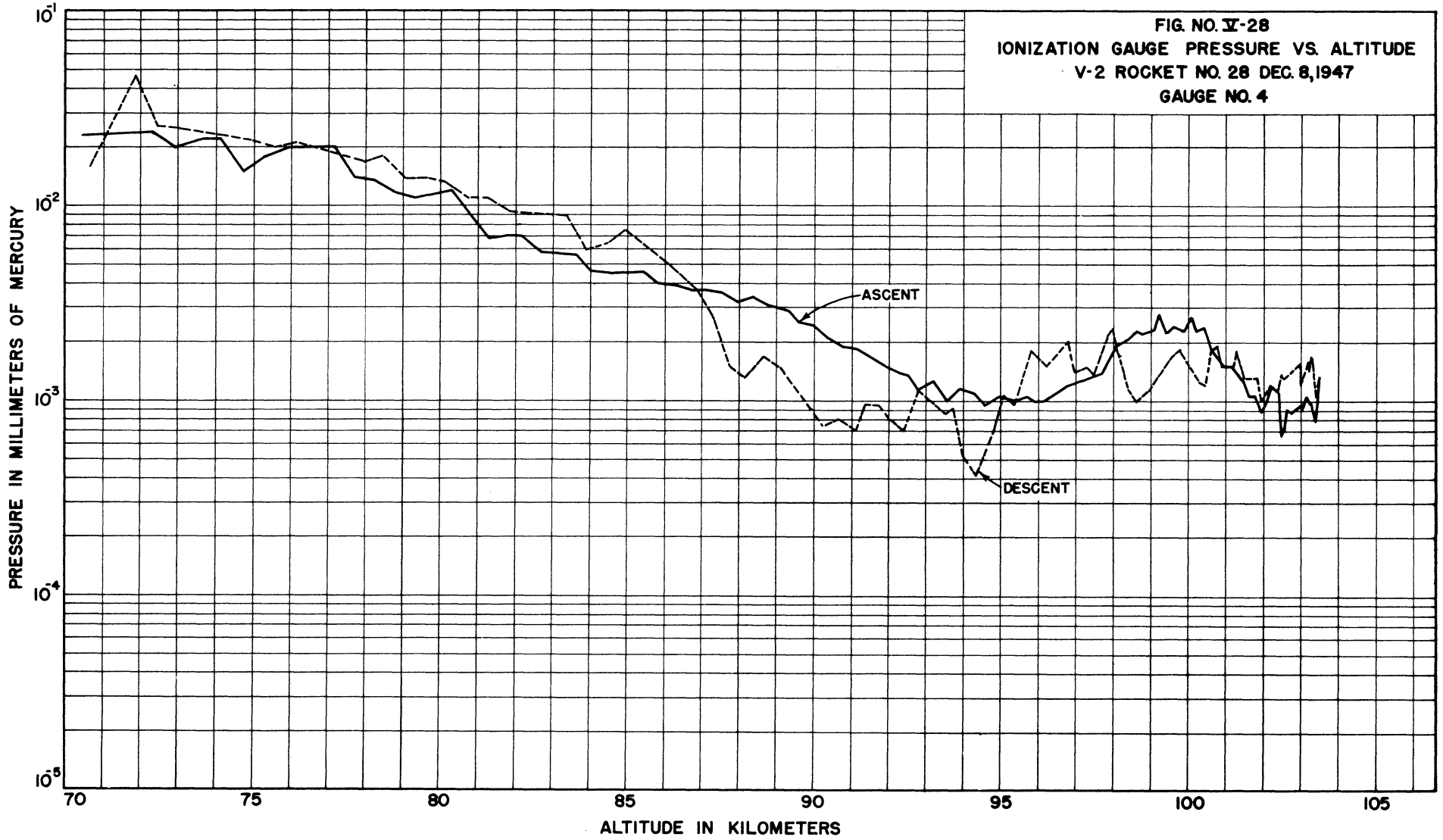
FIG. NO. V-28
IONIZATION GAUGE PRESSURE VS. ALTITUDE
V-2 ROCKET NO. 28 DEC. 8, 1947
GAUGE NO. 4
ASCENT
DESCENT
PRESSURE IN MILLIMETERS OF MERCURY
10^{-1}
10^{-2}
10^{-3}
10^{-4}
10^{-5}
70
75
80
85
90
95
100
105
ALTITUDE IN KILOMETERS

FIG. NO. V-28

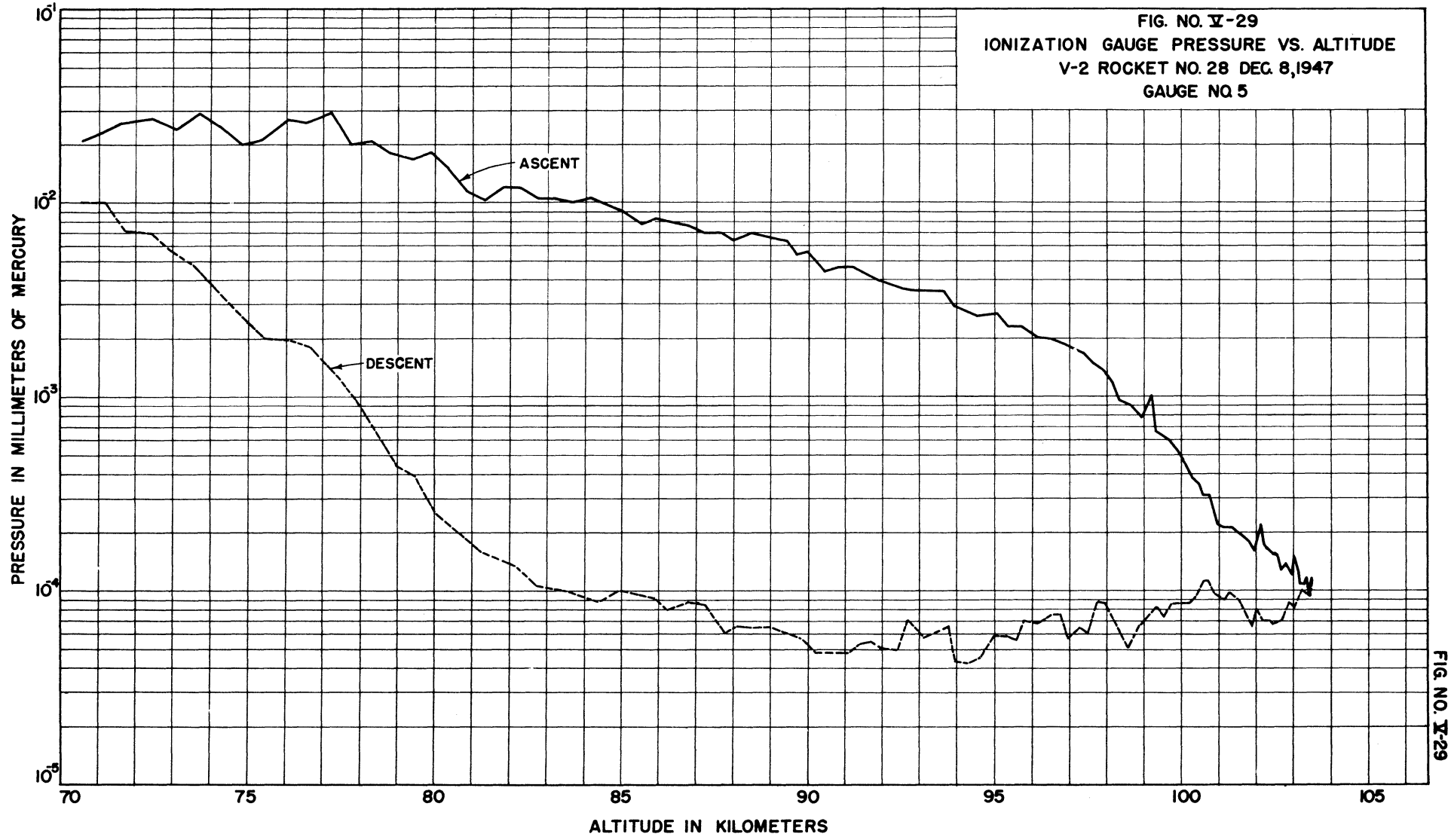
FIG. NO. V-29
IONIZATION GAUGE PRESSURE VS. ALTITUDE
V-2 ROCKET NO. 28 DEC. 8,1947
GAUGE NO. 5
ASCENT
DESCENT
PRESSURE IN MILLIMETERS OF MERCURY
10^{-1}
10^{-2}
10^{-3}
10^{-4}
10^{-5}
70
75
80
85
90
95
100
105
ALTITUDE IN KILOMETERS

FIG. NO. V-29

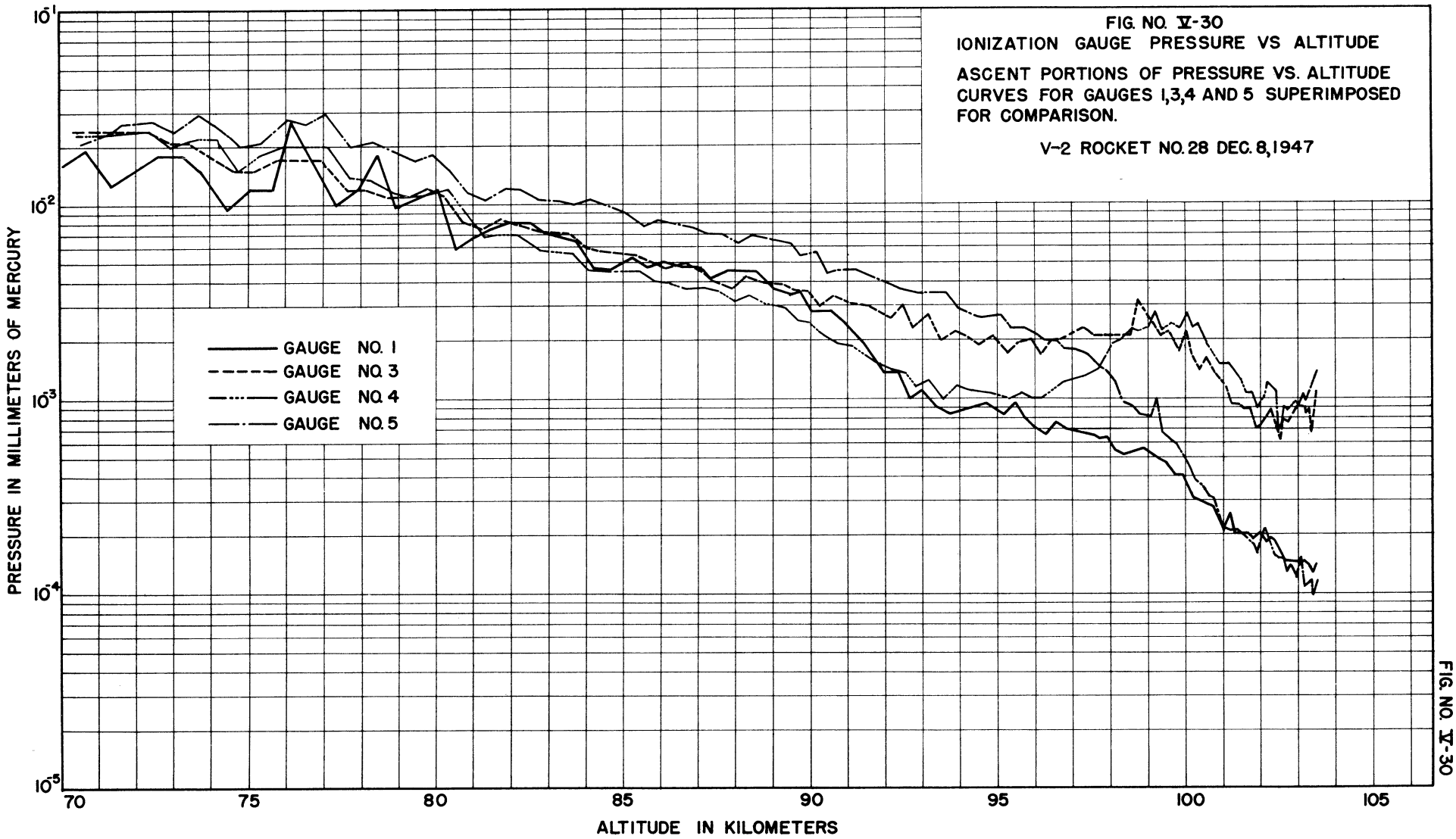
FIG. NO. V-30
IONIZATION GAUGE PRESSURE VS ALTITUDE
ASCENT PORTIONS OF PRESSURE VS. ALTITUDE CURVES FOR GAUGES 1,3,4 AND 5 SUPERIMPOSED FOR COMPARISON.
V-2 ROCKET NO. 28 DEC. 8, 1947
GAUGE NO. 1
GAUGE NO. 3
GAUGE NO. 4
GAUGE NO. 5
PRESSURE IN MILLIMETERS OF MERCURY
10^{-1}
10^{-2}
10^{-3}
10^{-4}
10^{-5}
70
75
80
85
90
95
100
105
ALTITUDE IN KILOMETERS
FIG. NO. V-30

FIG. NO. V-31

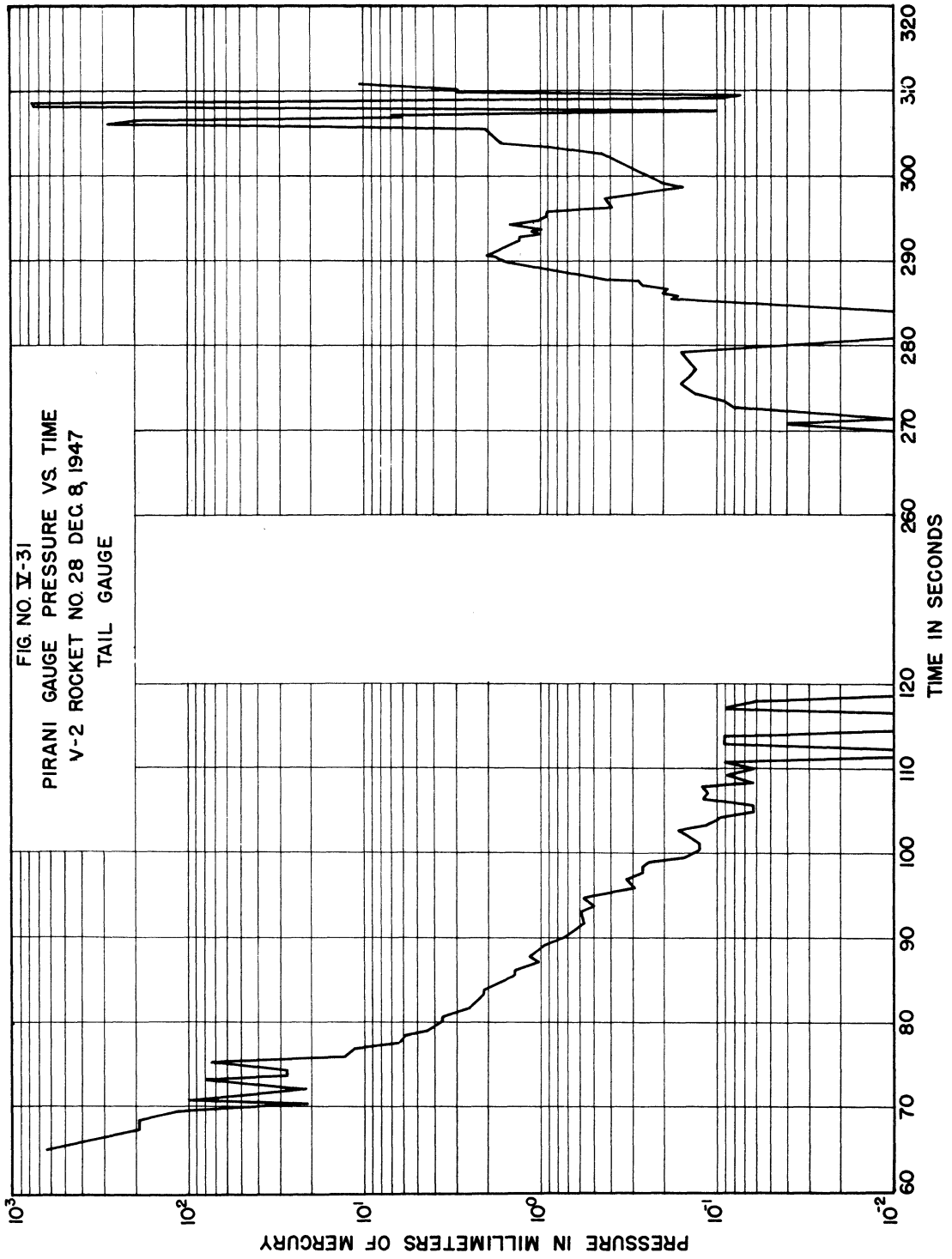
FIG. NO. V-31
PIRANI GAUGE PRESSURE VS. TIME
V-2 ROCKET NO. 28 DEC. 8, 1947
TAIL GAUGE
PRESSURE IN MILLIMETERS OF MERCURY
10^{3}
10^{2}
10^{1}
10^{0}
10^{-1}
10^{-2}
60
70
80
90
100
110
120
260
270
280
290
300
310
320
TIME IN SECONDS

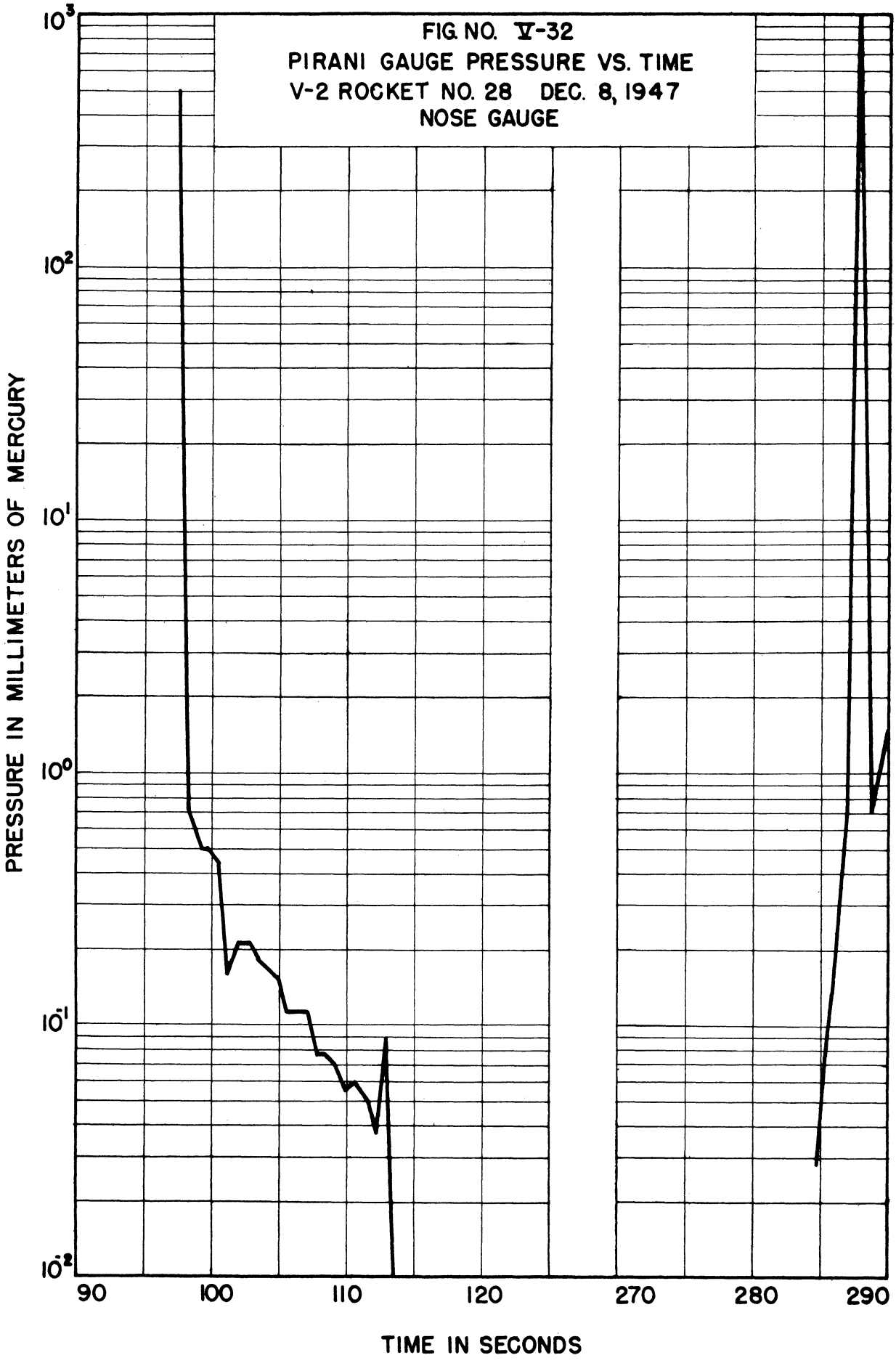
FIG. NO. V-32
PIRANI GAUGE PRESSURE VS. TIME
V-2 ROCKET NO. 28 DEC. 8, 1947
NOSE GAUGE
PRESSURE IN MILLIMETERS OF MERCURY
10^3
10^2
10^1
10^0
10^{-1}
10^{-2}
90
100
110
120
270
280
290
TIME IN SECONDS

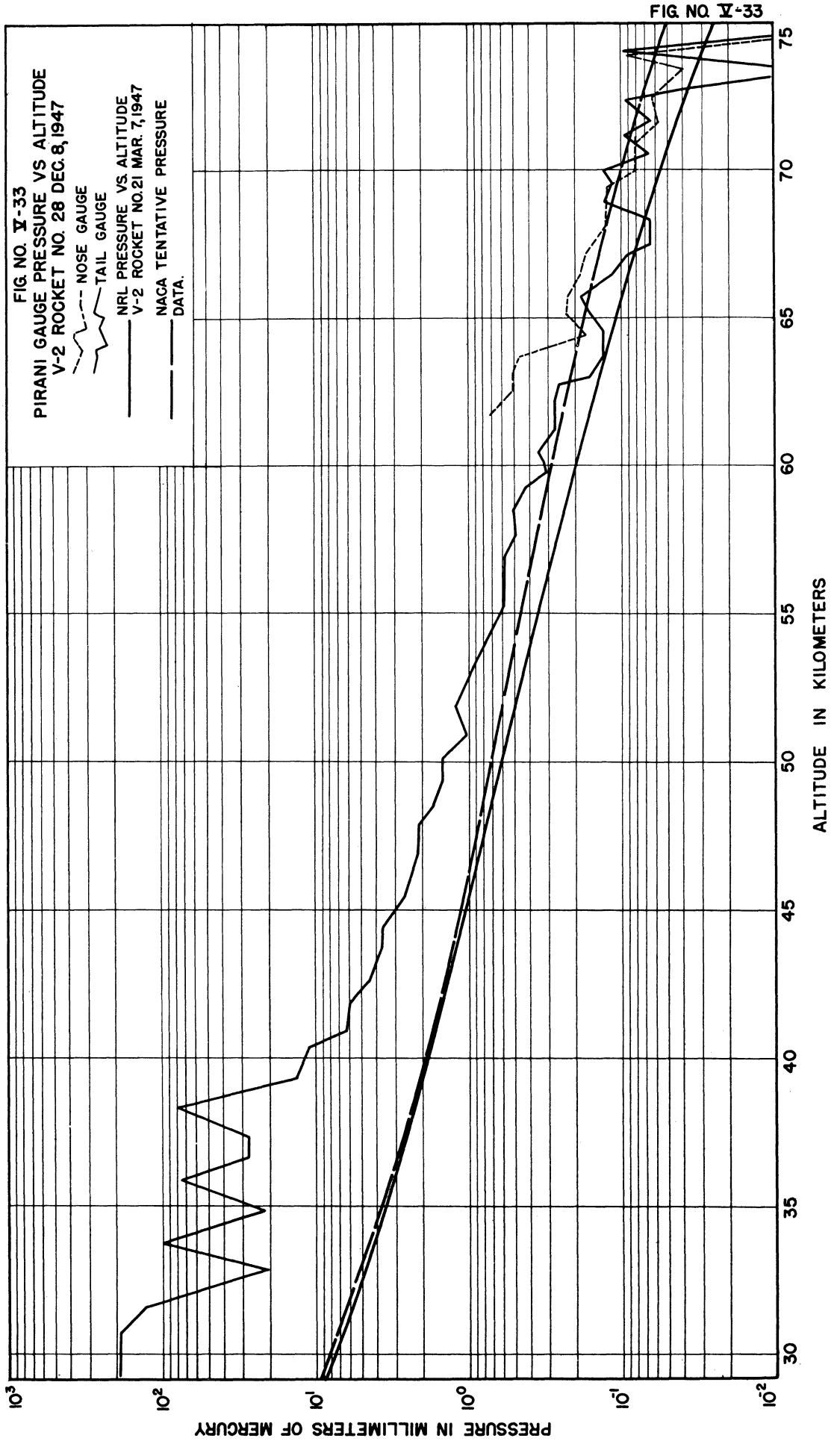
FIG. NO. V-33
FIG. NO. V-33
PIRANI GAUGE PRESSURE VS ALTITUDE
V-2 ROCKET NO. 28 DEC. 8, 1947
NOSE GAUGE
TAIL GAUGE
NRL PRESSURE VS. ALTITUDE
V-2 ROCKET NO. 21 MAR. 7, 1947
NACA TENTATIVE PRESSURE
DATA.
PRESSURE IN MILLIMETERS OF MERCURY
10^{3}
10^{2}
10^{1}
10^{0}
10^{-1}
10^{-2}
ALTITUDE IN KILOMETERS
30
35
40
45
50
55
60
65
70
75

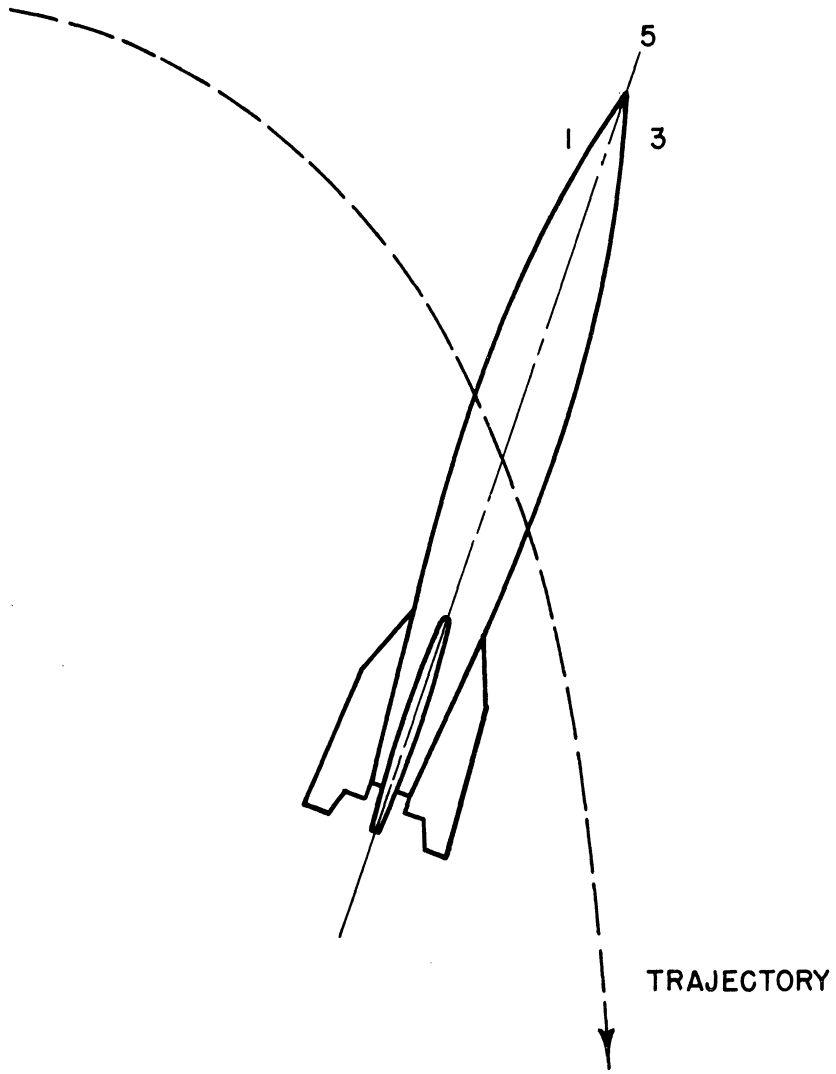

FIG. NO. V-34
ORIENTATION OF ROCKET AT BEGINNING OF DESCENT

APPENDIX A

DATA CONCERNING ROCKET FLIGHTS AND EXPERIMENTS

A-1. Firing of August 22, 1946: Unsuccessful Rocket Performance.

1. White Sands Proving Ground serial number for this Firing: No. 11.

2. Time of firing: 10:15 a.m., August 22, 1946.

3. Rocket performance: The rocket stabilization control equipment failed to function, beginning at take-off. The rocket plunged to earth after an approximately horizontal and eastward flight of about one mile, the maximum altitude reached being about 300 feet. The planned program setting called for the angle of flight trajectory with the vertical to be 5 degrees at the end of the powered flight, with the objective of producing a maximum-altitude flight. Duration of flight was about 11 seconds.

4. Trajectory data: None available.

5. Cloud conditions at time of firing: Clear overhead; a few scattered clouds elsewhere.

6. Ionization gauge provisions: The nosepiece carried five ionization gauges, one with a forward exposure, the other four with slant exposures, equally spaced circumferentially. The timing program called for the gauges to be exposed to the atmosphere at 100 seconds after take-off, the expectation being that the altitude would then be about 85 kilometers.

7. Variable-voltage probe: The nosepiece design provided for the variable-voltage probe to be exposed to the atmosphere simultaneously with the ionization gauges.

8. Ionosphere low-frequency pulsed transmitter arrangements, for providing a pulsed signal to be delayed in transit to the rocket through the ionosphere: The transmitter was a pulsed oscillator; pulse repetition frequency 569 pulses per second (triggered by the Signal Corps SCR-584 radar tracking unit); pulse duration about 10 microseconds; frequency 4.45 megacycles; average power during a pulse about 30 kilowatts. The transmitter was located about one mile south of the launching platform, and within 100 yards or so of the Signal Corps SCR-584 tracking radar. The antenna was of horizontal end fed design.

9. Ionosphere high-frequency pulsed transmitter arrangements for providing a signal not delayed in transit to the rocket through the ionosphere: The SCR-584 radar tracking signal served this purpose; pulse repetition rate 569 pulses per second, pulse duration about one microsecond, frequency about 3000 megacycles.

10. Ionosphere beacon responder provisions in the rocket: The Signal Corps beacon used for giving the SCR-584 tracking response was triggered, first normally by the radar signal, second by a triggering impulse originating in a 4.45 megacycle receiver in the rocket. Delay circuits built into the equipment caused this latter impulse to arrive at the beacon about 13 or 14 microseconds after the arrival of the microwave pulse. Of course, to this would be added the time delay due to the lower velocity of propagation of the 4.45 megacycle signal in passing through the ionosphere. This latter added time interval between the two responses was to provide the essential experimental information. The beacon response frequency was about 3000 megacycles.

11. Receivers for registering ionosphere beacon response: Both of the response signals were received by the SCR-584 radar set receivers, and the data presentation was in the form of two adjacent pips on the radar range scope. Of course no change of time interval between the pips was observed, because of rocket failure.

12. Properties of the ionospheric "E" layer at time of firing: Advance predictions were that the critical frequency of the "E" layer would be 3.8 megacycles at the time of firing; the 4.45 megacycle transmitter frequency was chosen with reference to this prediction and certain other limitations. The

National Bureau of Standards ionospheric field station at White Sands obtained no data concerning the characteristics of the ionosphere at the time of the firing.

13. Provisions for determination and control of rocket roll, pitch, and yaw: Complete interpretation of ionization gauge information requires a complete knowledge of positions of the rocket in roll, pitch, and yaw. In an attempt to provide this information, the roll control system employing the tail surfaces was set to continue to function after fuel cut-off, in the hope that the residual atmosphere above fuel cut-off altitude would be sufficient to prevent roll; then additional gyroscopes were installed and connected to the telemetering system, which would transmit pitch and yaw information provided the rocket did not spin, and provided the pitch and yaw did not exceed modest angles. These limitations were related to gyro tumbling.

Provision and installation of the ionospheric pulse delay measuring equipment for the August 22 firing was a cooperative activity involving members of the technical staffs of the AMC Cambridge Field Station, of the Aircraft Radiation Laboratory at Wright Field, and of the University of Michigan.

The air pressure and temperature measuring equipment, and the variable voltage probe, were provided and installed by the University of Michigan. The experimental information from the ionization gauges and the probe were transmitted to earth and recorded by the Naval Research Laboratory telemetering equipment.

Because of the rocket failure, no experimental data were obtained on August 22. However, the telemetering records and the ionospheric delay scope presentation indicated that all experimental equipment was functioning as intended during the eleven seconds that the rocket was in flight.

The firing was scheduled to take place at 9:00 a.m. This time was chosen because at that time of day there was little or no radio noise interference due to atmospheric conditions. Experience during airplane flight tests on preceding days had indicated that atmospheric radio noise increased rapidly later in the morning. With sufficiently severe noise the 4.45 megacycle receiver to be carried in the rocket experienced random triggering, which could result in severe "counting down" of the tracking beacon response. The 9:00 a.m. schedule was set up to avoid this random triggering. Last minute troubles in the tracking beacon, and with air-line coupling to the rocket, accounted for the delay from 9:00 to 10:15 a.m.

A-2. Firing of November 21, 1946.

1. White Sands Proving Ground serial number for this firing: No. 15.

2. Time of firing: 9:55 a.m., November 21, 1946.

3. Rocket performance:

Maximum altitude: 101.5 kilometers (63 miles).
Maximum range: 20.3 kilometers (12.6 miles).
Direction of flight: Approximately 5 degrees west of north.
Program setting for angle of rocket with vertical at end of powered flight: 5 degrees (trajectory indicates angle was actually 3.5 degrees).
Time from take-off to fuel cut-off: 61.5 seconds.
Height at fuel cut-off: 26.5 kilometers (16.5 miles).
Duration of flight: 340 seconds.
Horizontal velocity component after fuel cut-off: 67.9 meters per second (.042 mile per second).
Roll, pitch, yaw: Ionization gauges give firm evidence of a roll or spin, approximately about the rocket axis of figure, having a period of about 30 seconds. Ionization gauges give indirect indications of a rate of change of pitch angle, in the forward direction, of about 0.145 degree per second.

4. Trajectory data: Figures A-1, A-2, A-3, A-4 and A-5 show graphs of altitude versus range, altitude versus time, velocity versus time, and velocity versus altitude. This information is based on Signal Corps Master Beacon radar data. Figures A-1 and A-2 show the same altitude versus range data, but different abscissa scales are used. Figure A-1 gives a better concept of the actual shape of the trajectory, whereas Figure A-2 can be read more accurately.

5. Cloud conditions at time of firing: Partly cloudy. Rocket went through clouds.

6. Ionization gauge provisions: Five ionization gauges were placed in the nosepiece, one with a forward exposure, the other four with slant exposures, equally spaced circumferentially. The gauges were exposed to the atmosphere at 97 seconds after take-off, at an altitude of 62 kilometers.

7. Variable-voltage probe: The variable-voltage probe in the nose was exposed to the atmosphere simultaneously with the ionization gauges.

8. Ionosphere low-frequency pulsed transmitter arrangements: The transmitter was a multi-stage tuned-radio-frequency amplifier, with a low-level pulsed oscillator for controlling frequency and pulse duration precisely, and for providing synchronism with the high-frequency signal. The pulse repetition frequency was 570 pulses per second, pulse duration about 8 microseconds, frequency 4.45 megacycles and the average power during a pulse was about 50 kilowatts. The transmitter was located about four miles south of the launching platform, and within about 300 feet of the high-frequency pulse transmitter and ground station for receiving beacon responses. The antenna was of horizontal end-fed design.

9. Ionosphere high-frequency pulsed transmitter: For this purpose a 470 megacycle pulsed transmitter was provided, synchronized with the 4.45 megacycle transmitter and located about 300 feet from it. Its pulse duration was about one microsecond and the average power during a pulse about ten kilowatts.

10. Ionosphere beacon responder provisions in the rocket: The high frequency airborne beacon receiver operated at 470 megacycles, had a five-microvolt sensitivity and a three-megacycle bandwidth. The beacon transmitter operated at a carrier frequency of 493.5 megacycles with a peak output of 100 watts. The low-frequency receiver had a 100-microvolt sensitivity, a bandwidth of one megacycle and a carrier frequency of 4.45 megacycles.

11. Receiver for registering ionosphere beacon response: This receiver had a carrier frequency of 493.5 megacycles, a two-microvolt sensitivity and a three-megacycle bandwidth.

12. Properties of the ionospheric "E" layer at time of firing: Advance predictions were that the critical frequency of the "E" layer would be 3.4 megacycles at time of firing. The 4.45 megacycle transmitter frequency was chosen with reference to this prediction and certain other matters of convenience. The National Bureau of Standards ionospheric field station at White Sands reported an actual critical frequency of 3.5 megacycles at time of firing, and a virtual height of 120 kilometers.

13. Provisions for determining rocket roll, pitch, and yaw: No provisions were made for determining these quantities.

For the November 21 firing, the University of Michigan provided and operated the 4.45 megacycle pulsed ground transmitter and interpreted the ionosphere records, but all of the other activities connected with the ionospheric delay experiment were carried out by the Air Materiel Command Cambridge Field Station. The entire ionospheric delay program is completely discussed in an AMC Cambridge Field Station report, "Upper Air Research Program," Report No. 1 by the Navigation Laboratory, September 1, 1947.[4]

The air pressure and temperature measuring equipment, using ionization gauges, and the variable-voltage probe were provided and installed by the University of Michigan. The experimental information from the ionization gauges and the probe were transmitted to earth and recorded by the Naval Research Laboratory telemetering equipment.

Experimental data obtained on November 21, 1946 from the ionization gauges are presented and discussed in the body of this report. The experimental data obtained from the variable-voltage probe will be presented in a subsequent report.

A-3. Firing of February 20, 1947.

1. White Sands Proving Ground serial number for this firing: No. 20.

2. Time of firing: 11:16 a.m., February 20, 1947.

3. Rocket performance:

Maximum altitude: 108.5 kilometers (67.4 miles).
Maximum range: 25.15 kilometers (15.6 miles).
Direction of flight: Approximately 50 degrees west of north.
Program setting for angle of rocket with vertical at end of powered flight: 7 degrees (trajectory indicates angle was actually 4.2 degrees).
Time from take-off to fuel cut-off: 59.75 seconds.
Height at fuel cut-off: 32.5 kilometers (20.2 miles).
Duration of flight: 425 seconds.
Horizontal velocity component after fuel cut-off: 99.5 meters per second (.0618 mile per second).
Roll, pitch, yaw: Periodic interference with the telemetering channel, presumably by the rocket blast, gives evidence of a spin or roll periodicity of about 30 r.p.m. prior to fuel cut-off. The ionization gauges give definite evidence of a rotational period of about seven seconds during rocket descent from the crest of its trajectory. The gauges give no evidence as to presence or absence of spin during ascent to the crest. The ionization gauge evidence suggests that the axis of spin (presumably the axis of least moment of inertia) did not quite coincide with the axis of figure of the rocket. The gauges offer no interpretable evidence as to rate of change of pitch or yaw, except to the extent of a broad general similarity to the November 21 records, which suggested a moderate, but definite, forward rate of change of pitch.

4. Trajectory data: Figures A-6, A-7, A-8, A-9, and A-10 are of altitude versus range, altitude versus time, velocity versus time, and velocity versus altitude. These curves are based on the Signal Corps Master Beacon radar data.

5. Cloud conditions at time of firing: Light scattered clouds. Missile passed through clouds on ascent.

6. Ionization gauge provisions: Ionization gauges located as on November 21; the gauges were exposed to the atmosphere at 115.5 seconds after launching, at an altitude of 83 kilometers.

7. Variable-voltage probe: Exposed to the atmosphere simultaneously with the ionization gauges.

8. Ionosphere low-frequency pulsed transmitter arrangements: The transmitter employed was the same pulsed oscillator transmitter used on August 22, 1946; frequency 4.5 megacycles.

9, 10, 11. Ionosphere high-frequency pulse transmitter, beacons in the rocket, and receiving equipment on the ground: All these were the same as in the November 21 firing; that is, the 500 megacycle system was employed. The responder beacon failed in flight, so that no ionosphere information was obtained.

12. Properties of the ionospheric "E" layer at the time of firing: Advance predictions were that the critical frequency of the "E" layer would be 3.6 megacycles at time of firing. The National Bureau of Standards ionospheric field station at White Sands reported an actual critical frequency of 3.7 megacycles at time of firing, and a virtual height of 120 kilometers.

13. Provisions for determining rocket roll, pitch, and yaw: No such provisions were made.

For the February 20 firing, all the ionospheric measurement activities were carried out by the AMC Cambridge Field Station, with no active University of Michigan participation. Facts as to equipment provided are included here for completeness of the record.

The atmospheric pressure and temperature measuring equipment, using ionization gauges, and the variable-voltage probe were provided and installed by the University of Michigan. The experimental information from the ionization gauges and the probe were transmitted to earth and recorded by the Naval Research Laboratory telemetering equipment.

Experimental data obtained on February 20, 1947 from the ionization gauges are presented and discussed in the body of this report. The variable-voltage probe measurements will be included in a later report.

A-4. Firing of April 17, 1947.

The Cambridge Field Station personnel provided and installed ionospheric delay measuring equipment for a firing which took place April 17, 1947, employing equipment very similar to that installed on February 20, 1947. The University of Michigan did not participate in the April 17 firing, but the fact that ionospheric delay measurements were made at that time is stated here for reference purposes. The April 17 rocket attained a height of 88 miles (141.7 kilometers) and substantial pulse signal delays were observed.

A-5. Firing of December 8, 1947.

1. White Sands Proving Ground serial number for this firing: No. 28.

2. Time of firing: 2:40 p.m., December 8, 1947.

3. Rocket Performance:

Maximum altitude: 103 kilometers (64 miles)
Maximum range: approximately 42.5 kilometers (26.4 miles)
Direction of flight: approximately 1 deg. East of North
Program setting for angle of rocket with vertical at end of powered flight: 7 deg.
Time from take-off to fuel cut-off: 67.5 seconds
Height at fuel cut-off: 29.2 kilometers (18.2 miles)
Duration of flight: approximately 340 seconds
Horizontal velocity component after fuel cut-off: 149 meters (0.093 miles) per second
Roll, pitch, and yaw: Information from the three aspect cameras mounted in the mid-body of the rocket clearly shows the motion of the missile in roll, pitch, and yaw. A slow roll with a period of approximately 80 seconds is indicated, and this is substantiated by the action of the ionization gauges. The aspect camera information shows rather irregular motions in both pitch and yaw.

From this aspect camera information it is possible to deduce the actual spatial motion of the rocket, and this work is being carried on at present. Time, however, does not permit its inclusion in this report.

4. Trajectory data: Figures A-11, A-12, A-13, and A-14 are graphs of altitude versus horizontal range, altitude versus time, total velocity versus time and total velocity versus altitude. These curves are based on the Signal Corps Master Beacon Radar data.

5. Cloud conditions at time of firing: The sky was clear and unclouded.

6. Ionization gauge provisions: The ionization gauges were located as on November 21, 1946 and February 20, 1947. The gauges were exposed to the atmosphere after 81.5 seconds of flight at an altitude of 45 kilometers.

7. Variable-voltage probe: The variable voltage probe in the nose was exposed to the atmosphere simultaneously with the ionization gauges.

8. Pirani gauge provisions: Two Pirani gauges were included in the instrumentation. One of these was mounted on the side of the nose cone a few inches aft of the ionization gauges. The other was mounted a few inches forward of the tail fins, and 10 degrees toward No. 4 fin from No. 1 fin. Both Pirani gauges were exposed to the atmosphere from the ground up.

9. Ionosphere pulse-delay measurement: Inasmuch as the University of Michigan had responsibility only for the construction and operation of the low-frequency transmitter, no discussion of it is included here.

10. Provisions for determining rocket roll, pitch, and yaw: Four cameras were mounted in the mid-body of the rocket for the purpose of obtaining a continuous record of the aspect of the missile during flight. One of these cameras was destroyed upon rocket impact with the earth. The information from these cameras is contained in the Ohio State University Report No. 9 on missile aspect determination.

FIG NO. A-1
ALTITUDE VS. HORIZONTAL RANGE
TRAJECTORY OF V-2 ROCKET NO 15
NOV 21, 1946
BASED ON MASTER BEACON RADAR DATA

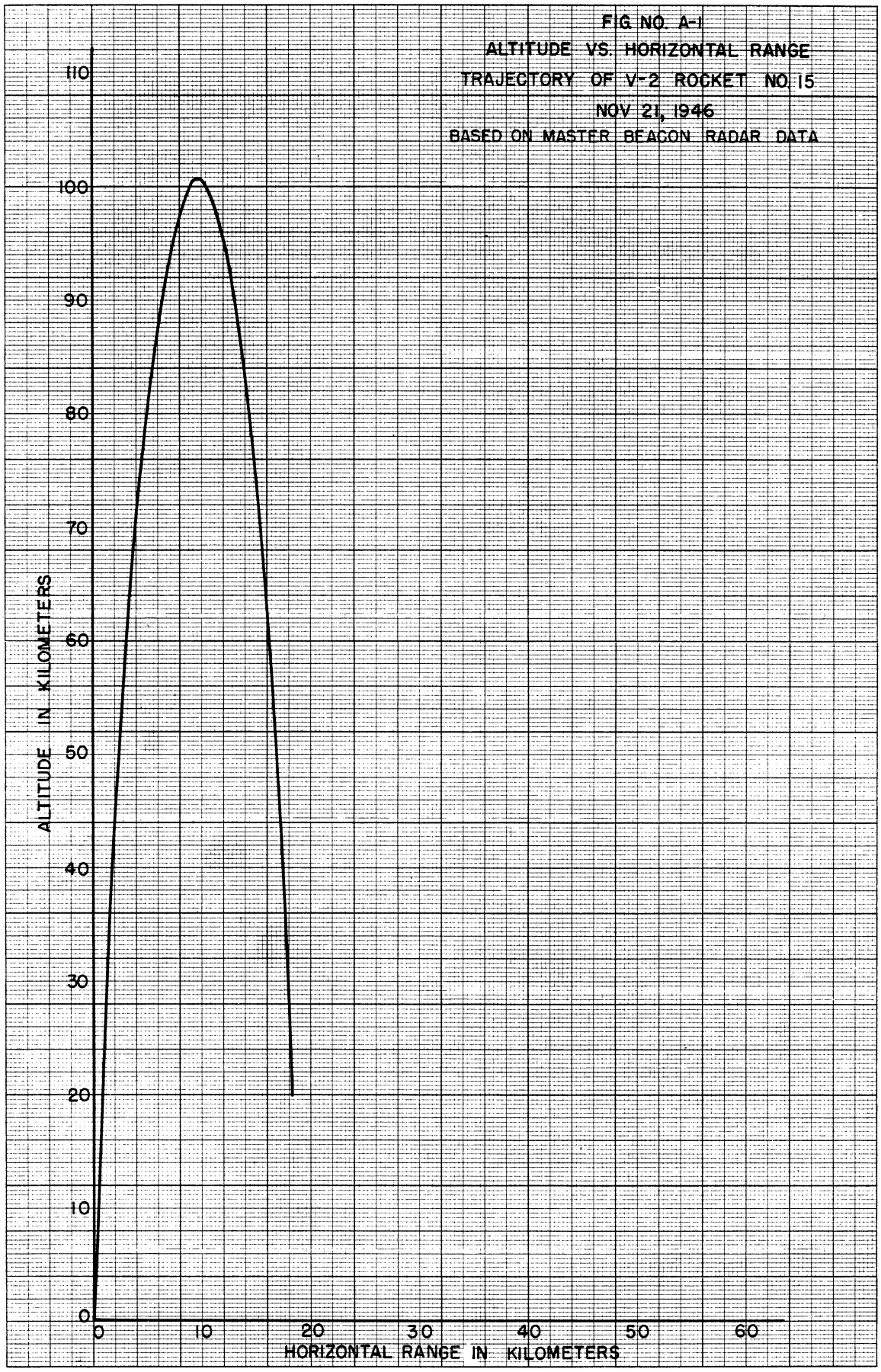

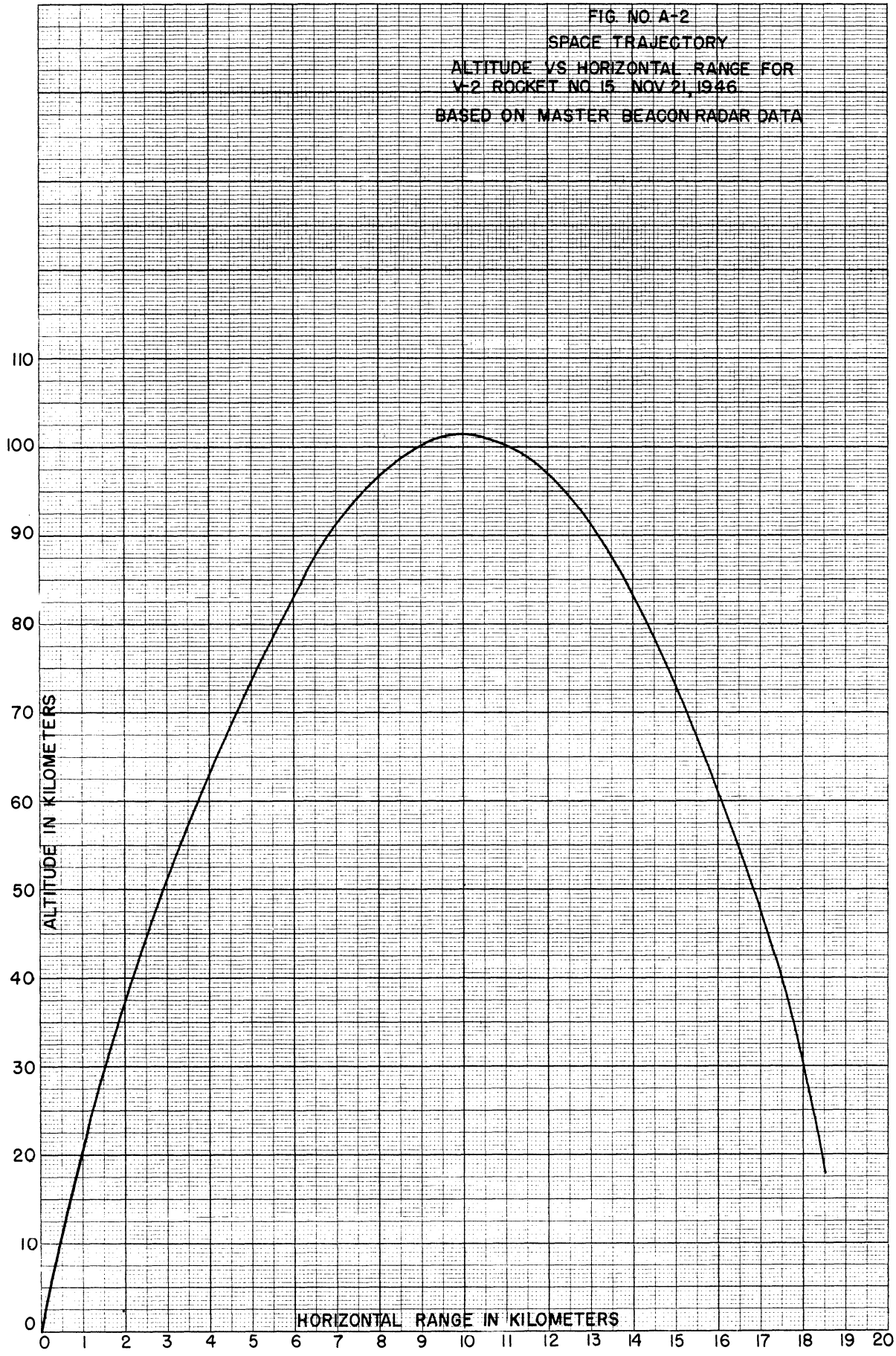
FIG. NO. A-2
SPACE TRAJECTORY
ALTITUDE VS HORIZONTAL RANGE FOR
V-2 ROCKET NO. 15 NOV 21, 1946
BASED ON MASTER BEACON RADAR DATA
ALTITUDE IN KILOMETERS
0
10
20
30
40
50
60
70
80
90
100
110
HORIZONTAL RANGE IN KILOMETERS
0 1 2 3 4 5 6 7 8 9 10 11 12 13 14 15 16 17 18 19 20

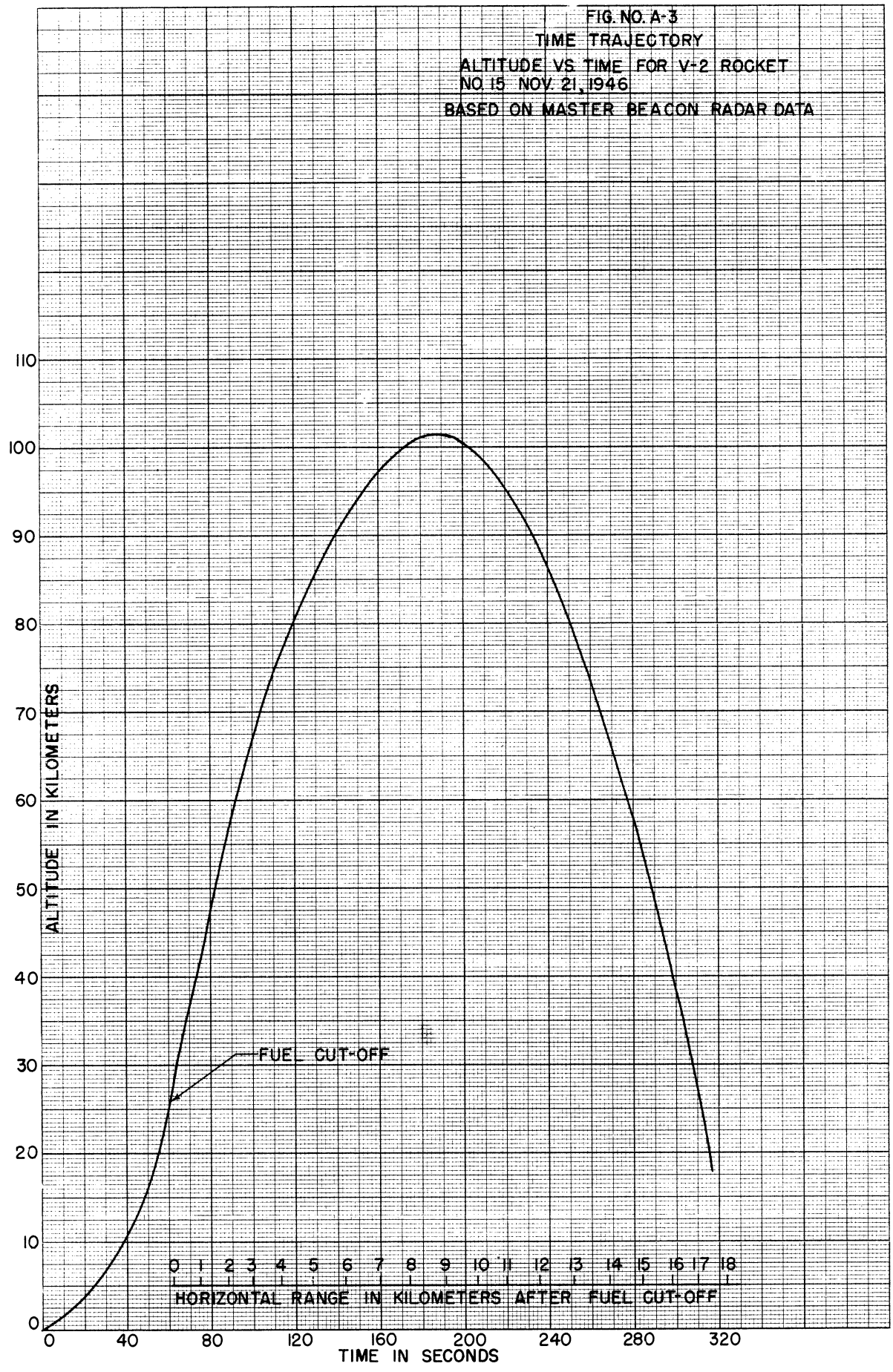
FIG. NO. A-3
TIME TRAJECTORY
ALTITUDE VS TIME FOR V-2 ROCKET
NO. 15 NOV. 21, 1946
BASED ON MASTER BEACON RADAR DATA
ALTITUDE IN KILOMETERS
0
10
20
30
40
50
60
70
80
90
100
110
FUEL CUT-OFF
0 1 2 3 4 5 6 7 8 9 10 11 12 13 14 15 16 17 18
HORIZONTAL RANGE IN KILOMETERS AFTER FUEL CUT-OFF
0
40
80
120
160
200
240
280
320
TIME IN SECONDS

FIG. NO. A-4
TOTAL VELOCITY VS. TIME
V-2 ROCKET NO. 15
NOV. 21, 1946

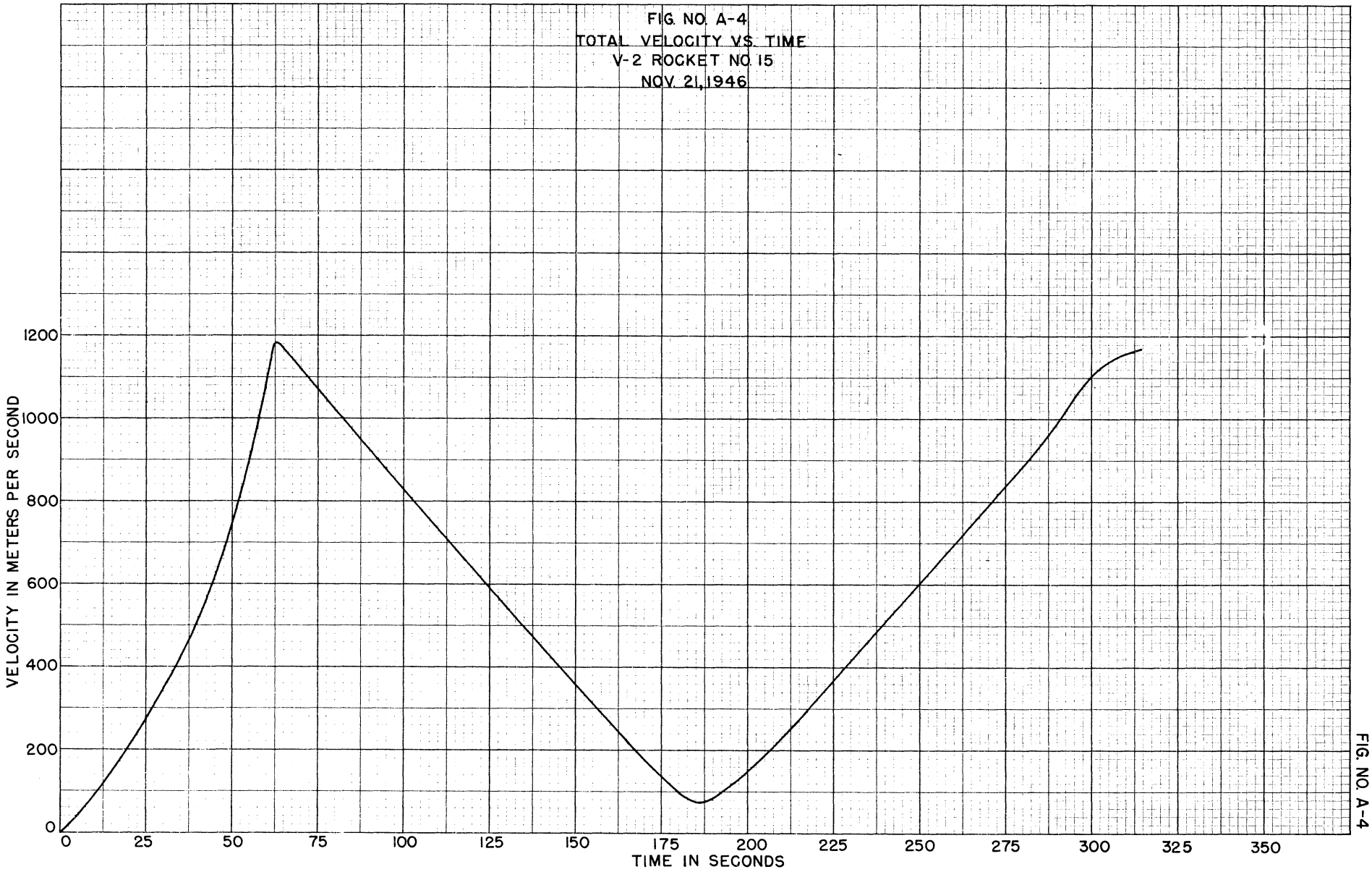

FIG. NO. A-4

FIG. NO. A-5

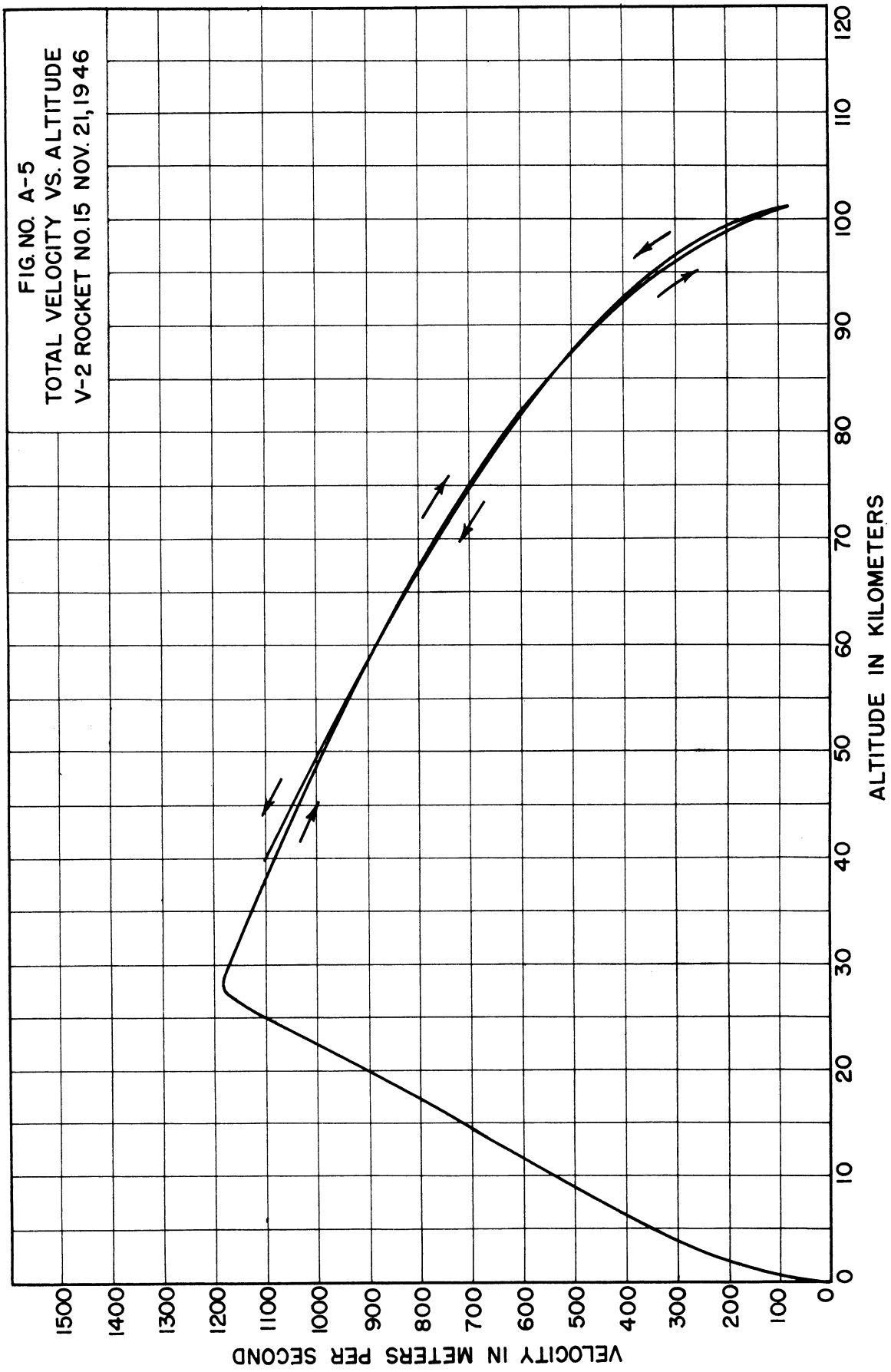
FIG. NO. A-5
TOTAL VELOCITY VS. ALTITUDE
V-2 ROCKET NO. 15 NOV. 21, 1946
VELOCITY IN METERS PER SECOND
0
100
200
300
400
500
600
700
800
900
1000
1100
1200
1300
1400
1500
ALTITUDE IN KILOMETERS
0
10
20
30
40
50
60
70
80
90
100
110
120

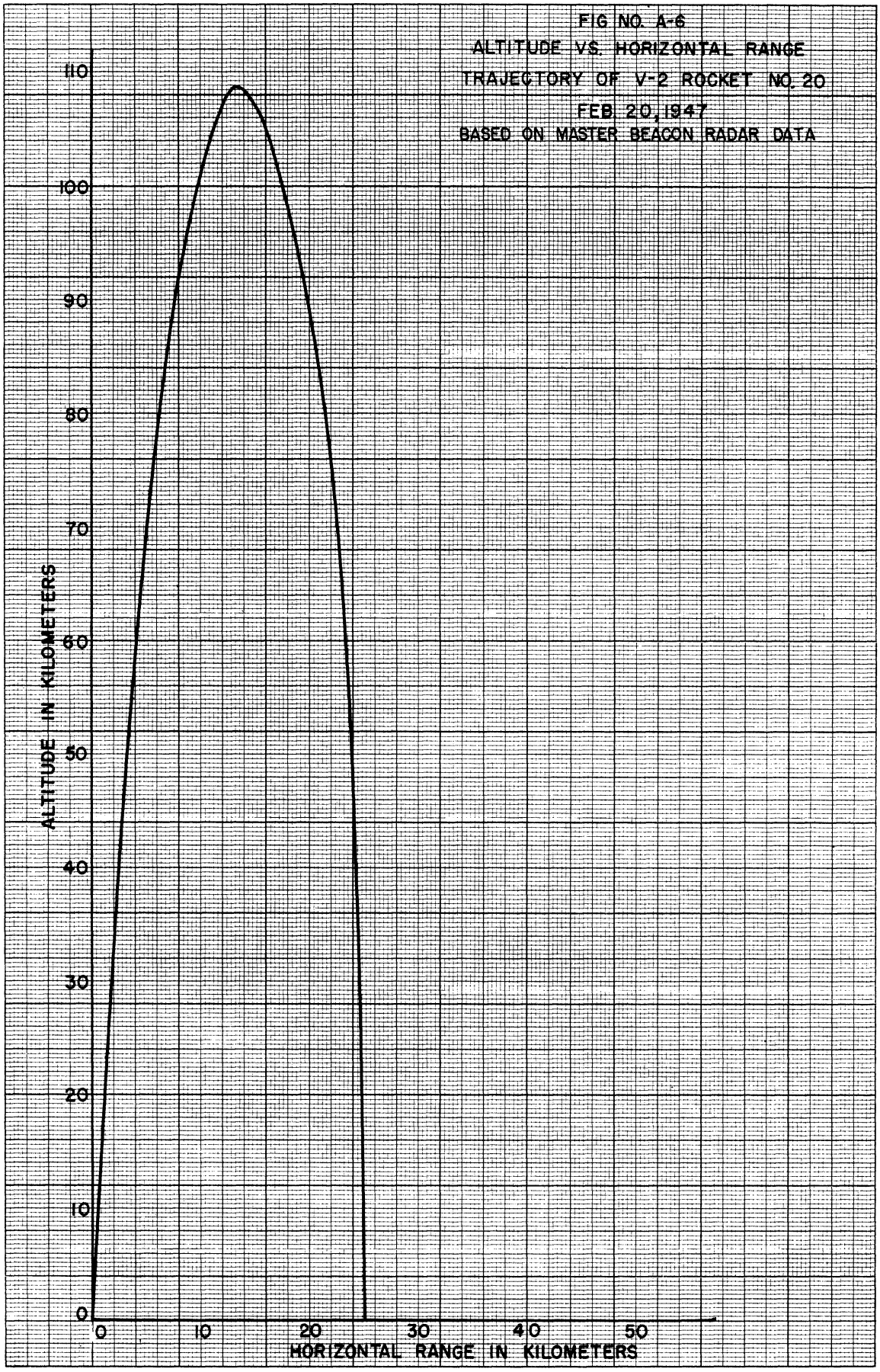
FIG NO. A-6
ALTITUDE VS. HORIZONTAL RANGE
TRAJECTORY OF V-2 ROCKET NO. 20
FEB 20, 1947
BASED ON MASTER BEACON RADAR DATA
ALTITUDE IN KILOMETERS
110
100
90
80
70
60
50
40
30
20
10
0
0
10
20
30
40
50
HORIZONTAL RANGE IN KILOMETERS

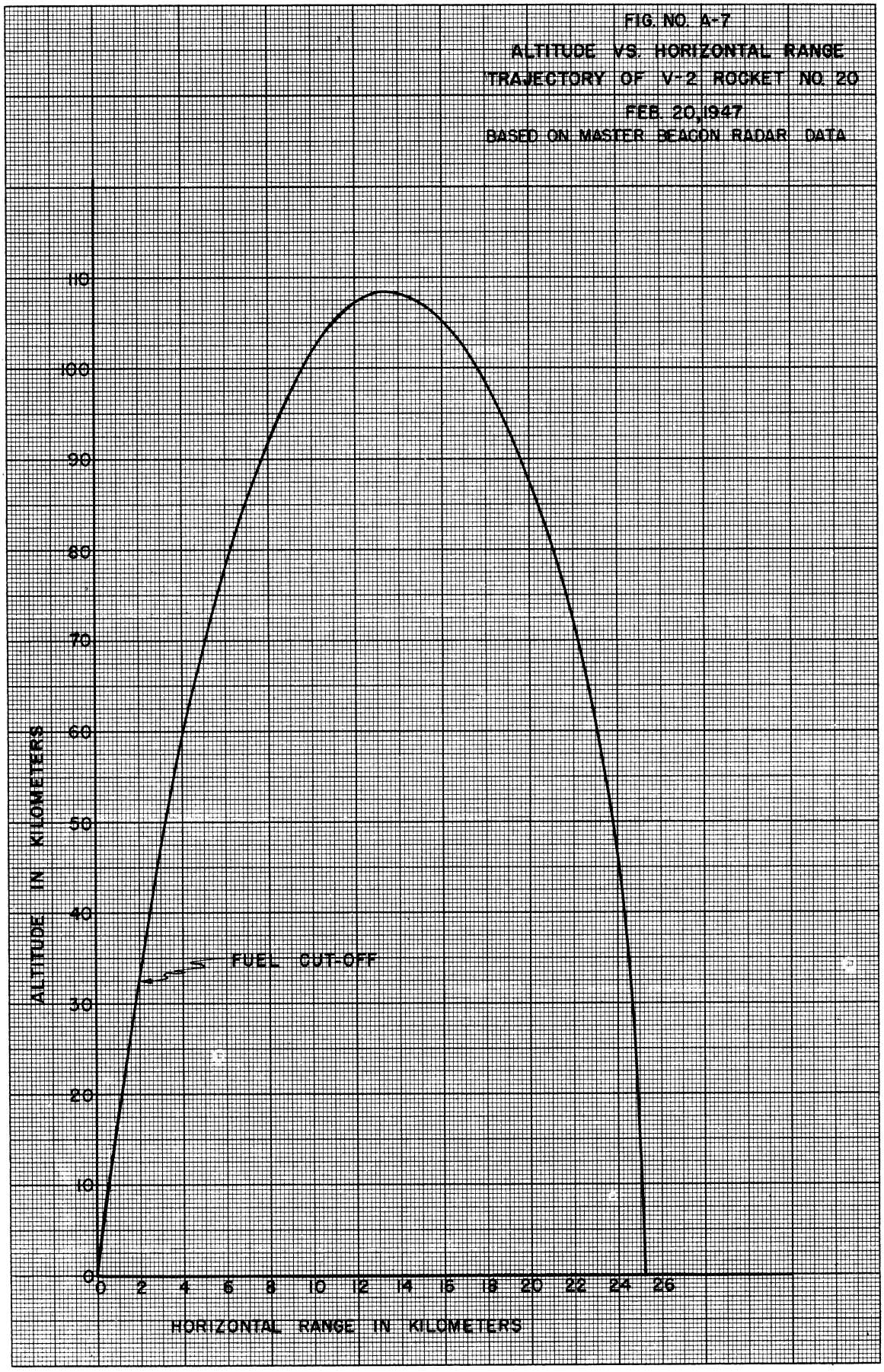
FIG. NO. A-7
ALTITUDE VS. HORIZONTAL RANGE
TRAJECTORY OF V-2 ROCKET NO. 20
FEB. 20, 1947
BASED ON MASTER BEACON RADAR DATA
ALTITUDE IN KILOMETER'S
HORIZONTAL RANGE IN KILOMETER'S
FUEL CUT-OFF
0
10
20
30
40
50
60
70
80
90
100
110
0
2
4
6
8
10
12
14
16
18
20
22
24
26

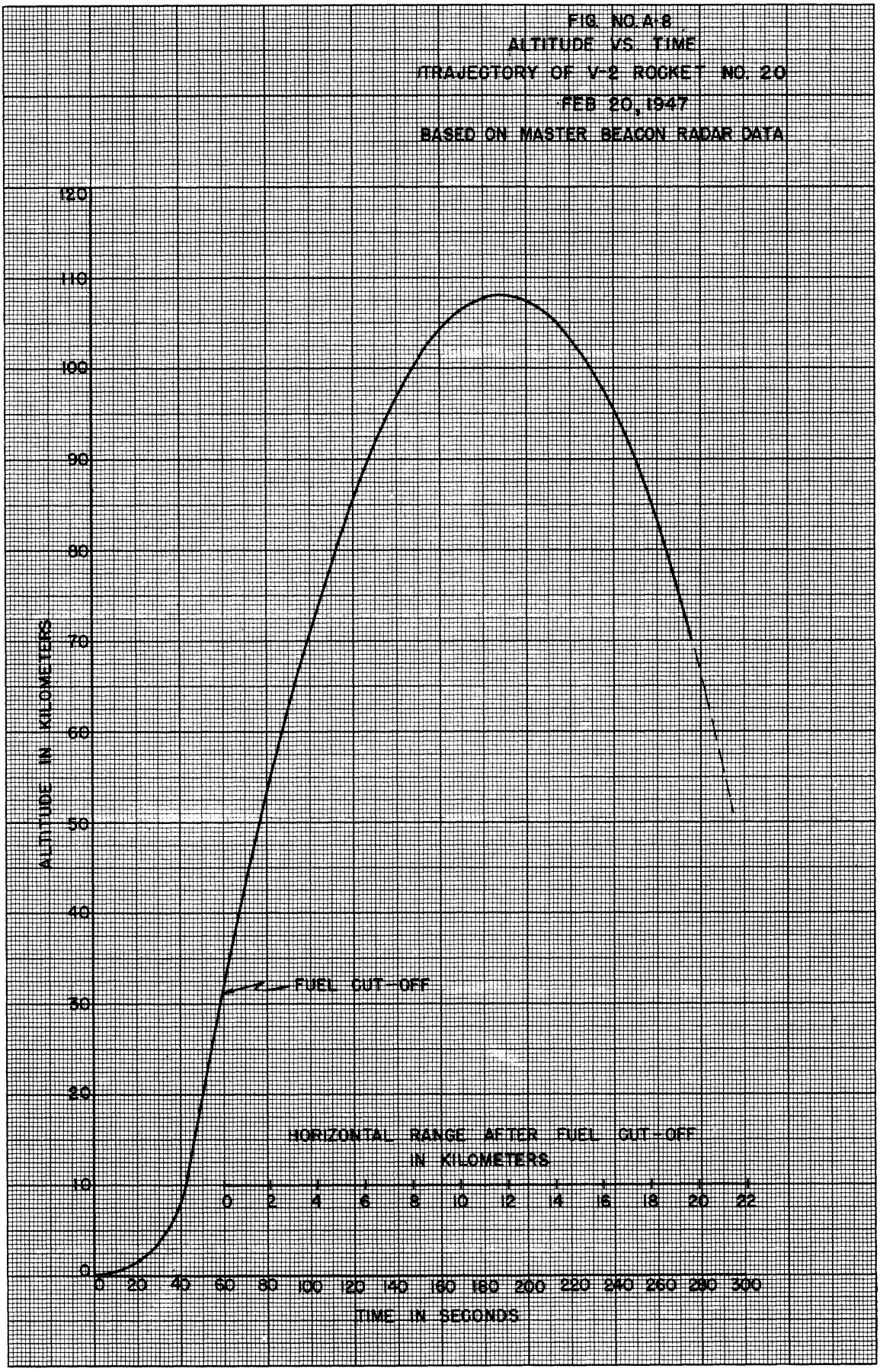
FIG. NO. A-8
ALTITUDE VS. TIME
TRAJECTORY OF V-2 ROCKET NO. 20
FEB 20, 1947
BASED ON MASTER BEACON RADAR DATA
ALTITUDE IN KILOMETERS
120
110
100
90
80
70
60
50
40
30
20
10
0
FUEL CUT-OFF
HORIZONTAL RANGE AFTER FUEL CUT-OFF
IN KILOMETERS
0 2 4 6 8 10 12 14 16 18 20 22
0 20 40 60 80 100 120 140 160 180 200 220 240 260 280 300
TIME IN SECONDS

FIG. NO. A-9

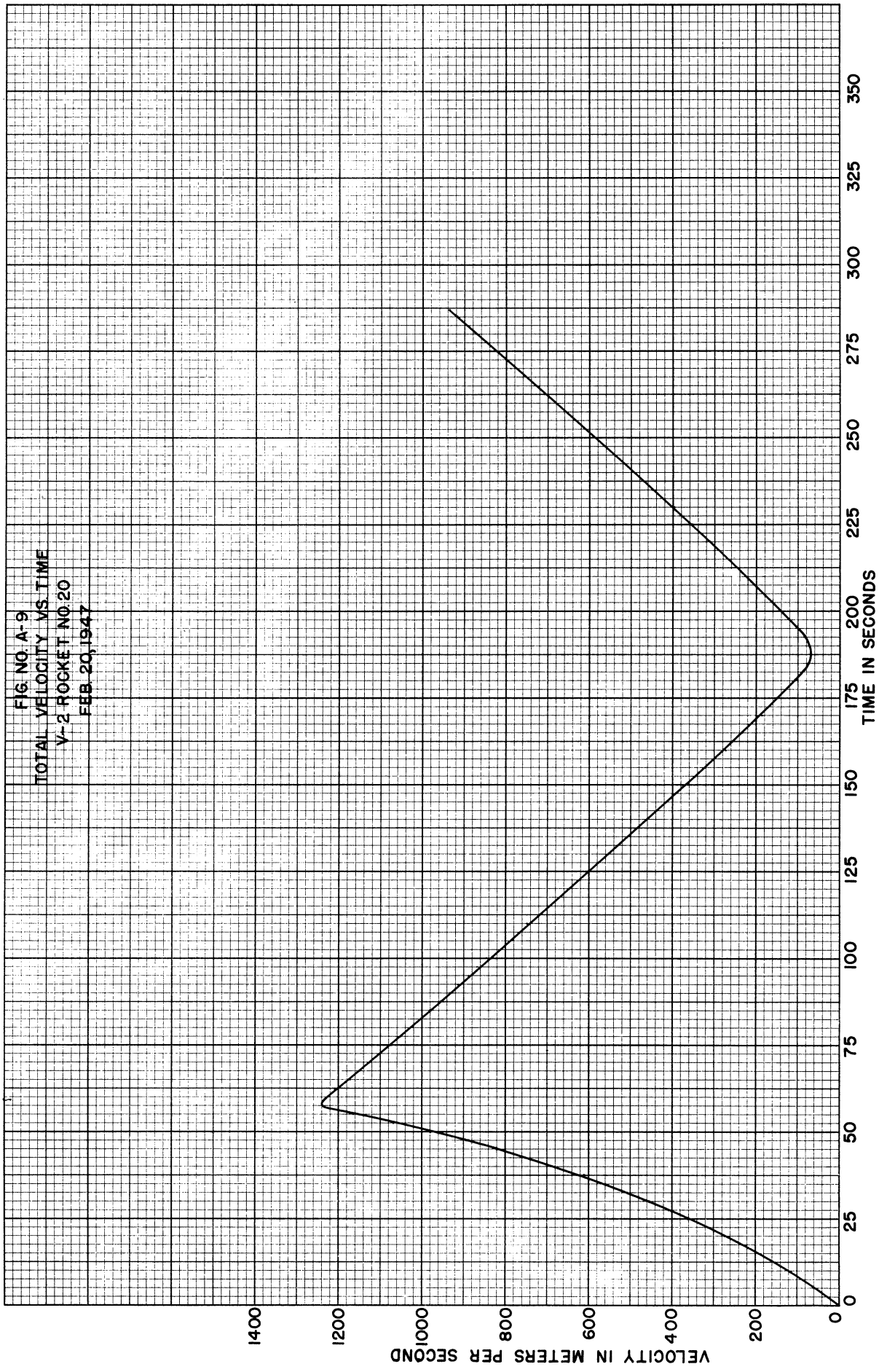
FIG. NO. A-9
TOTAL VELOCITY VS. TIME
V-2 ROCKET NO. 20
FEB. 20, 1947
VELOCITY IN METERS PER SECOND
0
200
400
600
800
1000
1200
1400
TIME IN SECONDS
0
25
50
75
100
125
150
175
200
225
250
275
300
325
350

FIG. NO. A-10

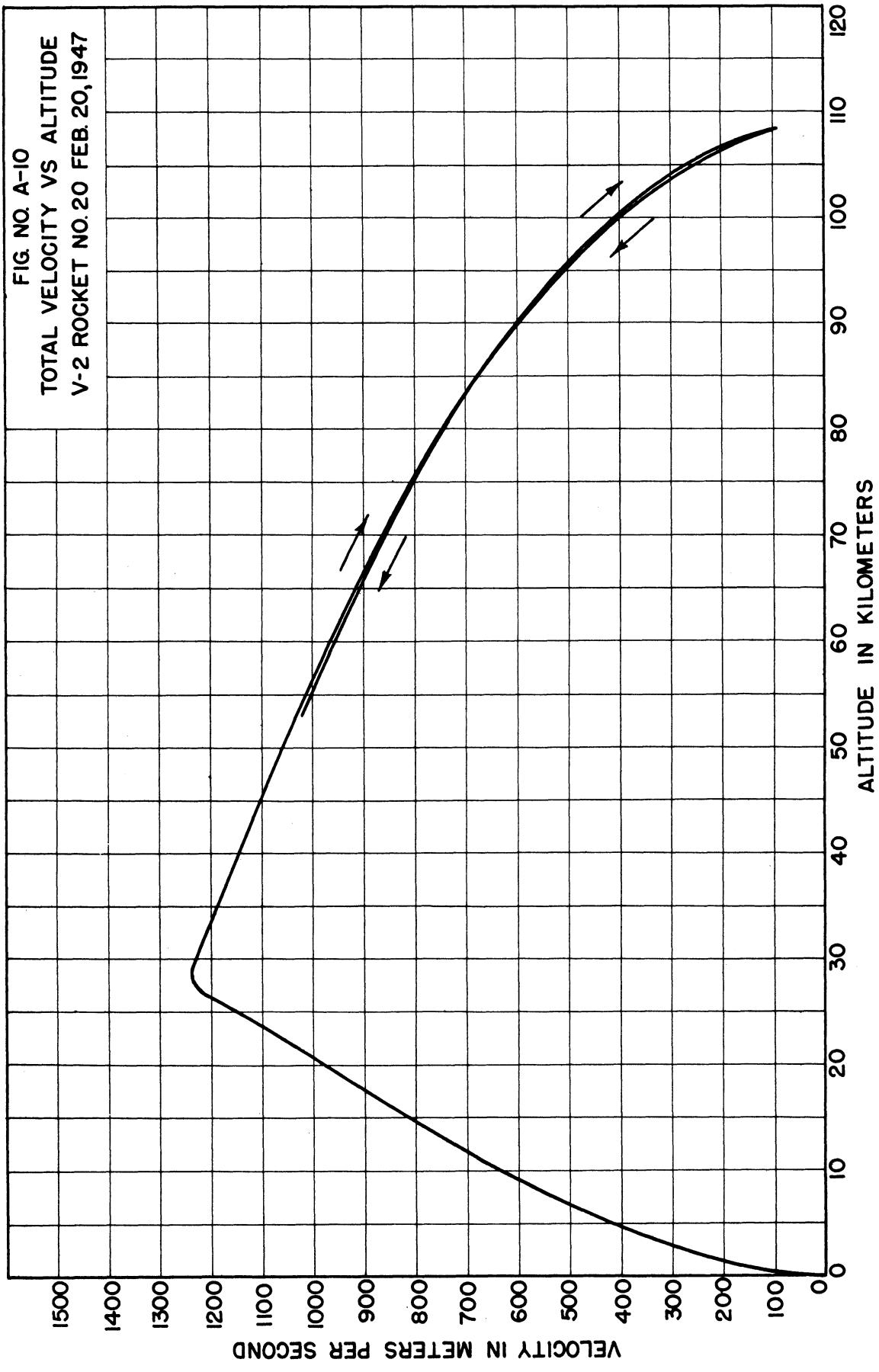
FIG. NO. A-10
TOTAL VELOCITY VS ALTITUDE
V-2 ROCKET NO. 20 FEB. 20, 1947
VELOCITY IN METERS PER SECOND
0
100
200
300
400
500
600
700
800
900
1000
1100
1200
1300
1400
1500
ALTITUDE IN KILOMETERS
0
10
20
30
40
50
60
70
80
90
100
110
120

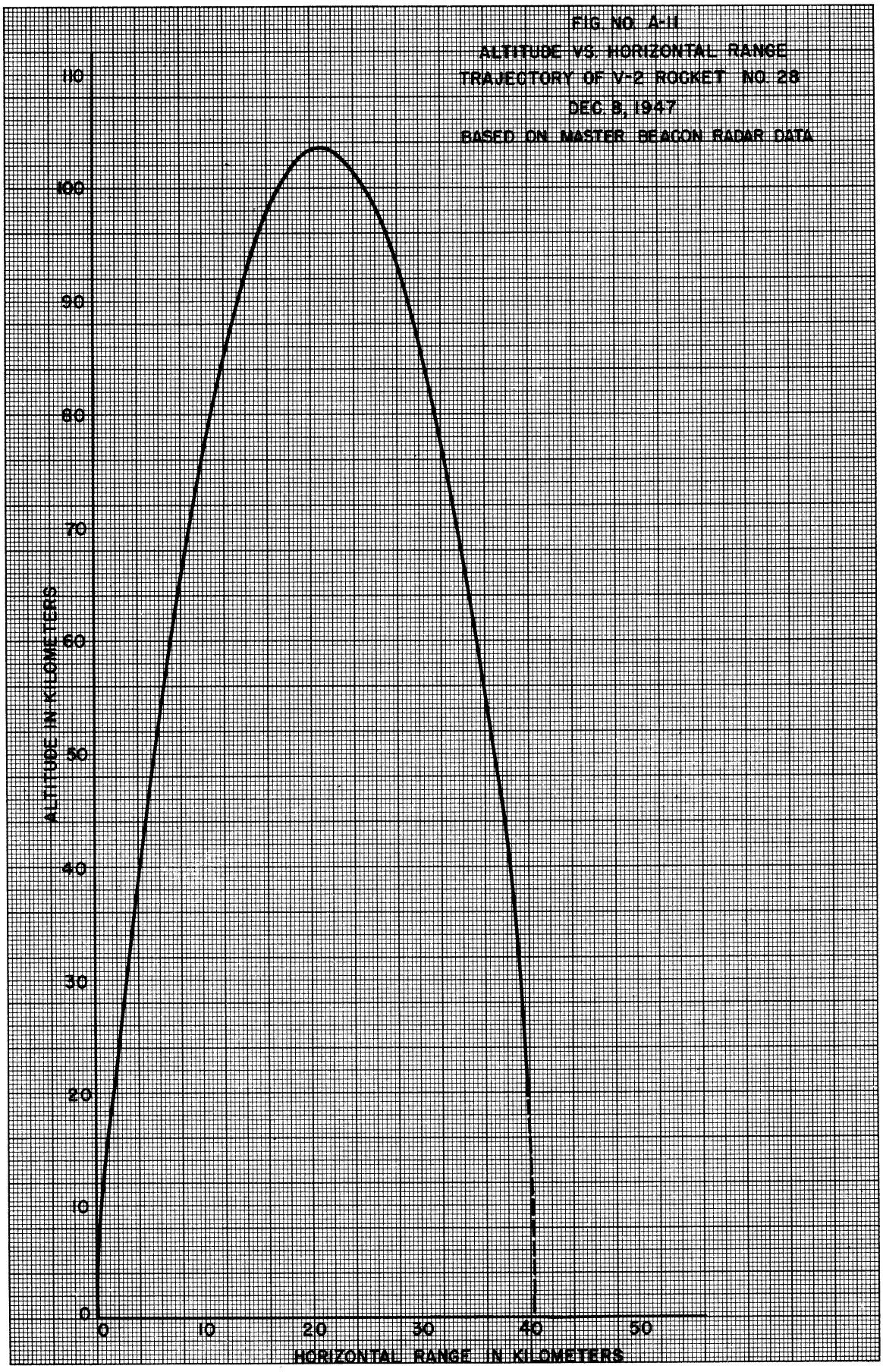
FIG. NO. A-II
ALTITUDE VS. HORIZONTAL RANGE
TRAJECTORY OF V-2 ROCKET NO. 28
DEC. 8, 1947
BASED ON MASTER BEACON RADAR DATA
ALTITUDE IN KILOMETERS
110
100
90
80
70
60
50
40
30
20
10
0
0
10
20
30
40
50
HORIZONTAL RANGE IN KILOMETERS

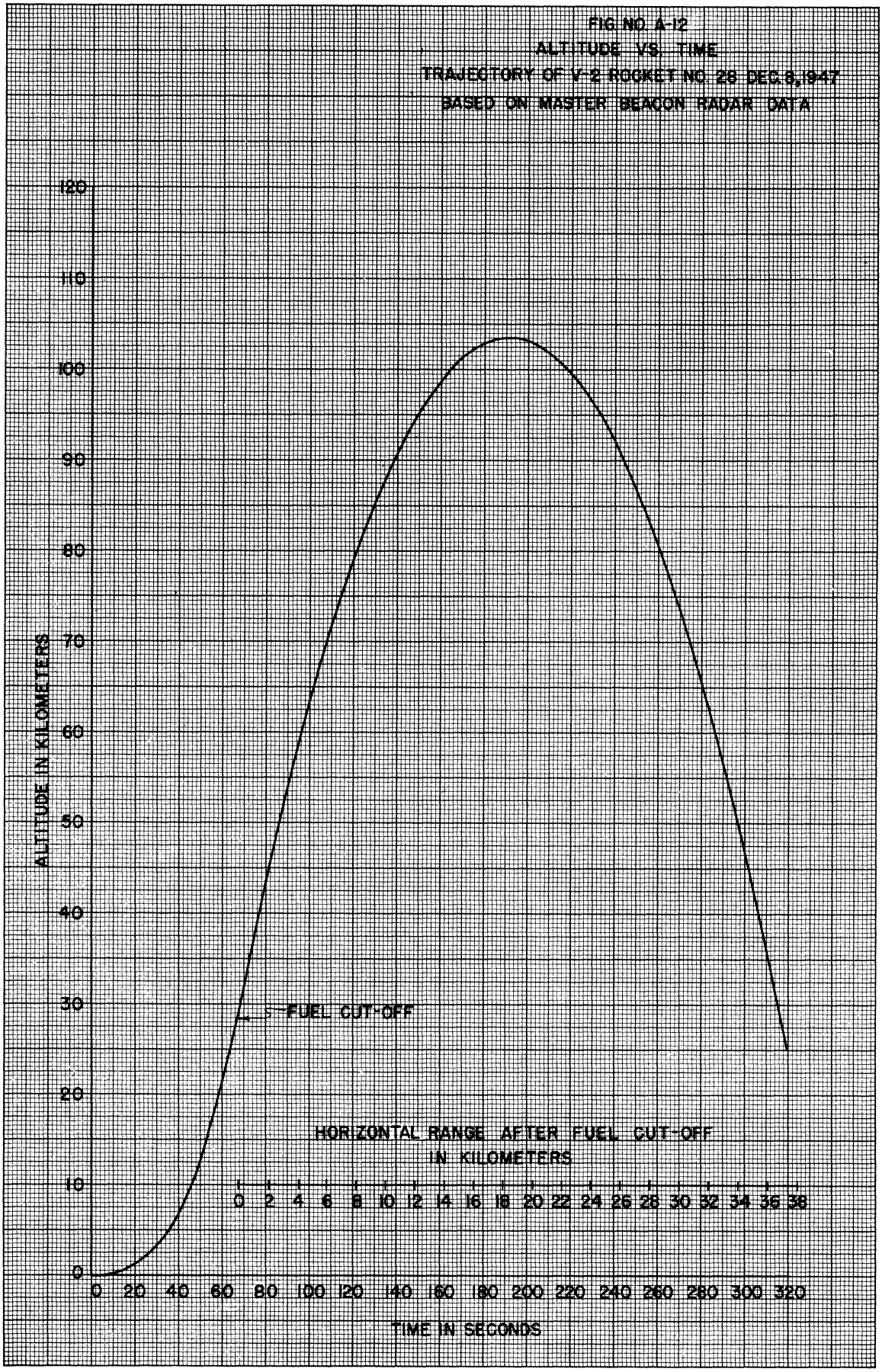
FIG NO A-12
ALTITUDE VS. TIME
TRAJECTORY OF V-2 ROCKET NO. 28 DEC. 8, 1947
BASED ON MASTER BEACON RADAR DATA
ALTITUDE IN KILOMETERS
120
110
100
90
80
70
60
50
40
30
20
10
0
S-FUEL CUT-OFF
HORIZONTAL RANGE AFTER FUEL CUT-OFF
IN KILOMETERS
0 2 4 6 8 10 12 14 16 18 20 22 24 26 28 30 32 34 36 38
0 20 40 60 80 100 120 140 160 180 200 220 240 260 280 300 320
TIME IN SECONDS

FIG. NO. A-13
TOTAL VELOCITY VS. TIME
V-2 ROCKET NO. 28
DEC. 8, 1947

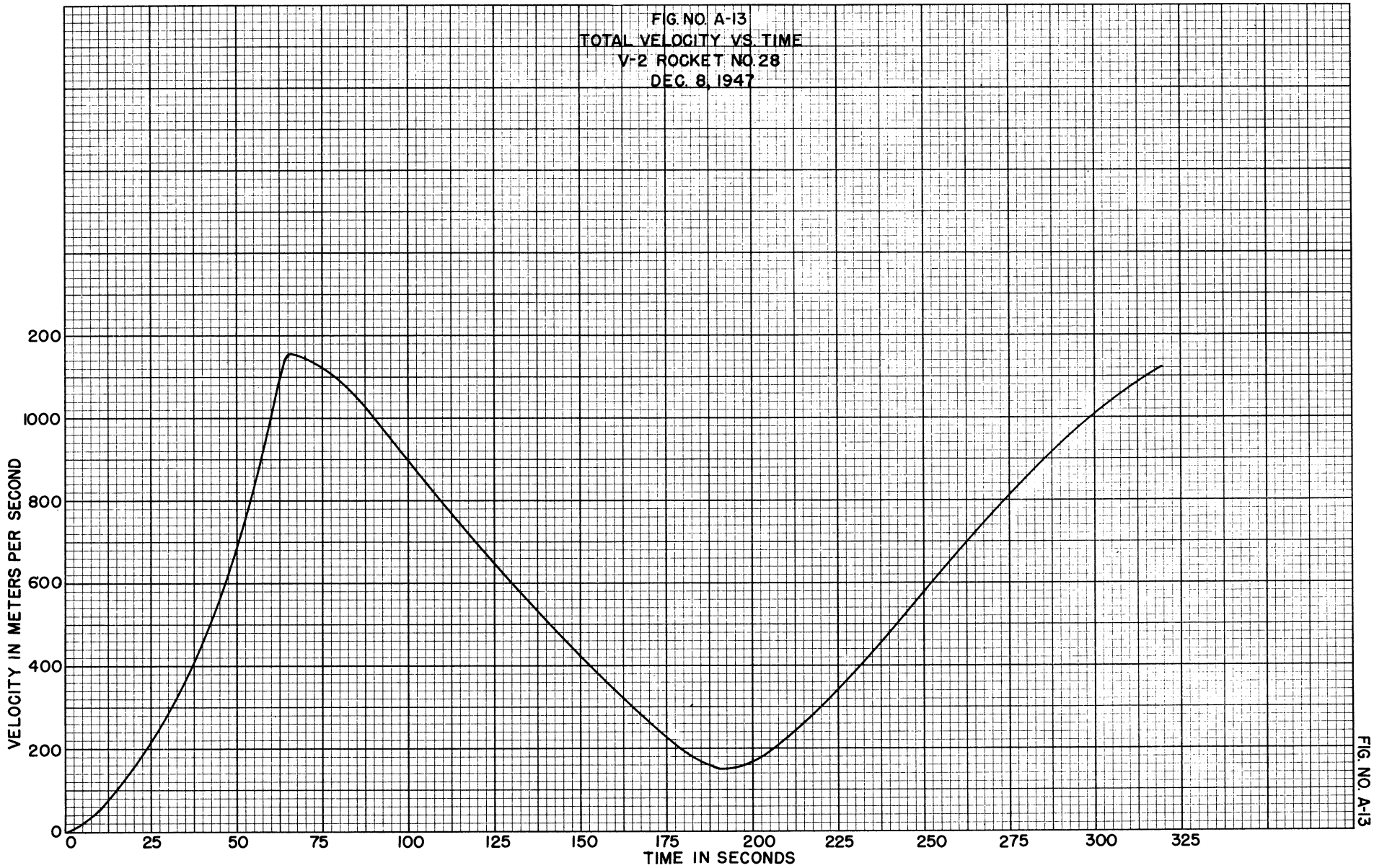

FIG. NO. A-13

FIG. NO. A-14

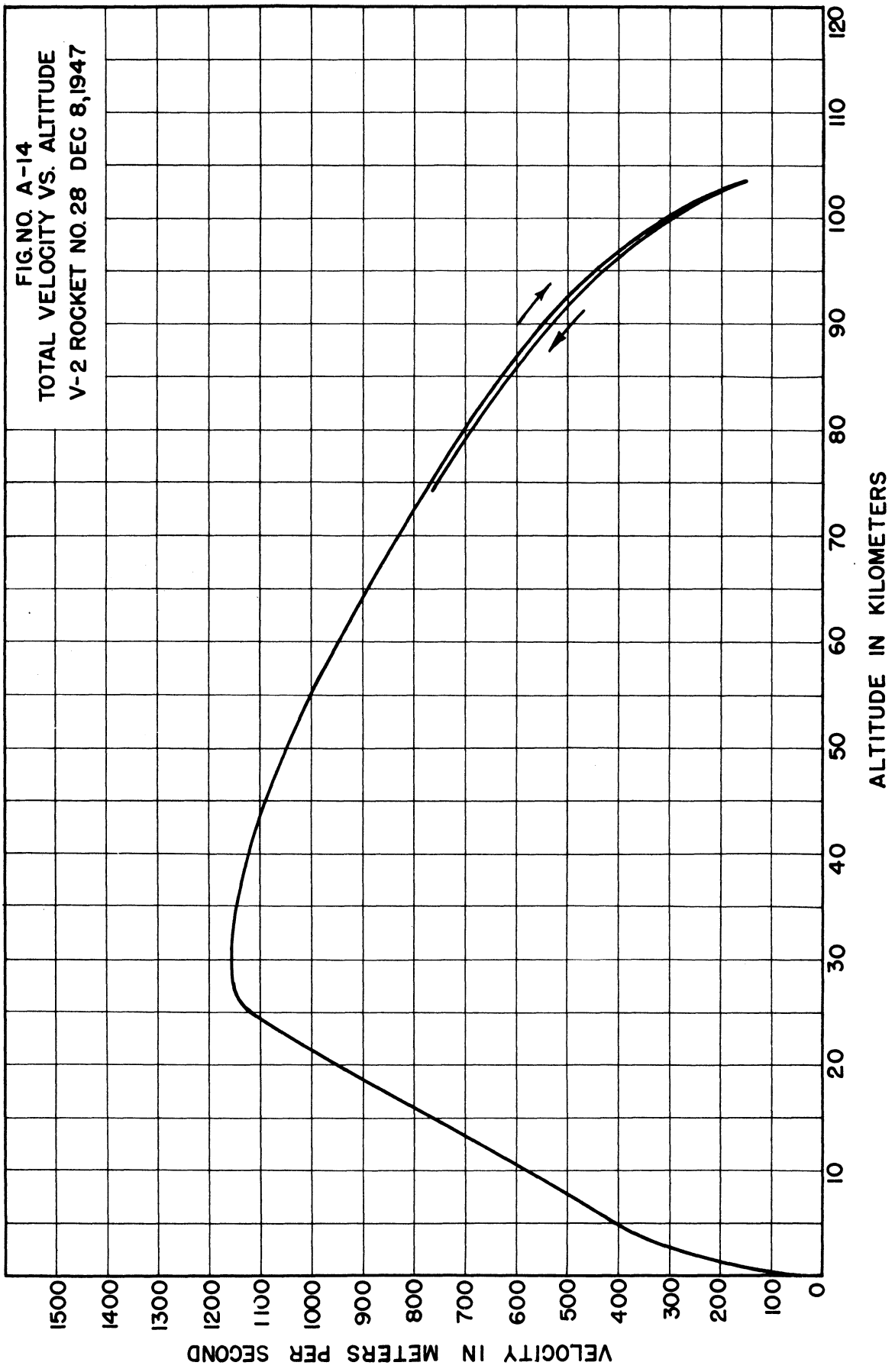
FIG. NO. A-14
TOTAL VELOCITY VS. ALTITUDE
V-2 ROCKET NO. 28 DEC 8, 1947
VELOCITY IN METERS PER SECOND
0
100
200
300
400
500
600
700
800
900
1000
1100
1200
1300
1400
1500
ALTITUDE IN KILOMETERS
10
20
30
40
50
60
70
80
90
100
110
120

APPENDIX B

PRESSURE-MEASUREMENT INSTRUMENTATION

B-1. Introduction

In this appendix will be described the apparatus used in obtaining pressure data on the V-2 rocket flight of December 8, 1947. The instrumentation consisted of five ionization gauges and two Pirani gauges, together with the necessary circuitry for converting the significant data obtained from these pressure gauges into suitable voltages, which could be used by the telemetering system for transmittal from the rocket to the ground.

The rockets fired on November 21, 1946 and February 20, 1947 carried five ionization gauges each, but no Pirani gauges.

The ionization gauge circuits used on these three successful rockets were basically the same. They differed only in minor details from one rocket to the next, the modifications having been made on the basis of experience gained from the previous flights. As mentioned above, the circuit to be discussed here is that which was used on the V-2 fired December 8, 1947.

B-2. Mechanical Design and Construction.

As is pointed out in Appendix D of this report, theoretical considerations showed the desirability of using five ionization gauges for obtaining pressure and temperature information at altitudes from about 100 to 160 kilometers, which originally was the range of altitudes over which it was desired to obtain this information. On the basis of these considerations a nosepiece was designed, which is shown diagrammatically in Figure V-1, and pictorially in Figure B-1. This nosepiece replaced the regular nosepiece of the V-2 (which nosepiece carried the warhead firing mechanism) and was fastened to the warhead by means of bolts. The warhead was rebuilt to carry experimental equipment.

It was intended that the nosepiece would be exposed only at altitudes above about 100 kilometers, so no attempt was made to streamline it. This was justified because of the relatively long mean free path of the gas particles at altitudes above 100 kilometers. Table V-1 shows that at sea level the mean free path is about 7.37×10^{-6} centimeter and from Figure II-4 it can be seen that at an altitude of 100 kilometers the mean free path probably is of the order of 3 centimeters. Therefore, the flat nose of the truncated cone has a diameter equal to only about three or four mean free paths at a 100 kilometer altitude. At sea level a disc having a diameter of three or four mean paths would be only about 25×10^{-6} centimeter (0.00001 inch) across.

During the flight of the rocket from ground level to some altitude at which the truncated-cone nosepiece would be aerodynamically satisfactory, it was necessary to cover this nosepiece with an outer, smooth cone, which is shown in Figure B-2.

Also, it was considered undesirable to expose the ionization gauges (with filaments heated) to ground level pressures because of the possibility of poisoning the gauges and causing them to read pressure inaccurately. Therefore, as pointed out in Appendix C, the ionization gauges were sealed off at a pressure of about 3×10^{-6} millimeter of mercury immediately after calibration. It was not necessary that the gauges be exposed to outside pressures until the rocket had reached the minimum altitude at which it was desired that the pressure readings be started. At this altitude the outer cone would have to be thrown off the rocket. Therefore, it was decided to use the motion involved in throwing off the outer cone to open the ionization gauges to the outside atmosphere.

The details of the outer cone, of its throw-off mechanism, and of the arrangement for opening the ionization gauges, are shown in Figures B-3, B-4, and B-5.

As shown in Figure B-3, the outer cone was made in two pieces by cutting the cone through its axis. Separation of the two halves and "throw-off" were brought about by the action of a 100-pound

spring, which is shown in Figure B-4. In order to insure that both halves of the outer cone would be thrown off, they were geared together.

A latch mechanism was utilized to hold together the two halves of the outer cone until such time as it was desired that they be discarded from the rocket. This latch mechanism was designed to open the outer cone at the end of a predetermined time interval following the initiation of the mechanism. The latch was driven by an electric motor, operating through a gear train, as shown in Figure B-5. The drive mechanism had a speed reduction ratio of 72,000 to 1, and thus provided for very slow movement of the latch. It was in this way that the required time delay in opening the latch was obtained. This time delay depended upon the position of the latch driving lever (see Figure B-5) at the time of starting the motor. By changing this initial position the required time delay could be obtained.

As mentioned previously in this appendix, the ionization gauges were opened to the outside atmosphere by the motion involved in discarding the outer cone. This was accomplished by means of straps mounted on the inside of the outer cone. One each of these straps (visible in Figure B-3) encircled the exposed upright tubulation of each of the ionization gauges and, when the outer cone was thrown off, the tubulation of each ionization gauge was broken off at the break-off groove (illustrated in Figure C-1 and C-6). Numerous laboratory tests proved that the gauge tubulations break off cleanly at the constriction.

The ionization gauge is not readily applicable to the measurement of pressures of greater than about 10^{-2} millimeter of mercury. Reference to Figure II-2 indicated that this pressure should exist at an altitude of about 85 kilometers, and reference to Figure D-4 (using trajectory marked "Complete Use of Fuel for Most Probable Motor Efficiency") indicated that an altitude of 85 kilometers should be attained after about 100 seconds of flight. Therefore, before closing the nosepiece of the rocket prior to launching, the latch mechanism was set to open 120 seconds after the starting of the latch mechanism motor. The additional 20 seconds was to allow for pre-flight circuit testing. Because of variations in motor speed, friction, time spent in testing, etc., the actual opening time varied somewhat for the various flights, the minimum being 81.5 seconds on December 8, 1947, and the maximum being 115 seconds on February 20, 1947. Laboratory tests have shown that this earlier opening time of 81.5 seconds should not have damaged the ionization gauges. Also, the opening time of 115 seconds on the February 20, 1947, rocket was not too late, since the altitude of the rocket at that time was only about 82 kilometers, for this particular flight.

B-3. Electrical Circuits.

As mentioned in the Introduction to this appendix, the circuit design has varied from rocket to rocket, as desirable improvements became evident on the basis of experience gained from previous flights. The circuit discussed here is the one used on the rocket fired December 8, 1947, and thus is of the latest design. This circuit is shown in Figure B-9.

The circuitry consisted of five interrelated sections, which will be discussed separately. These are:

1. Ionization gauge circuit.
2. Pirani gauge circuits.
3. Thermometer circuit.
4. Control circuit.
5. Power supply.

B-3.1. Ionization Gauge Circuit.

This circuit was designed to measure the grid and plate currents of the five ionization gauges, and to convert these current readings into voltages which could be used by the telemetering system for transmission of the information to the ground.

On this rocket (fired December 8, 1947) five ionization gauges were used. Referring to Figure V-1, the particular gauges were used in the numbered positions as follows:

APPENDIX B

Gauge number	Gauge used
1	VG-1A (Distillation Products, Inc.)
2	NRC-507 (National Research Corp.)
3	VG-1A
4	NRC-507
5	VG-1A

On previous rockets all the gauges used were VG-1A. On the December 8, 1947 rocket the two NRC gauges were used in order to determine whether or not any characteristic of the VG-1A gauge might be affecting the pressure readings obtained. The results indicate no such effect.

The Naval Research Laboratory telemetering system, in use at the White Sands Proving Ground, has 23 channels. A brief description of this telemetering system is included in Appendix F. Five of these telemetering channels were made available to the University of Michigan for the December 8, 1947 rocket. These five channels were used for transmitting the following information:

Channel No. 1: Ionization gauge grid currents.
Channel No. 2: Ionization gauge plate currents.
Channel No. 3: Gauge wall thermometer and calibration voltages.
Channel No. 4: Variable-voltage probe current (to be discussed in a later report).
Channel No. 5: Pirani gauge circuit output voltages.

It was necessary to transmit the values of all the ionization gauge grid currents on a single channel, and all the plate current values on a second channel. Therefore, it was necessary to use a commutator. The brushes of this commutator were turned at about 70 R.P.M. The three sections of the commutator were utilized as follows:

Section A commutated the grid currents for Telemetering Channel No. 1; Section B commutated the plate currents for Telemetering Channel No. 2 and Section C commutated the various quantities carried on Telemetering Channel No. 3. Each section of the commutator had six segments. These segments were utilized as follows:

SECTION A (grid currents)	SECTION B (plate currents)	SECTION C (miscellaneous)
Segment	Segment	Segment
No. 1 Gauge No. 1	No. 3 Gauge No. 1	No. 5 Thermometer output voltage
No. 2 Gauge No. 2	No. 4 Gauge No. 2	No. 6 Variable-voltage probe current
No. 3 Gauge No. 3	No. 5 Gauge No. 3	No. 1 Plus 3.1-volt calibration
No. 4 Gauge No. 4	No. 6 Gauge No. 4	No. 2 Grounded to rocket body
No. 5 Gauge No. 5	No. 1 Gauge No. 5	No. 3 Plate current of ionization gauge No. 5
No. 6 Grid current calibration value.	No. 2 Open, corresponding to zero plate current, for calibration.	No. 4 Same as Segment No. 6 of Section A.

The brushes on successive commutator sections were displaced from each other by 120 degrees, and this accounts for the shift, by two segments, from one section to the next, as shown in the above listing of functions. The information carried on the various segments of the commutator appears on the various channels of the telemetering record in the same order that it is listed above. That is, Segment No. 1 of Section A of the commutator carried the data shown in Position No. 1 of Channel No. 1 of the telemetering record (shown in Figure F-2); Segment No. 3 of Section B of the commutator carried the information shown in Position No. 1 of Channel No. 2 on the record; Segment No. 5 of Section C corresponded to Position No. 1 of Channel No. 3 on the record; and so on.

The NRL telemetering system automatically inserts into each telemetering channel, at regular intervals, one pulse corresponding to a telemetering voltage in the rocket of zero volts and one pulse corresponding to a telemetering voltage of 3.5 volts. These pulses furnish a continuous calibration of the telemetering system during the flight of the rocket. It was decided that it would be well, as in insurance against failure of the NRL calibration pulses, to provide a calibration means within the University of Michigan equipment. One way to do this would be to introduce periodically into each telemetering channel several different known voltages. However, a highly satisfactory alternative method was devised which utilized equipment already required for other purposes.

Four segments were available on Section C of the commutator. A calibration voltage of three volts was connected to Segment No. 1, and Segment No. 2 was grounded to the body of the rocket and thus had zero voltage on it. The telemetering voltage corresponding to the plate current of ionization gauge No. 5 was connected to Segment No. 3 of Section C of the commutator, as well as to Segment No. 1 of Section B. The voltage corresponding to the value of current used as a grid current calibration value on Channel No. 1 (appearing on Segment No. 6 of Section A of the commutator) was connected to Segment No. 4 of Section C. Thus, Telemetering Channel No. 3 was continuously calibrated by the two calibration voltages mentioned above. Then the currents appearing on Segments No. 3 and No. 4 of Section C of the commutator could be determined. These known currents also appeared in Telemetering Channels No. 1 and No. 2 and thus could be used as calibration values on these channels.

The ionization gauge circuitry (illustrated in the circuit diagram of Figure B-9) was contained in a circuit box which was mounted in the warhead, just behind the nosepiece. This circuit box is shown in Figures B-6 and B-7. Figure B-8 is a photograph of the bottom of the nosepiece and shows how connections were made between it and the connectors on the pressurized cover of the warhead, for connection to the circuit box.

As pointed out in the Introduction to this appendix, the complete ionization gauge and control circuit is shown in Figure B-9, and reference to this figure will be necessary in reading the following discussion of the circuitry.

The theory of the ionization gauge is discussed in Appendix C, and, as stated there, the ionization gauge operates at a positive grid voltage and at a negative plate voltage. The positive grid voltage (approximately 150 volts) was supplied by Vibrator B and it was switched from one ionization gauge to another by Section A of the commutator. However, it was found that undesirable transients were set up when the grid voltage was reapplied, if the grids of the ionization gauges were left open-circuited while the grid voltage was being applied to the other gauges. To prevent this, a fixed positive potential of 135 volts was supplied by Vibrator A and fed through a crystal directly to each of the ionization gauge grids. When the plus 150 volts was applied through Section A of the commutator to the grid of an ionization gauge, the grid side of the 1N34 crystal connected to that particular grid became more positive than the power supply side of the crystal, so the crystal became in effect an open circuit and disconnected the power supply of Vibrator A from the grid. This insured that essentially all the ionization gauge grid current would flow through the network of R_1, R_4 and the 1N34, and thus be measured.

From the circuit diagram, it can be seen that the voltage applied to Telemetering Channel No. 1 was:

$$E_{T_1} = 4.5 - 1500\, I_g \qquad \text{(B-1)}$$

up to a grid current (I_g) of one milliampere. When the grid current exceeded one milliampere, the voltage drop across R_1 was greater than 1.5 volts, and of such a polarity as to cause the 1N34 crystal (connected in series with R_4) to conduct, in spite of the 1.5-volt battery in series with the 1N34 crystal. Then, for grid currents greater than one milliampere, the telemetering voltage was:

$$E_{T_1} = 4.5 - \frac{I_g (R_4 + R_X) + 1.5}{R_1 + R_4 + R_X} R_1 \qquad \text{(B-2)}$$

where R_X is the forward resistance of the 1N34 crystal. Of course, R_X was nonlinear but this caused no difficulty since a calibration was made of E_{T_1} versus I_g. R_X amounted to about 200 or 300 ohms. Therefore:

$$R_1 \cong R_1 + R_4 + R_X \qquad \text{(B-3)}$$

Assuming that this equation is true, there results from Equation B-2:

$$E_T = 3.0 - I_g (R_4 + R_X) \qquad \text{(B-4)}$$

This allowed a maximum value of I_g of about ten milliamperes, for $E_T = 0$.

The plate current of the ionization gauges varied from a few tenths of a microampere to several hundred microamperes. The useful range of voltage which may be applied to the telemetering system is from a few tenths of a volt to about six volts. Therefore, it was necessary to provide a non-linear relation between gauge plate current and telemetering voltage. This was done by using the diode V1A. This diode was so biased that it did not conduct until the voltage drop across R_9 became about three volts (corresponding to a plate current of about 25 microamperes). For larger values of plate current, the diode V1A conducted, and the plate load of the ionization gauge became the network composed of R_9, R_{10}, V1A and the 3-volt battery. This resulted in a much lower plate load. In fact, after diode V1A started to conduct, the plate current of the ionization gauge produced a grid voltage on the cathode follower (V2A) of:

$$E_G = 3.0 + 10{,}000\ I_p \qquad \text{(B-5)}$$

The maximum allowable value of E_G was about 8 volts for a telemetering voltage of 5 volts, so this circuit was capable of measuring values of ionization gauge plate current up to about 500 microamperes. However, somewhat larger values of plate current could be measured, even though they caused the telemetering voltage to exceed five volts, because the telemetering system will accept input voltages up to a maximum of six volts, although it is desirable (for reasons of accuracy) to keep this input below five volts.

The cathode follower (V2A) was used so that the output impedance, used to feed the plate current information to Telemetering Channel No. 2, was a few hundred ohms rather than of the order of 100,000 ohms, which was the approximate output impedance of the ionization gauge, as used.

The filament current of the ionization gauges could be adjusted by the filament rheostats (R_7 and R_8 of Figure B-9). The filament rheostats were so adjusted, before rocket take-off, that the filament emission during flight would result in a grid current which remained within reasonable limits. This adjustment was made on the basis of experience gained from previous firings, tempered with judgement.

B-3.2. Pirani Gauge Circuit.

Two Pirani gauges were used on the rocket fired December 8, 1947. One (a WL-762 gauge, manufactured by the Westinghouse Electric Corp.) was mounted near the tail of the rocket, a few inches forward of Fin No. 1, and about 10 degrees toward Fin No. 4 from Fin No. 1. The other (a special gauge constructed at the University of Michigan) was mounted near the nose of the rocket, about two feet back from the tip of the outer cone. Its azimuthal position was the same as that of the other Pirani gauge.

Photographs of the two Pirani gauges used are shown in Figures C-17 and C-18, and diagrams of these gauges are contained in Figures C-15 and C-16. The theory of operation and the method of calibration of the Pirani gauges are contained in Appendix C.

The circuits used in the rocket for the two Pirani gauges were identical to the circuits used for their calibration. The calibration circuits are shown in Figures C-19 and C-20. The power supply for the WL-762 gauge was a special 22.5-volt battery, and that for the special gauge was the 105-volt B-supply of the ionization gauge circuit.

A separate commutator and commutator motor were used for the Pirani gauges. This commutator motor was connected directly across the main storage battery of the system. The circuit was energized by means of an acceleration switch, which was designed to close when the net upward acceleration became one g. This occurred at about 5 seconds after launching. The commutation speed was about 90 R. P. M.

The Pirani gauge commutator had eight segments, which were used as follows:

Segment	
1	Ground
2	Battery voltage (22.5 volts)
3	Special calibrating voltage (from a special 4.5-volt battery)
4	Nose gauge output voltage (special Pirani gauge)
5	Tail gauge output voltage (WL-762 Pirani gauge)
6	Nose gauge output voltage
7	Tail gauge output voltage
8	Nose gauge output voltage

The output of this Pirani gauge commutator was supplied to Telemetering Channel No. 5.

B-3.3. Thermometer Circuit.

As pointed out in Appendix D, it was important that information be obtained concerning the temperature of the envelope of the ionization gauges during the flight of the rocket, since the assumption was made that the temperature of the gas was that of the envelope of the gauge. Therefore, a platinum wire (0.001 inch in diameter) was wrapped around ionization gauge No. 1, to be used as a thermometer in determining the temperature of the wall of this gauge. A photograph of this arrangement is shown in Figure C-2. An essentially constant current was passed through the platinum wire thermometer and the voltage across the thermometer was measured. The resistance of the platinum wire increased with an increase of temperature, thus the voltage drop across the thermometer was a function of temperature. The output voltage of the thermometer was applied to Segment No. 5 of Section C of the commutator.

A thermometer was used on only one gauge, since a thermometer had been used on each ionization gauge of the rockets fired November 21, 1946 and February 20, 1947 and these showed that the temperatures of all five gauges were practically the same.

B-3.4. Control Circuit.

The control circuit is illustrated in Figure B-9. The circuit was used for testing all the University of Michigan apparatus which was carried on the rocket after the rocket had been erected on the launching stand, and for turning on this apparatus just prior to launching of the rocket. The control circuit was operated, remotely, from the blockhouse at the launching site.

The control circuit consisted of three relays. Relay A was operated by the blockhouse control called "Test"; Relay B by the blockhouse control called "Lock-on"; and Relay C by the control called "Cut-off."

For testing, prior to rocket launching, Relay A was energized from the blockhouse. When Relay A was energized, its single pair of contacts were closed. The closing of the Relay A contacts connected the main storage battery to the rest of the circuit (as shown in Figure B-9). This started the two vibrator power supplies and heated the filaments of all the tubes. The latch motor (which drove the latch mechanism for throwing off the outer cone) was not turned on by the energizing of Relay A.

Relay B was energized from the blockhouse about five seconds before rocket take-off. The closing of the contacts of this relay accomplished the following:

1. Energized Relay A, which connected the main storage battery, which, in turn, started the two vibrator power supplies and energized all the tube filaments.

2. Connected the ionization gauge commutator motor and the latch motor to the main storage battery.

3. Connected the coil of Relay B to the main storage battery, so that Relay B would continue to be energized after the rocket left the ground. In this way, the disconnecting of the power leads from the blockhouse to the rocket would have no effect upon the circuit.

Relay C was provided so that all the University of Michigan equipment in the rocket could be turned off from the blockhouse in the event the rocket was not launched after Relay B was energized

and self-locked. The blockhouse controls were so arranged that closing of the blockhouse "Cut-off" control would de-energize Relays A and B and completely shut-off the rocket-borne equipment.

B-3.5. Power Supply.

The prime source of power was a 6-volt, 100-ampere-hour automobile storage battery. The load on it was between 30 and 40 amperes. This proved to be a very reliable source of power. During much of the downward flight the battery was subjected to the rather wild gyrations of the rocket, but the records indicate that the output was stable, even under these rather extreme operating conditions.

Two vibrator power supplies were used to convert d-c power, available from the 6-volt storage battery, to higher voltage d-c power. Vibrator A, with its associated filter and voltage regulators, supplied power for the ionization gauge grids and for most of the other high voltage needs. Vibrator B supplied the power for the ionization gauge grids during the measurement of grid current. These vibrator power supplies performed very satisfactorily on all three of the successful rockets carrying University of Michigan equipment.

Miscellaneous small dry-cell batteries were used in the circuit. In general, their use was confined to that of biasing, where little or no power was required of them. The 45-volt battery, used to supply the plate voltage for the ionization gauges, had a current drain of less than one milliampere, since the plate current of the ionization gauges was always less than this amount.

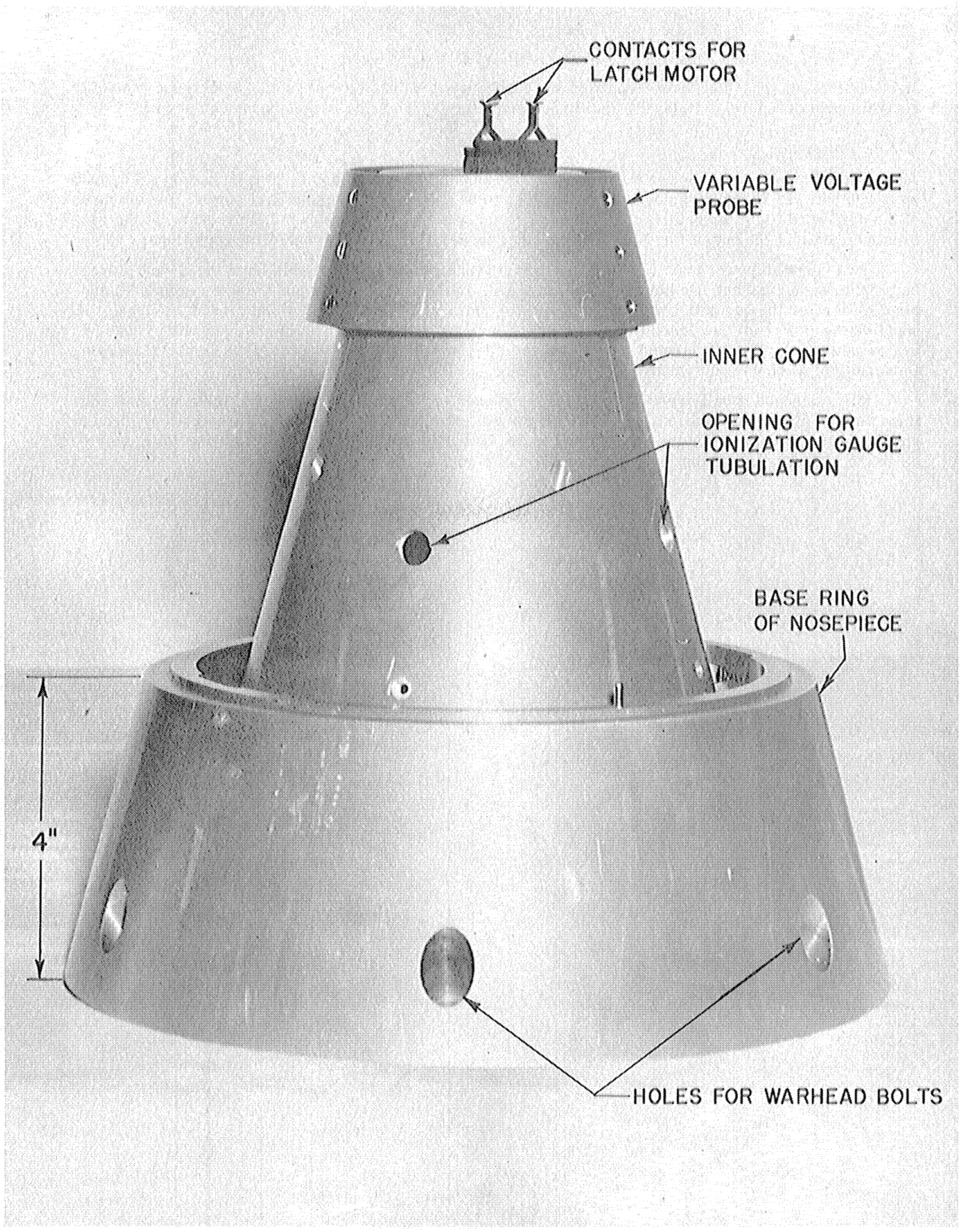

FIG. NO. B-1
NOSEPIECE WITH OUTER CONE SURFACES REMOVED

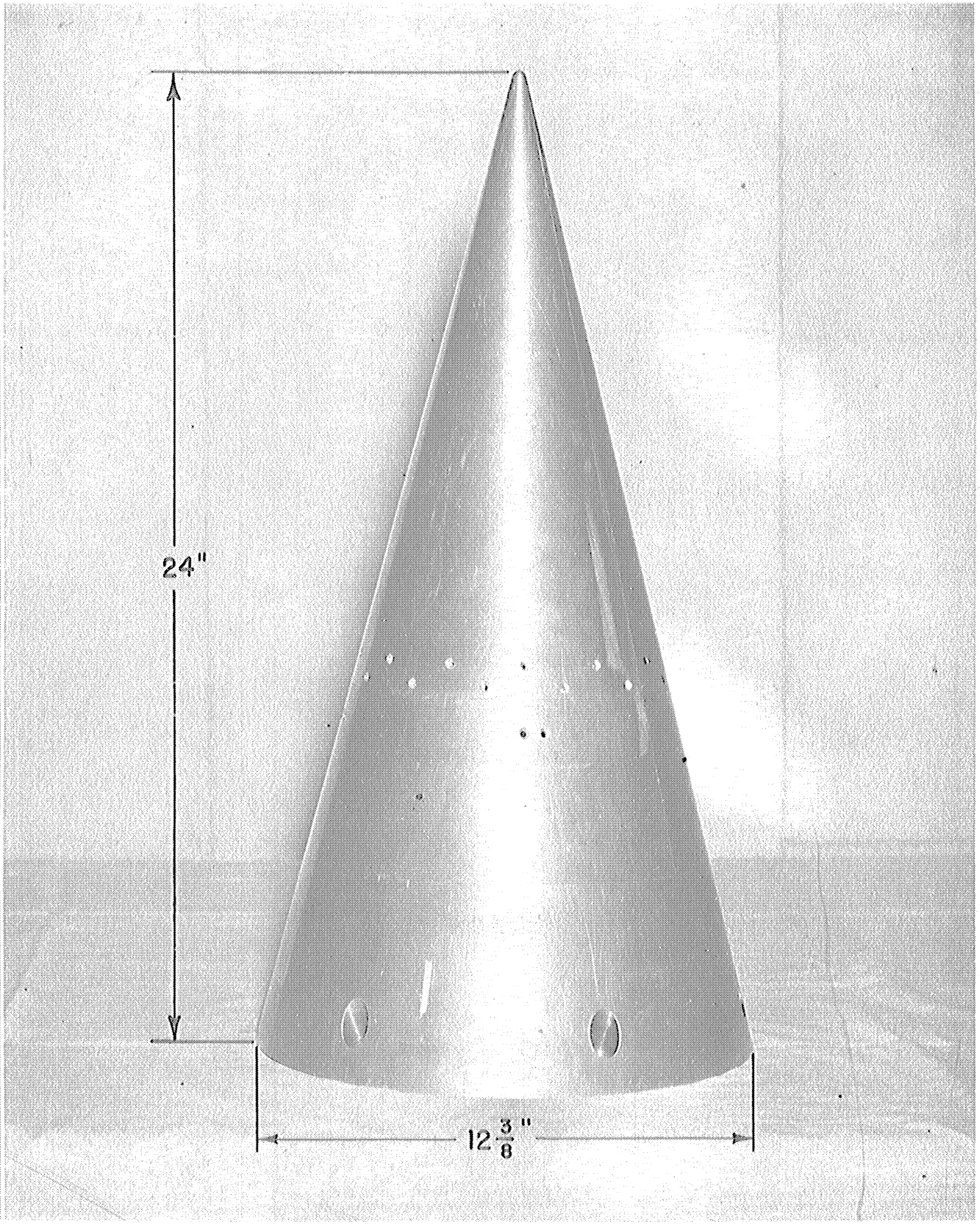

FIG. NO. B-2
NOSEPIECE WITH OUTER CONE IN PLACE

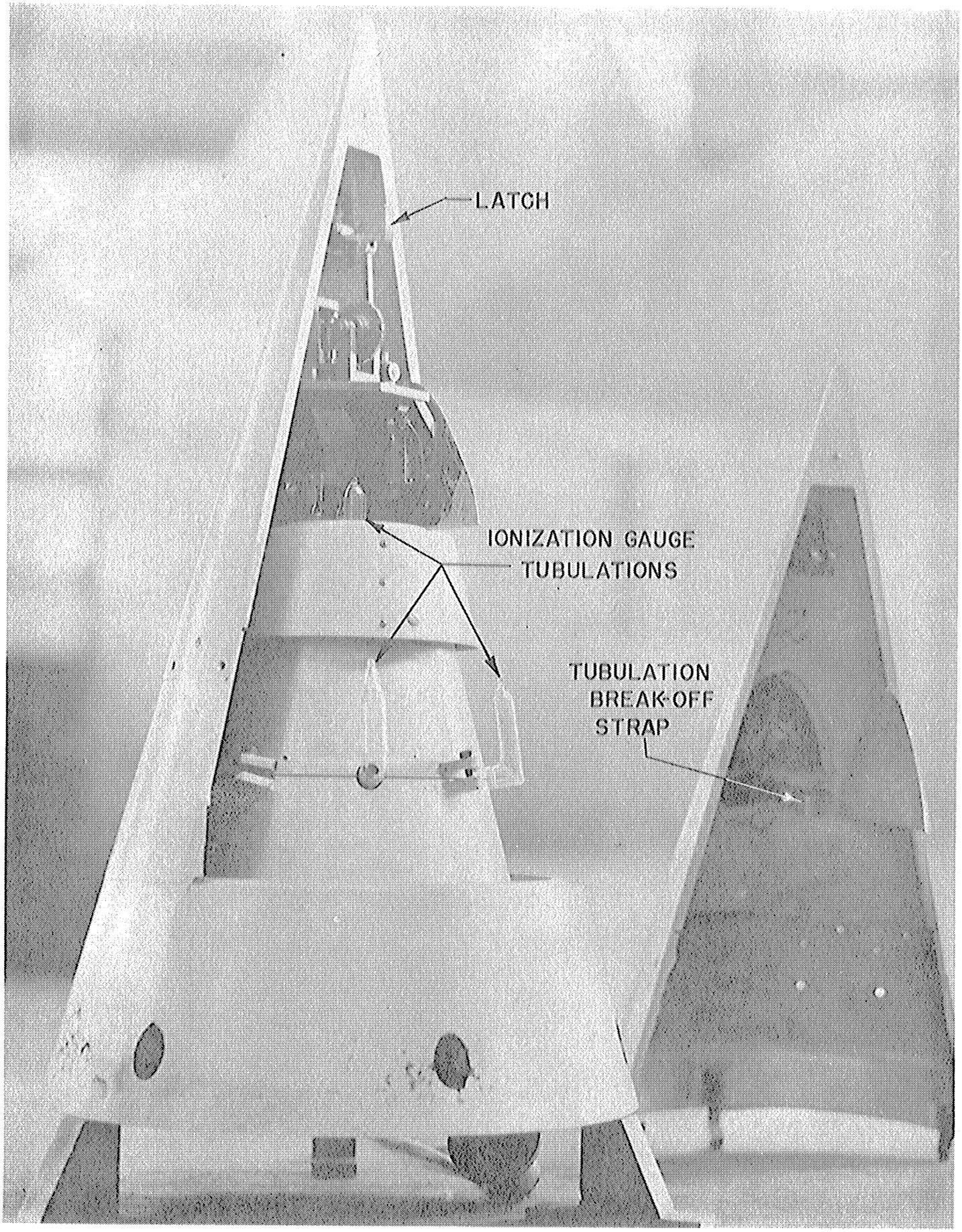

FIG. NO. B-3
NOSEPIECE WITH ONE HALF OF OUTER CONE REMOVED

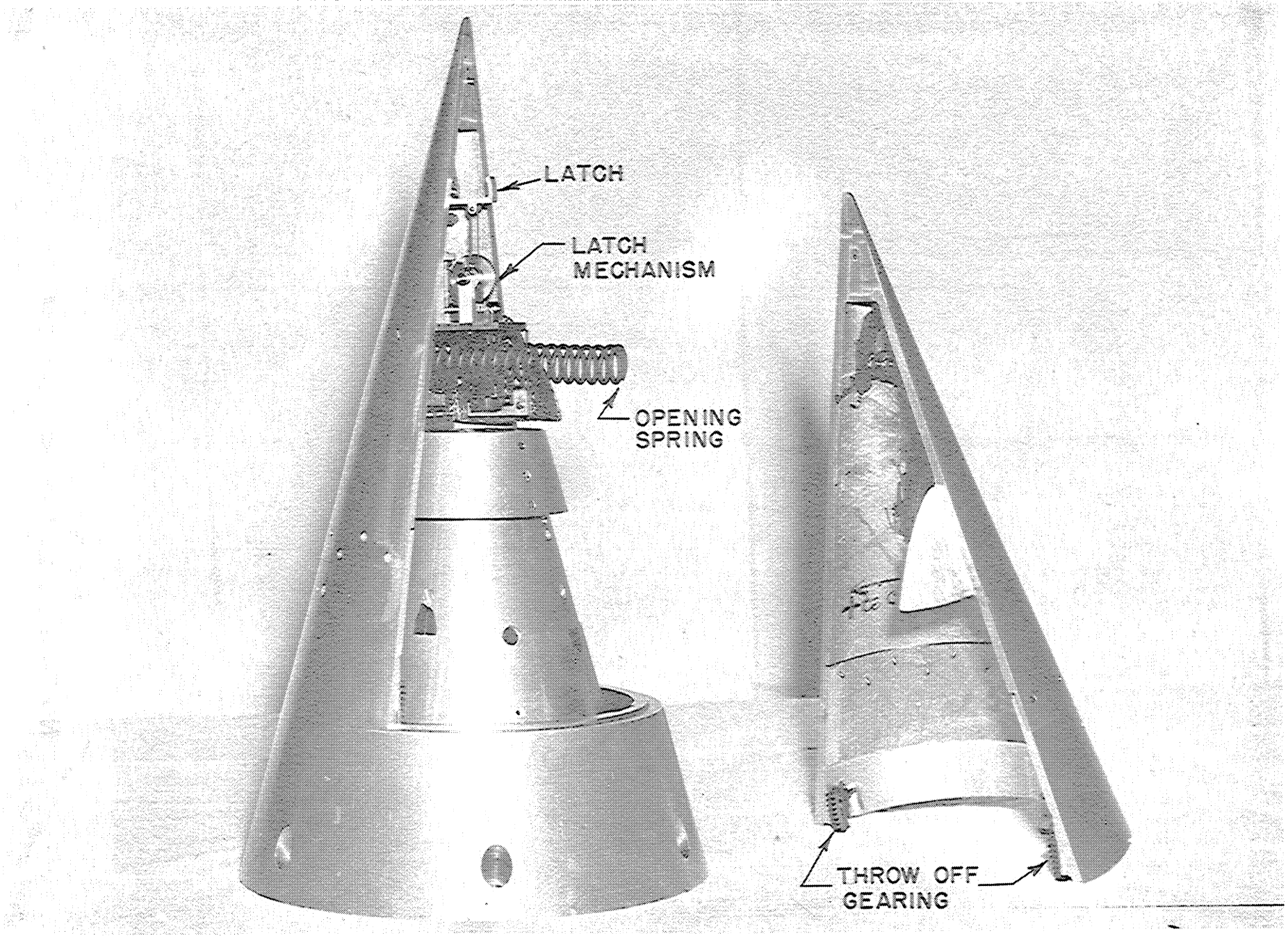

FIG. NO. B-4
VIEW OF NOSEPIECE WITH OPENING SPRING IN PLACE

FIG. NO. B-4

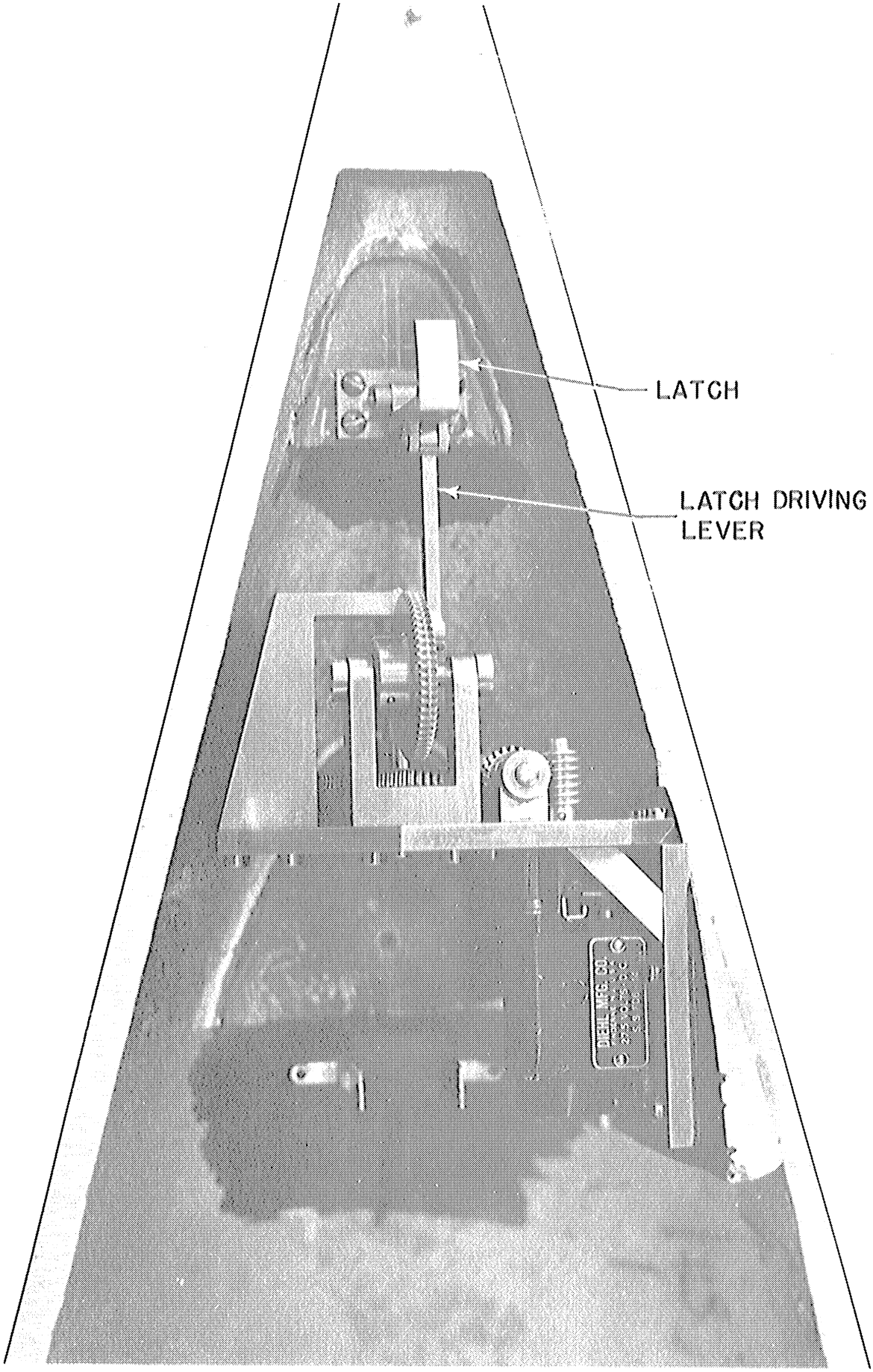

FIG. NO. B-5
NOSEPIECE LATCH MECHANISM

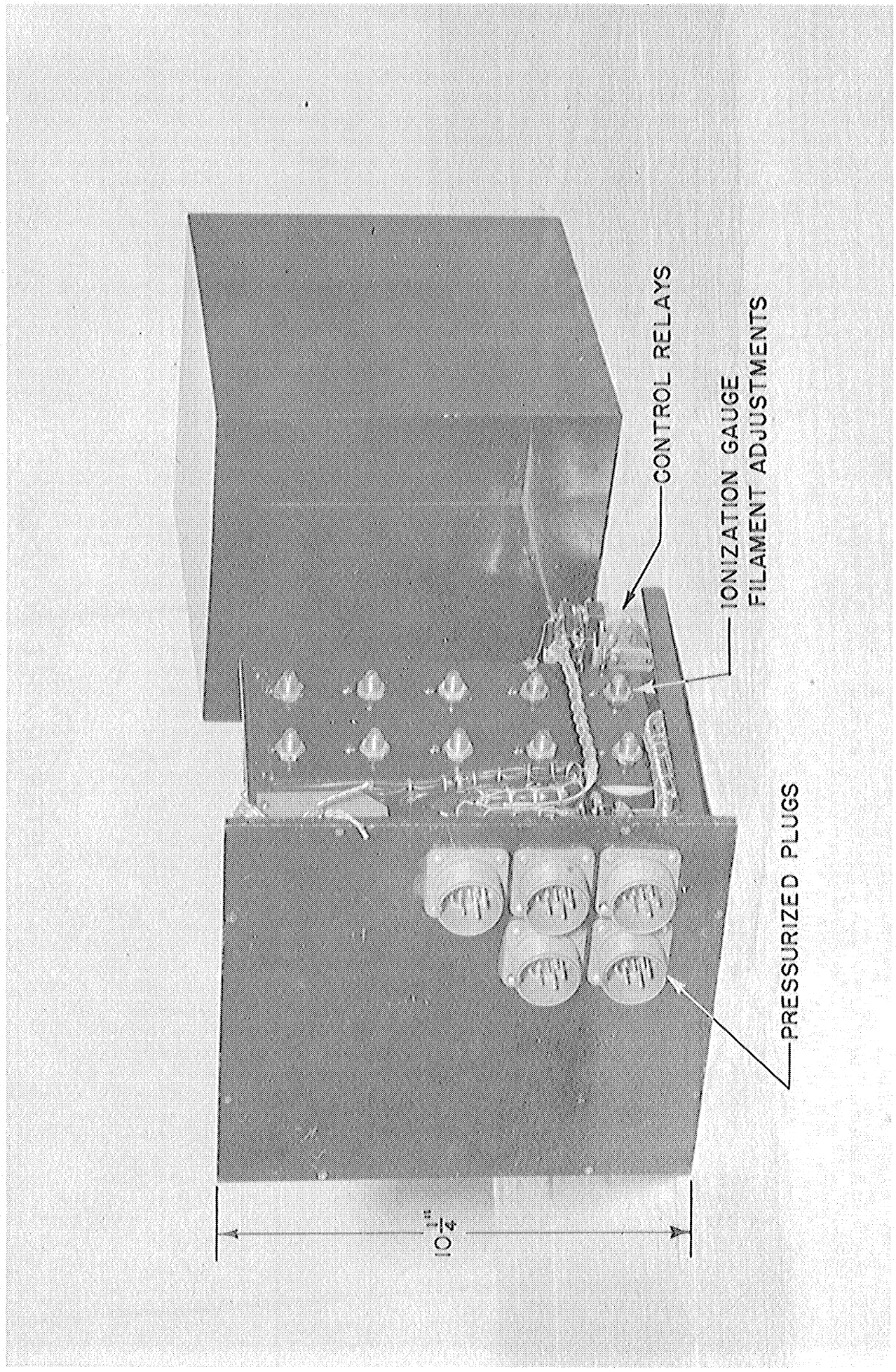

FIG. NO. B-6
FRONT VIEW OF CIRCUIT BOX

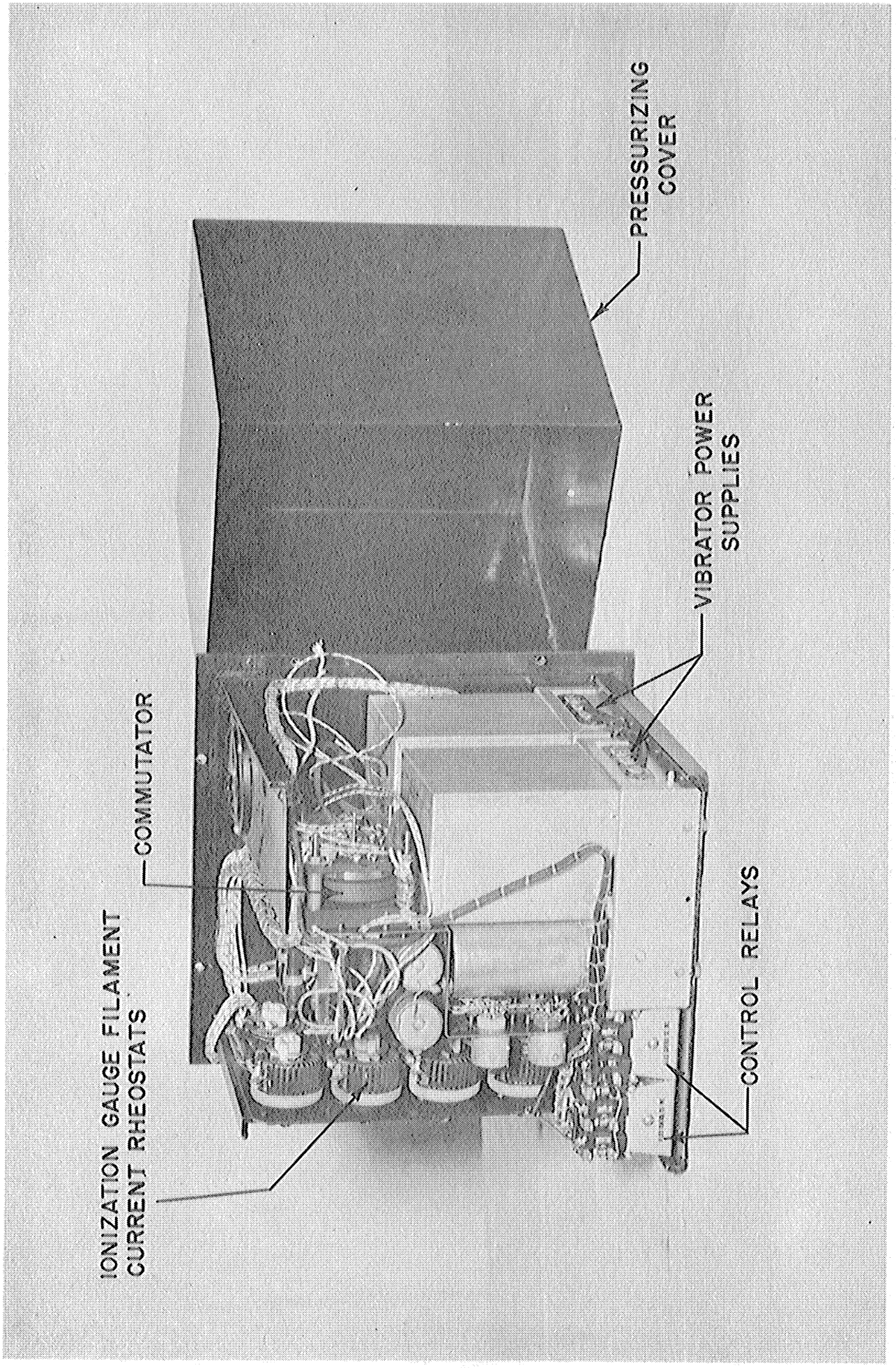

FIG. NO. B-7
INTERIOR OF CIRCUIT BOX

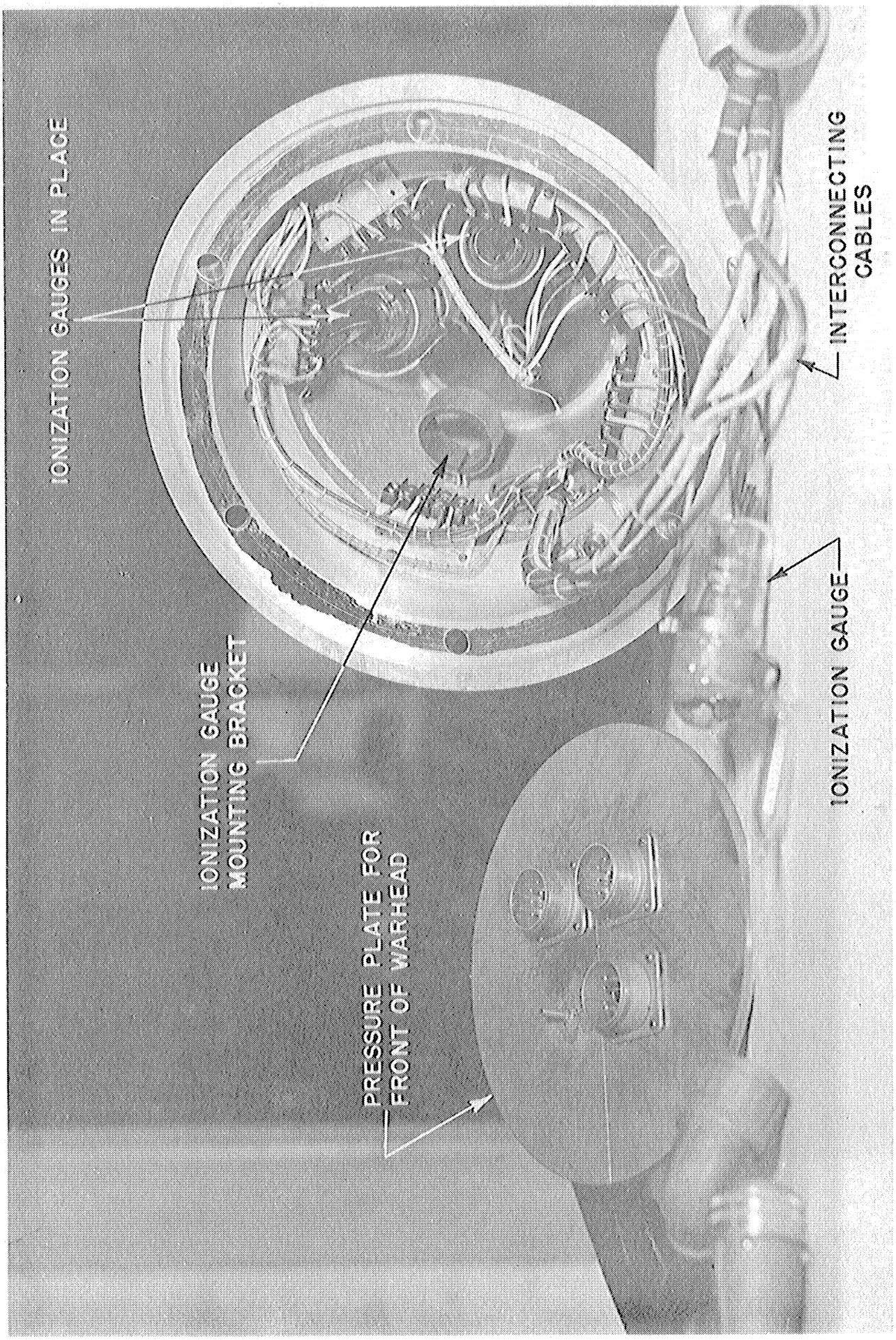

FIG. NO. B-8
BOTTOM VIEW OF NOSEPIECE

FIG. NO. B-9

IONIZATION GAUGE AND CONTROL CIRCUIT

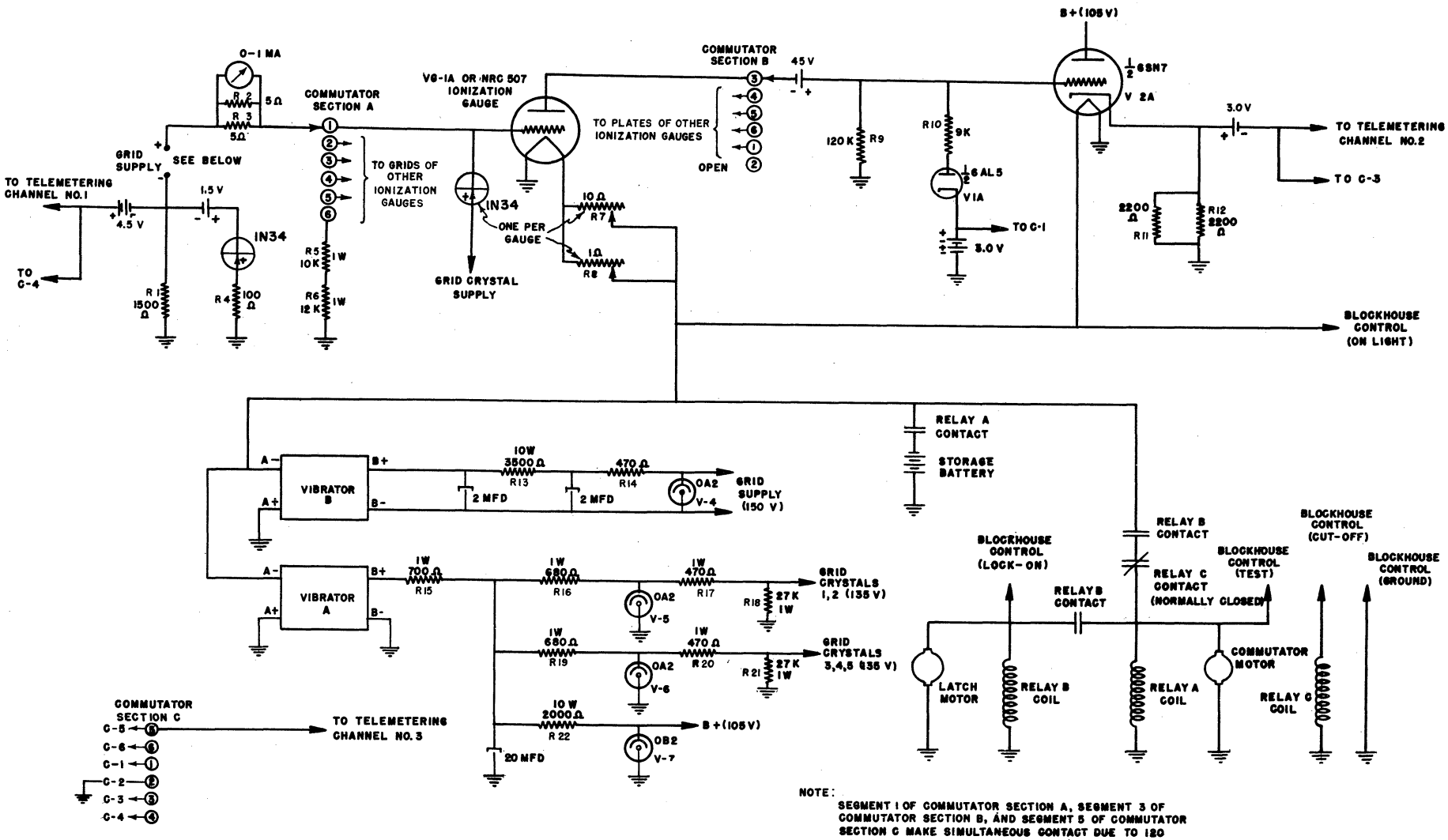

NOTE:

SEGMENT 1 OF COMMUTATOR SECTION A, SEGMENT 3 OF COMMUTATOR SECTION B, AND SEGMENT 5 OF COMMUTATOR SECTION C MAKE SIMULTANEOUS CONTACT DUE TO 120 DEGREES SEPARATION OF THREE COMMUTATOR BRUSHES. SIMILARLY FOR OTHER SEGMENT.

APPENDIX C

THEORY AND PROCEDURE FOR CALIBRATION OF PRESSURE GAUGES USED

C-1. Introduction.

As is pointed out in Section V of this report, only ionization gauges were carried on the rockets fired August 22, 1946, November 21, 1946 and February 20, 1947. This was done because early in the project the objective was to measure only pressures and temperatures in the ionosphere. On the basis of indirect estimates of the type presented in Figure II-2, it appeared that the pressure range to be measured was from about 3×10^{-5} to 2×10^{-3} millimeter of mercury. The ionization gauge is admirably suited to measuring pressures in this range, but not easily adapted to reading higher values of pressure. In the fall of 1947 circumstances arose which made it important to obtain pressure data from near ground level to rocket ceiling. Therefore, on the December 8, 1947 rocket two Pirani gauges also were carried, in order to measure pressures at altitudes from about 40 to 75 kilometers, or over a pressure range of about 5×10^{-2} to 5 millimeters of mercury.

The gauges carried on each of the successful University of Michigan rockets were as follows:

November 21, 1946

5 VG-1A Ionization Gauges (Manufactured by Distillation Products, Inc.)

February 20, 1947

5 VG-1A Ionization Gauges (Manufactured by Distillation Products, Inc.)

December 8, 1947

3 VG-1A Ionization Gauges (Manufactured by Distillation Products, Inc.)

2 NRC-507 Ionization Gauges (Manufactured by National Research Corp.)

1 WL-762 Pirani Gauge (Manufactured by Westinghouse Electric Corp.)

1 Special Pirani Gauge (See Figures C-16 and C-18)

In this appendix the theory of operation of ionization and Pirani gauges will be discussed, and the methods used at the University of Michigan for calibrating them will be described.

C-2. Theory of Operation of Ionization Gauges.

Details of the VG-1A ionization gauge are shown in Figures C-1 through C-4. Figure C-1 is a cross-sectional drawing of the gauge showing internal details and, in addition, details of the tubulation and of the thermometer which was attached to some of the gauges used. Figure C-2 is a photograph of the same gauge. Figures C-3 and C-4 are photographs of ionization gauges designed for use on the side and on the flat nose, respectively, of the truncated cone forming the nosepiece of the rocket. These gauges are shown without thermometers.

Details of the NRC-507 ionization gauge are shown in a photograph in Figure C-5 and in a diagram in Figure C-6.

An ionization gauge is essentially a three element tube which consists of a heated filament, a grid and a plate. The filament of an ionization gauge serves as the electron source. It is operated under emission-limited conditions and the electron current is controlled by adjusting the filament temperature (by adjusting applied filament voltage) to obtain the desired emission current. The grid, which operates at a positive voltage with respect to the filament, attracts (and thus accelerates) the negative electrons from the filament, and also serves as the electron collector.

If an electron, in its trajectory from filament to grid, collides with a gas particle, the electron will ionize the latter if the following relation is satisfied:

$$\frac{1}{2} mu^2 > Ve \qquad (C\text{-}1)$$

where m = mass of the electron
u = velocity of the electron
V = ionization potential of the gas
e = charge of the electron.

The electron released from the ionized particle, as well as the bombarding electron, will be attracted to the grid, whereas the positively charged ion will be attracted to the plate, which is at a slightly negative potential relative to the filament.

The ratio of the positive ion current (plate current) to the electron current is approximately proportional to the density of the gas within the tube-element structure, for a given set of applied voltages, provided the mean free path of the gas particles is greater than the order of magnitude of the spacings between the elements, as explained later in this appendix. Since, for a fixed temperature, the gas pressure is proportional to the gas density, the following relation holds approximately:

$$P = K \frac{I_p}{I_e} \qquad (C\text{-}2)$$

where I_p = positive ion current
I_e = electron bombarding current
K = proportionality factor.

The proportionality factor, K, is dependent on internal gauge dimensions, on electrode voltages and on the nature of the gas.

The sensitivity of the ionization gauge (defined as the ratio of plate current to pressure with other factors held constant) as a function of plate voltage and of grid voltage may be inferred from Figures C-7 and C-8, respectively, since each of these curves was obtained at a constant pressure, and thus the sensitivity is directly proportional to the plate current shown in these curves. For a given set of values of grid voltage, electron current and pressure, the plate current reading is almost independent of the value of plate voltage used, provided it is above a certain critical value. Below this critical value, which is around -3 volts, the electrons have sufficient energy to strike the plate in spite of the repulsion due to its negative potential, thereby producing a "negative" component of plate current. Above this critical value the plate voltage affects the rate of ion production by reducing the length of the electron path due to repulsion by the negative plate.

For a given set of values of plate voltage, electron current and pressure, the plate current reading is approximately proportional to grid voltage. The higher grid voltages will give a higher rate of ion production by increasing the length of the trajectory of some of the electrons due to their higher energy. With the higher grid voltage, the electrons which do not strike the grid on the first flight towards the grid will oscillate more times between the filament-grid region and the grid-plate region before they finally strike the grid. Of course this increases the number of gas molecules struck, and ionized.

The lower limit of pressure which can be measured with an ionization gauge depends on the sensitivity of the plate current measuring device, and on the current leakage occurring in the circuit and in the gauge. This lower limit of pressure is of the order of 10^{-6} to 10^{-8} millimeter of mercury. The upper limit of pressure is approximately 10^{-2} millimeter of mercury, above which a glow discharge is set up within the electrode structure of the gauge. Also, prolonged operation at such relatively high pressures results in destruction of the filament. However, this effect is of no importance in the present use, due to the short time during which the heated filament is exposed to the outside atmosphere in the course of a rocket flight.

Typical calibration data for the two types of ionization gauges (the VG-1A and NRC-507 ionization gauges) are shown in Figures C-9 and C-10, respectively. The non-linearity of the curves in the high grid current and high pressure region is due, in part, to electrons colliding with more than one gas par-

ticle because of the short mean free path of the gas. The non-linearity of the curves is also due, in part, to measurement of the electron current in the grid circuit instead of in the cathode circuit. After a collision of an electron with a gas particle, the additional electron produced, as a result of the ionization, is attracted to the grid along with the colliding electron. The plate current return circuit, therefore, is through the grid and is in such a direction as to increase the electron current reading. Hence, for high values of positive ion current, the electron current as measured in the grid circuit is not the true bombarding current but it is high by the magnitude of the plate current. In both the calibration and in the rocket instrumentation circuits the bombarding current is measured in series with the grid. Thus, no error is introduced because of this effect. Figure C-11 shows the block diagram of the ionization gauge control circuit used during calibration, and illustrates how the plate and grid currents are actually measured.

C-3. Ionization Gauge Calibration Procedure.

Each ionization gauge is individually calibrated by comparison with a McLeod gauge. The vacuum system on which the gauges are calibrated is shown diagrammatically in Figure C-12. This diagram shows the arrangement of the vacuum pumps, stopcocks, cold trap and vacuum gauges. Figure C-13 is a photograph of this vacuum system.

The McLeod gauge, which is used as the calibrating standard, is an absolute vacuum gauge. This means that the calibration of the McLeod gauge depends only on its physical characteristics and it need not be calibrated against any other instrument. The McLeod gauge takes a known volume of the gas, the pressure of which is to be measured, and compresses it to a measurable volume and pressure. By the use of the gas law the unknown pressure can be calculated. The diagram of a McLeod gauge is shown in Figure C-14. The gas, the pressure of which is to be measured, is entrapped in the volume, V, by raising the mercury reservoir slowly until the mercury level is at C-C'. The gas is then compressed further, by raising the mercury reservoir, until the mercury rises in the comparison capillary to the same level as the top of the closed capillary, which is connected to the volume V. The area of the comparison capillary is the same as the area of the closed capillary on top of the bulb, in order to eliminate errors due to the capillarity effect of the small diameter bores of the two tubes. After compression, the mercury in the closed capillary will be at a distance, h, below the top of this capillary. The unknown pressure of the gas can now be calculated by using the gas law:

$$PV = P'V' \tag{C-3}$$

where: P = pressure (in millimeters of mercury) of the gas under test, prior to compression.
V = volume (in cubic millimeters) of the gas under test, prior to compression, which is the volume of the McLeod guage bulb plus the volume of the closed capillary.
P' = pressure (in millimeters of mercury) of the gas under test after compression.
V' = volume (in cubic millimeters) of the gas under test, after compression.

Then

$$P' = h + P \tag{C-4}$$

$$V' = Ah \tag{C-5}$$

where: h = distance (in millimeters) of top of mercury volumn in closed capillary below top of this capillary.
A = cross-sectional area (in square millimeters) of closed capillary.

Now, using Equation C-4 and C-5 in Equation C-3, we obtain:

$$PV = (h + P)(Ah) \tag{C-6}$$

or, solving for the unknown P:

$$P = \frac{Ah^2}{V + Ah} \tag{C-7}$$

In gauges where the bulb volume is large and the capillary is small the denominator is practically V. Therefore:

$$P = \frac{Ah^2}{V} \tag{C-8}$$

All the above analysis depends on the validity of the gas law, which, for all practical purposes, is valid at the pressures with which we are dealing.

The ratio of area to volume $\left(\frac{A}{V}\right)$ is known as the calibration constant of the gauge. The McLeod gauge used for calibrating the ionization gauges has a calibration constant of 5.421×10^{-6} millimeter.$^{-1}$ The second McLeod gauge (used for calibrating the Pirani gauges) has a calibration constant of 7.514×10^{-4} millimeter.$^{-1}$

The step-by-step procedure used for calibrating the ionization gauges is as follows (reference to Figure C-12 will be helpful in reading the following):

1. The gauge to be calibrated is sealed onto the vacuum system and the vacuum pumps are started.

2. As soon as the system has been pumped down to a pressure of approximately 10^{-1} millimeter of mercury, the liquid air is applied to the cold trap. This is to prevent mercury vapor, from the mercury diffusion pump and the McLeod gauge, from entering the ionization gauge.

3. When the pressure is below 10^{-4} millimeter of mercury the ionization gauge is degassed. This is done by heating the grid (by passing approximately 6.5 amperes of a-c current through the spiral grid) and by simultaneously heating the bulb with a gas hand-torch. These processes are continued for approximately 10 to 20 minutes.

4. After the degassing is completed, the points of calibration are taken. This is done by admitting sufficient air to the vacuum system to obtain the desired pressure. The stopcock between the diffusion pump and the vacuum system is then closed. After a waiting period of 30 to 60 seconds to allow the pressure in the whole system to reach equilibrium, the pressure is measured with the McLeod gauge. The plate and electron currents of the ionization gauge are read just before the McLeod gauge compression chamber is closed off by elevating the mercury reservoir.

5. Step No. 4 is repeated as often as necessary to obtain a complete calibration curve.

6. The gauge is again degassed as in step No. 3 for about 30 minutes.

7. After degassing with the pressure at 3×10^{-6} millimeter of mercury or lower, the gauge is sealed off from the vacuum system at the constriction shown in Figures C-1 and C-6.

C-4. Theory of Operation of the Pirani Gauge.

The Pirani gauge is a device for measuring gas pressures through the range from about 10^{-2} to 10 millimeters of mercury. It consists of a glass envelope containing a resistance element, which has a high temperature coefficient of resistance. This resistance element is heated by passing a small current through the wire. Diagrams of the WL-762 and the special Pirani gauges are shown in Figures C-15 and C-16, respectively, and photographs in Figures C-17 and C-18.

In a gas where the mean free path is not less than a modest fraction of the dimensions of the chamber around the temperature-sensitive filament, the thermal heat conductivity of the gas is dependent on the pressure of the surrounding gas. This principle is utilized in the Pirani gauge.

The Pirani gauge may be used in any one of the following three ways:

1. Maintain constant filament voltage and measure the filament resistance as a function of temperature.

2. Maintain constant filament current and measure the filament resistance as a function of temperature.

3. Maintain constant filament resistance and measure the required power input as a function of temperature.

In the rocket fired December 8, 1947 there were two Pirani gauges used. One of these gauges was operated at nearly constant filament voltage, as in Method 1, listed above, and the other was operated at nearly constant filament current, as in Method 2. The circuits used in the rocket were essentially the same as those used during calibration, which circuits are described in the next sub-section of this appendix.

APPENDIX C

C-5. Calibration of Pirani Gauges.

The circuit used for calibrating the WL-762 gauge is shown in Figure C-19. In this circuit the gauge is operated at nearly constant voltage, since there is only a small resistor in series with the filament and the power supply. The change in current, caused by the change in resistance of the Pirani gauge filament, produces a change in voltage across the 17.60 ohm resistance, which voltage is the output voltage.

The circuit used for calibrating the special Pirani gauge is shown in Figure C-20. In this circuit the gauge is operated at nearly constant current. The change in resistance of the Pirani gauge filament results in a change in voltage across it. The output voltage is measured directly across the Pirani gauge filament.

Such practical matters as the availability of power, and of space, in the rocket were the factors which made it expedient to operate the one Pirani gauge under constant voltage conditions and the other under constant current conditions.

The WL-762 gauge was calibrated by essentially the same procedure as was used for the ionization gauges except the gauge was not degassed and it was not sealed when it was taken off the vacuum system. Therefore, steps No. 3, 6 and 7 of the previously discussed ionization gauge calibration procedure were eliminated, and the gauge was broken off from the system with the length of tubulation shown in Figure C-15. The calibration data for this gauge are shown in Figure C-21. This figure is self-explanatory.

The special Pirani gauge was calibrated by placing the gauge inside a bell jar which was evacuated by a Cenco Hypervac-20 pump. The points of calibration were taken by simultaneously taking readings of the gauge and of another Pirani gauge which was also placed in the bell-jar. The gauge used for calibration had previously been calibrated on the vacuum system by the method outlined for the WL-762 Pirani gauge. The calibration data for the special Pirani gauge are shown in Figure C-22. This figure, also, is self-explanatory.

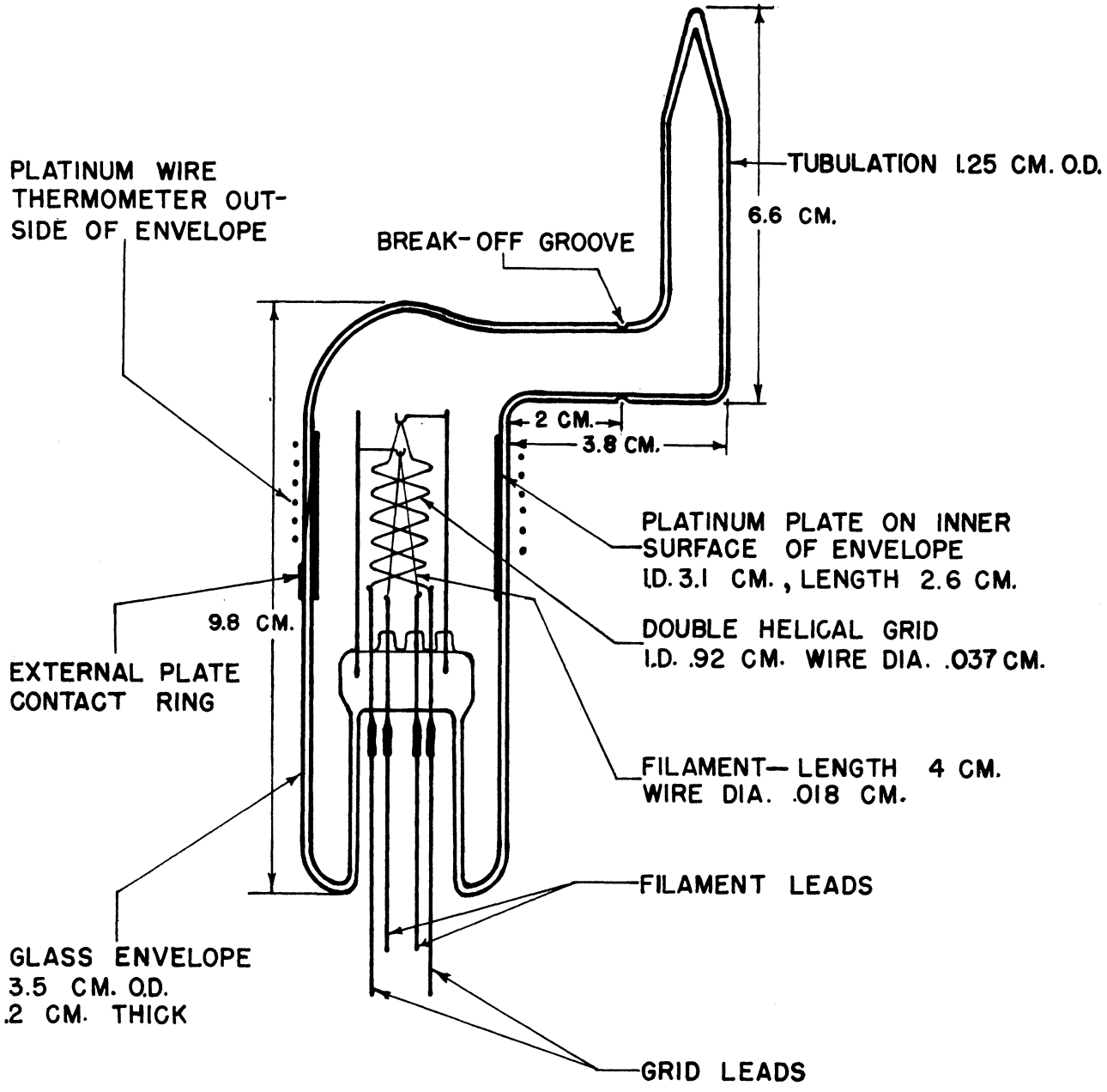

FIG. NO. C-1

D.P.I. TYPE VG-1A IONIZATION GAUGE

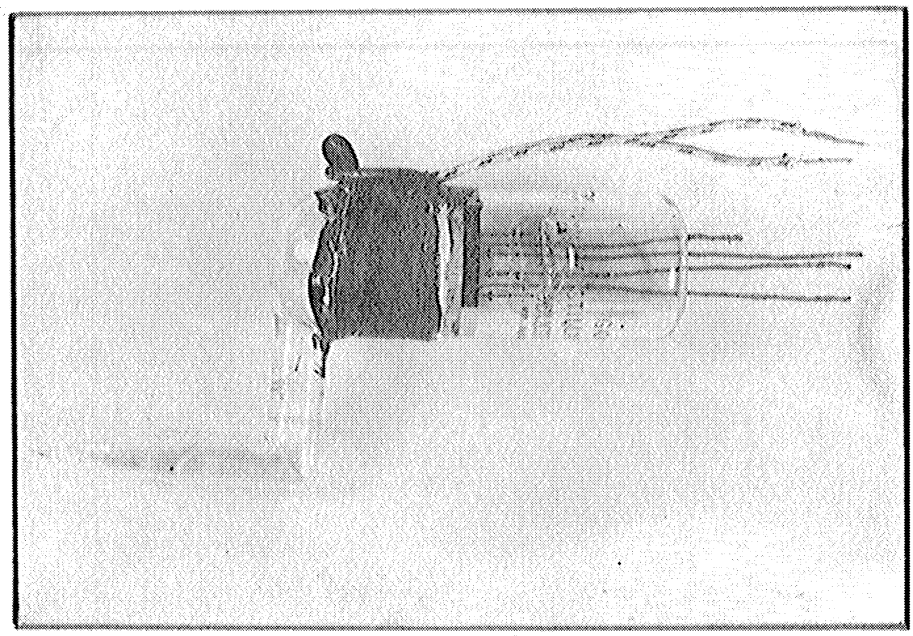

FIG. NO. C-2
VG-IA IONIZATION GAUGE WITH PLATINUM WIRE THERMOMETER FOR MEASURING GAUGE WALL TEMPERATURE.

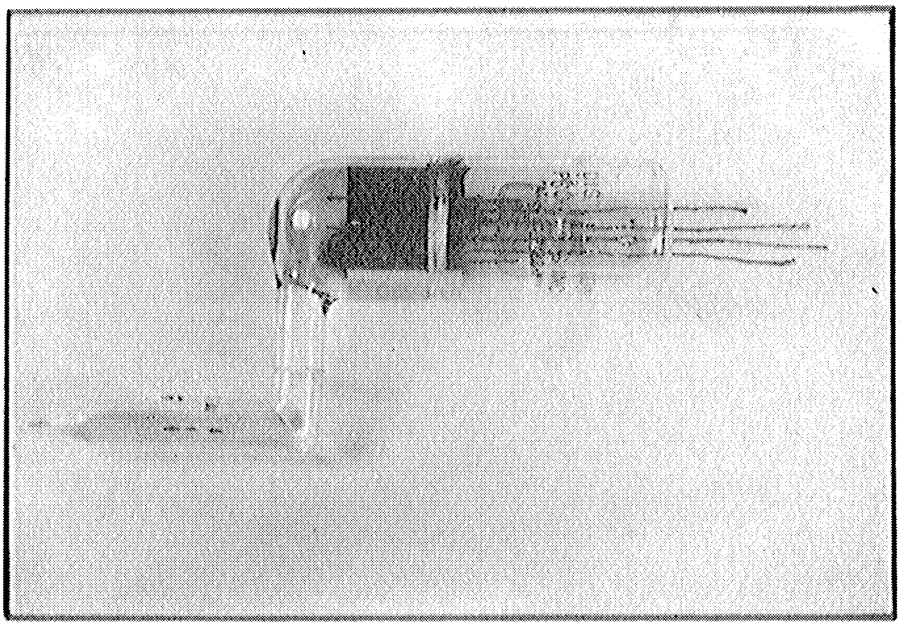

FIG. NO. C-3
VG-IA IONIZATION GAUGE FOR SIDE WALL OF TRUNCATED 15° CONE. (GAUGES 1 THROUGH 4 OF FIG. NO. V-1)

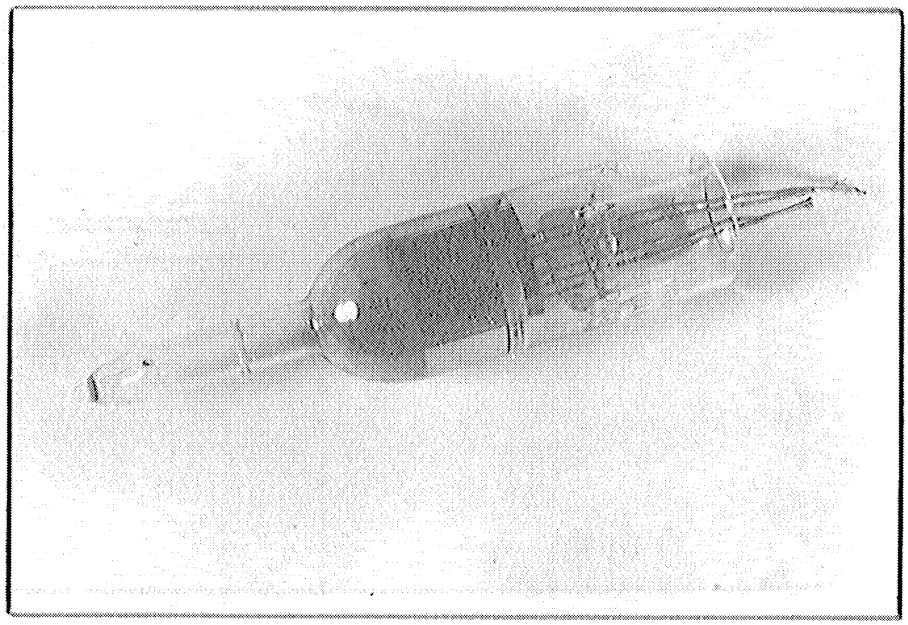

FIG. NO. C-4
VG-1A IONIZATION GAUGE FOR FLAT END OF TRUNCATED 15° CONE (NOSE GAUGE).(GAUGE NO. 5 FIG. NO. V-1)

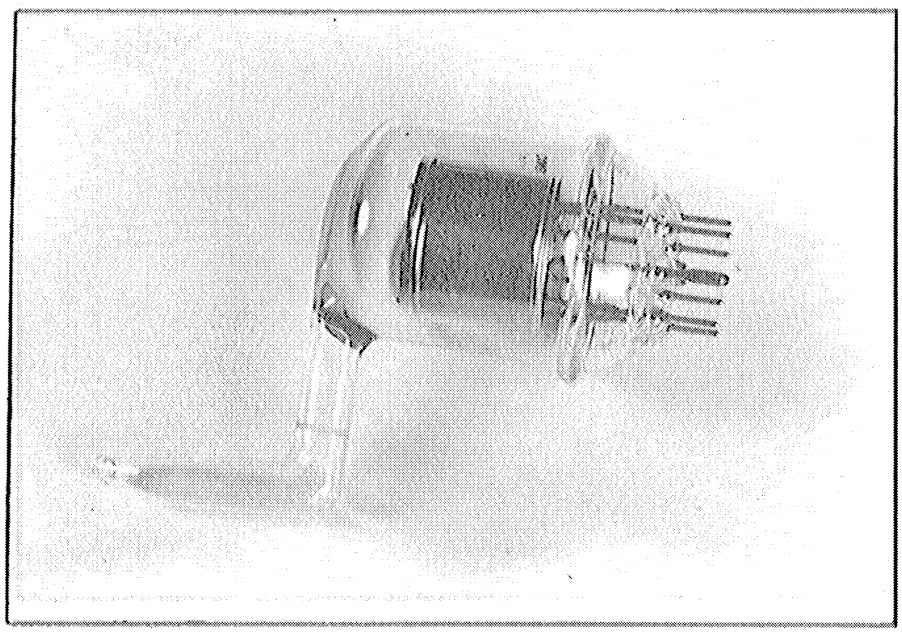

FIG. NO. C-5
NRC-507 IONIZATION GAUGE USED IN ROCKET NO. 28 DEC. 8,1947 (GAUGES 2 AND 4)

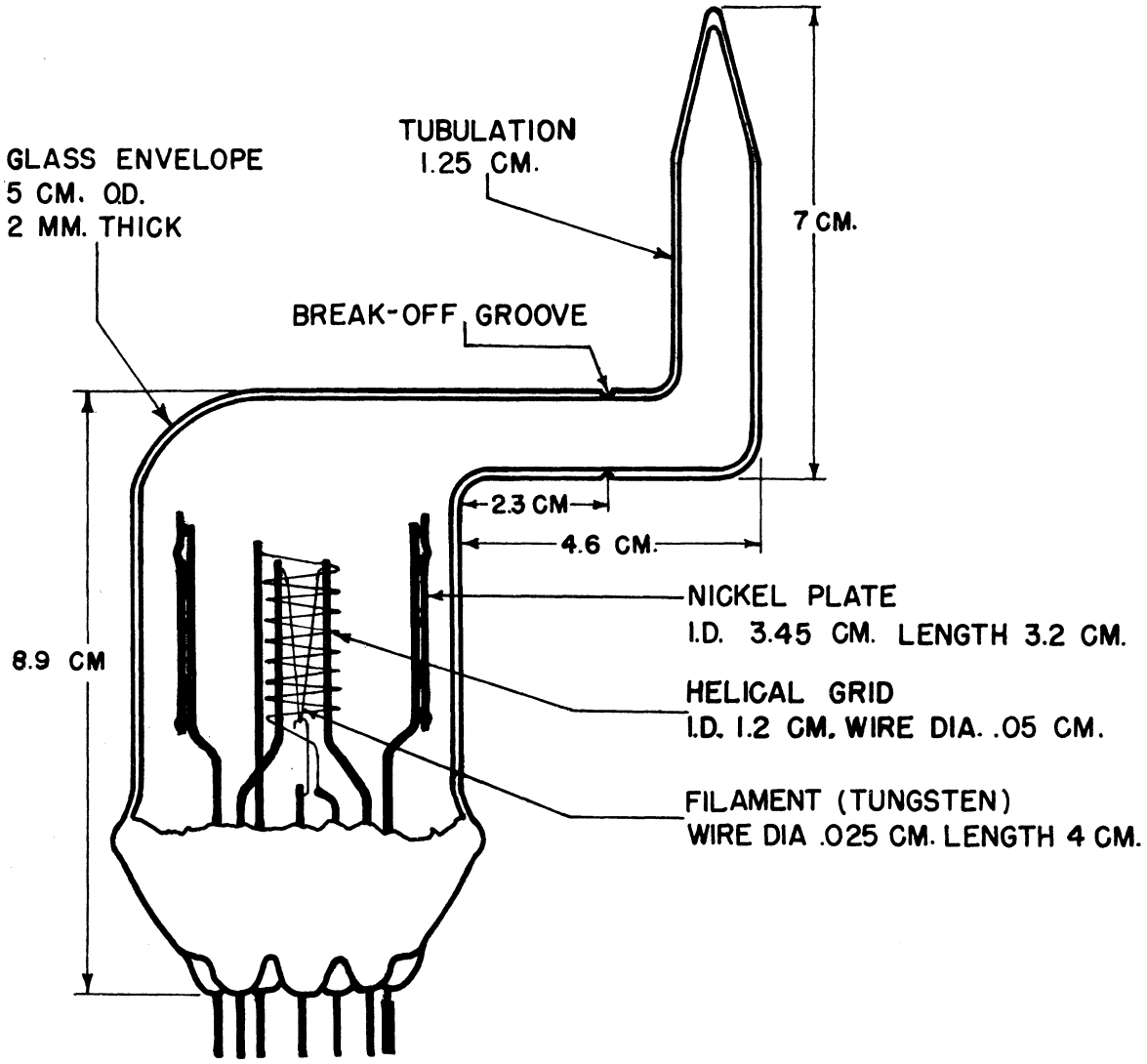

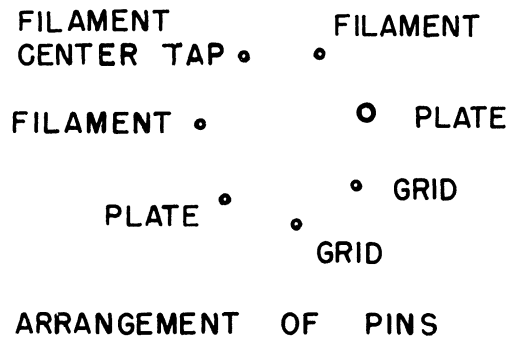

ARRANGEMENT OF PINS

FIG. NO. C-6
NRC-507 IONIZATION GAUGE

FIG. NO. C-7

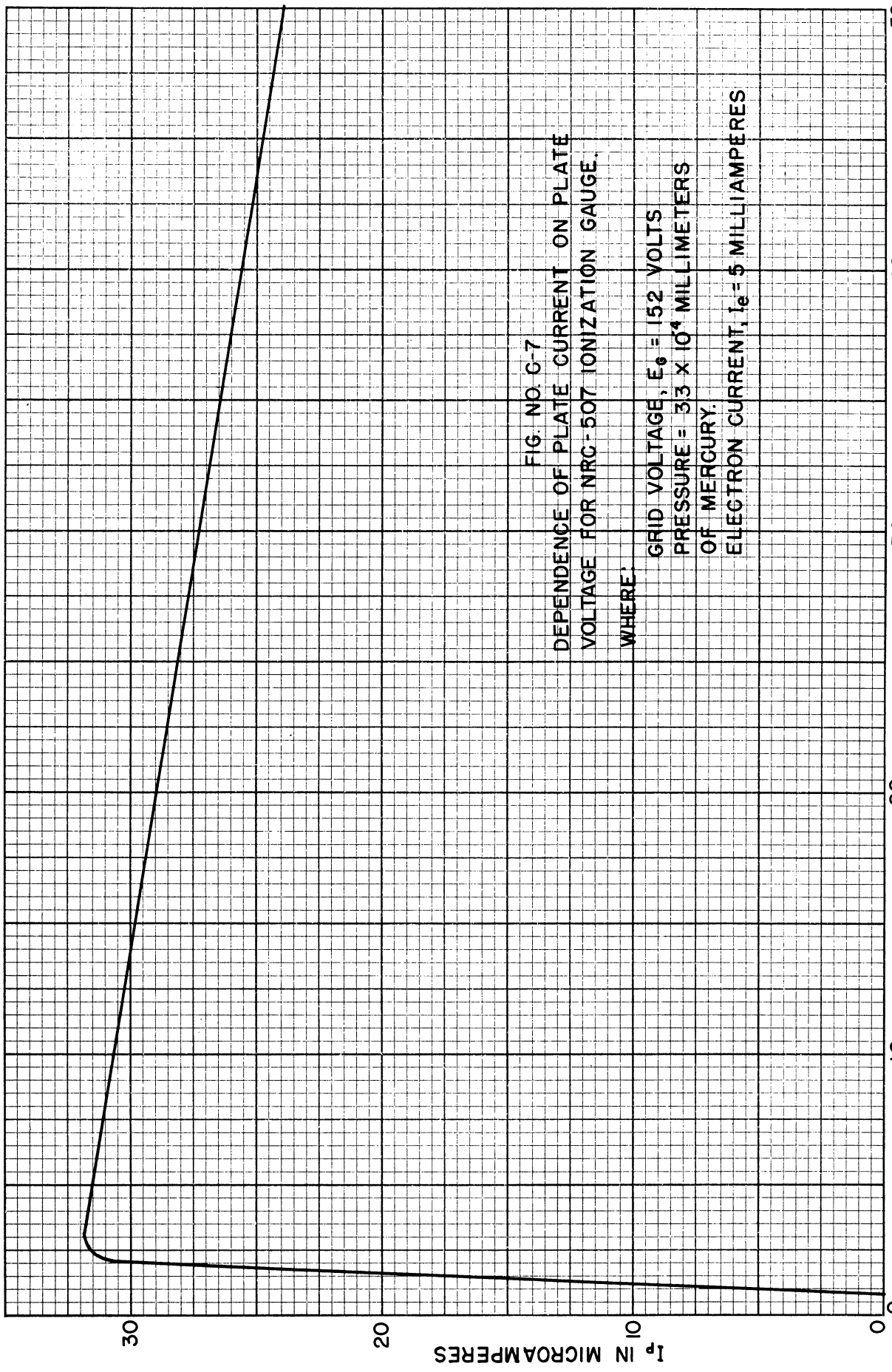
FIG. NO. C-7
DEPENDENCE OF PLATE CURRENT ON PLATE VOLTAGE FOR NRC-507 IONIZATION GAUGE.
WHERE:
GRID VOLTAGE, E_c = 152 VOLTS
PRESSURE = 33 X 10^{-4} MILLIMETERS OF MERCURY.
ELECTRON CURRENT, I_e = 5 MILLIAMPERES
I_p IN MICROAMPERES
0
10
20
30
E_p IN VOLTS
0
-10
-20
-30
-40
-50

FIG. NO. C-8

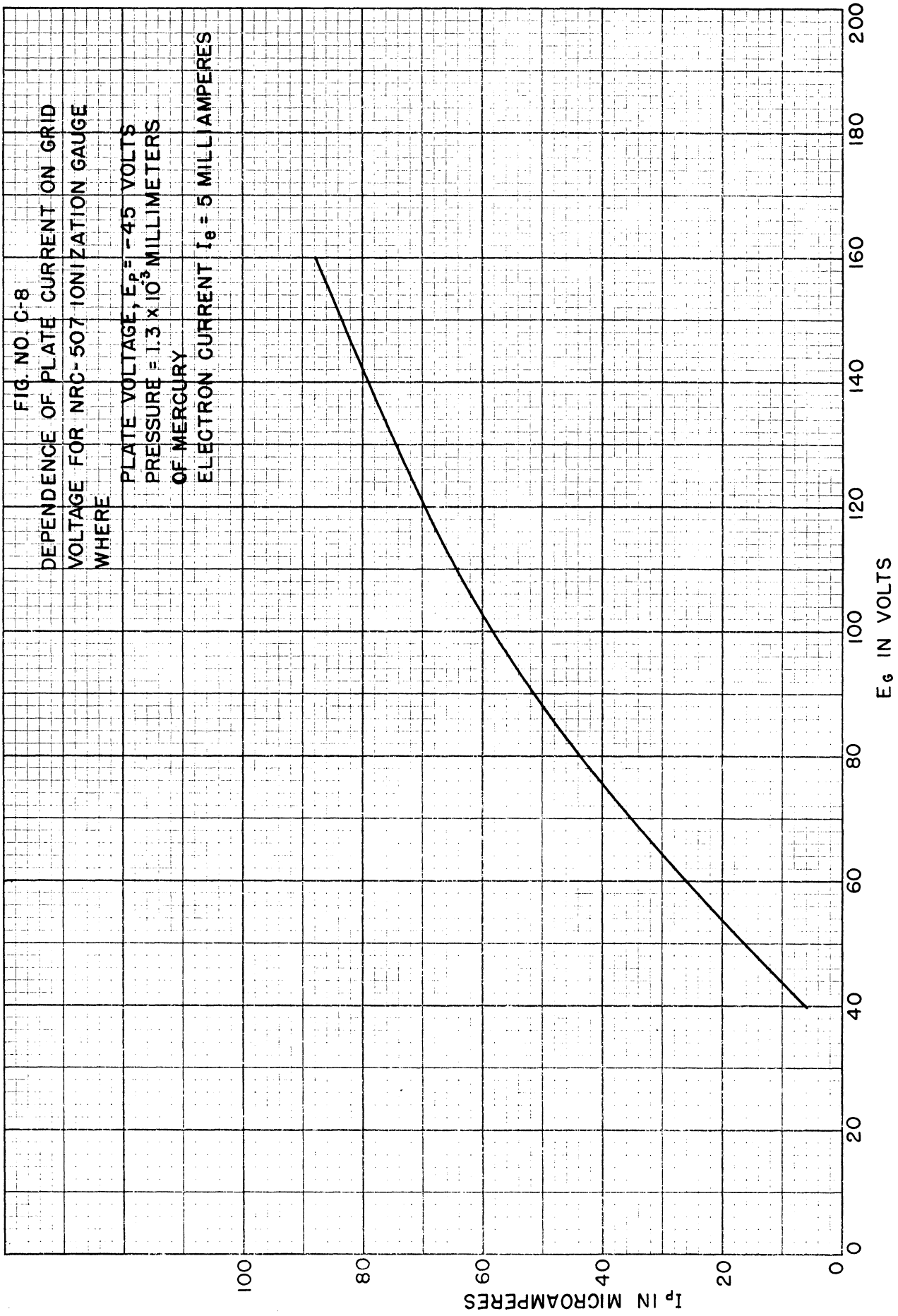
FIG. NO. C-8
DEPENDENCE OF PLATE CURRENT ON GRID VOLTAGE FOR NRC-507 IONIZATION GAUGE
WHERE
PLATE VOLTAGE, E_p = -45 VOLTS
PRESSURE = 1.3 x 10^{-3} MILLIMETERS OF MERCURY
ELECTRON CURRENT I_e = 5 MILLIAMPERES
I_p IN MICROAMPERES
0
20
40
60
80
100
E_G IN VOLTS
0
20
40
60
80
100
120
140
160
180
200

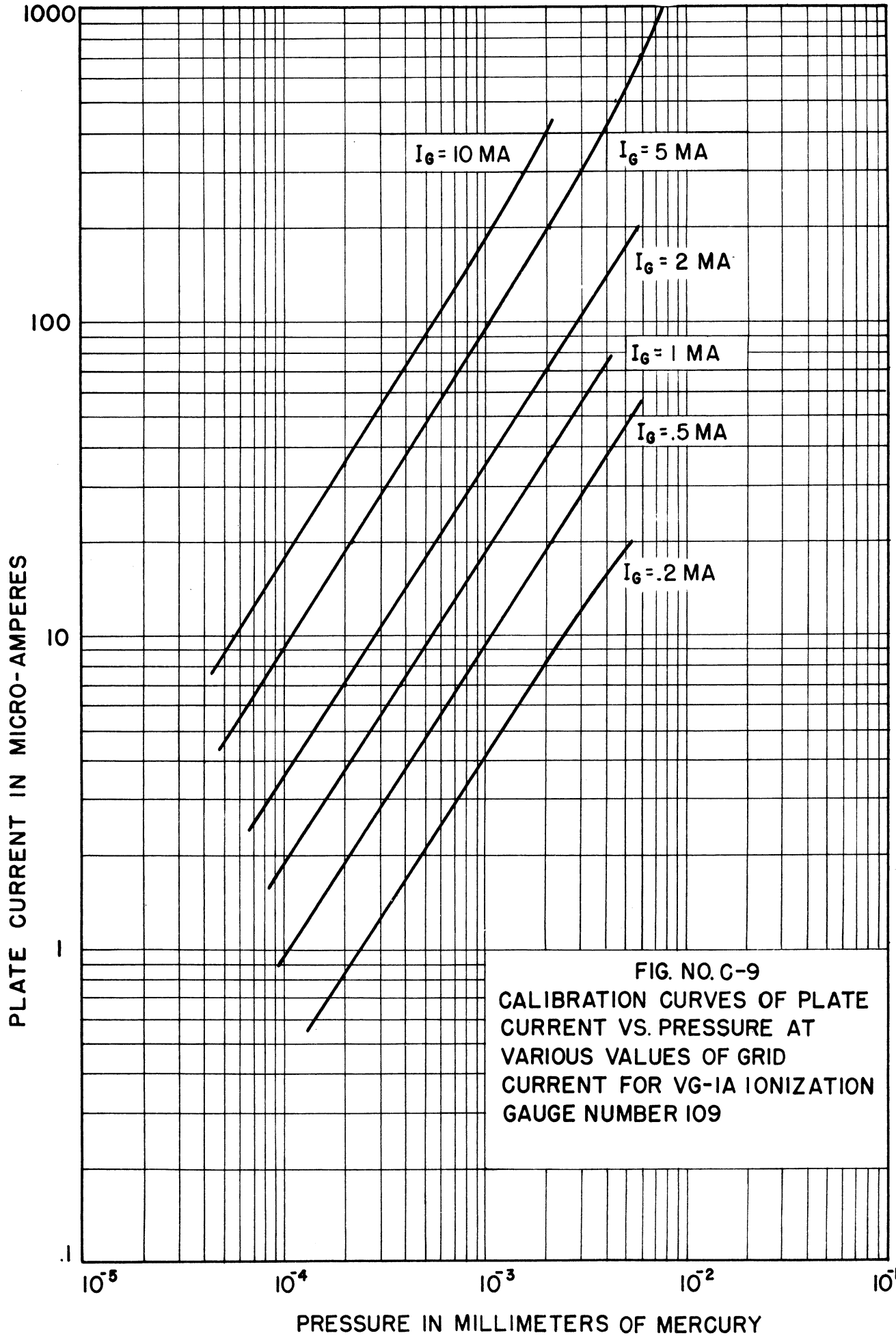

FIG. NO. C-9
CALIBRATION CURVES OF PLATE CURRENT VS. PRESSURE AT VARIOUS VALUES OF GRID CURRENT FOR VG-1A IONIZATION GAUGE NUMBER 109

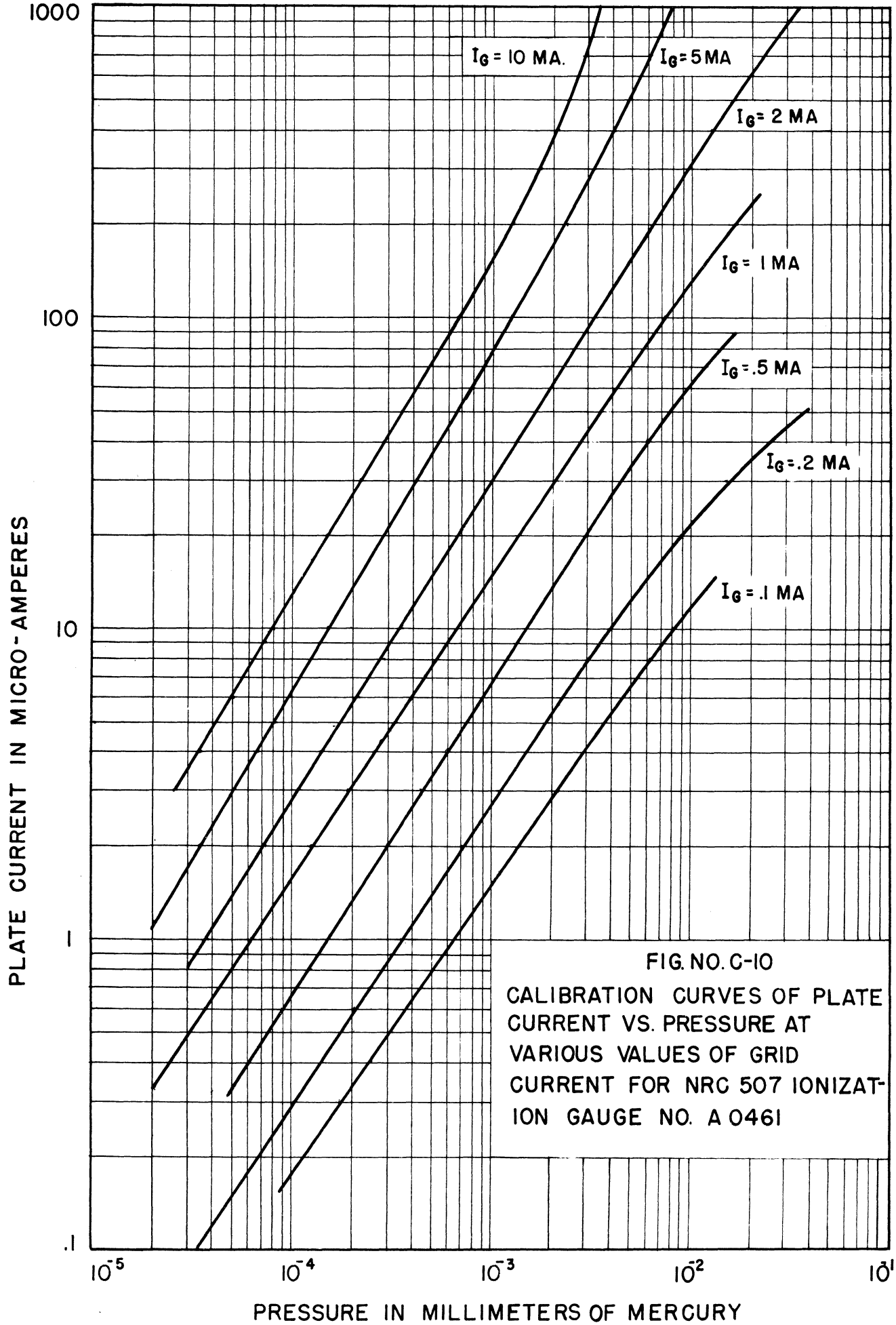

FIG. NO. C-10

CALIBRATION CURVES OF PLATE CURRENT VS. PRESSURE AT VARIOUS VALUES OF GRID CURRENT FOR NRC 507 IONIZATION GAUGE NO. A 0461

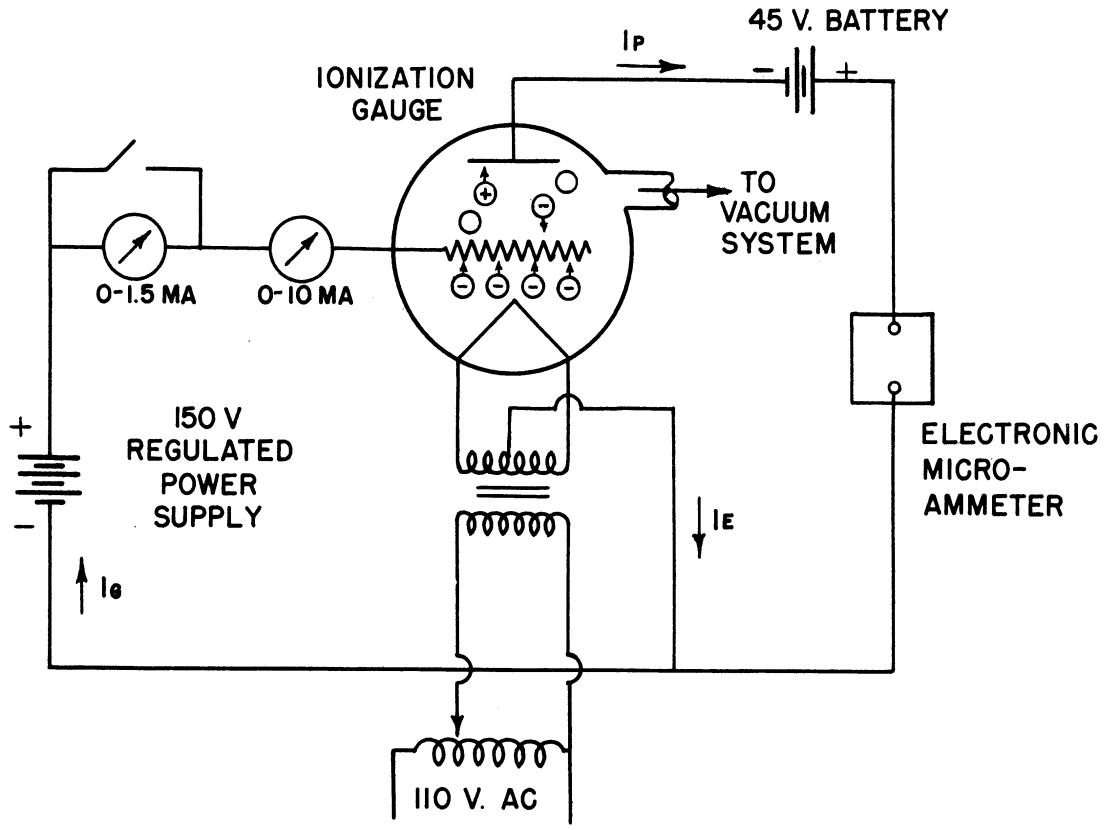

FIG. NO. C-11
CALIBRATION CIRCUIT FOR IONIZATION GAUGE

I_P = POSITIVE-ION OR PLATE CURRENT
I_G = GRID CURRENT
I_E = ELECTRON BOMBARDING CURRENT
$I_G = I_P + I_E$
○ = NEUTRAL GAS PARTICLES
⊕ = POSITIVE IONS
⊖ = ELECTRONS

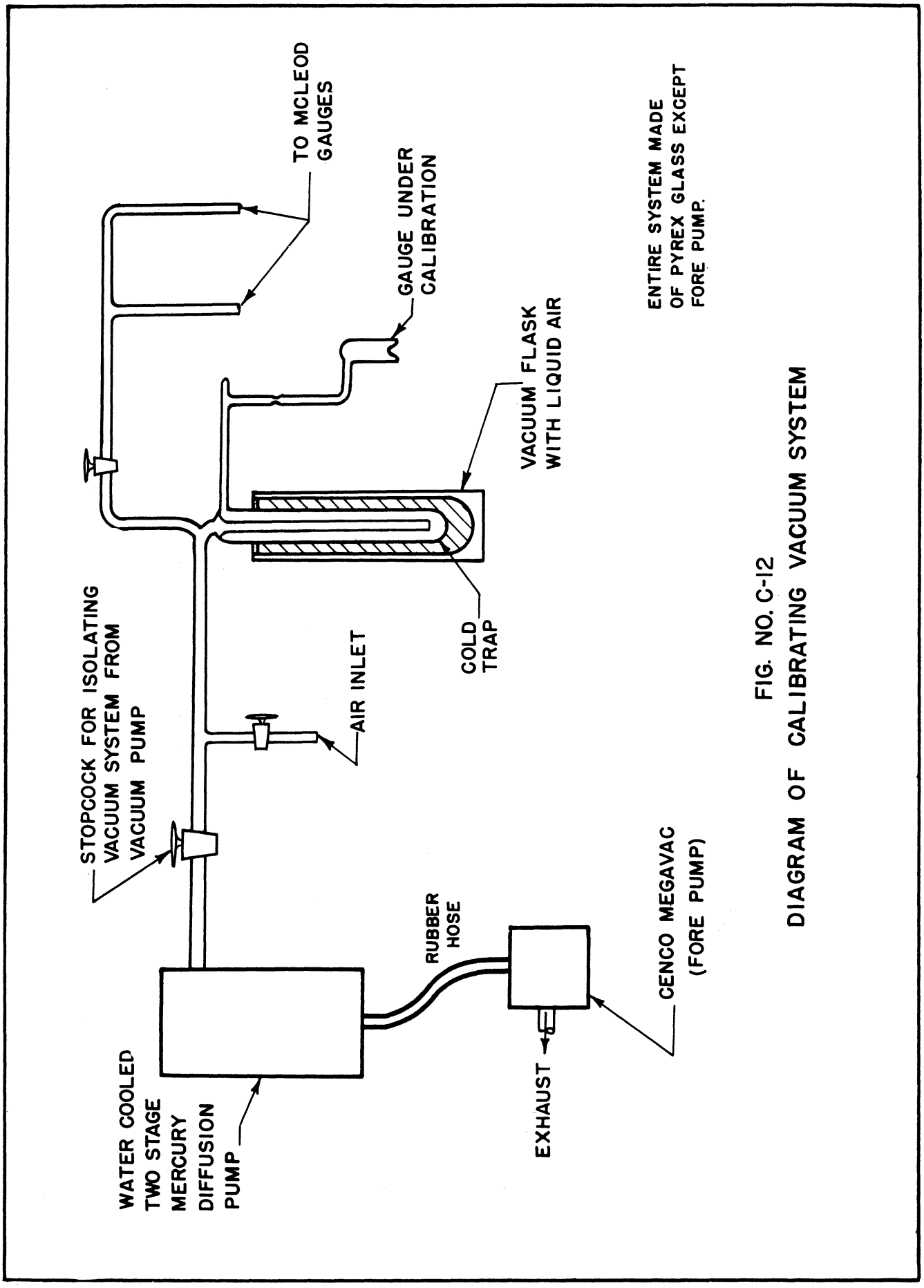

FIG. NO. C-12

DIAGRAM OF CALIBRATING VACUUM SYSTEM

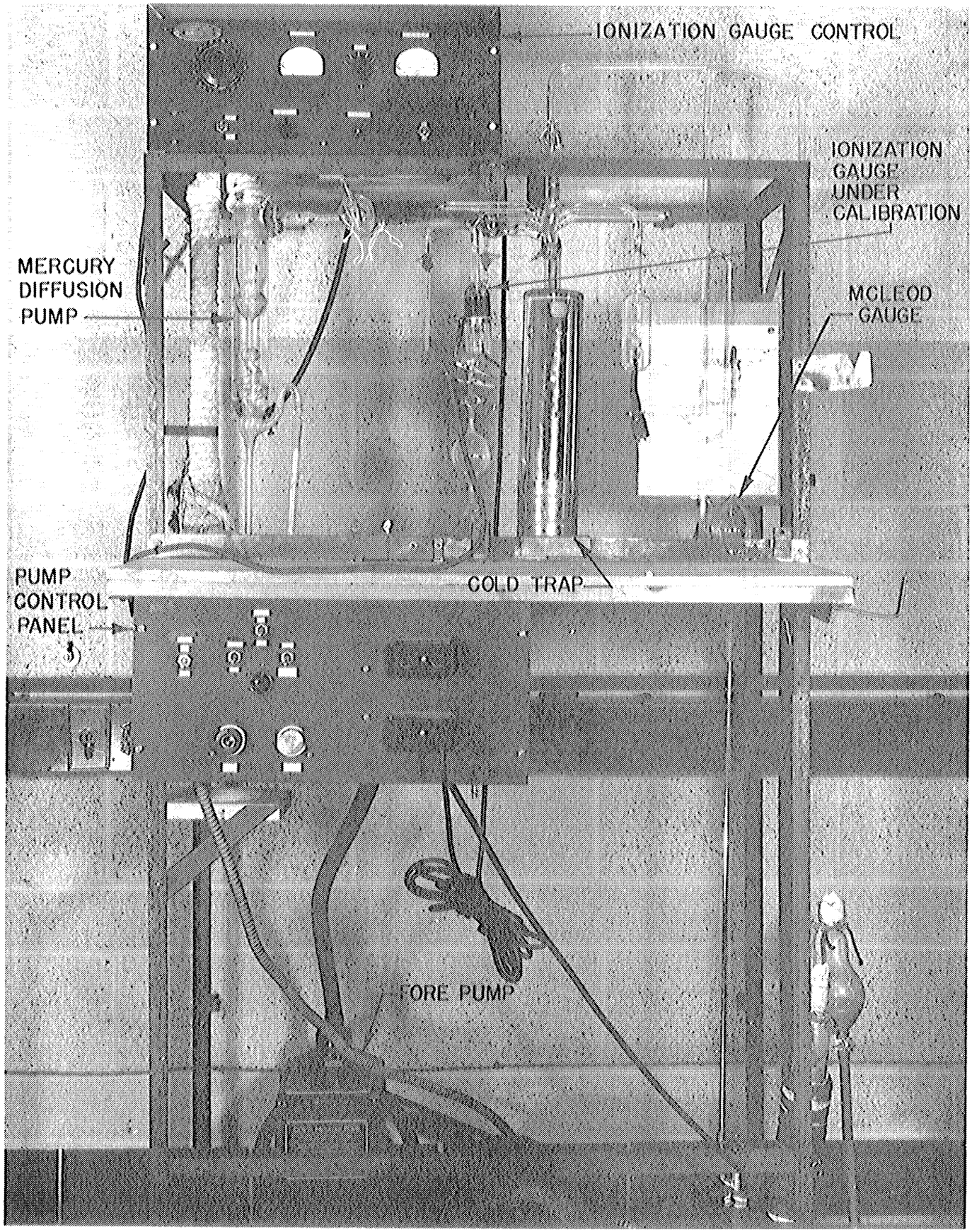

FIG. NO. C-13
VACUUM SYSTEM FOR CALIBRATING IONIZATION GAUGES

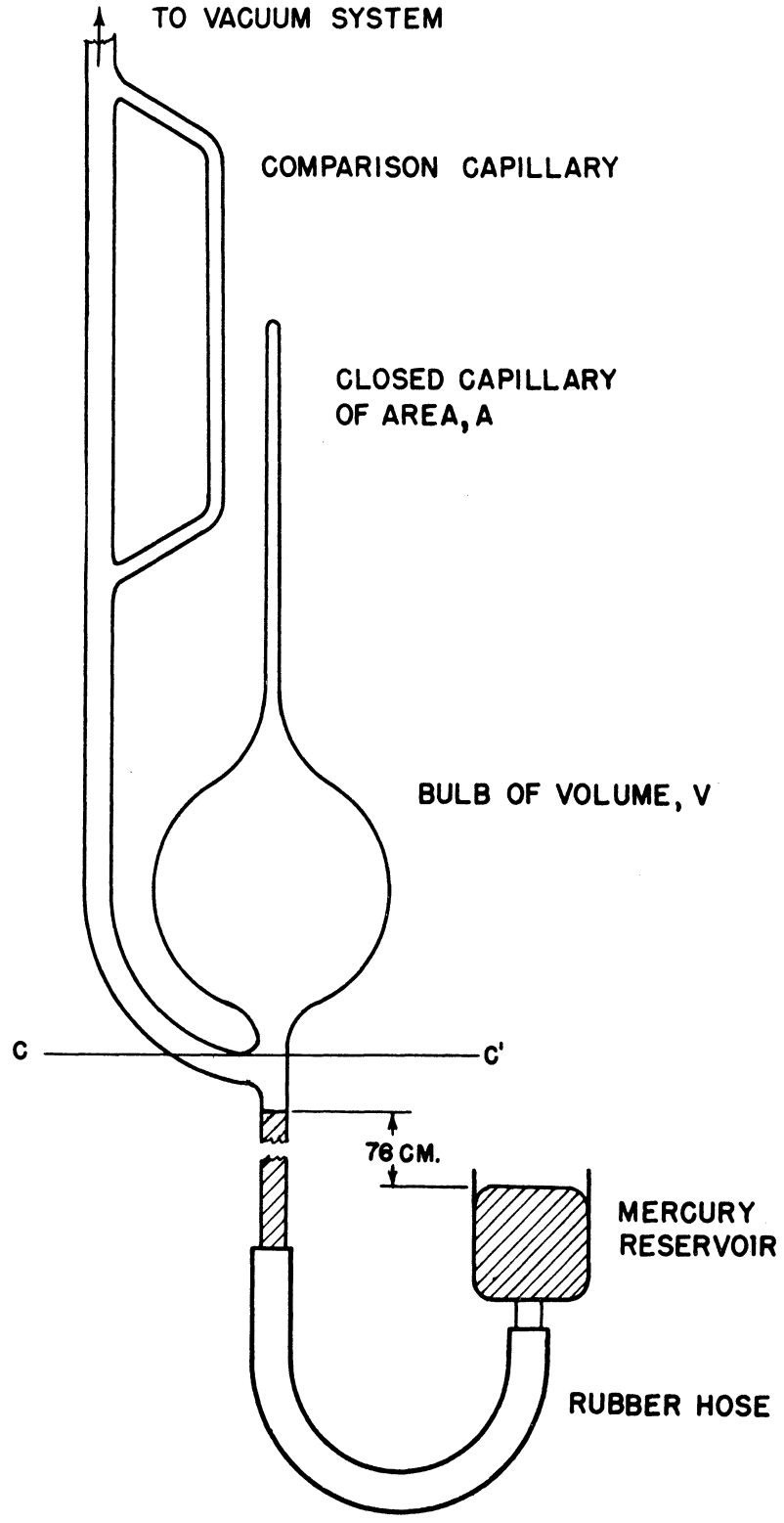

FIG. NO. C-14
DIAGRAM OF McLEOD GAUGE

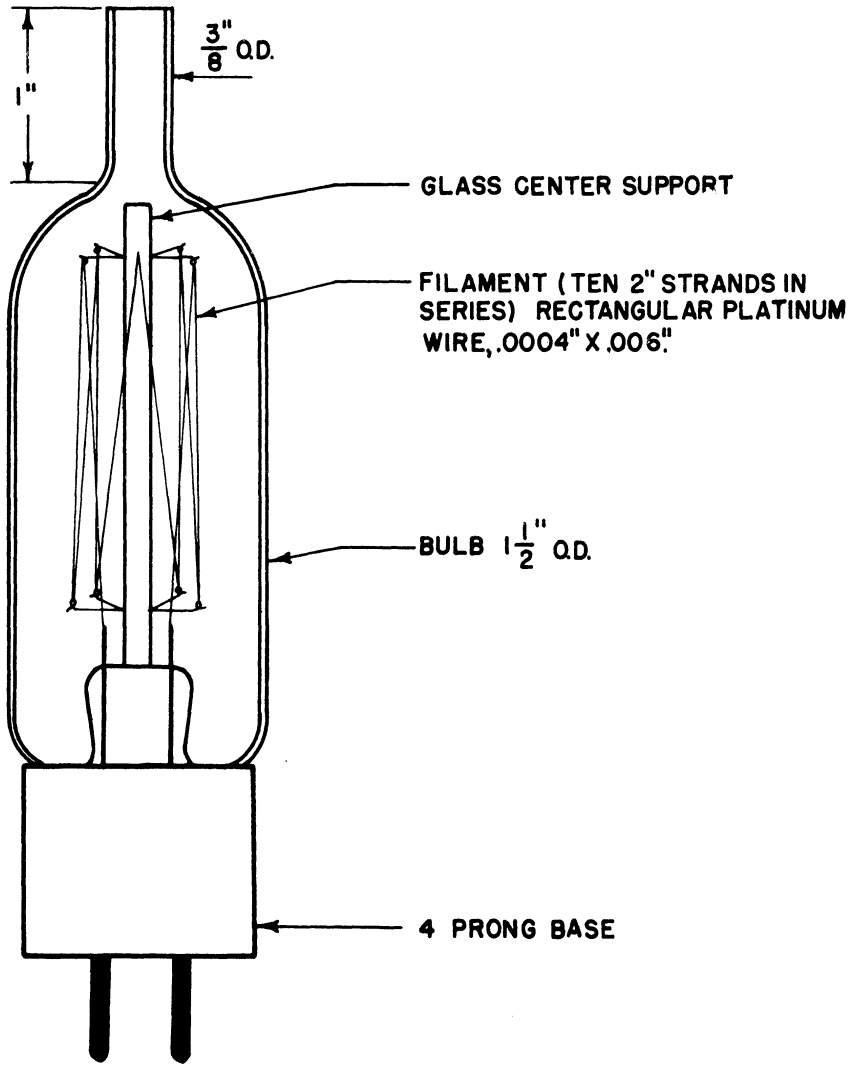

FIG. NO. C-15

WL 762 PIRANI GAUGE

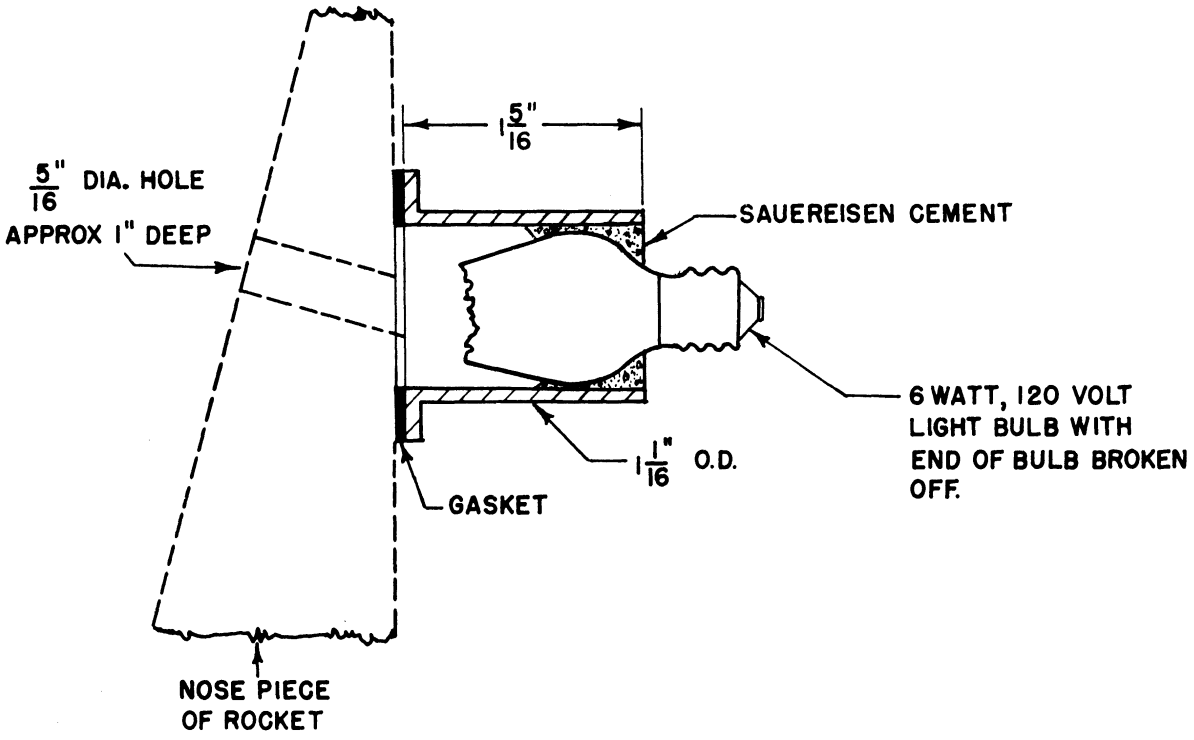

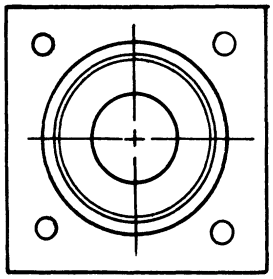

END VIEW

FIG. NO. C-16
SPECIAL PIRANI GAUGE

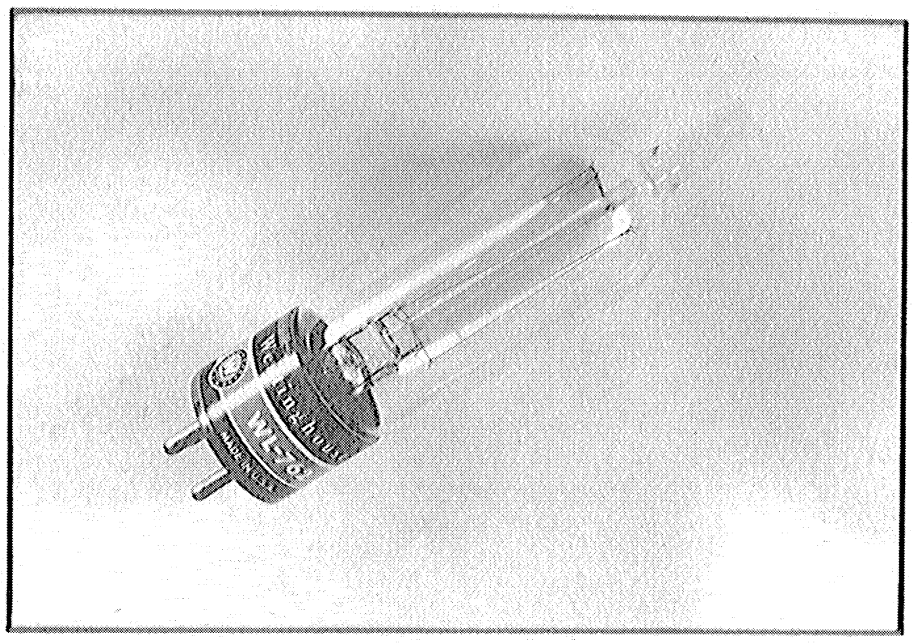

FIG. NO. C-17

WL-762 PIRANI GAUGE MOUNTED NEAR TAIL OF ROCKET

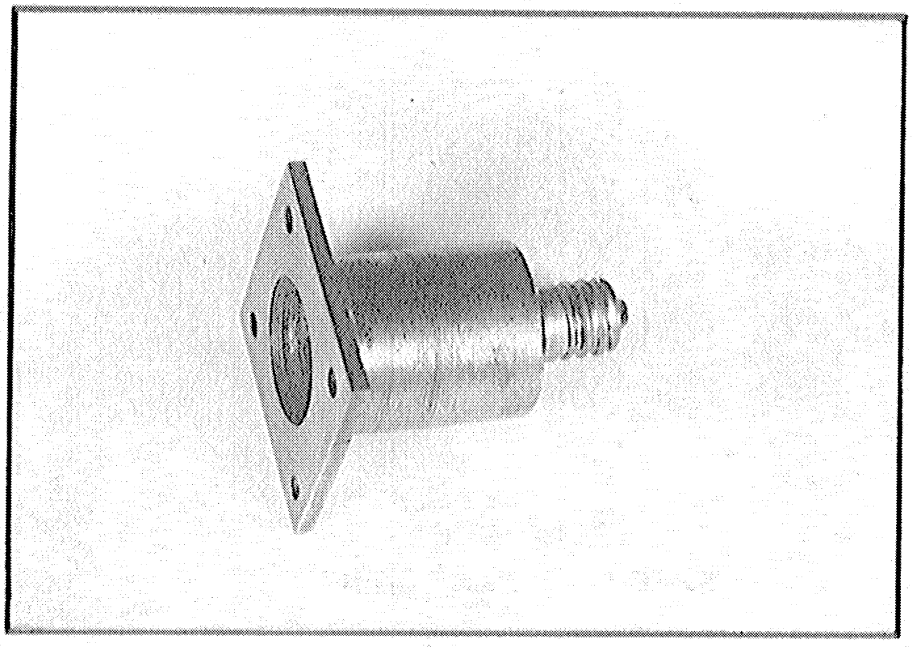

FIG. NO. C-18

SPECIAL PIRANI GAUGE MOUNTED ON SIDE OF TRUNCATED 15° CONE BELOW IONIZATION GAUGES.

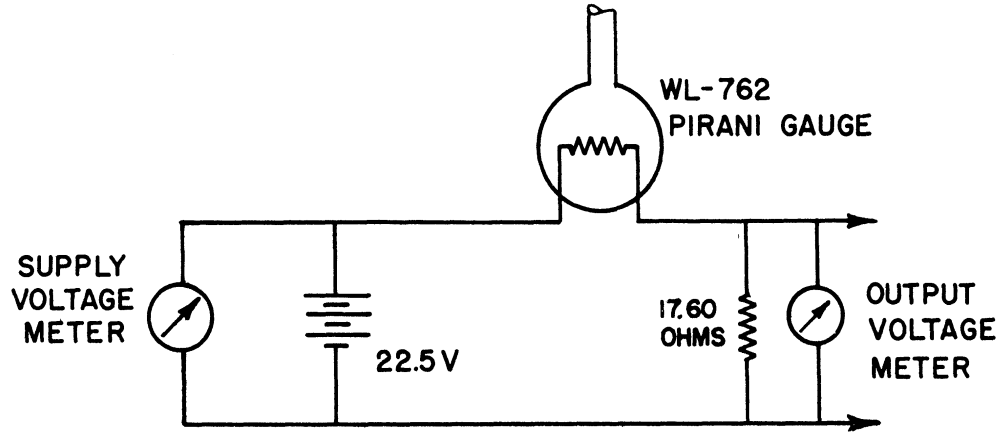

FIG. NO. C-19
CALIBRATION CIRCUIT FOR WL-762 PIRANI GAUGE

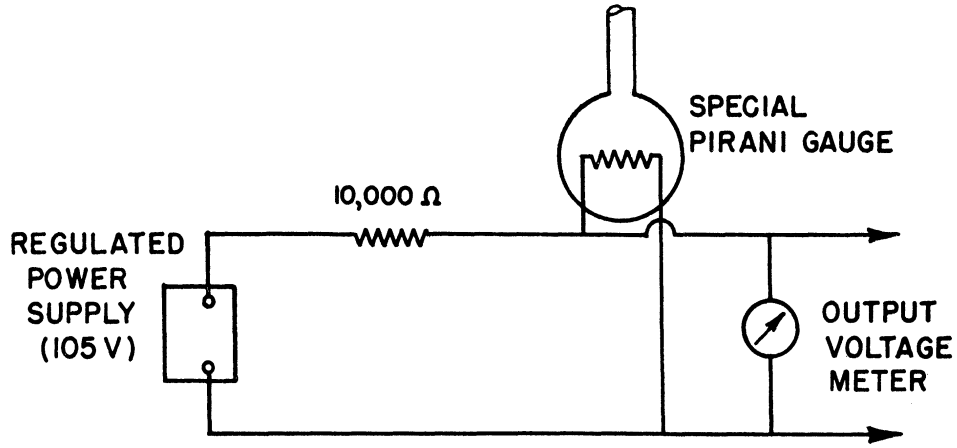

FIG. NO. C-20
CALIBRATION CIRCUIT FOR SPECIAL PIRANI GAUGE

FIG. NO. C-21

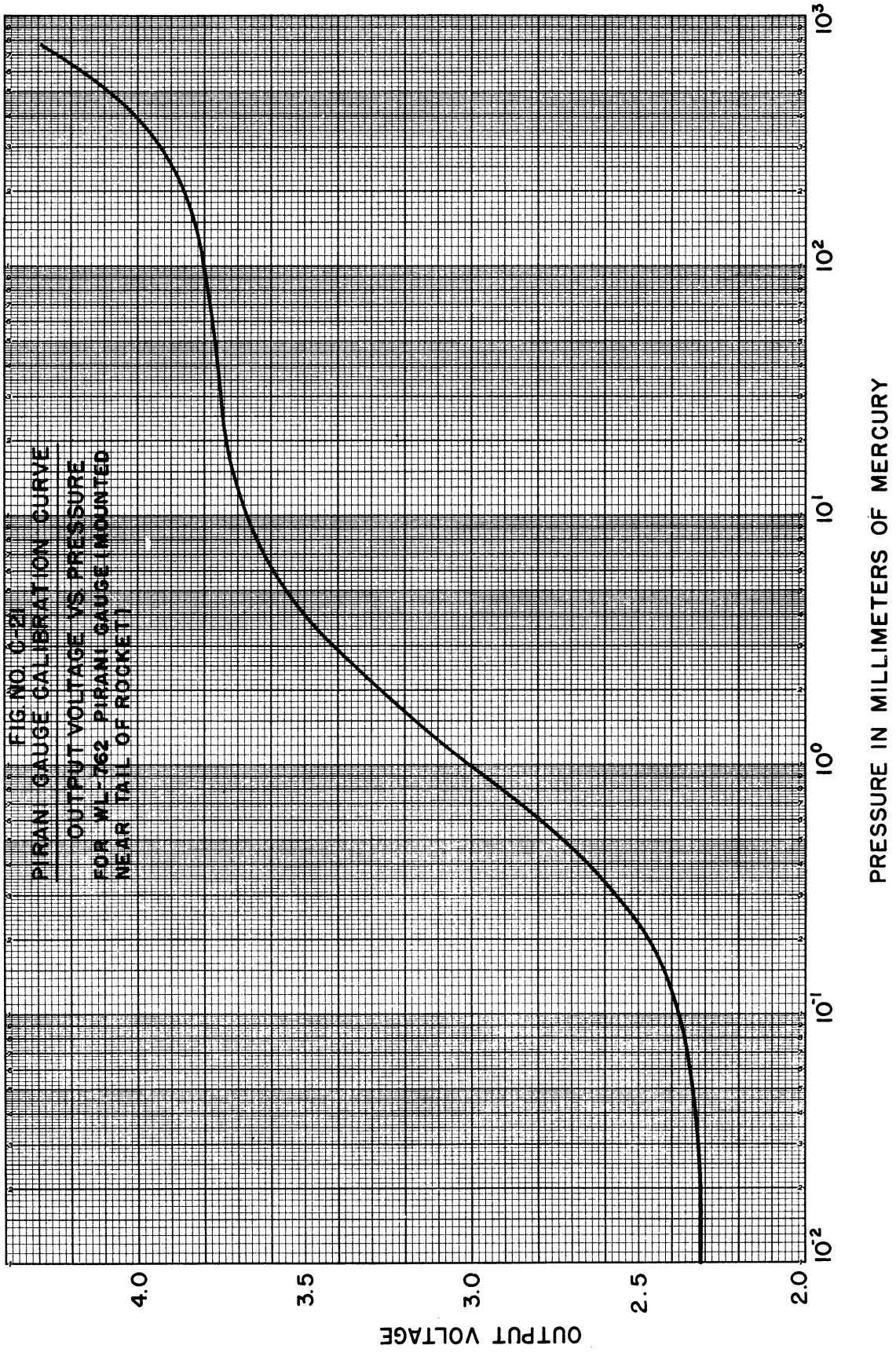
FIG NO. C-21
PIRAN GAUGE CALIBRATION CURVE
OUTPUT VOLTAGE VS. PRESSURE
FOR WL-762 PIRANI GAUGE (MOUNTED
NEAR TAIL OF ROCKET)
OUTPUT VOLTAGE
4.0
3.5
3.0
2.5
2.0
10^{-2}
10^{-1}
10^{0}
10^{1}
10^{2}
10^{3}
PRESSURE IN MILLIMETERS OF MERCURY

FIG. NO. C-22

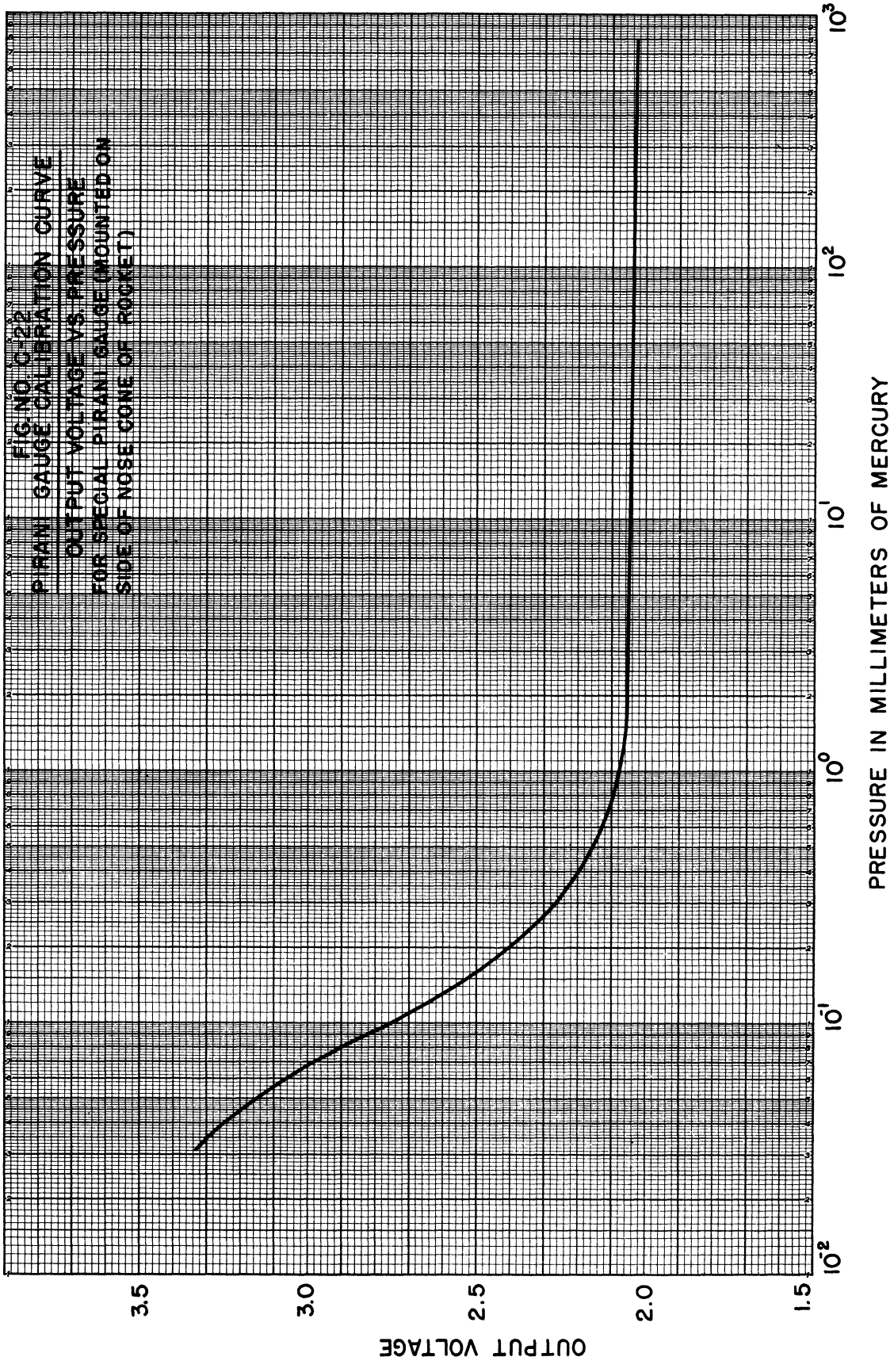
FIG. NO. C-22
PIRANI GAUGE CALIBRATION CURVE
OUTPUT VOLTAGE VS. PRESSURE
FOR SPECIAL PIRANI GAUGE (MOUNTED ON SIDE OF NOSE CONE OR ROCKET)
OUTPUT VOLTAGE
3.5
3.0
2.5
2.0
1.5
10^{-2}
10^{-1}
10^{0}
10^{1}
10^{2}
10^{3}
PRESSURE IN MILLIMETERS OF MERCURY

APPENDIX D

INTERPRETATION OF PRESSURE GAUGE READINGS IN TERMS OF AMBIENT PRESSURE OF THE ATMOSPHERE, AND CONSIDERATION OF ATMOSPHERIC TEMPERATURE CALCULATIONS FROM PRESSURE DATA

D-1. Introduction.

In the first section of the present report it is pointed out that the original objective of the work being done on this project was, with regard to the atmospheric pressure and temperature measurements, the determination of these properties of the atmosphere at altitudes from about 80 kilometers to 160 kilometers (expected altitude of crest of V-2 trajectory). Therefore, immediately after the initiation of the project an investigation was made of possible methods of measuring pressure and temperature by means of instruments carried on a rocket moving at a very high velocity through this range of altitudes. From estimates, of the type presented in Figure II-4 of this report, it appeared that the mean free path of the gas particles over the greater part of this region would be long compared to the dimensions of the measuring instruments and of the nose of the V-2, where the instruments were to be mounted. On this basis, a system of instrumentation was designed. The analysis of the entire problem was presented in the University of Michigan report[2] "Technical Report on the Measurement of Temperature and Pressure in the Ionosphere" by W. G. Dow and A. Reifman, issued July 25, 1946. This report did not have a wide circulation and, since it formed the basis for the design of the pressure-measuring instrumentation, the essential material from it is included in this appendix of the present report.

However, the three successful V-2's carrying University of Michigan instruments attained maximum altitudes of only slightly more than 100 kilometers. Therefore, each of these rockets had lower velocities over its entire trajectory than was anticipated, with the result that the pressure gauges on each rocket were first exposed to the atmosphere at an altitude somewhat lower than the intended 80 kilometer altitude. (The instrumentation was designed to open the pressure gauges at approximately 100 seconds after rocket take-off.) Therefore, the theory developed in the summer of 1946 was applicable only to a small part of the data obtained.

In order to obtain as much information as possible from the readings of the pressure gauges, it has been necessary to consider the problem of motion of the rocket through a gas in which the mean free path of the gas particles is of the same order of magnitude as the dimensions of the nosepiece of the rocket and of the pressure gauges. This is a very difficult problem and the complete solution likely will not be obtained for some time. However, a first approximation to the solution has been made, which approximation is discussed in this appendix.

In arriving at this first-order solution it has been necessary to find relations between the following quantities:

1. The pressure (P_{1C}) within the pressure gauge during its calibration and the pressure (P_{OC}) read by the calibrating McLeod gauge during this calibration.

2. The pressure (P_{1F}) within the pressure gauge during rocket flight and the pressure (P_{OF}) at the opening port of this gauge during flight.

3. The pressure (P_{OF}) at the opening port of the ionization gauge during rocket flight and the ambient pressure (P_A) at that altitude prior to the intrusion of the rocket. It is assumed that P_A as defined in the preceding sentence is also the pressure existing at a sufficiently great horizontal distance from the rocket so that this pressure is substantially unaffected by the passage of the rocket. This horizontal distance would amount to only a few score feet.

The relation between P_{OC} (the known calibrating pressure) and P_A (the unknown quantity under measurement) follows at once, with the establishment of the relations mentioned in the above paragraphs.

It must be emphasized that this theoretical analysis of the relation between P_A and P_{OC} is only a first approach to the problem and must not be considered as a final solution. The assumptions on which the analysis is based are pointed out in the text where they are made, and an evaluation of their validity is included.

Also included in this appendix are theoretical calculations of the response time of the ionization gauges.

The analyses contained in this appendix are based largely on theory taken from the fields of the kinetic theory of gases, thermodynamics and fluid mechanics[5,6,7]. The following is a list of the symbols used:

T = temperature in degrees, Kelvin.

T_{1C}, T_{2C}, etc. = gas temperature within the ionization gauges during their calibration.

T_{OC} = gas temperature in the vacuum system connected to the ionization gauge during calibration.

T_{1F}, T_{2F}, etc. = gas temperature within the ionization gauges during rocket flight.

T_{OF} = gas temperature at the opening port of the ionization gauge during rocket flight.

T_A = ambient temperature of the undisturbed gas outside the influence of the motion of the rocket during rocket flight.

R = gas constant per mole = 8.315×10^7 ergs per degree, Kelvin.

k = gas constant per molecule = 1.381×10^{-16} erg per degree, Kelvin.

n = number of moles of gas under consideration.

L = Avogadro's Number = 6.02×10^{23} molecules per mole.

N = gas concentration (number of particles per cubic centimeter).

dN = number of gas particles per cubic centimeter with x-directed component of velocity between u_x and $u_x + du_x$ centimeters per second.

m = mass of a single particle, in grams.

$\mathfrak{m}$ = molecular weight.

v = volume occupied by one mole of gas, in cubic centimeters.

V = volume of gas under consideration, in cubic centimeters.

M' = mass of volume (V) of gas, in grams.

γ = ratio of specific heats = C_p/C_v.

C_p = specific heat at constant pressure.

C_v = specific heat at constant volume.

P = gas pressure, in dynes per square centimeter.

$\overline{P}$ = average gas pressure, in dynes per square centimeter.

P_{1C}, P_{2C}, etc. = gas pressure within the ionization gauges during their calibration.

P_{OC} = gas pressure in the vacuum system connected to the ionization gauge during calibration.

P_{1F}, P_{2F}, etc. = gas pressure within the ionization gauges during rocket flight.

P_{OF} = gas pressure at the opening port of the ionization gauge during rocket flight.

P_A = ambient pressure of the undisturbed gas outside the influence of the motion of the rocket during rocket flight.

ρ = density of gas, in grams per cubic centimeter.

$\bar{\rho}$ = average density of gas, in grams per cubic centimeter.

u = instantaneous velocity of a single particle, in centimeters per second.

u_x = x-directed component of instantaneous velocity (u) of a single particle, in centimeters per second.

c = average particle velocity, in centimeters per second.

$\bar{c}$ = root-mean-square velocity, in centimeters per second.

c_m = most probable particle velocity, in centimeters per second.

a = velocity of sound, in centimeters per second.

w = relative drift velocity between fluid and body under consideration, in centimeters per second.

w_x = x-directed component of w.

$S = \frac{w_x}{c_m}$

λ = mean-free-path of a gas particle, in centimeters.

h = altitude above earth's surface, in centimeters.

g = acceleration due to gravity, in centimeters per second per second.

M = Mach number.

Re = Reynolds number.

μ = coefficient of viscosity, in poises per dyne-seconds per square centimeter.

ν = kinematic viscosity, in square centimeters per second.

r = a characteristic dimension of the body under consideration, in centimeters.

δ = thickness of boundary layer, in centimeters.

The following equations are taken from the fields of thermodynamics, kinetic theory of gases and fluid mechanics[5,6,7] and are used at various places in the development:

$$P = NkT \tag{D-1}$$

$$Pv = RT \tag{D-2}$$

$$PV = nRT \tag{D-3}$$

$$R = kL \tag{D-4}$$

$$P = \frac{1}{2} Nmc_m^2 \tag{D-5}$$

$$RT = \frac{Lm\bar{c}^2}{3} \tag{D-6}$$

$$v = \frac{mV}{M'} = \frac{m}{\rho} \tag{D-7}$$

$$\rho = \frac{M'}{V} \tag{D-8}$$

$$m = Lm \tag{D-9}$$

$$N = \frac{L}{v} \tag{D-10}$$

$$a = \sqrt{\frac{\bar{P}\gamma}{\bar{\rho}}} = \sqrt{\frac{\gamma kT}{m}} = \sqrt{\frac{\gamma RT}{m}} \tag{D-11}$$

$$c_m = \sqrt{\frac{2kT}{m}} \tag{D-12}$$

$$c = \frac{2}{\sqrt{\pi}}\, c_m = \sqrt{\frac{8kT}{\pi m}} \tag{D-13}$$

$$\bar{c} = \sqrt{\frac{3}{2}}\, c_m = \sqrt{\frac{3kT}{m}} \tag{D-14}$$

$$\mu = 0.499\, c \rho \lambda \tag{D-15}$$

$$M = \frac{w}{a} \tag{D-16}$$

$$Re = \frac{rw\rho}{\mu} = \frac{rw}{\nu} \tag{D-17}$$

$$\nu = \frac{\mu}{\rho} \tag{D-18}$$

$$\delta = \frac{3.4r}{\sqrt{Re}} \quad \text{(for a flat plate with fluid moving tangentially to plate)} \tag{D-19}$$

$$\frac{dP}{dh} = -g\rho \tag{D-20}$$

$$dN = \frac{N}{\sqrt{\pi}}\, e^{-\frac{u_x^2}{c_m^2}}\, d\left(\frac{u_x}{c_m}\right) \tag{D-21}$$

D-2. Conditions for Gas Flow Equilibrium at Entrance to a Chamber.

In this section we shall consider the relations which exist under conditions of gas flow equilibrium at the entrance to a chamber. This analysis is important because of its application to the conditions which must hold when gas flow equilibrium exists between the gas within a pressure gauge and that external to the gauge.

We shall direct our attention to a chamber with an opening in one face. The situation is illustrated in Figure D-1. The chamber shown has a drift velocity relative to the outside atmosphere, which velocity is assumed to have a component of w_x centimeters per second normal to the face of the chamber containing the opening. The gas particles external to the container are assumed to have instantaneous thermal agitation velocities of u centimeters per second which, of course, vary from particle to particle, and are a function of time, temperature and density for a single particle. The x-directed component of u is u_x. The temperature and pressure within the chamber will be denoted by T_1 and P_1, respectively, and those outside the chamber by T_0 and P_0.

We shall assume, further, that the particles both inside and outside the box obey the Maxwell-Boltzmann velocity distribution law and that the particles within the chamber are in temperature equilibrium with the walls of the chamber. T_0, P_0, T_1, P_1 and w_x are assumed to be independent of time for a period of the order of 0.01 seconds. As will be shown in Section D-8 of this appendix, this is a long enough period of time to ensure that an equilibrium state exists and yet it is a short enough time so that T_0, P_0 and w_x will not vary appreciably during this period.

For equilibrium to exist, the number of particles entering the chamber through the opening must equal the number leaving. Let us first consider the number of external particles striking a square centimeter of chamber surface per second, assuming there exists no relative drift velocity between the box and the gas as a whole.

Consider an imaginary cylinder $u_x \triangle t$ centimeters long and one square centimeter in cross-sectional area normal to the box opening, as illustrated in Figure D-1. Any particle within this cylinder that has a velocity with an x-component of at least u_x centimeters per second will reach the box surface

in $\triangle t$ seconds, providing it does not collide with another particle before entering the box. We shall assume that $\triangle t$ (and thus $u_x \triangle t$) is sufficiently small to ensure that the number of particles suffering such a collision is negligible.

Now assume that there is a relative drift velocity (w) between the box and the gas as a whole, and that this drift velocity has an x-directed component of w_x centimeters per second. Then it is necessary to change the length of the imaginary cylinder mentioned above, from $u_x \triangle t$ centimeters to $(u_x + w_x) \triangle t$ centimeters. Either u_x or w_x may be negative, as long as their sum is positive, otherwise no particles will enter the chamber.

The number of particles (dG_0) with x-directed velocities between u_x and $(u_x + du_x)$ centimeters per second that strike the chamber opening in $\triangle t$ seconds can be determined by multiplying the volume of the cylinder by dN_0, which is the number of such particles per cubic centimeter. That is:

$$dG_0 = (u_x + w_x) \triangle t dN_0 \tag{D-22}$$

u_x varies from very large negative values to very large positive values so, in order to find the total number (G_0) of particles entering the box in $\triangle t$ seconds, it is necessary to integrate over all possible positive values of $(u_x + w_x)$, remembering that dN_0 is a function of u_x.

$$G_0 = \int_{u_x + w_x = 0}^{u_x + w_x = \infty} (u_x + w_x) \triangle t dN_0 \tag{D-23}$$

Now

$$dN_0 = \frac{N_0}{\sqrt{\pi}} e^{-\frac{u_x^2}{c^2 m_0}} d\left(\frac{u_x}{c_{m_0}}\right) \tag{D-24}$$

This is the x-directed Maxwell-Boltzmann distribution of velocities. Hence:

$$G_0 = \int_{\frac{u_x}{c_{m_0}} = -\frac{w_x}{c_{m_0}}}^{\frac{u_x}{c_{m_0}} = \infty} (u_x + w_x) \frac{\triangle t N_0}{\sqrt{\pi}} e^{-\frac{u_x^2}{c^2 m_0}} d\left(\frac{u_x}{c_{m_0}}\right) \tag{D-25}$$

$$G_0 = \frac{\triangle t N_0 c_{m_0}}{\sqrt{\pi}} \int_{-\frac{w_x}{c_{m_0}}}^{\infty} \frac{u_x}{c_{m_0}} e^{-\frac{u_x^2}{c^2 m_0}} d\left(\frac{u_x}{c_{m_0}}\right) + \frac{\triangle t N_0 w_x}{\sqrt{\pi}} \int_{-\frac{w_x}{c_{m_0}}}^{\infty} e^{-\frac{u_x^2}{c^2 m_0}} d\left(\frac{u_x}{c_{m_0}}\right) \tag{D-26}$$

Let: $S = \frac{w_x}{c_{m_0}}$ and $s = \frac{u_x}{c_{m_0}}$ (D-27)

Then:

$$G_0 = \frac{\Delta t N_0 c_{m_0}}{\sqrt{\pi}} \int_{-S}^{\infty} s e^{-s^2}\, ds + \frac{\Delta t N_0 w_x}{\sqrt{\pi}} \int_{-S}^{\infty} e^{-s^2}\, ds \tag{D-28}$$

Separating the latter integral:

$$G_0 = \frac{\Delta t N_0 c_{m_0}}{\sqrt{\pi}} \int_{-S}^{\infty} s e^{-s^2} ds + \frac{\Delta t N_0 w_x}{\sqrt{\pi}} \int_{-S}^{o} e^{-s^2} ds + \frac{\Delta t N_0 w_x}{2} \frac{2}{\sqrt{\pi}} \int_{o}^{\infty} e^{-s^2} ds \tag{D-29}$$

These are well-known integrals:[8]

$$\frac{\Delta t N_0 c_{m_0}}{\sqrt{\pi}} \int_{-S}^{\infty} s e^{-s^2} ds = \frac{\Delta t N_0 c_{m_0}}{2\sqrt{\pi}} \left[- e^{-s^2} \right]_{-S}^{\infty} = \frac{\Delta t N_0 c_{m_0}}{2\sqrt{\pi}} e^{-S^2} \tag{D-30}$$

$$\frac{\Delta t N_0 w_x}{\sqrt{\pi}} \int_{-S}^{o} e^{-s^2} ds = \frac{\Delta t N_0 w_x}{2} \left[\frac{2}{\sqrt{\pi}} \int_{o}^{S} e^{-s^2} ds \right] = \frac{\Delta t N_0 w_x}{2} \text{ erf } S \tag{D-31}$$

$$\frac{\Delta t N_0 w_x}{2} \left[\frac{2}{\sqrt{\pi}} \int_{o}^{\infty} e^{-s^2} ds \right] = \frac{\Delta t N_0 w_x}{2} \tag{D-32}$$

Therefore:

$$G_0 = \frac{\Delta t N_0 c_{m_0}}{2\sqrt{\pi}} e^{-S^2} + \frac{\Delta t N_0 w_x}{2} \text{ erf } S + \frac{\Delta t N_0 w_x}{2} \tag{D-33}$$

$$G_0 = \frac{\Delta t N_0 c_{m_0}}{2\sqrt{\pi}} \left[e^{-S^2} + \frac{\sqrt{\pi}\, w_x}{c_{m_0}} \text{ erf } S + \frac{\sqrt{\pi}\, w_x}{c_{m_0}} \right] \tag{D-34}$$

Now: $S = \frac{w_x}{c_{m_0}}$, so:

$$G_0 = \frac{\Delta t N_0 c_{m_0}}{2\sqrt{\pi}} \left[e^{-S^2} + S\sqrt{\pi}\, (1 + \text{erf } S) \right] \tag{D-35}$$

APPENDIX D

The number of particles (G_1) leaving the chamber per square centimeter of the opening in Δt seconds can be calculated in the same way, remembering that now $w_x = o$. Also we must use the values of N, dN and c_m for the interior of the box. Then:

$$G_1 = \int_{u_x = o}^{u_x = \infty} \Delta t u_x dN_1 \tag{D-36}$$

$$dN_1 = \frac{N_1}{\sqrt{\pi}} e^{-\frac{u_x^2}{c_{m_1}^2}} d\left(\frac{u_x}{c_{m_1}}\right) \tag{D-37}$$

$$G_1 = \frac{\Delta t N_1 c_{m_1}}{\sqrt{\pi}} \int_{\frac{u_x}{c_{m_1}} = o}^{\frac{u_x}{c_{m_1}} = \infty} \frac{u_x}{c_{m_1}} e^{-\frac{u_x^2}{c_{m_1}^2}} d\left(\frac{u_x}{c_{m_1}}\right) \tag{D-38}$$

This can be easily integrated, yielding

$$G_1 = \frac{\Delta t N_1 c_{m_1}}{2\sqrt{\pi}} \tag{D-39}$$

Since the chamber is of a finite size, some objection may be raised because of the use of an infinite upper limit for u_x in Equation D-36. This objection is met by assuming that Δt is so small that when the length $u_x \Delta t$ is equal to the x-dimension of the chamber, u_x is so large that only a negligible fraction of the gas particles has velocities greater than this value of u_x.

As remarked before, equilibrium exists when the number of particles entering the chamber is equal to the number leaving. That is,

$$G_1 = G_0 \tag{D-40}$$

or

$$\frac{\Delta t N_1 c_{m_1}}{2\sqrt{\pi}} = \frac{\Delta t N_0 c_{m_0}}{2\sqrt{\pi}} \left[e^{-S^2} + S\sqrt{\pi}(1 + \text{erf } S)\right] \tag{D-41}$$

$$\frac{N_1 c_{m_1}}{N_0 c_{m_0}} = \left[e^{-S^2} + S\sqrt{\pi}(1 + \text{erf } S)\right] \tag{D-42}$$

The pressure within the chamber can be expressed as follows:

$$P_1 = \frac{1}{2} N_1 m_1 c_{m_1}^2 \tag{D-43}$$

and that outside the chamber as:

$$P_0 = \frac{1}{2} N_0 m_0 c_{m_0}^2 \tag{D-44}$$

It will be assumed that the particle mass (m_1) is the same within the box as it is outside (m_0). It is realized that there is some dissociation of the oxygen molecules above an altitude of about 80 kilometers and it is possible that there may be some recombination within the chamber, where the gas is not subject to the strong radiation fields which originally cause the dissociation. The magnitude of this effect is being investigated, but it is believed to be of little practical significance and will be neglected for the present.

Then:

$$\frac{P_1}{P_0} = \frac{\frac{1}{2} N_1 m c_{m_1}^2}{\frac{1}{2} N_0 m c_{m_0}^2} = \frac{N_1 c_{m_1}^2}{N_0 c_{m_0}^2} \tag{D-45}$$

Combining Equations (D-42) and (D-45), one obtains:

$$\frac{P_1}{P_0} = \frac{c_{m_1}}{c_{m_0}} \left[e^{-S^2} + S\sqrt{\pi}(1 + \text{erf } S) \right] \tag{D-46}$$

From Equations (D-1) and (D-5) we have:

$$\frac{1}{2} m c_m^2 = kT \tag{D-47}$$

Using Equation (D-47) in Equation (D-46), remembering that $m_1 = m_0$, we obtain:

$$\frac{P_1}{P_0} = \sqrt{\frac{T_1}{T_0}} \left[e^{-S^2} + S\sqrt{\pi}(1 + \text{erf } S) \right] \tag{D-48}$$

Now let us define f(S) in the following way:

$$f(S) = e^{-S^2} + S\sqrt{\pi}(1 + \text{erf } S) \tag{D-49}$$

A curve of f(S) plotted as ordinate with S plotted as abscissa is shown in Figure D-2.

It is interesting to note that, for S = o (corresponding to w_x = o), f(S) is unity. That is:

$$\frac{P_1}{P_0} = \sqrt{\frac{T_1}{T_0}} \tag{D-50}$$

when there is no normal component of relative drift velocity between the chamber opening and the gas as a whole.

It will be recalled that $S = \frac{w_x}{c_{m_0}}$. We shall now establish a coordinate system to be used throughout the remainder of this appendix in order to find w_x, in case the relative drift velocity (w) between

the chamber and the gas as a whole is not normal to the plane of the opening in the chamber. The situation is illustrated in Figure D-3. The x-axis is taken normal to the plane of the opening of the chamber. The angle Ψ, between the x-axis (thus the normal to the chamber opening) and the relative drift velocity vector (w), will be called the angle of attack.

From Figure D-3 it can be seen that:

$$w_x = w \cos \Psi \tag{D-51}$$

D-3. Proposed Method for Obtaining both Temperature and Pressure Data at Altitudes above about 140 Kilometers.

As is pointed out in the Introduction of this report, one of the original objectives of the project was to determine atmospheric pressure and temperature in the "E" layer of the ionosphere. That is, the primary interest was in obtaining data at altitudes above about 100 kilometers.

The General Electric Company had made calculations concerning the likely trajectories of the V-2's to be fired at White Sands. The results of these calculations were plotted and are shown in Figure D-4. It seemed reasonable to expect that most of the rockets fired would attain heights of the order of 160 kilometers, as indicated on the curve of Figure D-4 marked "Complete Use of Fuel for Most Probable Motor Efficiency."

On the basis of the above, a method was developed during the summer of 1946 for determining pressure and temperature at altitudes great enough that the laws of the kinetic theory of gases could be assumed to hold.

This method of determining pressure and temperature is based on Equation D-48:

$$\frac{P_1}{P_0} = \sqrt{\frac{T_1}{T_0}} \left[e^{-S^2} + S \sqrt{\pi}(1 + \text{erf } S) \right] \tag{D-48}$$

where

$$S = \frac{w_x}{c_{m_0}} = \frac{w \cos \Psi}{c_{m_0}} \tag{D-52}$$

The angle Ψ is defined in Figure D-3.

A single chamber, moving with respect to the outside atmosphere (as described in Section D-2 of this report), gives rise to Equation D-48. It may be assumed that P_1 and T_1 are measurable, since they are quantities existing within the chamber.

Now, c_{m_0} is a function of T_0 and m_0, as shown by this equation:

$$c_{m_0} = \sqrt{\frac{2kT_0}{m_0}} \tag{D-53}$$

It is assumed that m_0, the average mass of the external particles, is known. Therefore, Equation D-48 really contains two unknowns: T_0 and P_0. Thus this equation cannot be used directly, unless either T_0 or P_0 is known.

Now suppose that we have two chambers (1 and 2) fastened together and moving with a velocity (w) relative to the outside gas. Then, for Chamber No. 1:

$$\frac{P_1}{P_0} = \sqrt{\frac{T_1}{T_0}} \left[e^{-S_1^2} + S_1 \sqrt{\pi}(1 + \text{erf } S_1) \right] \tag{D-54}$$

and for Chamber No. 2:

$$\frac{P_2}{P_0} = \sqrt{\frac{T_2}{T_0}} \left[e^{-S_2^2} + S_2 \sqrt{\pi}(1 + \text{erf } S_2) \right] \tag{D-55}$$

where

$$S_1 = \frac{w_{x_1}}{c_{m_0}} = \frac{w \cos \Psi_1}{c_{m_0}} \tag{D-56}$$

and

$$S_2 = \frac{w_{x_2}}{c_{m_0}} = \frac{w \cos \Psi_2}{c_{m_0}} \tag{D-57}$$

If we divide Equation D-54 by Equation D-55 we obtain:

$$\frac{P_1}{P_2} = \sqrt{\frac{T_1}{T_2}} \left[\frac{e^{-S_1^2} + S_1 \sqrt{\pi}(1 + \text{erf } S_1)}{e^{-S_2^2} + S_2 \sqrt{\pi}(1 + \text{erf } S_2)} \right] \tag{D-58}$$

P_1, P_2, T_1 and T_2 are values occurring within Chambers 1 and 2, and can be measured. S_1 and S_2 are given by Equations D-56 and D-57. w, Ψ_1, and Ψ_2 in these equations can be determined. c_{m_0} is given by Equation D-53. In Equation D-53 it may be assumed that m_0 is known. T_0 is the quantity to be determined. Therefore, Equation D-58 is an equation in a single unknown, T_0, which occurs implicitly in S_1 and S_2; hence T_0 should be determinable from this equation. Details of how this may be done will be discussed in the latter part of this section.

On the basis of the theory developed immediately above, it was decided, early in the summer of 1946, to use a conical nosepiece on the rocket for carrying the pressure gauges. A cylindrical nosepiece was considered, also, but, for several reasons, was rejected in favor of the conical shaped nosepiece.

Figure D-5 illustrates the application of the theory, developed in the first part of this sub-section, to the actual nosepiece used on the V-2 rockets.

The angle Ψ_5 is the angle of attack of ionization gauge No. 5 with respect to the total relative velocity w. This is also the angle of attack of the missile as a whole. Similarly Ψ_1 and Ψ_3 are the angles of attack of gauges No. 1 and No. 3, respectively. For simplicity, it is assumed that the three ionization gauges shown, the center-line of the rocket, and the velocity vector w are in the same plane.

Then:

$$\Psi_1 = 75^0 - \Psi_5 \tag{D-59}$$

$$\Psi_3 = 75^0 + \Psi_5 \tag{D-60}$$

To illustrate the possible variations of individual gauge readings over the crest of a typical V-2 trajectory, Figures D-6 and D-7 have been prepared. These curves were computed using the following relations and data:

$$\frac{P_{1,3,5}}{P_0} = \sqrt{\frac{T_{1,3,5}}{T_0}} \left[e^{-S_{1,3,5}^2} + S_{1,3,5} \sqrt{\pi}(1 + \text{erf } S_{1,3,5}) \right]$$

$T_1 = T_3 = T_5 = 313$ degrees, Kelvin.

$$S_{1,3,5} = \frac{w}{c_{m_0}} \cos \Psi_{1,3,5} \qquad c_{m_0} = \sqrt{\frac{2kT_0}{m_0}}$$

P_0 taken from Figure II-2.

T_0 taken from Figure II-3.

w and Ψ taken from data contained in the General Electric Company Report No. 45779, "Report of A-4 Trajectory Calculations Preliminary to A-4 Missile Tests at White Sands, New Mexico."[9]

m_0 assumed constant at ground-level value. In Figure D-7 there have been plotted the same data as in Figure D-6, but with altitude instead of flight time as the abscissa. In both Figures D-6 and D-7 it has been assumed that there was no spin of the rocket about its longitudinal axis, or axis of figure.

If the rocket were spinning about its axis of figure, the readings of the nose gauge (gauge No. 5) would not be affected. However the readings of gauges No. 1 and No. 3 would oscillate between curves No. 1 and No. 3 of Figures D-6 and D-7 as limits, and, of course, at the same period as the period of spin. If the spin were not about the true axis of figure of the rocket, but about some axis other than the axis of figure, the readings of gauge No. 5 might vary above and below the values shown in Figures D-6 and D-7. This is an important point, and an application of it is discussed in Section V.

We shall now discuss the use of Equation D-58 for determining the value of the temperature (T_0) external to the chambers (or ionization gauges). We shall apply Equation D-58 to ionization gauges No. 1 and No. 3, as shown in Figure D-5.

Now, from Equation D-56, D-59 and D-60, we have:

$$S_1 = \frac{w \cos \Psi_1}{c_{m_0}} = \frac{w}{c_{m_0}} \cos (75^\circ - \Psi_5) \tag{D-61}$$

$$S_3 = \frac{w \cos \Psi_3}{c_{m_0}} = \frac{w}{c_{m_0}} \cos (75^\circ + \Psi_5) \tag{D-62}$$

It is assumed that Ψ_5 is known as a function of altitude on both ascent and descent. Also, it is assumed that the rocket is not spinning, and that the other assumptions hold that were postulated in drawing Figure D-5. Then let:

$$b = \frac{S_3}{S_1} = \frac{\cos (75^\circ + \Psi_5)}{\cos (75^\circ - \Psi_5)} \tag{D-63}$$

and b will be known as a function of altitude, since Ψ_5 is known.

Now:

$$f(S_3) = e^{-S_3^2} + S_3 \sqrt{\pi}(1 + \operatorname{erf} S_3) \tag{D-64}$$

$$f(S_3) = e^{-b^2 S_1^2} + bS_1 \sqrt{\pi}(1 + \operatorname{erf} bS_1) = f(bS_1) \tag{D-65}$$

Then Equation D-58 can be rewritten thus:

$$\frac{P_1}{P_3}\sqrt{\frac{T_3}{T_1}} = \frac{e^{-S_1^2} + S_1 \sqrt{\pi}(1 + \operatorname{erf} S_1)}{e^{-S_3^2} + S_3 \sqrt{\pi}(1 + \operatorname{erf} S_3)} = \frac{f(S_1)}{f(bS_1)} \tag{D-66}$$

In this equation all quantities are known, except S_1, which is the quantity whose magnitude is desired, since from it we may determine T_0.

In order to facilitate the determination of S_1, let us take the logarithm of both sides of Equation D-66:

$$\log [f(S_1)] - \log [f(bS_1)] = \log \left[\frac{P_1}{P_3}\sqrt{\frac{T_3}{T_1}}\right] \qquad \text{(D-67)}$$

Curves of $\log [f(S_1)]$ and $\log [f(bS_1)]$ can be drawn, with S_1 as the independent variable, where $f(S)$ is defined by Equation D-49. Then the value of S_1 is determined at which the distance between the curve of $\log [f(S_1)]$ and the curve of $\log [f(bS_1)]$ is equal to $\log \left[\frac{P_1}{P_3}\sqrt{\frac{T_3}{T_1}}\right]$. Having determined S_1, c_{m_0} can be found from Equation D-61 and then T_0 can be calculated using Equation D-53.

None of the three rockets carrying University of Michigan instruments have reached altitudes above about 110 kilometers. Therefore, the above method of determining T_0 and P_0 cannot be expected to be valid for these three flights.

D-4. Theory of Ionization Gauge Calibration.

The detailed procedure for calibrating the pressure gauges is described in Appendix C of this report. In the present section the significance of these calibration results is to be discussed. The relation between the pressure (P_{1C}) within the pressure gauge during its calibration, and the pressure (P_{OC}) read by the calibrating McLeod gauge during this calibration will be analyzed. This is the first relation mentioned in the introduction to this appendix.

Figure D-8 is a simplified diagram of the calibration system showing a pressure gauge (ionization gauge), the calibrating McLeod gauge and position (x), where the ionization gauge is opened in flight. The ionization gauges are calibrated against the McLeod gauge through connecting tubes approximately 1-1/4 to 2 centimeters in diameter and about 200 centimeters in total length. The ionization gauge is thoroughly degassed and the walls are allowed to reach a constant equilibrium temperature before the calibration run is made. Hence, throughout the test the air temperature in the ionization gauge is fairly constant at the gauge wall temperature. The air in the McLeod gauge is at room temperature.

Ionization gauge plate current data then are obtained as a function of the McLeod gauge pressure. Various sets of readings are obtained for various fixed values of ionization gauge grid current. Figures C-9 and C-10 show typical calibration curves obtained in this way. During the flight the ionization gauge plate and grid currents are recorded and, from the gauge calibration curve, the corresponding ionization gauge pressures can be determined. This procedure is described in Appendix F.

We shall now analyze the significance of the calibration results.

When the mean free path of the gas particles is much smaller than the diameter of the connecting tube between the ionization and McLeod gauges, the gas moves by convection and the pressure difference between the two gauges becomes zero. Then:

$$P_{1C} = P_{OC} \qquad \text{(D-68)}$$

This occurs at pressures greater than about 10^{-2} millimeter of mercury, where the mean free path is a small fraction of the connecting tube diameter. This can be seen from Figure D-9, which shows mean free path as a function of pressure. However, pressures in this range are not reliably indicated by an ionization gauge; therefore the calibration curves are accurately determined down to a pressure of only about 10^{-2} millimeter of mercury. The relation between P_{1C} and P_{OC} for the higher pressure range is included here only to indicate a limiting condition.

When the mean free path of the gas particles is many times the inside diameter of the tube connecting the ionization and McLeod gauges, the gas no longer moves as a whole and a pressure difference can exist between the two gauges. This phenomenon is known as "thermal transpiration" and has been the subject of extensive experimental and theoretical work[10,11]. Under these conditions Equation D-50 of this report is valid:

$$\frac{P_{1C}}{P_{OC}} = \sqrt{\frac{T_{1C}}{T_{OC}}} \qquad \text{(D-69)}$$

The magnitudes of T_{1C} and T_{OC} are determined at the time of gauge calibration and the following are representative values:

$$T_{1C} = 345 \text{ degrees, Kelvin.}$$

$$T_{OC} = 290 \text{ degrees, Kelvin.}$$

Then:

$$P_{1C} = P_{OC} \sqrt{\frac{T_{1C}}{T_{OC}}} \cong P_{OC} \sqrt{\frac{345}{290}} = 1.09\, P_{OC} \qquad \text{(D-70)}$$

The mean free path of the gas particles is long compared to the diameter of the connecting tube for pressures less than about 10^{-3} millimeter of mercury. Therefore, this is the range of pressures over which the relation derived above holds.

For pressures between 10^{-2} and 10^{-3} millimeter of mercury, the mean free path of the gas is of the same order of magnitude as the diameter of the tube connecting the McLeod and ionization gauges. The precise analysis of the relation between P_{1C} and P_{OC} is quite involved under these conditions. Knudsen[10,11] has solved the problem by semi-empirical methods and his results show that the ratio of P_{1C} to P_{OC} is equal to the ratio of T_{1C} to T_{OC} raised to a fractional power. This fractional power is a function of the ratio of the mean free path to the tube radius, and includes several empirical constants. However, to the order of accuracies involved here, it can be shown that over this range of pressures P_{1C} and P_{OC} are essentially equal.

Therefore, we may conclude that, under all conditions met with during ionization gauge calibration:

$$P_{1C} = P_{OC}$$

with a maximum error of about ten per cent.

D-5. Analysis of Relations between Ambient Pressure (P_A) and the Pressure (P_{OF}) at the Ionization Gauge Opening during Flight.

The relation between P_A and P_{OF}, which we are to consider in this section, is the third of the three relations mentioned in the Introduction to this appendix. The relations between P_A and P_{OF} are being discussed prior to the discussion of the relations between P_{OF} and P_{1F} because some of the considerations concerning the motion of the rocket through the atmosphere which arise in the discussion of the relations between P_A and P_{OF} are also of importance in discussing the relation of P_{OF} to P_{1F}.

D-5.1. Considerations of Rocket Motion through the Atmosphere.

Up to this point only brief mention has been made of the gas flow conditions adjacent to the cone wall of the nosepiece during the rocket flight. In order to further interpret P_{OF} (pressure at the ionization gauge opening during flight) in terms of the ambient pressure (P_A), the nature of this flow and its relationship to the mean free path of the gas particles must first be determined.

Figures V-1 and D-10 help in visualizing the flight situation. Figure V-1 is a diagram of the V-2 nosepiece used which shows the placement of the five ionization gauges. Figure D-10 illustrates flight conditions for one of the side-wall gauges.

In the lower atmosphere the mean free path is short compared with the dimensions of any equipment employed, whereas at a sufficiently high altitude the mean free path is long relative to equipment dimensions. There is, however, an appreciable range of altitudes, between about 90 and 120 kilometers in our case, in which the mean free path is substantially longer than the dimensions of the measuring instruments and substantially shorter than the major dimensions of the rocket itself. Above about 140 or 150 kilometers the mean free path is long relative to even the major dimensions of the rocket.

Figure II-4 is a plot of estimated mean free path versus altitude, which helps one to understand over what ranges of altitudes the mean free path can be considered long and over what ranges it can be

considered short. This curve has been extrapolated from an altitude of 120 kilometers to an altitude of 160 kilometers by using straight-line extrapolations of the NACA temperature and mean-molecular-weight curves. Since this was an arbitrary procedure, the reliability of the mean free path extrapolation is uncertain. However, it does give one an idea of the order of magnitude of the mean free paths involved between the altitudes of 120 and 160 kilometers.

Theoretical analyses, and intuitive concepts, of value in instrument design and in measurement interpretation, differ radically between the short mean free path and the long mean free path situations. If the mean free path can be called short, then analysis and intuition alike must relate to the continuum of a compressible fluid. If the mean free path can be considered long, analysis and intuition depend on pure kinetic theory considerations. Under the latter conditions we shall say that we are dealing with a "Knudsen gas." Both of these extreme conditions are reasonably well understood as the results of years of experimental and theoretical study.

In the intermediate condition, such that the mean free path cannot be considered either short or long, there as yet exists no simplified general theory. However, this condition has been thoroughly studied for low velocity flows and the effect of increased mean free path appears in a "slip" at the wall.[12] Slip is said to exist when the relative velocity between the wall and the immediately adjacent gas is not zero. That is, the gas "slips" along the wall.

A potentially powerful method of attack on this intermediate condition which is based on the non-uniform gas theory has been introduced by Chapman.[13] However the equations resulting from this method of approach are, in their present form, too involved to be of much use.

In order to make a quantitative estimate as to which regime of flow is applicable at the various altitudes traversed by a V-2, the mean free path must be compared with the thickness of the "boundary layer," rather than with the major dimensions of the rocket. The boundary layer may be thought of as the region adjacent to the surface, in which region velocity and temperature gradients are of importance. These gradients are set up by the relative motion between the gas, as a whole, and the surface. Therefore, within the boundary layer viscous effects and heat conduction are important.

If we denote by λ the length of the mean free path of the gas particles and by δ the thickness of the boundary layer, the ratio of importance is $\frac{\lambda}{\delta}$. Considerations based on the experimental work of many investigators indicate the following very approximate boundaries for the three regions of flow[10,11,14]:

Continuum	$\frac{\lambda}{\delta} \lesssim 0.05$	(D-71)
Intermediate, or slip	$0.05 \lesssim \frac{\lambda}{\delta} \lesssim 10$	(D-72)
Knudsen gas	$\frac{\lambda}{\delta} \gtrsim 10$	(D-73)

In order to evaluate $\frac{\lambda}{\delta}$, it is convenient to express this ratio as a function of Mach number (M) and Reynolds number (Re). This can be done as follows:

$$\frac{\lambda}{\delta} = \frac{\lambda}{r} \cdot \frac{r}{\delta} \tag{D-74}$$

where r is some characteristic dimension of the missile (for example, its length).

The thickness of the boundary layer is[15]:

$$\delta = r \frac{b}{\sqrt{Re}} \tag{D-75}$$

where b is a function of wall temperature, boundary layer temperature and Mach number. However, in view of approximations to be made later, we shall be justified in using for δ the value given for the flow

of an incompressible fluid over a flat plate[7,16]. That is:

$$\delta = \frac{3.4r}{\sqrt{Re}} \tag{D-76}$$

$$\frac{r}{\delta} = \frac{\sqrt{Re}}{3.4} \tag{D-77}$$

We must now evaluate the term $\frac{\lambda}{r}$ appearing in Equation D-74. This will be done by starting with the definition of the Reynolds number. We shall use symbols and relations as defined in the introduction to this appendix. Thus:

$$Re = \frac{wr}{\nu} = \frac{wr}{.499c\,\lambda} \tag{D-78}$$

$$\frac{\lambda}{r} = \frac{w}{.499cRe} \tag{D-79}$$

Now:

$$w = Ma = M\sqrt{\frac{\gamma kT}{m}} \tag{D-80}$$

$$c = \sqrt{\frac{8kT}{\pi m}} \tag{D-81}$$

Using Equations D-80 and D-81 in Equation D-79:

$$\frac{\lambda}{r} = \frac{1}{.499Re}\ M\sqrt{\frac{\gamma kT}{m}}\ \sqrt{\frac{\pi m}{8kT}} \tag{D-82}$$

$$\frac{\lambda}{r} = \frac{M}{.499Re}\sqrt{\frac{\gamma\pi}{8}} \tag{D-83}$$

For a diatomic gas, such as the atmosphere largely is, for all altitudes considered here, γ has the value 1.4. Evaluating the constants in Equation D-83, we have:

$$\frac{\lambda}{r} = 1.49\,\frac{M}{Re} \tag{D-84}$$

Then:

$$\frac{\lambda}{\delta} = \frac{\lambda}{r}\frac{r}{\delta} = \frac{1.49M\sqrt{Re}}{Re\ 3.4} = 0.438\,\frac{M}{\sqrt{Re}} \tag{D-85}$$

or, to the degree of accuracy justifiable:

$$\frac{\lambda}{\delta} = \frac{1}{2}\,\frac{M}{\sqrt{Re}} \tag{D-86}$$

Thus the regions of flow can be approximately separated if the Mach number and the Reynolds number are known. In Figure D-11, D-12 and D-13, $\frac{\lambda}{\delta}$ has been plotted as a function of altitude for the three successful University of Michigan firings. Two different values of Reynolds number were used,

one based upon the total missile length of approximately 14 meters, and the other based upon the distance of the cone-side ionization gauges from the rocket tip (about 0.14 meters). Thus, two curves of $\frac{\lambda}{\delta}$ are shown for each rocket.

In computing these curves of $\frac{\lambda}{\delta} = \frac{\frac{1}{2}M}{\sqrt{Re}}$ values of Mach number (M) were used which were computed by using rocket velocity values (w) as given in Figures A-5, A-10 and A-14. The values for the velocity of sound (a) were the NACA values, as given in Figure II-7 of this report. Then the calculations were made using the equation:

$$M = \frac{w}{a}$$

Curves of Mach number versus altitude are shown in Figure D-14.

The values of Reynolds number (Re) were computed using the equation:

$$Re = \frac{wr}{.499c\lambda}$$

Values of c were computed using the equation:

$$c = \sqrt{\frac{8kT}{\pi m}}$$

NACA values of T, λ and m, as given in Figures II-3, II-4 and II-6, respectively were used in calculating c and Re. The values of Reynolds number for each flight are shown in Figures D-15, D-16 and D-17.

The curves of $\frac{\lambda}{\delta}$ versus altitude could have been computed directly using the equation:

$$\frac{\lambda}{\delta} = 7.32 \times 10^3 \sqrt{\frac{w\lambda}{r}} \left(\frac{m}{T}\right)^{\frac{1}{4}} \qquad \text{(D-87)}$$

where the values of T, λ and m would be taken from the curves of NACA data (Figures II-3, II-4 and II-6 of this report). The calculations of $\frac{\lambda}{\delta}$ were not made directly in this way since it is instructive to have the curves of Mach number and Reynolds number versus altitude. Equation D-87 follows directly from Equation D-74, using values of δ, Re and c, as given in Equations D-76, D-78 and D-81, respectively.

It will be noted that the values of temperature, mean free path, velocity of sound and mean gas particle velocity, which have been used, are ambient values. The actual values existing in the immediate vicinity of the rocket undoubtedly differ considerably from the ambient values, due to the disturbances set up by the motion of the rocket. However, it would be extremely difficult to evaluate accurately the changes in T, λ, a and c which are caused by these disturbances (which disturbances appear as a shock wave and, possibly, as turbulence). In view of the uncertainties existing even in the ambient values of T, λ, a and c, and due to the fact that the present analysis is intended only as a first approximation to the solution of the extremely difficult problem of the interpretation of the readings of the pressure gauges, it is considered that the use of ambient values is justified. It is believed that the use of ambient values for T, λ, a and c will not introduce an error in $\frac{\lambda}{\delta}$ of more than a factor of 1.5 or 2, which is not serious. This would simply shift somewhat the boundaries of the flow regions marked on Figures D-11, D-12 and D-13, which boundaries, after all, are not at all well defined.

Figures D-11, D-12 and D-13 indicate that, throughout the altitudes attained by these three rockets, the atmosphere can be regarded as a continuum in considering the full length of the V-2.

In considering the flow around the nose of the rocket, Figures D-11, D-12 and D-13 show that below an altitude of about 80 kilometers the atmosphere can be regarded as a continuum, or compressible

fluid. Above this altitude the motion of the rocket must be considered as taking place in a "slip" region, since here $\frac{\lambda}{\delta} \gtrsim 0.05$.

D-5.2. Relations between Ambient Pressure (P_A) and the Pressure (P_{OF}) at the Ionization Gauge Opening during Flight.

It has been shown in Section D-5.1 of this report that the flow in the vicinity of the nose of the rocket can be considered as that due to a continuum for all altitudes below about 80 kilometers and as a slip from 80 kilometers to the maximum altitude attained by the three rockets carrying University of Michigan instruments. Of course this division at 80 kilometers holds only for these three flights and would not necessarily apply to other flights where the curve of $\frac{\lambda}{\delta}$ might be different due to different curves of Mach number and of Reynolds number versus altitude. Therefore, it is necessary that we investigate the relations between P_A and P_{OF} under both conditions, i.e., assuming the existence of a continuum and assuming that slip flow exists.

First we shall discuss the flow below 80 kilometers, using the results obtained by assuming a compressible fluid. A strong normal detached shock wave forms directly in front of the truncation of the nosepiece cone. This shock wave tapers off, farther back from the nose of the rocket, until it falls along the direction expected for an ogive (such as the V-2), which is roughly the same as that due to a cone with a 15-degree half-angle. However, since the mean free path is of the order of a millimeter, the shock wave can not be idealized as a line. It has a finite thickness, perhaps two to five mean free paths.

The flow in the neighborhood of the nose (near the ionization gauge openings) is a complicated mixture of the flow through the curved shock wave set up by the flat nose of the nosepiece and that through the shock wave due to a 15-degree half-angle cone. No analysis has ever been made of such a situation, and it is far too big a job to be covered in this first approach to the final solution of the overall problem.

Taylor and Maccoll[17] have analyzed the flow of a compressible fluid about true cones. On the basis of the Taylor-Maccoll analysis, Kopal[18] has prepared tables relating the cone-wall pressure to the ambient pressure. Due to the lack of more exact information we must assume that the Taylor-Maccoll theory holds in the vicinity of the ionization gauges. Figure D-18 prepared using the Kopal tables, shows the ratio of the cone-wall pressure (P_{OF}) to ambient pressure (P_A) as a function of Mach number for cones of half-angles of 10 degrees, 15 degrees or 20 degrees.

From Figure D-14, which shows the values of Mach numbers which occurred during the three V-2 flights under consideration, it can be seen that between the altitudes of 60 and 80 kilometers the Mach numbers ranged between 2.0 and 2.5. This range of altitudes is that over which we are at present interested in finding the relation between P_A and P_{OF}. Figure D-18 shows that for a 15-degree half angle cone, at Mach numbers between 2.0 and 2.5, the ratio of P_{OF} to P_A varies from 1.55 to 1.75.

It is well-known that the angle between the longitudinal axis of the rocket and the relative velocity vector (between the rocket and the air) is not zero over much of the rocket's trajectory. This angle will be referred to as the "angle of attack of the rocket." The angle relations are discussed in Appendix E of the present report. The Kopal tables do not contain data covering this situation, therefore there are included in Figure D-18 curves for cones whose half-angles are 20 degrees and 10 degrees. It is believed that these curves will give some information concerning the ratio of P_{OF} to P_A when the rocket's angle of attack differs from zero by perhaps as much as five degrees. From these curves it appears that, for an angle of attack of five degrees, the ratio of P_{OF} to P_A may vary between 1.25 and 2.35 over the range of Mach numbers under consideration, depending upon the position of the periphery of the cone at which P_{OF} is being measured. Thus, in case the rocket is spinning about its longitudinal axis, the pressure read by an ionization gauge might vary between limits whose ratio is 2.35/1.25 if the angle of attack were about five degrees. This fact has been taken into account, in interpreting the pressure readings, by drawing mean curves.

We must now consider the conditions existing between the altitudes of 80 and 110 kilometers. The proper method of approach would be to analyze the flow when $\frac{\lambda}{\delta}$ is of the order of 0.1. Here a definite

slip motion occurs and it could very well be that the shock wave is so thick (10-30 centimeters) that the ionization gauge openings are actually immersed in the shock wave. This would lead one to expect the gauges to read some value of pressure intermediate between ambient pressure and the pressure existing behind the shock wave.

Since no analysis exists on the basis of which the ratio of P_{OF} to P_A can be calculated in a slip region, we shall have to apply naively the results of Taylor-Maccoll here. They should be fairly valid up to the maximum altitudes attained by the University of Michigan rockets. The value of 0.05 for $\frac{\lambda}{\delta}$ which is supposed to separate the regions of compressible flow and slip flow is not a hard-and-fast limiting value and, after all, the maximum value of $\frac{\lambda}{\delta}$ occurring on any of the three flights is a little less than 0.3. The Mach numbers for this portion of the flight do not exceed 2.3 so, from Figure D-18, we see that the average ratio of P_{OF} to P_A should not exceed about 1.7. It may be less than this if the ionization gauges are actually immersed in the shock wave.

We may conclude that, for the pressure data presented in this report, the ratio of P_{OF} to P_A for mean values of pressure readings should never exceed about 1.75.

D-6. Relations between Pressure (P_{1F}) within Ionization Gauge during Flight, to Pressure (P_{OF}) at the Port of the Ionization Gauge.

The relation between P_{1F} and P_{OF}, which will be considered in this section, is the second of the three relations mentioned in the Introduction to this appendix.

The situation under flight conditions is somewhat similar to that encountered during the calibration of the ionization gauge. However, during flight the external gas may have an important drift velocity relative to the gauge opening. The effect of this drift velocity depends upon the nature of the gas flow and upon the angle of attack of the opening of the gauge.

As has been pointed out in Section D-5 of this report, the air flow about the nose of the rocket can be considered from the standpoint of a compressible fluid at altitudes below about 80 kilometers. That is, the air can be considered as a continuum and the random motions of the gas particles do not have to be taken into account. This means that a shock wave is set up by the rocket and that the air flow at the surface of the rocket is, therefore, parallel to the surface. Thus, there is no component of velocity of air flow normal to the openings of the side-wall ionization gauges.

Reference to Figure II-4 shows that at altitudes below 80 kilometers the mean free path probably is less than 0.2 centimeter. Therefore, the mean free path is considerably less than the diameter of the tubulation leading from the ionization gauge proper to the outside air, which diameter is about 1-1/4 centimeters. It has been shown in Section D-4 (Ionization Gauge Calibration Theory) that under these conditions the gauge reads the true outside pressure (Equation D-68). Therefore, we can say that at altitudes below 80 kilometers:

$$P_{1F} = P_{OF}$$

Between the altitudes of 80 and 108.5 kilometers (the maximum altitude reached by any of the three rockets carrying University of Michigan instruments) it has been shown in Section D-5 of this report that the air flow about the rocket takes place according to the laws of slip flow. However, as pointed out in Section D-5, the maximum value of $\frac{\lambda}{\delta}$ attained during any one of the three rocket flights was a little less than 0.3. Thus, the flow takes place in the region only slightly above the vague boundary ($\frac{\lambda}{\delta} = 0.05$) between the continuum and slip regions. Therefore, it was assumed in Section D-5 that the laws of the flow of a continuum hold between the altitudes of 80 and 108.5 kilometers, and this same assumption will be made here. Hence, it may be said that there is no component of air velocity normal to the openings of the side-wall ionization gauges.

Reference to Figure II-4 shows that, between the altitudes of 80 and 108.5 kilometers, the mean free path may vary from about 0.2 centimeter to 6 centimeters. Thus, the mean free path is of the same

order of magnitude as the diameter (1-1/4 centimeters) of the tubulation connecting the ionization gauge to the outer atmosphere. This situation was discussed in Section D-4 of this report and it was concluded that the pressure within the ionization gauge was approximately equal to the pressure outside. That is:

$$P_{1F} = P_{OF}$$

There are indications that the values of mean free path predicted by the NACA (shown in Figure II-4) may be somewhat smaller than those which actually exist. On the V-2 fired March 7, 1947, the Naval Research Laboratory had installed pressure measuring equipment. From these pressure measurements they calculated values of temperature which results are contained in a report issued by the Naval Research Laboratory.[19] The NRL pressure readings, which show pressure values somewhat lower than those predicted by the NACA, are in close agreement with the University of Michigan ionization gauge readings. Figure i-1 shows the pressure values as determined by the NACA, the Naval Research Laboratory and the University of Michigan, and Figure i-2 illustrates the temperature values obtained by these three organizations.

Using NRL values of pressure and temperature and NACA values for average molecular weight, a second curve of mean free path versus altitude has been prepared. This is shown in Figure D-19 (marked "NRL"), together with a plot of mean free path as predicted by the NACA. According to the curve of mean free path, marked "NRL," at altitudes above 100 kilometers the mean free path is greater than ten centimeters, and thus long relative to the diameter of the ionization gauge tubulation.

It was shown in Section D-2 that under these conditions the relation between P_{1F} and P_{OF} is:

$$\frac{P_{1F}}{P_{OF}} = \sqrt{\frac{T_{1F}}{T_{OF}}} \qquad \text{(D-88)}$$

This equation holds if there is no normal component of drift velocity of the external gas relative to the opening of the pressure gauge. It has been shown in Section D-5.1 that, up to the maximum altitudes attained by the three rockets being considered in this report, there is no such component.

The use of Equation D-88 requires a knowledge of the temperature (T_{1F}) of the gas within the gauge, and of the temperature (T_{OF}) of the external gas at the entrance to the gauge. Platinum wire thermometers were applied to ionization gauges carried on the rockets fired February 20, 1947 and December 8, 1947. The temperature data thus obtained are shown in Figures D-20 and D-21. A reasonable value for T_{1F} at altitudes above 100 kilometers is seen to be about 310 degrees, Kelvin.

It is necessary now to evaluate T_{OF}. It has been shown in Section D-5 that over the entire trajectories of the three rockets carrying University of Michigan apparatus the boundary layer very likely was laminar. Under these conditions, the gas adjacent to the wall of the rocket was at wall temperature. It is necessary, then, to determine the cone wall temperature (T_W). Since the thick-walled inner cone of the rocket nosepiece was not exposed to the atmosphere until an altitude of at least 45 kilometers was reached, it is reasonable to suppose that the wall temperature did not change much from the ground value (approximately 300 degrees, Kelvin). At these altitudes a calculation shows that the heat transferred from the boundary layer to the cone wall amounted to only about 4.4×10^{-6} BTU per second per degree Fahrenheit. The largest heat transfer was that received from the radiation of the sun, about 0.11 BTU per second. Also, the cone wall itself radiated about 3.6×10^{-2} BTU per second. Thus, the 1/4-inch-thick aluminum inner cone could hardly change in temperature by more than a fraction of a degree during the 80-100 seconds under consideration. Therefore, it may be assumed that

$$T_{OF} = 300 \text{ degrees, Kelvin.}$$

Using Equation D-88, we have:

$$\frac{P_{1F}}{P_{OF}} = \sqrt{\frac{310}{300}} = 1.015$$

Thus, to the order of approximation under consideration, it may be said that at all altitudes of importance on the three rocket flights:

$$P_{1F} = P_{OF}$$

D-7. Summary of Relations between Ambient Atmospheric Pressure (P_A) and Calibration Pressure (P_{OC}) of Ionization Gauges.

The procedure of reducing pressure data from the telemetering records is discussed in detail in Appendix F. The procedure is essentially this: The telemetering records give values of ionization gauge plate current and grid current. Using these current values, one determines, from the calibration curve for that particular ionization gauge, the values of calibration pressure (P_{OC}) corresponding to these current values. As mentioned previously, it is necessary to relate this pressure (P_{OC}) to the ambient pressure (P_A) in the vicinity of the rocket during flight.

In the preceding sections of this appendix we have concluded that probably the following relations are valid at all altitudes above 60 kilometers attained by the three rockets carrying University of Michigan equipment:

$$P_{1F} = 1.015\ P_{OF}$$

$$P_{OC} \leq P_{1C} \leq 1.09\ P_{OC}$$

$$P_A \leq P_{OF} \lesssim 1.75\ P_A$$

The uncertainty in the determination of the relation between P_A and P_{OF} is sufficiently great to warrant making the assumptions that $P_{1F} = P_{OF}$ and that $P_{1C} = P_{OC}$. Now in the reduction of data P_{1C} is set equal to P_{1F}, so we may conclude from these above relations that:

$$P_A \gtrsim \frac{P_{OC}}{1.75}$$

$$P_A \gtrsim 0.57\ P_{OC}$$

Also, it probably is true that:

$$P_A \lesssim P_{OC}$$

Therefore, we may conclude that the ambient pressure probably does not exceed the mean values of the ionization gauge readings on the ascent portion of the flight, and probably is not less than about one-half of these mean values.

D-8. Theoretical Analysis of Response Time of Ionization Gauges.

As is mentioned in Appendix C, the ionization gauges, for the firings discussed in this report, were sealed-off in the laboratory at a pressure of about 3×10^{-6} millimeter of mercury. The gauges were not opened until after the rockets reached fairly high altitudes. Therefore it was necessary, in the early planning, to make an estimate of the response time of the ionization gauges to changes in pressure. This analysis is included in this section because of its general interest and because of its importance as an aid to the correct interpretation of the ionization gauge pressure readings.

The following analysis is based on the theory developed in Section D-2 of this appendix, and therefore is applicable only to regions where the mean free path of the gas particles is long relative to the diameter of the ionization gauge tubulation.

From Equation D-35 we have, for the total number (G_0') of particles entering the chamber in a time dt:

$$G_0' = I\left[\frac{N_0 c_{m_0}}{2\sqrt{\pi}}\right] A\,dt \tag{D-89}$$

where

$$I = [e^{-S^2} + S\sqrt{\pi}(1 + \text{erf } S)] \tag{D-90}$$

A = area of chamber opening in square centimeters.

Similarly, the total number (G_1') of particles leaving the chamber in a time dt is (using Equation D-39):

$$G_1' = \left[\frac{N_1 c_{m_1}}{2\sqrt{\pi}}\right] A\,dt \tag{D-91}$$

The change in particle density, or concentration (dN_1), within the chamber is:

$$dN_1 = (G_0' - G_1')\frac{1}{V} \tag{D-92}$$

where V is the volume of the chamber in cubic centimers.

Then:

$$\frac{dN_1}{dt} = \frac{A}{2\sqrt{\pi}\,V}\left[IN_0 c_{m_0} - N_1 c_{m_1}\right] \tag{D-93}$$

Separating variables:

$$\frac{dN_1}{IN_0 c_{m_0} - N_1 c_{m_1}} = \frac{A}{2\sqrt{\pi}\,V}\,dt \tag{D-94}$$

This can be integrated at once, yielding:

$$-\frac{1}{c_{m_1}}\log\left[IN_0 c_{m_0} - N_1 c_{m_1}\right] = \frac{At}{2\sqrt{\pi}\,V} + C \tag{D-95}$$

In this integration it has been assumed that N_0 is a constant. This means that the gas concentration external to the chamber is independent of any flow of gas into, or out of, the chamber. Physically this is true, during flight, since the region external to the chamber is the unconfined atmosphere of the earth. During calibration of the ionization gauge this is not true, but we are not particularly concerned with the response time of the ionization gauge during calibration.

The integration constant (C) in Equation D-95 can be evaluated by calling N_{to} the value of the concentration (N_1) within the chamber at t = o, the instant at which the chamber is exposed to the external atmosphere.

Then:

$$\log\left[\frac{IN_0 c_{m_0} - N_1 c_{m_1}}{IN_0 c_{m_0} - N_{to} c_{m_1}}\right] = -\frac{Ac_{m_1}}{2\sqrt{\pi}\,V}\,t = -\frac{t}{\beta} \tag{D-96}$$

where

$$\beta = \frac{2\sqrt{\pi}\,V}{Ac_{m_1}} \tag{D-97}$$

Thus:

$$\frac{IN_0 c_{m_0} - N_1 c_{m_1}}{IN_0 c_{m_0} - N_{to} c_{m_1}} = e^{-\frac{t}{\beta}} \tag{D-98}$$

Multiplying both sides of Equation D-98 by -1, adding 1 to each side, and rearranging:

$$N_1 - N_{to} = \left[\frac{IN_0 c_{m_0} - N_{to} c_{m_1}}{c_{m_1}}\right]\left[1 - e^{-\frac{t}{\beta}}\right] \tag{D-99}$$

Now β is the time, in seconds, required for the gas concentration (N_1) within the chamber to change from its initial value (N_{to}) to $[N_{to} + 0.63\ (N_1 - N_{to})]$. This means that in β seconds the gas concentration inside the container will accomplish 63% of the change from the initial value to the final equilibrium value.

To determine the approximate response time (β) for a VG-1A ionization gauge we shall use the following values for the constants involved:

V = 100 cubic centimeters.

A = 1.25 square centimeters.

$c_{m_1} = 4.5 \times 10^4$ centimeters per second.

(based on: T = 350 degrees, Kelvin

m = 4.81×10^{-23} grams)

Then the response time (β) for the VG-1A ionization gauge should be approximately six milliseconds.

D-9. *Method for Determining Atmospheric Temperature.*

The method for determining atmospheric temperature is based on the barometric equation:

$$\frac{d}{dh}(\log P_A) = -\frac{Mg}{RT} \tag{D-100}$$

Earlier in this appendix the pressure readings of the ionization gauges were shown to be approximately equal to the ambient pressure. In computing temperature, using Equation D-100, we should consider the second-order approximation to true ambient pressure, instead of the first-order approximation, since the derivative of the pressure is used. However, if this were done it would be necessary to use the relationship between P_{OF} and P_A. Since this relationship is, at present, known to only a rough first order approximation it has been assumed, for the purpose of computing atmospheric temperature, that $P_{OF} = P_A$. Therefore, the equation used for the computation of the atmospheric temperature values shown in Figure i-II was this:

$$\frac{d}{dh}(\log P_{OF}) = -\frac{Mg}{RT} \tag{D-101}$$

Of course this equation yields only very approximate values for the temperature, but it is the best that can be done at present.

FIG. NO. D-1

PHYSICAL ILLUSTRATION FOR DETERMINING GAS FLOW EQUILIBRIUM CONDITIONS AT CHAMBER OPENING.

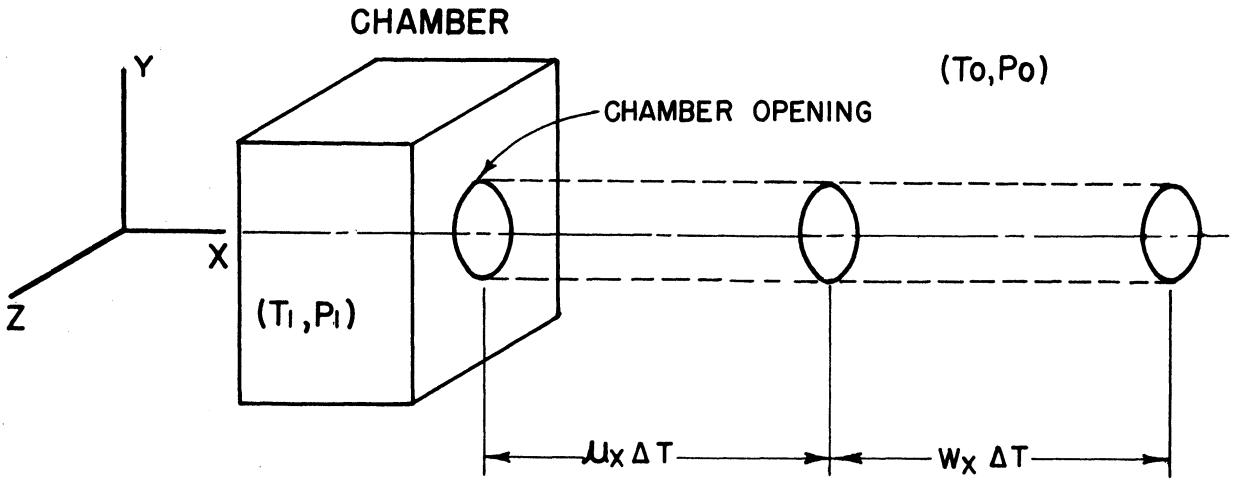

T_I = TEMPERATURE WITHIN CHAMBER

P_I = PRESSURE WITHIN CHAMBER

T_o = TEMPERATURE EXTERNAL TO CHAMBER

P_o = PRESSURE EXTERNAL TO CHAMBER

W_X = X-COMPONENT OF RELATIVE DRIFT VELOCITY BETWEEN CHAMBER AND GAS

μ_X = X-COMPONENT OF GAS PARTICLE VELOCITY

ΔT = TIME INTERVAL UNDER CONSIDERATION

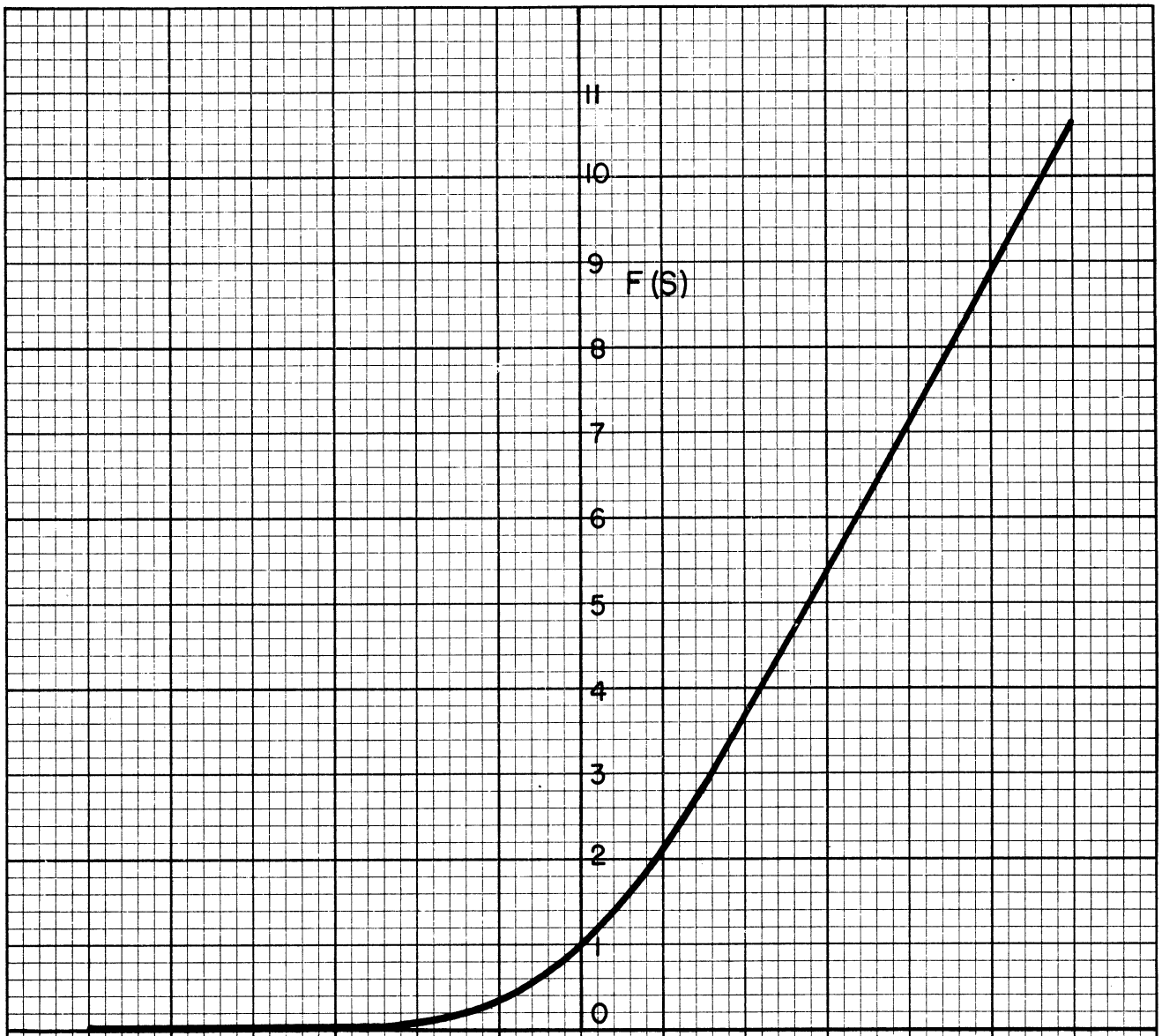

FIG. NO. D-2

CURVE OF F(S) VERSUS S

$$F(S) = e^{-S^2} + S\sqrt{\pi}\,(1 + \mathrm{ERF}\ S)$$

$$S = \frac{W_X}{C_{MO}}$$

W_X = X-COMPONENT OF RELATIVE DRIFT VELOCITY BETWEEN CHAMBER AND GAS

C_{MC} = MOST PROBABLE GAS PARTICLE VELOCITY

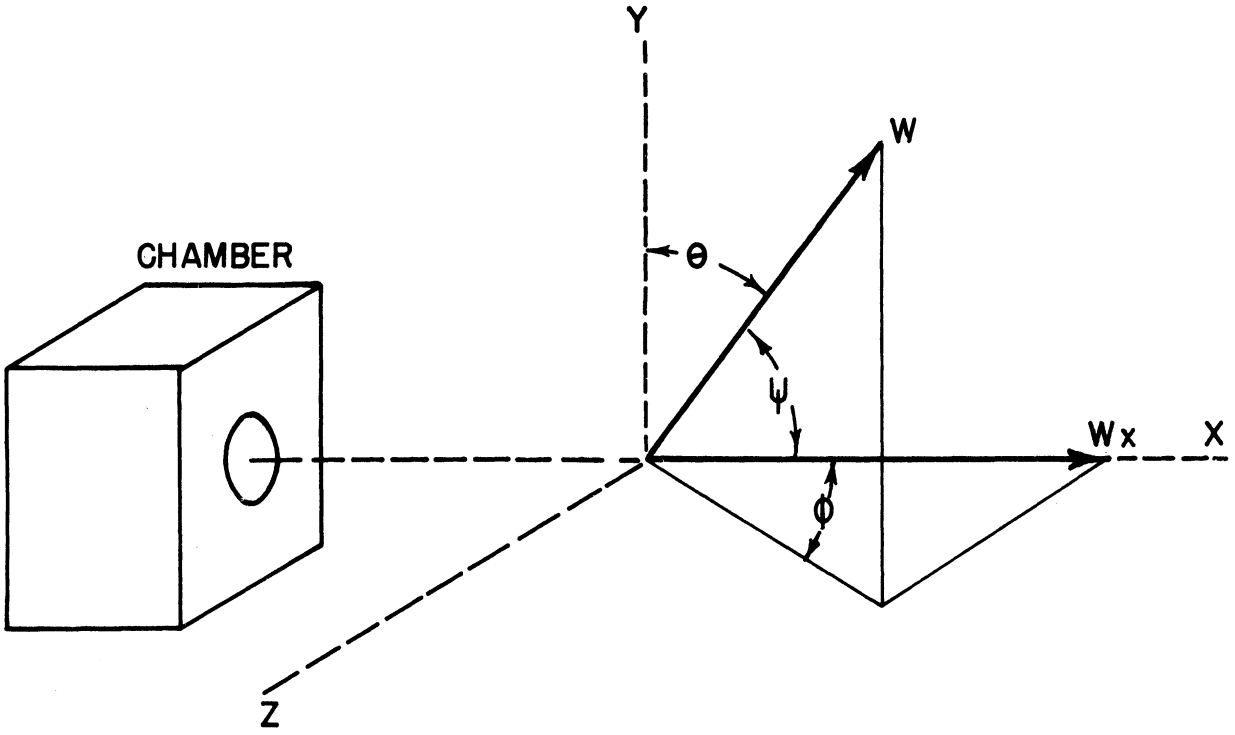

FIG. NO. D-3

ILLUSTRATION OF RELATIONSHIPS BETWEEN W, W_X, θ, ϕ, ψ AND RECTANGULAR COORDINATE SYSTEM.

W= TOTAL RELATIVE DRIFT VELOCITY BETWEEN CHAMBER AND GAS.

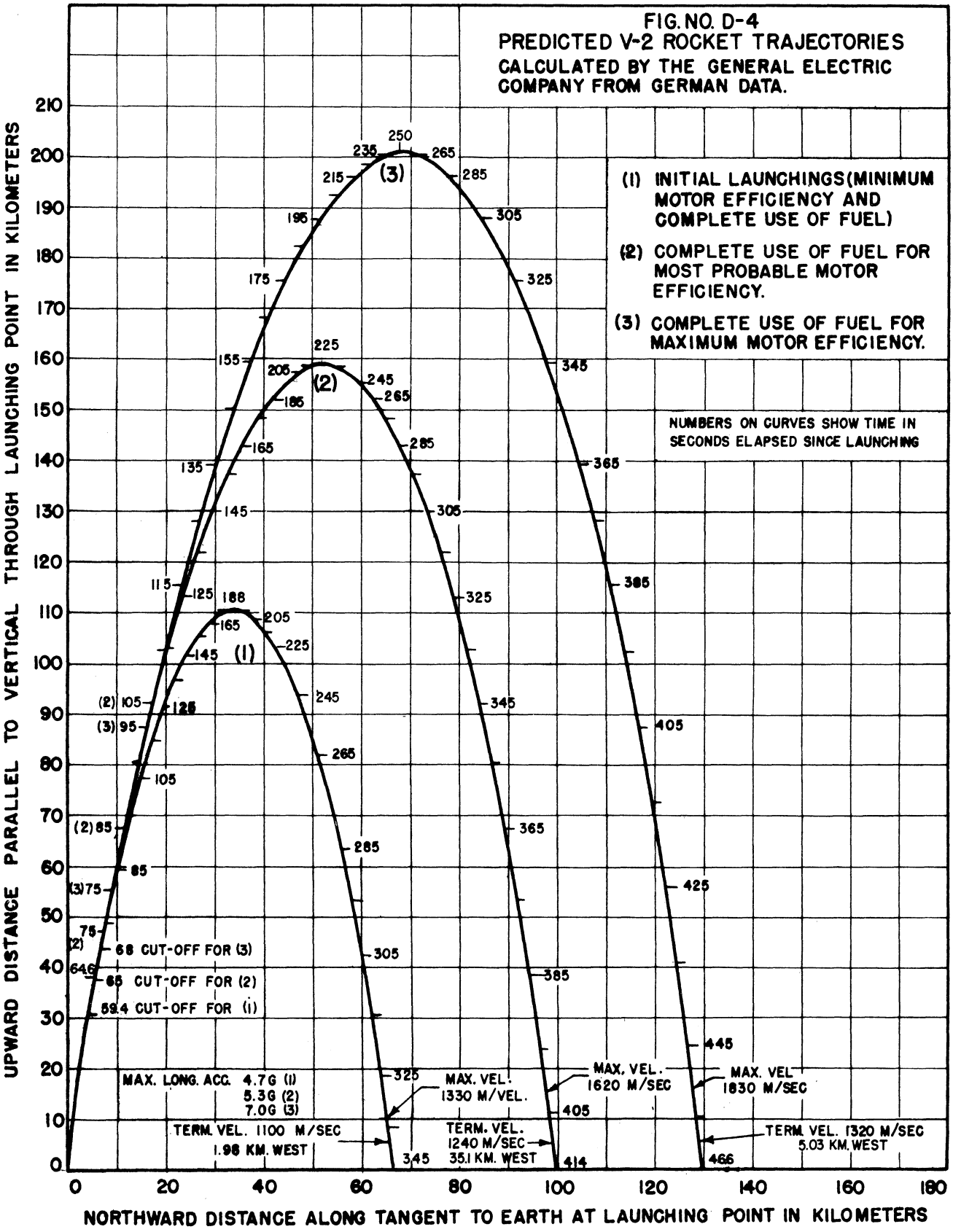
FIG. NO. D-4
PREDICTED V-2 ROCKET TRAJECTORIES
CALCULATED BY THE GENERAL ELECTRIC COMPANY FROM GERMAN DATA.
(1) INITIAL LAUNCHINGS (MINIMUM MOTOR EFFICIENCY AND COMPLETE USE OF FUEL)
(2) COMPLETE USE OF FUEL FOR MOST PROBABLE MOTOR EFFICIENCY.
(3) COMPLETE USE OF FUEL FOR MAXIMUM MOTOR EFFICIENCY.
NUMBERS ON CURVES SHOW TIME IN SECONDS ELAPSED SINCE LAUNCHING
UPWARD DISTANCE PARALLEL TO VERTICAL THROUGH LAUNCHING POINT IN KILOMETERS
NORTHWARD DISTANCE ALONG TANGENT TO EARTH AT LAUNCHING POINT IN KILOMETERS
MAX. LONG. ACC. 4.7G (1) 5.3G (2) 7.0G (3)
68 CUT-OFF FOR (3)
65 CUT-OFF FOR (2)
59.4 CUT-OFF FOR (1)
MAX. VEL. 1330 M/VEL.
MAX. VEL. 1620 M/SEC
MAX. VEL 1830 M/SEC
TERM. VEL. 1100 M/SEC 1.98 KM. WEST
TERM. VEL. 1240 M/SEC 35.1 KM. WEST
TERM. VEL. 1320 M/SEC 5.03 KM. WEST

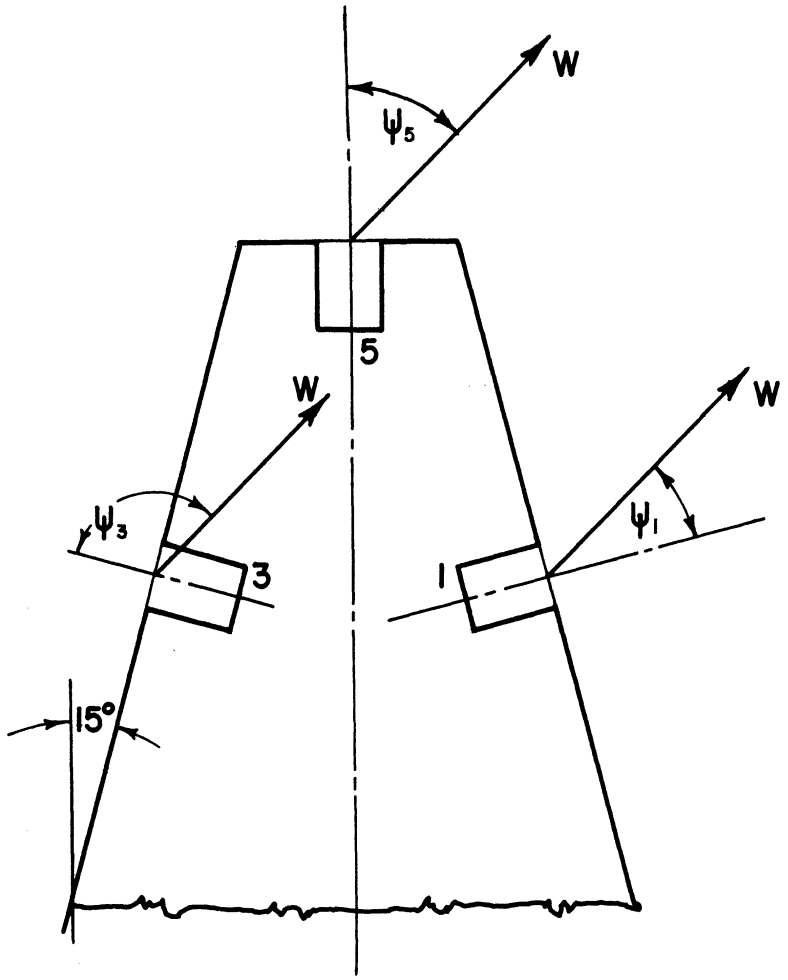

FIG. NO. D-5
DIAGRAM ILLUSTRATING ANGLES OF ATTACK
OF IONIZATION GAUGES IN THE NOSEPIECE

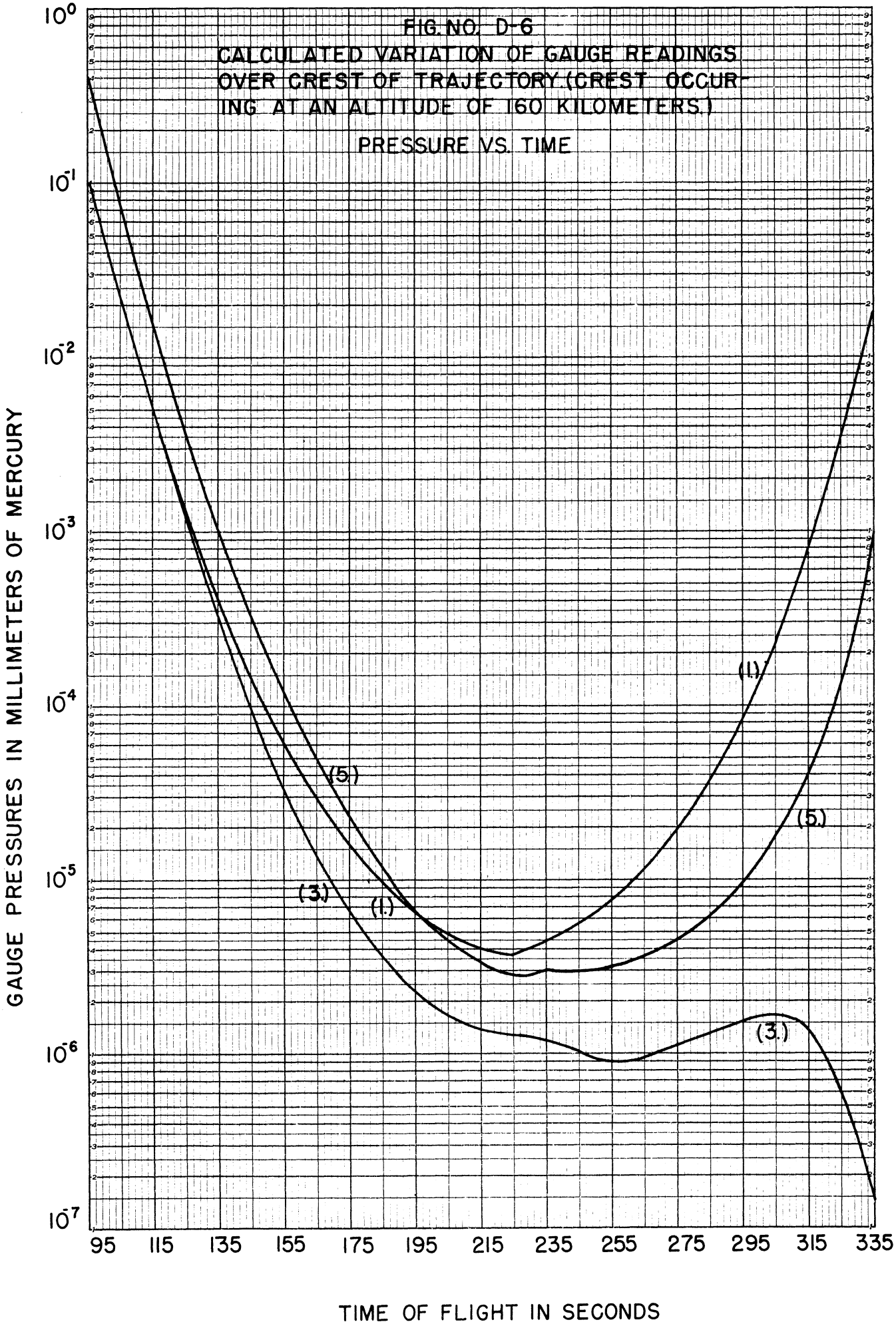
FIG. NO. D-6
CALCULATED VARIATION OF GAUGE READINGS OVER CREST OF TRAJECTORY (CREST OCCURING AT AN ALTITUDE OF 160 KILOMETERS.)
PRESSURE VS. TIME
GAUGE PRESSURES IN MILLIMETERS OF MERCURY
10^{0}
10^{-1}
10^{-2}
10^{-3}
10^{-4}
10^{-5}
10^{-6}
10^{-7}
95
115
135
155
175
195
215
235
255
275
295
315
335
TIME OF FLIGHT IN SECONDS
(1.)
(5.)
(3.)
(1.)
(5.)
(3.)

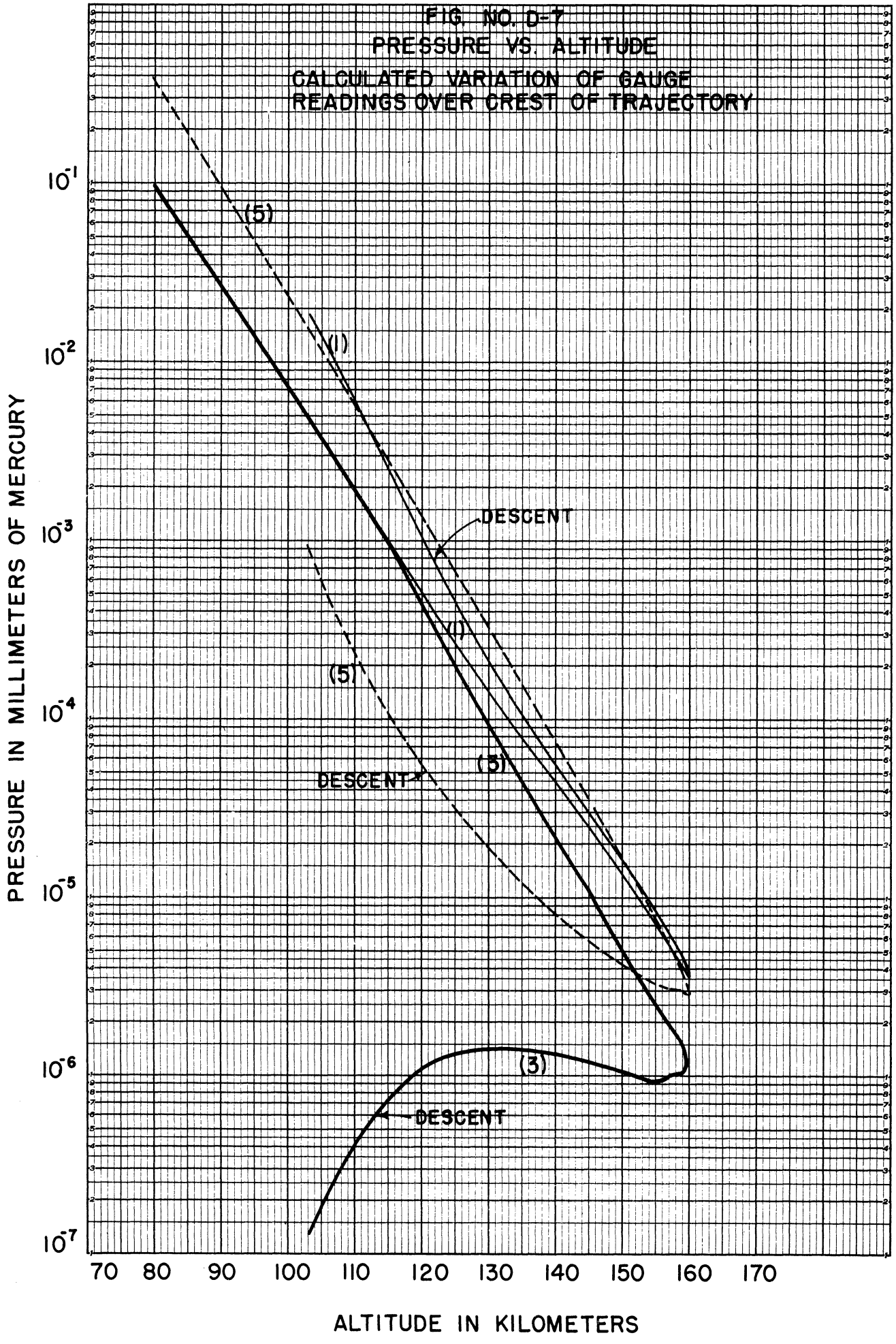
FIG. NO. D-7
PRESSURE VS. ALTITUDE
CALCULATED VARIATION OF GAUGE READINGS OVER CREST OF TRAJECTORY
PRESSURE IN MILLIMETERS OF MERCURY
10^{-1}
10^{-2}
10^{-3}
10^{-4}
10^{-5}
10^{-6}
10^{-7}
(5)
(1)
DESCENT
(1)
(5)
(5)
DESCENT
(3)
DESCENT
70 80 90 100 110 120 130 140 150 160 170
ALTITUDE IN KILOMETERS

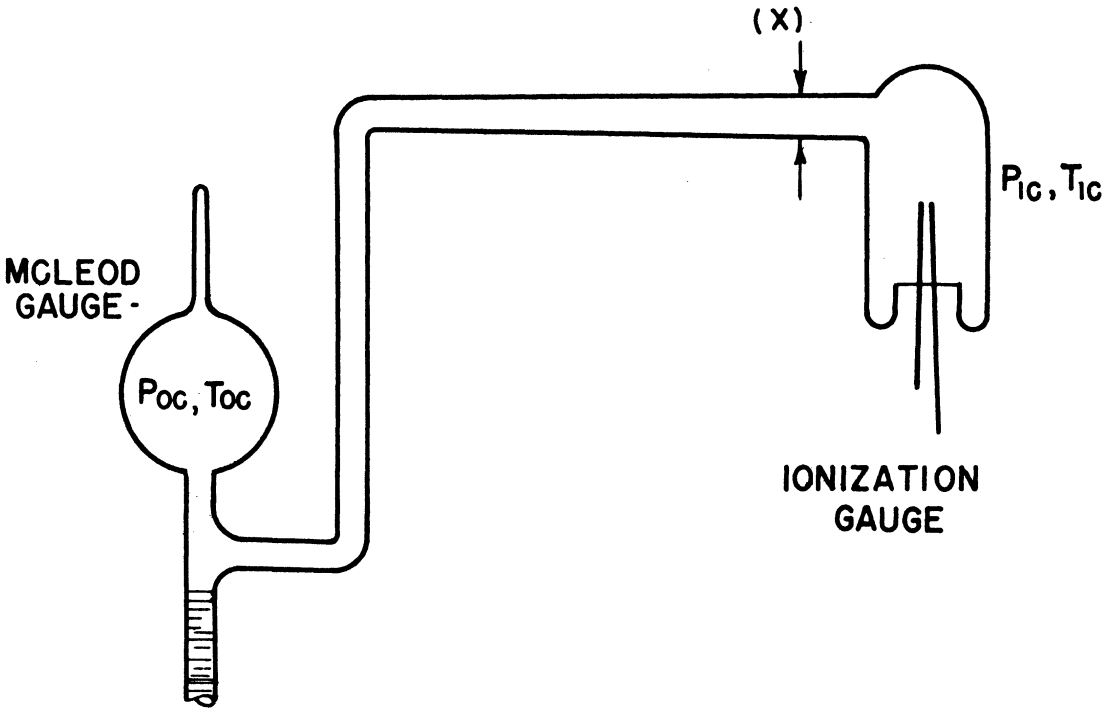

FIG. NO. D-8
SIMPLIFIED DIAGRAM ILLUSTRATING
GAUGE OPERATION DURING CALIBRATION

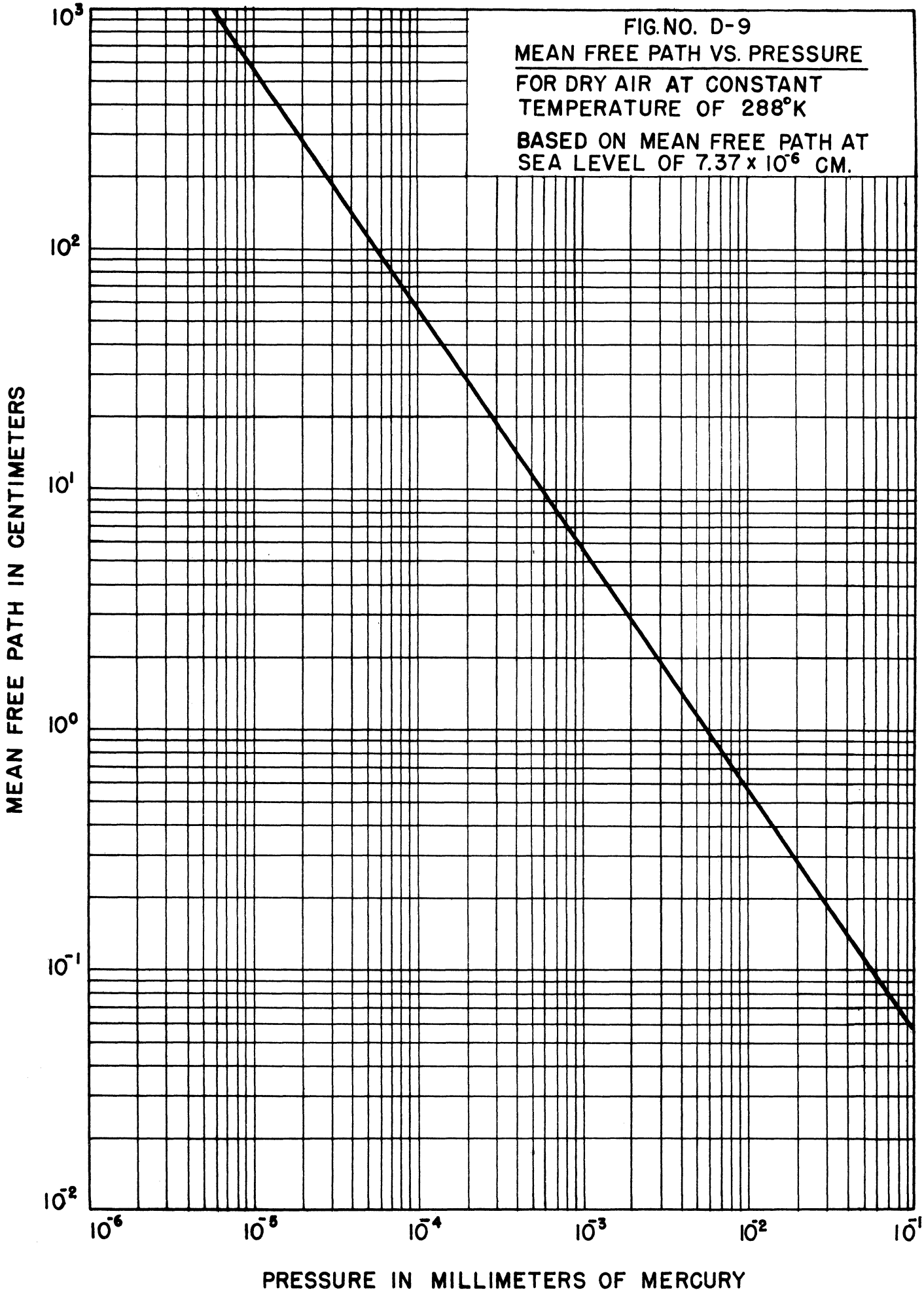
FIG. NO. D-9
MEAN FREE PATH VS. PRESSURE
FOR DRY AIR AT CONSTANT TEMPERATURE OF 288°K
BASED ON MEAN FREE PATH AT SEA LEVEL OF 7.37 x 10⁻⁶ CM.
MEAN FREE PATH IN CENTIMETERS
10³
10²
10¹
10⁰
10⁻¹
10⁻²
10⁻⁶
10⁻⁵
10⁻⁴
10⁻³
10⁻²
10⁻¹
PRESSURE IN MILLIMETERS OF MERCURY

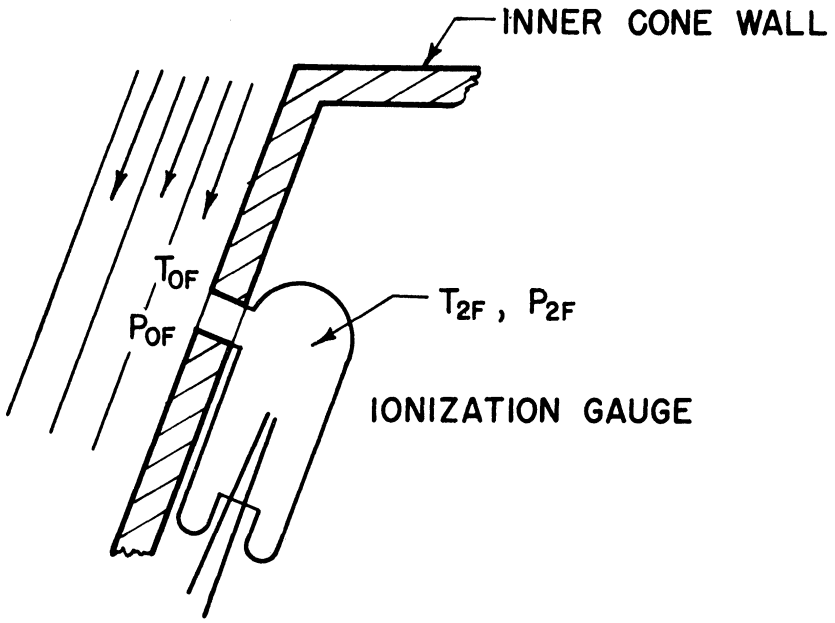

FIG. NO. D-10
SIMPLIFIED DIAGRAM ILLUSTRATING
GAUGE OPERATION DURING FREE FLIGHT

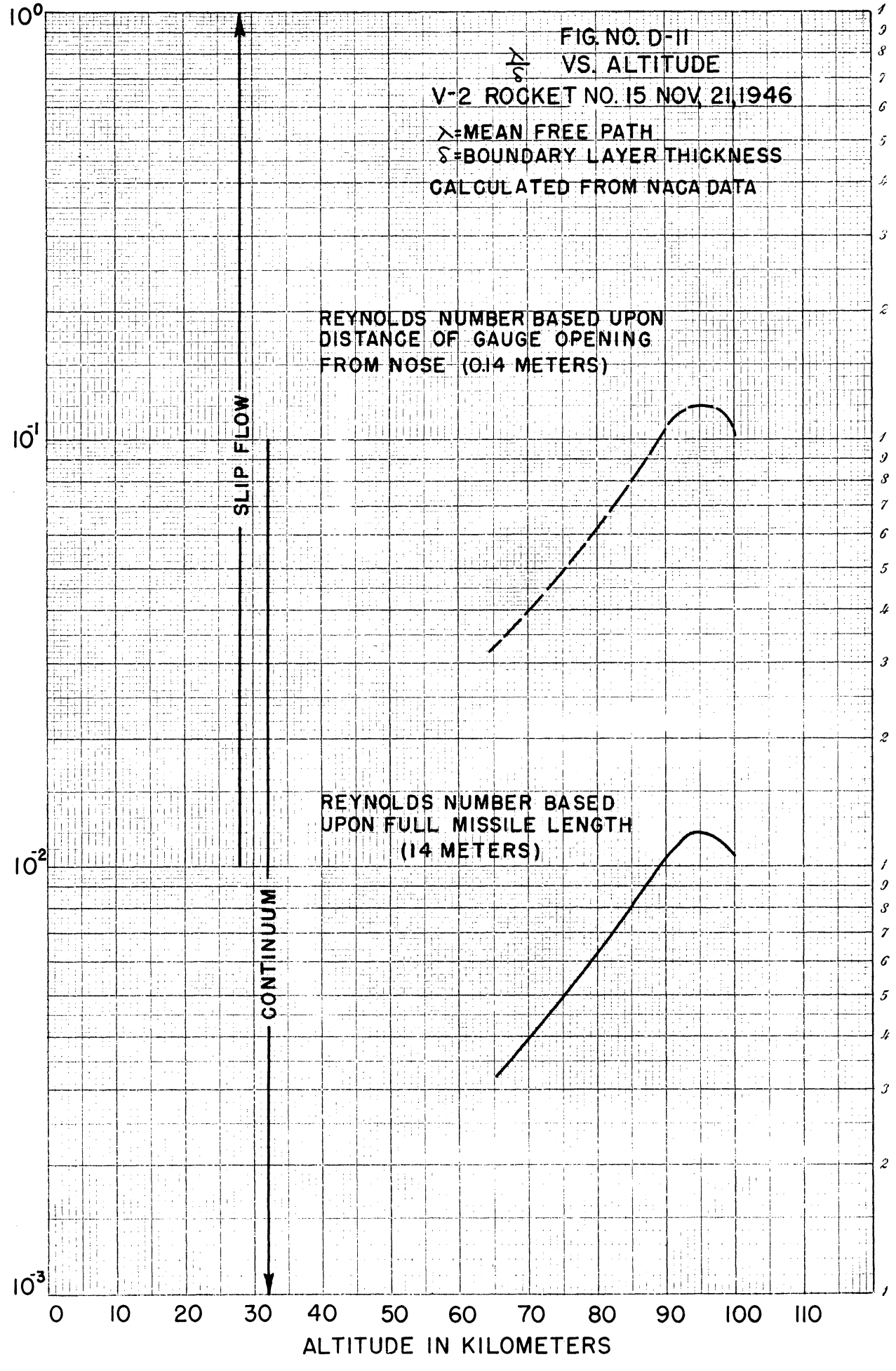
FIG. NO. D-11
λ/δ VS. ALTITUDE
V-2 ROCKET NO. 15 NOV. 21, 1946
λ=MEAN FREE PATH
δ=BOUNDARY LAYER THICKNESS
CALCULATED FROM NACA DATA
REYNOLDS NUMBER BASED UPON DISTANCE OF GAUGE OPENING FROM NOSE (0.14 METERS)
REYNOLDS NUMBER BASED UPON FULL MISSILE LENGTH (14 METERS)
SLIP FLOW
CONTINUUM
λ/δ
10^0
10^-1
10^-2
10^-3
0 10 20 30 40 50 60 70 80 90 100 110
ALTITUDE IN KILOMETERS

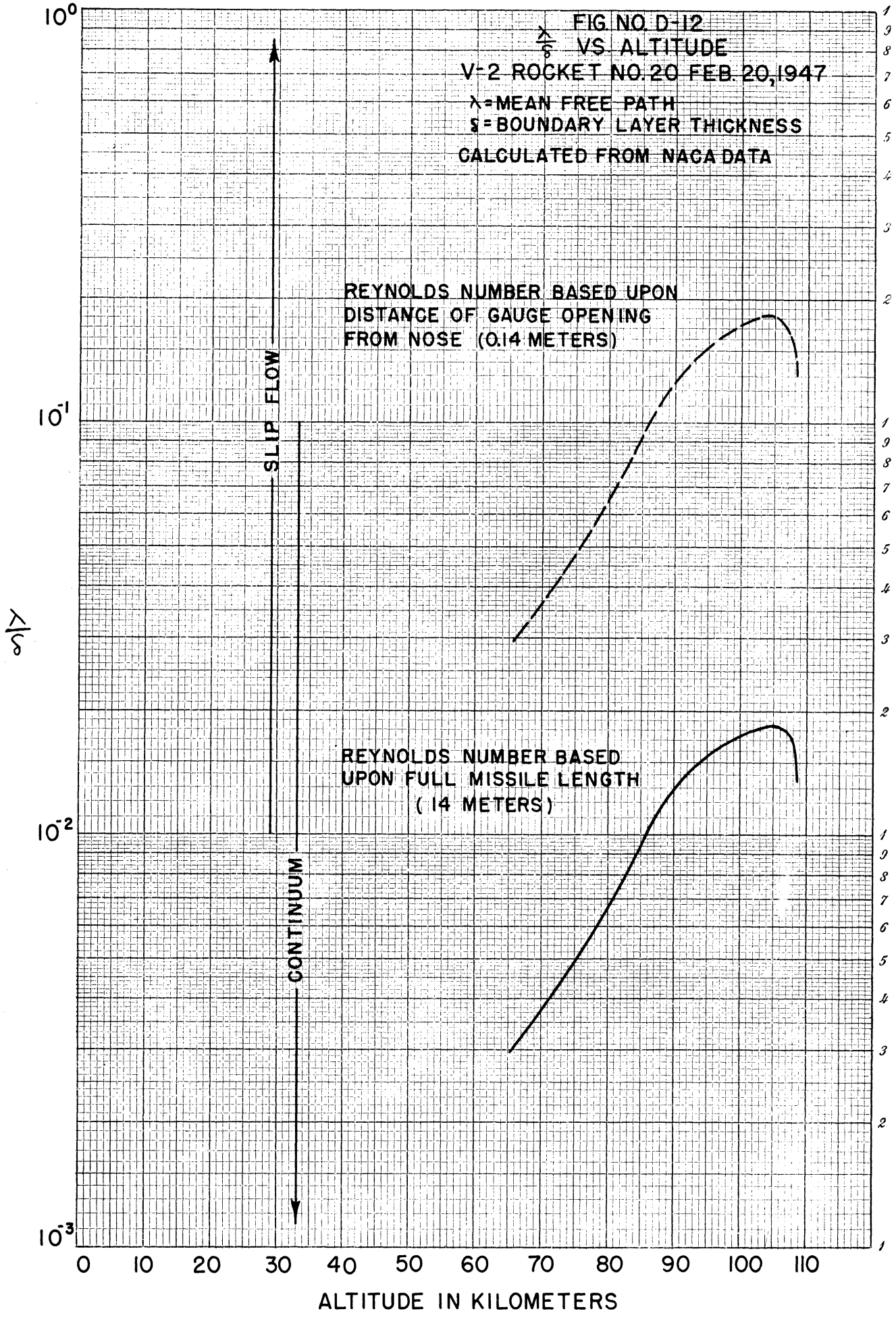
FIG NO. D-12
λ/δ VS. ALTITUDE
V-2 ROCKET NO. 20 FEB. 20, 1947
λ = MEAN FREE PATH
δ = BOUNDARY LAYER THICKNESS
CALCULATED FROM NACA DATA
REYNOLDS NUMBER BASED UPON DISTANCE OF GAUGE OPENING FROM NOSE (0.14 METERS)
REYNOLDS NUMBER BASED UPON FULL MISSILE LENGTH (14 METERS)
SLIP FLOW
CONTINUUM
λ/δ
10^0
10^-1
10^-2
10^-3
0 10 20 30 40 50 60 70 80 90 100 110
ALTITUDE IN KILOMETERS

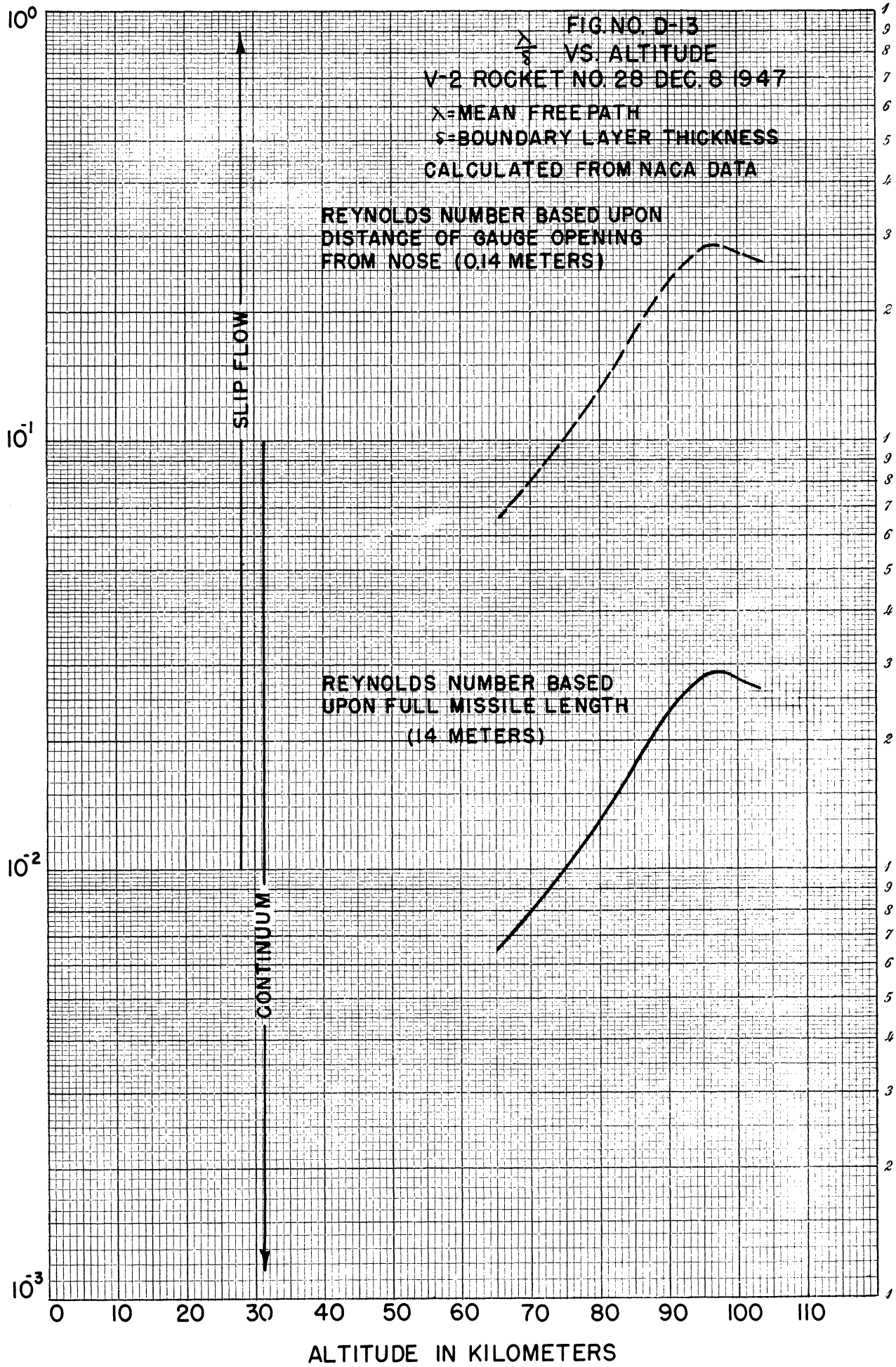
FIG. NO. D-13
λ/δ VS. ALTITUDE
V-2 ROCKET NO. 28 DEC. 8 1947
λ=MEAN FREE PATH
δ=BOUNDARY LAYER THICKNESS
CALCULATED FROM NACA DATA
REYNOLDS NUMBER BASED UPON DISTANCE OF GAUGE OPENING FROM NOSE (0.14 METERS)
REYNOLDS NUMBER BASED UPON FULL MISSILE LENGTH (14 METERS)
SLIP FLOW
CONTINUUM
λ/δ
10^0
10^-1
10^-2
10^-3
0 10 20 30 40 50 60 70 80 90 100 110
ALTITUDE IN KILOMETERS

FIG. NO. D-14

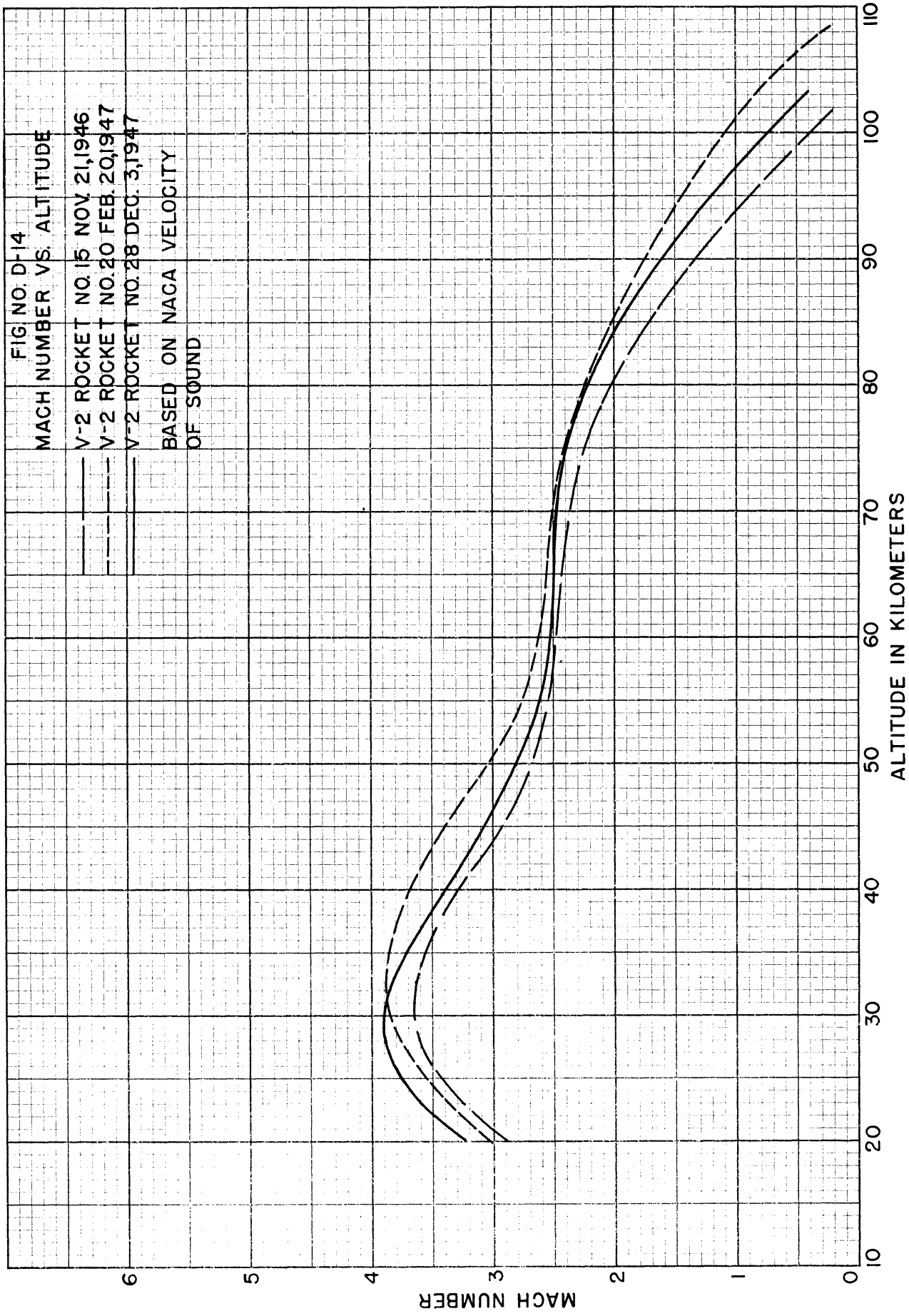
FIG. NO. D-14
MACH NUMBER VS. ALTITUDE
V-2 ROCKET NO. 15 NOV. 21, 1946
V-2 ROCKET NO. 20 FEB. 20, 1947
V-2 ROCKET NO. 28 DEC. 3, 1947
BASED ON NACA VELOCITY OF SOUND
MACH NUMBER
0
1
2
3
4
5
6
ALTITUDE IN KILOMETERS
10
20
30
40
50
60
70
80
90
100
110

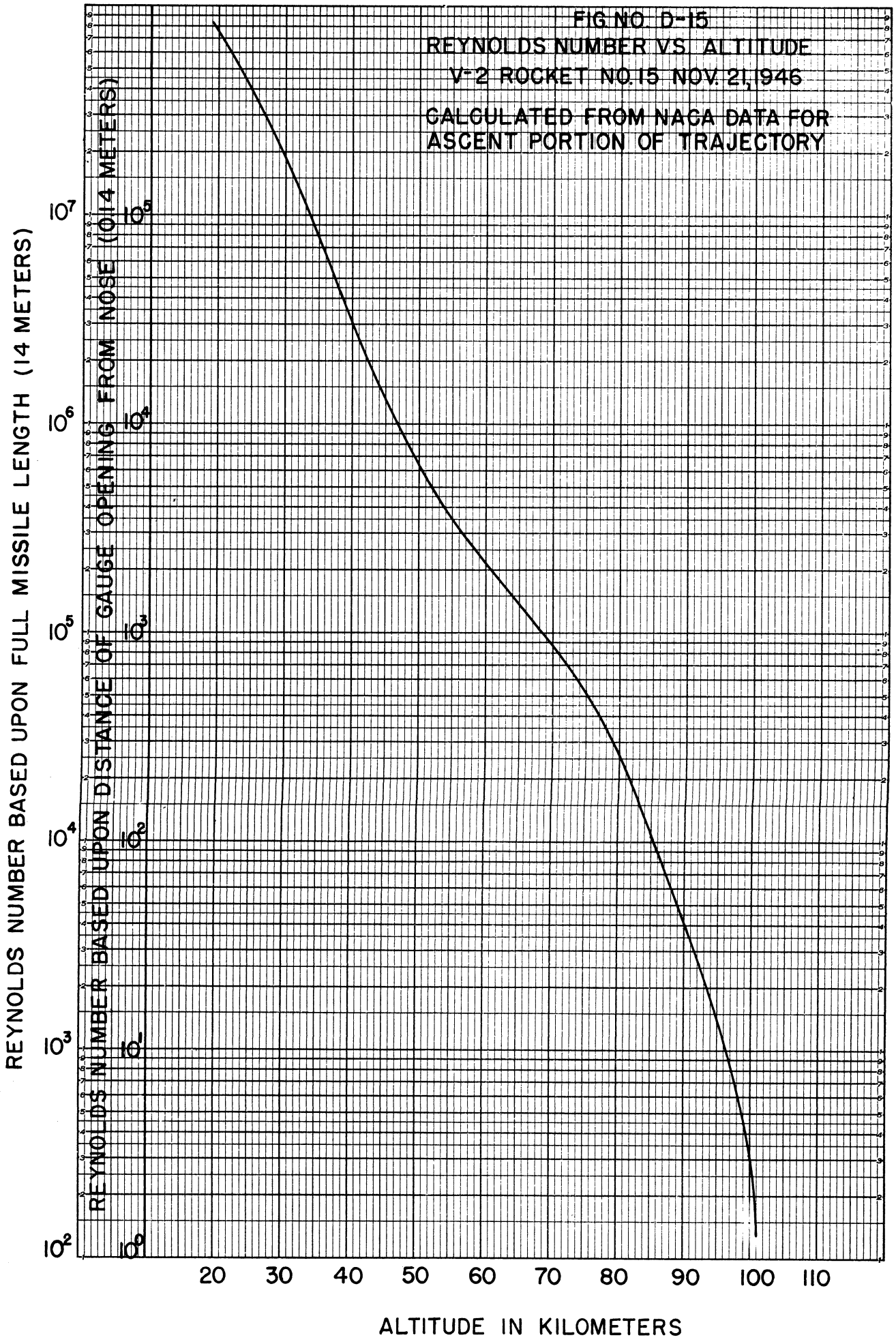
FIG NO. D-15
REYNOLDS NUMBER VS. ALTITUDE
V-2 ROCKET NO. 15 NOV. 21, 1946
CALCULATED FROM NACA DATA FOR
ASCENT PORTION OF TRAJECTORY
REYNOLDS NUMBER BASED UPON FULL MISSILE LENGTH (14 METERS)
REYNOLDS NUMBER BASED UPON DISTANCE OF GAUGE OPENING FROM NOSE (.0014 METERS)
10^7
10^6
10^5
10^4
10^3
10^2
10^5
10^4
10^3
10^2
10^1
20
30
40
50
60
70
80
90
100
110
ALTITUDE IN KILOMETERS

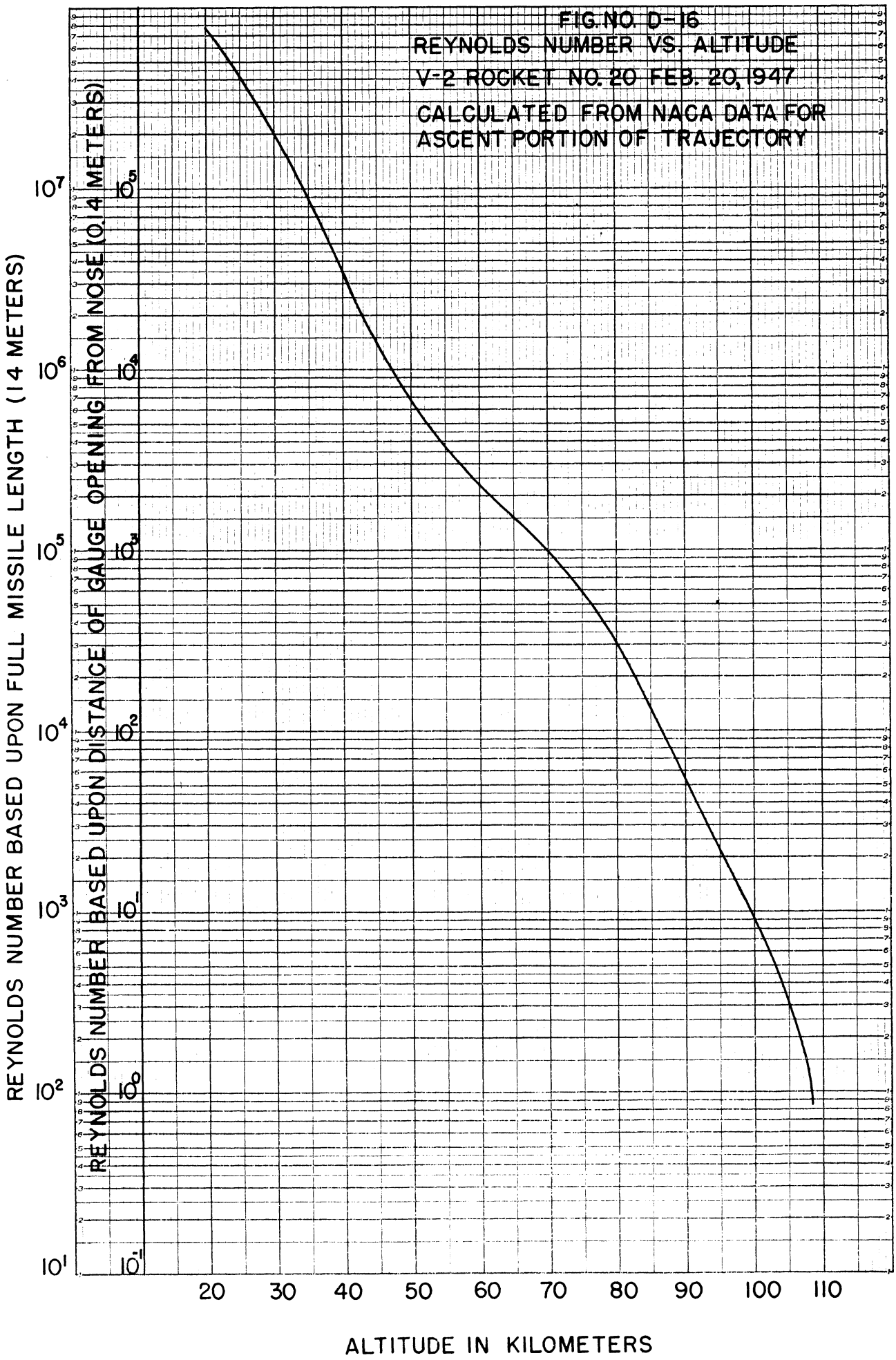
FIG. NO. D-16
REYNOLDS NUMBER VS. ALTITUDE
V-2 ROCKET NO. 20 FEB. 20, 1947
CALCULATED FROM NACA DATA FOR
ASCENT PORTION OF TRAJECTORY
REYNOLDS NUMBER BASED UPON FULL MISSILE LENGTH (14 METERS)
REYNOLDS NUMBER BASED UPON DISTANCE OF GAUGE OPENING FROM NOSE (0.14 METERS)
10^7
10^6
10^5
10^4
10^3
10^2
10^1
10^5
10^4
10^3
10^2
10^1
10^0
10^{-1}
20
30
40
50
60
70
80
90
100
110
ALTITUDE IN KILOMETERS

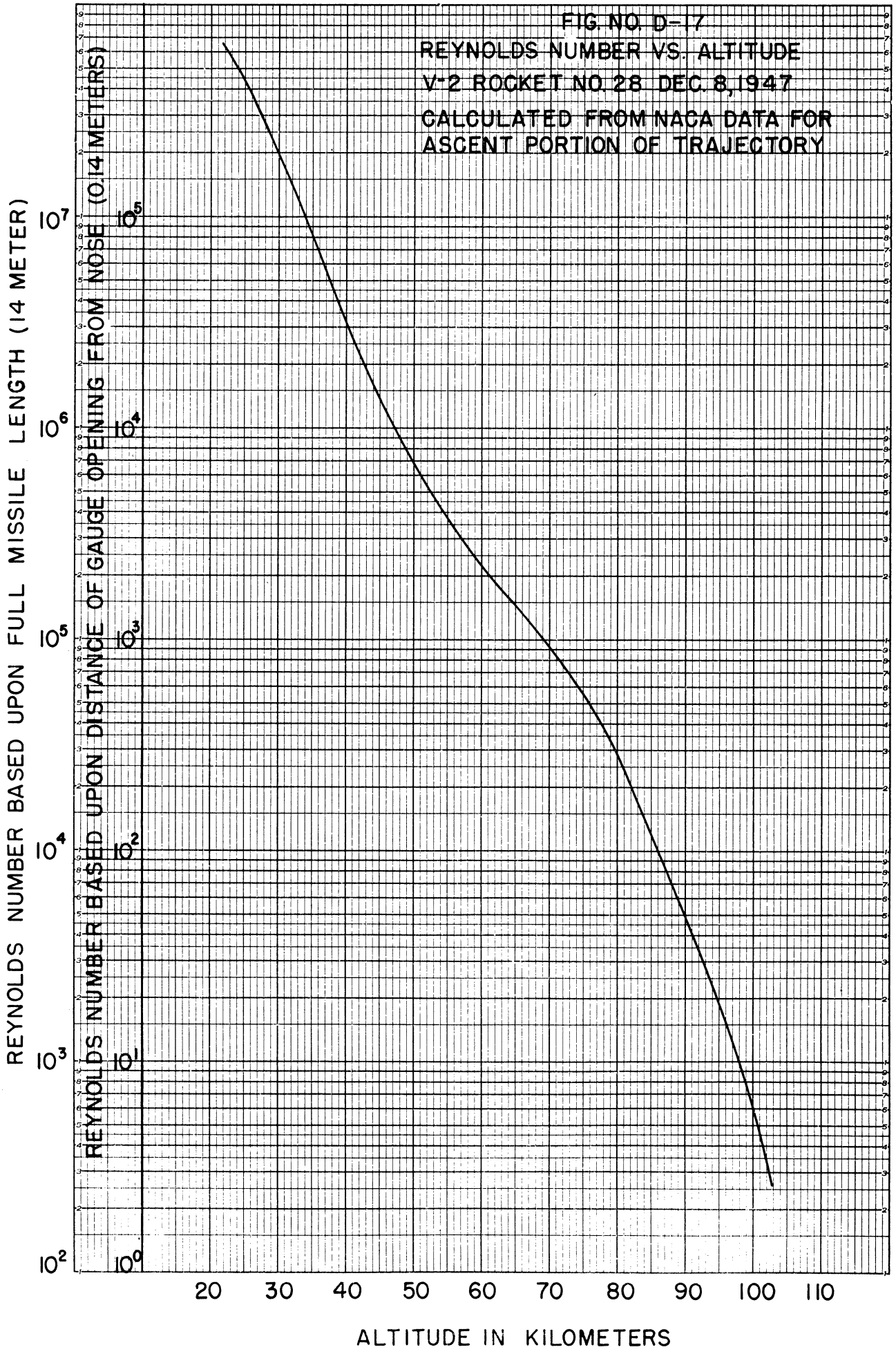
FIG. NO. D-17
REYNOLDS NUMBER VS. ALTITUDE
V-2 ROCKET NO. 28 DEC. 8, 1947
CALCULATED FROM NACA DATA FOR
ASCENT PORTION OF TRAJECTORY
REYNOLDS NUMBER BASED UPON FULL MISSILE LENGTH (14 METER)
REYNOLDS NUMBER BASED UPON DISTANCE OF GAUGE OPENING FROM NOSE (0.14 METERS)
10^7
10^6
10^5
10^4
10^3
10^2
10^5
10^4
10^3
10^2
10^1
10^0
20
30
40
50
60
70
80
90
100
110
ALTITUDE IN KILOMETERS

FIG. NO. D-18

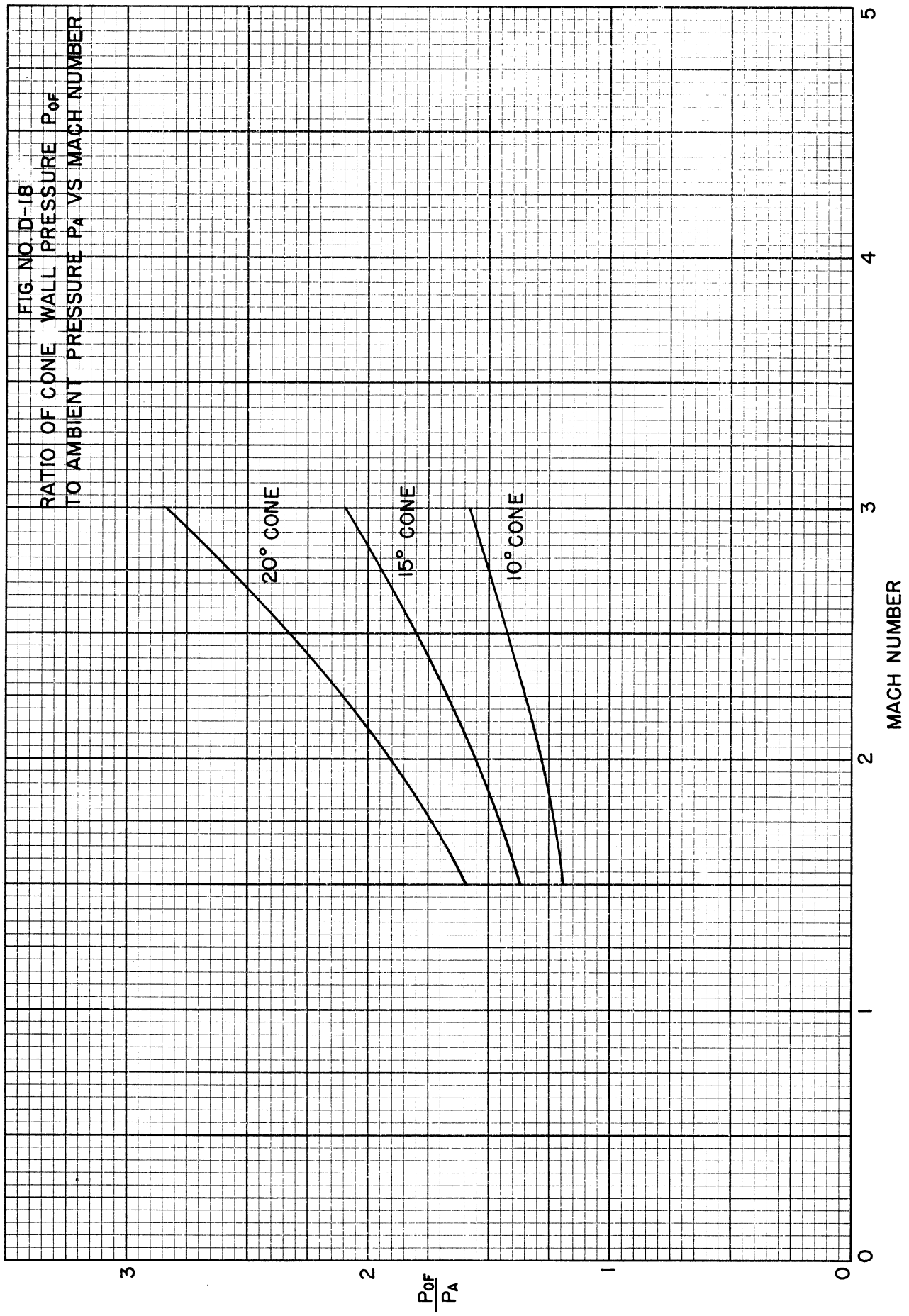
FIG NO. D-18
RATIO OF CONE WALL PRESSURE P_{OF}
TO AMBIENT PRESSURE P_A VS MACH NUMBER
20° CONE
15° CONE
10° CONE
$\frac{P_{OF}}{P_A}$
MACH NUMBER
0
1
2
3
4
5

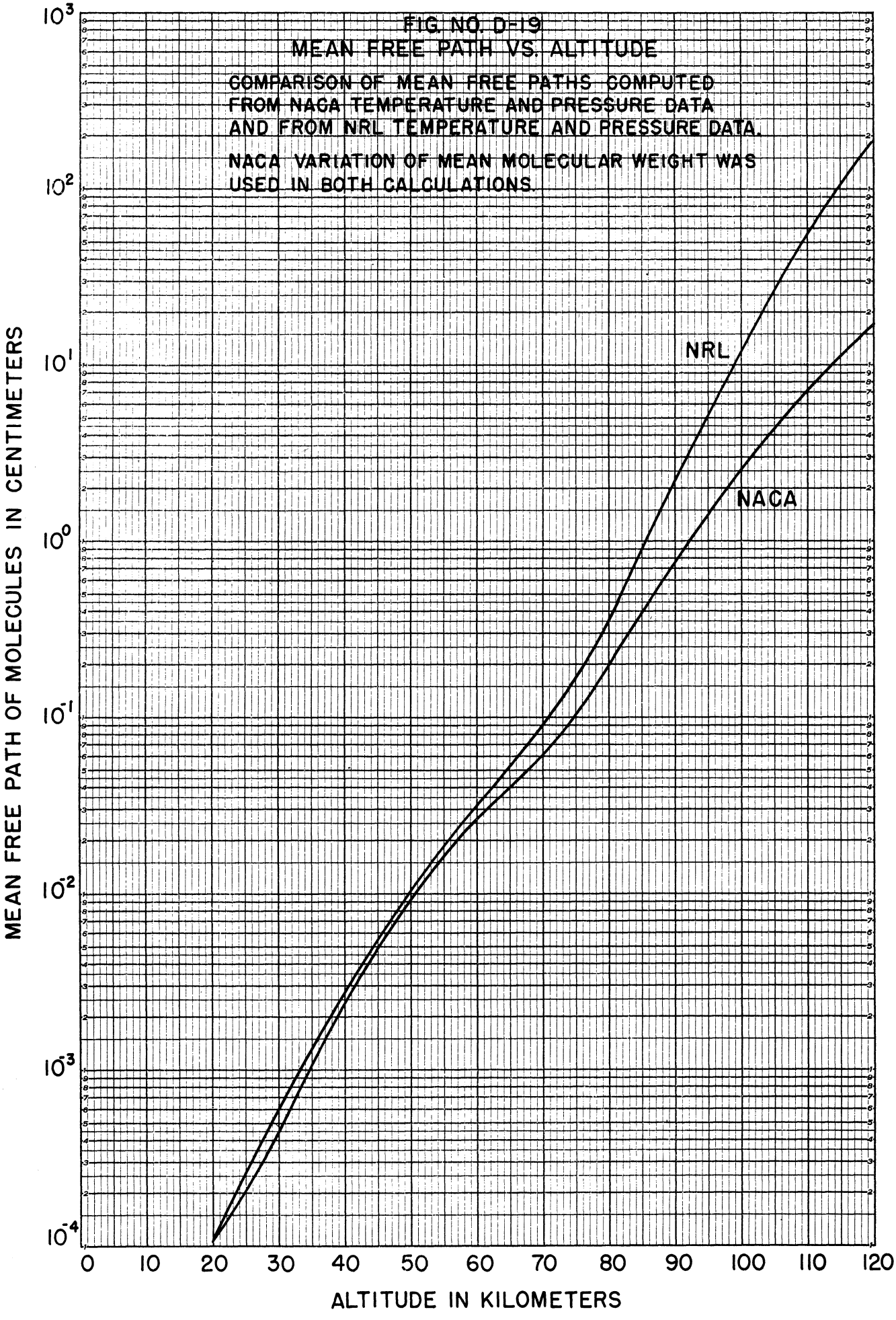
FIG. NO. D-19
MEAN FREE PATH VS. ALTITUDE
COMPARISON OF MEAN FREE PATHS COMPUTED FROM NACA TEMPERATURE AND PRESSURE DATA AND FROM NRL TEMPERATURE AND PRESSURE DATA.
NACA VARIATION OF MEAN MOLECULAR WEIGHT WAS USED IN BOTH CALCULATIONS.
NRL
NACA
MEAN FREE PATH OF MOLECULES IN CENTIMETERS
10^{3}
10^{2}
10^{1}
10^{0}
10^{-1}
10^{-2}
10^{-3}
10^{-4}
0
10
20
30
40
50
60
70
80
90
100
110
120
ALTITUDE IN KILOMETERS

FIG. NO. D-20

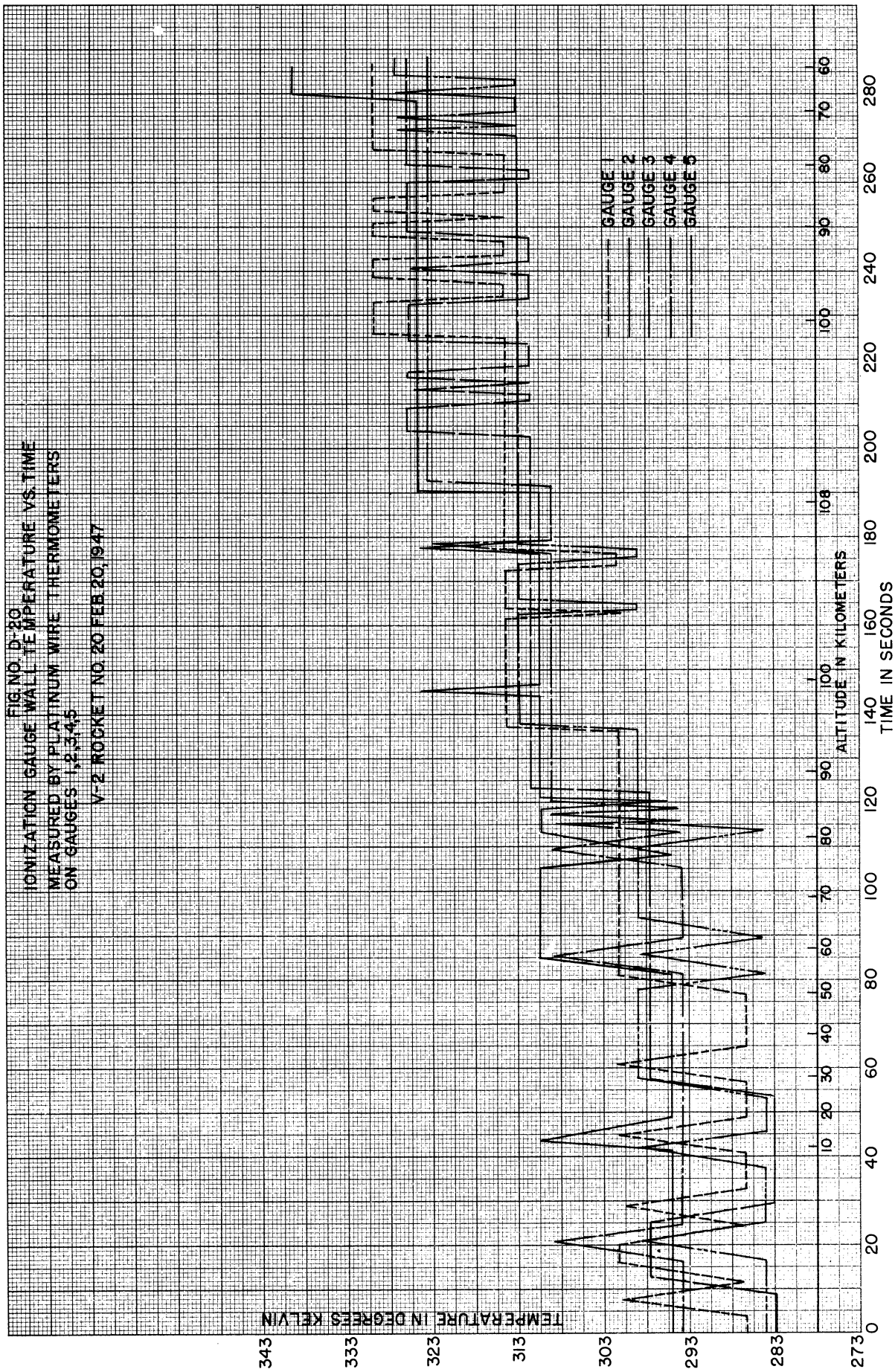
FIG. NO. D-20
IONIZATION GAUGE WALL TEMPERATURE VS. TIME
MEASURED BY PLATINUM WIRE THERMOMETERS
ON GAUGES 1,2,3,4,5
V-2 ROCKET NO. 20 FEB. 20, 1947
GAUGE 1
GAUGE 2
GAUGE 3
GAUGE 4
GAUGE 5
TEMPERATURE IN DEGREES KELVIN
343
333
323
313
303
293
283
273
ALTITUDE IN KILOMETERS
0
20
40
60
80
100
120
140
160
180
200
220
240
260
280
TIME IN SECONDS
10
20
30
40
50
60
70
80
90
100
108
60
70
80
90
100

FIG. NO. D-21
IONIZATION GAUGE WALL TEMPERATURE VS. TIME
MEASURED BY PLATINUM WIRE THERMOMETER ON GAUGE NO.1
V-2 ROCKET NO.28 DEC.8, 1947

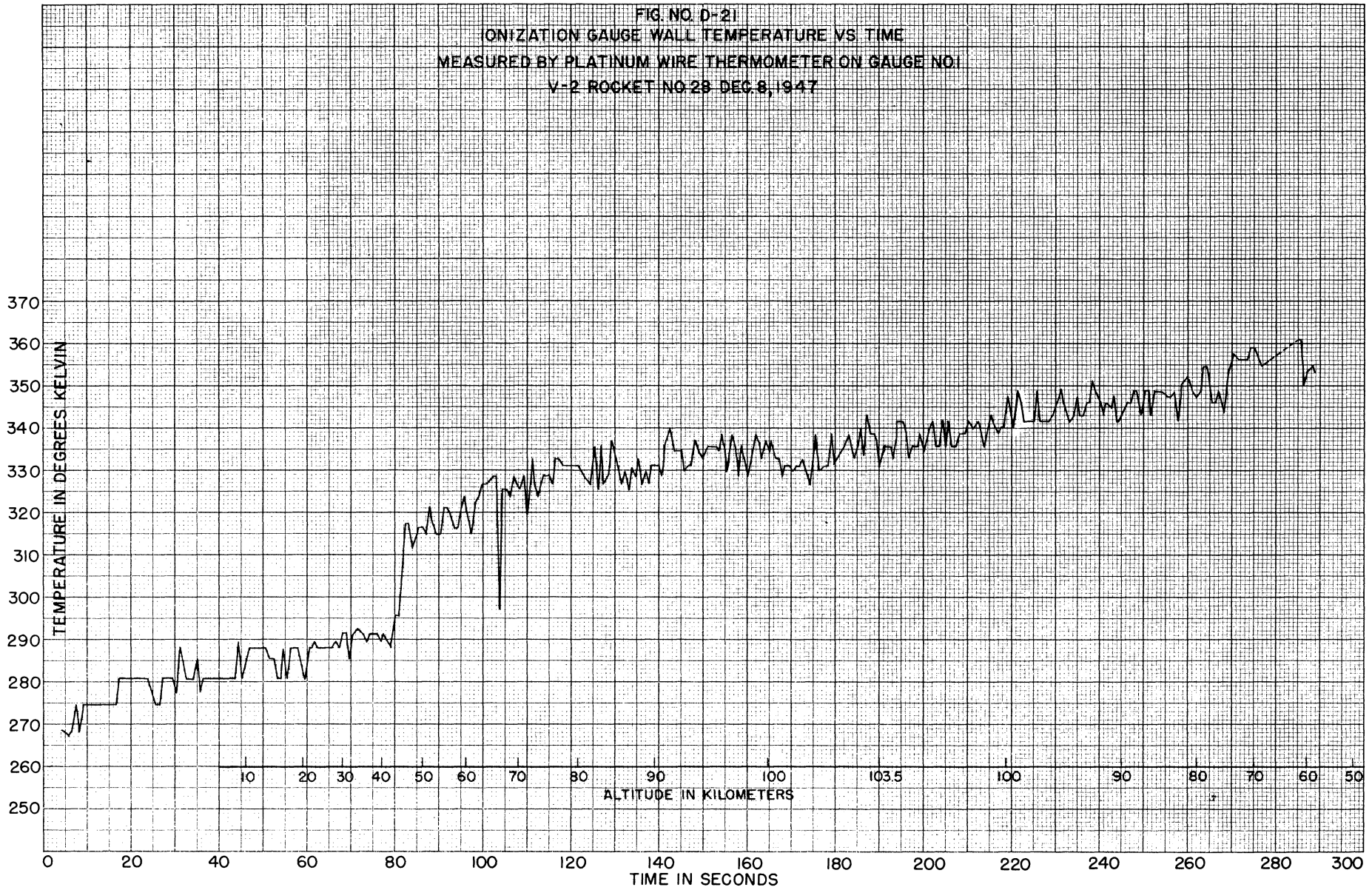

FIG. NO. D-21

APPENDIX E

THEORY OF POSSIBLE ROCKET ROTATIONS AND CONSEQUENCES THEREOF

E-1. Importance of Knowledge of Details of Rocket Angular Motion.

In the process of advancing the frontiers of science there are met, one after another, a series of apparent obstacles to progress. For example, in extending the frequency spectrum of the electronic art upward there came a time when electron transit time appeared to be limiting progress. The significant thing about the appearance of any such new limitation is that the experimenter has begun to work under conditions that make this limitation important, whereas up to that time it was not of significance. Now anything that is important may impede progress; it may almost always, however, be turned to advantage. Thus there are always two approaches to the problems that arise when a new phenomenon becomes important; one is to attempt to suppress it, to overpower it, or to modify conditions so that it ceases to be important; the other approach is to make use of it. Thus the klystron, the magnetron, and the traveling wave amplifier make use of electron transit time.

In the measurement of pressure and temperature of the upper atmosphere, particularly the latter, the existence of supersonic rocket velocities in very thin air presents certain obstacles to measurement. One of the policies that has been adopted in the approach of the University of Michigan to this problem is, wherever possible, to make use of the high rocket velocities rather than to try to force into the situation techniques which are inherited from previous, more nearly static, measurement situations. This policy insures at least the appearance of, and experience with, new measurement techniques. It probably also means that these new measurement techniques must go through a process of seasoning and a certain amount of repetition before the significance of their results becomes entirely clear.

If use is to be made of the rocket motion for measurement purposes, it is necessary that the details of that motion be known. Therefore it is important to the success of certain of the methods of V-2 experimentation employed by the University of Michigan that:

1. The possible types of motion, including angular motion as well as motion of the center of gravity, be clearly understood, and

2. That careful and accurate records be obtained of the details of motion of both general kinds.

From the beginning of the V-2 experimentation, records of the trajectory (movement of the center of gravity) have been available that have been satisfactory for measurement interpretation purposes, although there have at times been unfortunate delays in the availability of this trajectory information. However, it is only very recently that there has become available any reasonably accurate records of the angular positions of the rocket in roll, pitch, and yaw during the free flight that occurs after fuel cut-off. For that reason it is very difficult to assign complete significance to certain of the records that have been obtained. The significance of future measurements will, it is believed, be greatly enhanced by instrumentation being introduced by certain agencies for recording accurately the angular motions of the rocket.

It should also be pointed out that a factual knowledge of just what does happen to these rockets in flight is of very great direct importance in the broad research program dealing with guided missiles operating in the upper atmosphere. The indirect evidence as to angular motion that has been obtained so far in connection with V-2 rockets indicates that the rocket motion during free flight is not always the simple type of motion that early thinking indicated.

The next few sections give attention to various experimental and theoretical considerations bearing on the details of rocket motion, as observed, and in relation to theoretical limitations. With this material as a background, it will at least be possible to rule out certain impossible types of motion, and to gain an intuitive concept as to which types are likely to happen, and under what circumstances.

E-2. Analysis of Rocket Angular Motions in Free Flight.

The angular motions of the V-2 may or may not be affected strongly by aerodynamic forces after fuel cut-off. However, a reasonable approach to the consideration of the rocket's angular motion after fuel cut-off is to consider first the expected type of behavior in case there are no aerodynamic forces, then estimate the modifications to be expected as a result of aerodynamic forces. The following analysis neglects such forces. The basis for this method of attack may be found in various places in the literature on theoretical mechanics, notably Klein and Sommerfeld, "Uber Die Theorie des Kreisels."[20]

It is customary to discuss the angular motion of the rocket in terms of roll, pitch and yaw. Of course, spin, or roll, refers to rotation about the axis of figure of the rocket, that is, about the axis of essentially cylindrical symmetry. Pitch and yaw are used to describe the angular position of the axis of figure of the rocket with respect to the velocity vector.

In this present paper, a standard system of spherical coordinates will be used in referring to angular position. The origin of the coordinates will be taken at the center of gravity of the rocket, the polar axis of the system will be vertical (with respect to the earth), and the reference plane will be the plane containing the vertical polar axis and the trajectory of the center of gravity. (Plane $Y'Z'$ in Figure E-1.) In this report the term "pitch angle" will refer to the angle θ_F between the velocity vector U and the projection $F_{Y'Z'}$ of the axis of figure F on the plane $Y'Z'$, while "yaw angle" will refer to the angle θ_F between the plane $Y'Z'$ of the trajectory and the projection $F_{X'Y'}$ of the axis of figure on the $X'Y'$ plane.

Of course this same system of coordinates can be used to describe the angular direction of any vector; for example, the unchanging direction of the axis of the rocket's angular momentum while in free flight. However, the reference system of Figure E-1 and the terms "pitch angle" and "yaw angle" are not the most useful approaches to an understanding of the possible angular motions of a free symmetric body such as the V-2.

Probably the nature of the angular motions of a free rigid body can most easily be visualized by reference to Figure E-2. Any such body, whether symmetrical or not, will possess one unique axis (OZ in Figure E-2) which will be either an axis of least moment of inertia or an axis of greatest moment of inertia. For the V-2 this unique axis is one of least moment of inertia and is the axis of symmetry, also called the axis of figure. There will be an axis of angular momentum, and an angular momentum vector P lying along that axis. (OZ' in Figure E-2.) The angles θ, ϕ and Ψ in Figure E-2 are the Eulerian angles which express the position of one coordinate system with respect to the other at any instant of time. NN is a line perpendicular to both OZ and OZ'. The line OX is some particular body-fixed line through O and normal to OZ; similarly OX' is some particular space-fixed line through O and normal to OZ'.

Since we are dealing with angular motions only, it is quite unimportant whether the origin O is thought of as stationary or as moving with the center of gravity of the rocket. It is convenient to think of the angular motions as taking place in a frame of reference moving with the rocket, so that the origin O coincides with the center of gravity of the rocket and is stationary relative to the frame of reference employed.

In the general case the body is considered to rotate about its unique body-fixed axis OZ with a velocity $d\phi/dt$ relative to the space-fixed coordinate system $X'Y'Z'$. At the same time the body-fixed axis OZ precesses with velocity $d\Psi/dt$ about the angular momentum axis OZ'. Also, in the general case, the axis OZ nutates with respect to OZ', with a velocity $d\theta/dt$. It will be shown that for the V-2 the property of symmetry eliminates nutation, making θ constant. The axis of figure of the V-2 should, therefore, describe a cone about OZ', the half-angle of the cone being the constant value of θ.

It is characteristic of a rigid body that it possesses at any instant a definite single axis of rotation, corresponding to a definite instantaneous angular velocity vector W. However, this angular velocity vector varies periodically with time both as to magnitude and position, in contrast to the angular momentum vector, which never changes. The total angular velocity is the vector sum of $d\phi/dt$, $d\Psi/dt$ and $d\theta/dt$, these being the instantaneous angular velocities of the body-fixed coordinate system, or the rocket, about OZ, OZ' and NN respectively. It is convenient to relate these three components to three mutually perpendicular components directed along the instantaneous positions of the three principal axes of the rocket.

APPENDIX E

The principal axes consist of the axis of least or greatest moment of inertia, and two others at right angles to the first. The moments of inertia along the three principal axes will be symbolized as follows:

C is the moment of inertia about the unique axis (least or greatest); in the V-2 it is the moment of inertia about the axis of figure.

A, B are moments of inertia about two axes perpendicular to one another and to the axis of C. In case of the V-2, A and B are of equal magnitude. With reference to Figure E-2, A will be considered the moment of inertia about the body-fixed axis OX, and B that about OY.

The values of the components of angular velocity along the principal axes can be written as follows in terms of the rates of change of the Eulerian angles:

$$W_C = \frac{d\phi}{dt} + \frac{d\Psi}{dt} \cos\theta \tag{E-1}$$

$$W_A = \frac{d\theta}{dt} \cos\phi + \frac{d\Psi}{dt} \sin\phi \sin\theta \tag{E-2}$$

$$W_B = -\frac{d\theta}{dt} \sin\phi + \frac{d\Psi}{dt} \cos\phi \sin\theta \tag{E-3}$$

The total angular velocity W is of course

$$W = \sqrt{W_A^2 + W_B^2 + W_C^2} \tag{E-4}$$

The direction cosines of W relative to the A, B, C axes are

$$\frac{W_A}{W}, \quad \frac{W_B}{W}, \quad \frac{W_C}{W} \tag{E-5}$$

The position and magnitude of the total angular momentum vector P will remain constant during free flight, but the values of its components P_A, P_B, P_C will vary periodically. Angular momentum about any principal axis is the product of the moment of inertia about that axis by the corresponding component of angular velocity, thus

$$P_A = AW_A, \quad P_B = BW_B, \quad P_C = CW_C \tag{E-6}$$

If, in Equation (E-6), the P components are expressed in terms of P and the Eulerian angles, and the W's as in Equations (E-1), (E-2) and (E-3), the equations of angular motion are obtained as follows:

$$\frac{d\theta}{dt} \cos\phi + \frac{d\Psi}{dt} \sin\phi \sin\theta = \frac{P}{A} \sin\phi \sin\theta \tag{E-7}$$

$$\frac{d\theta}{dt} \sin\phi - \frac{d\Psi}{dt} \cos\phi \sin\theta = -\frac{P}{B} \cos\phi \sin\theta \tag{E-8}$$

$$\frac{d\phi}{dt} + \frac{d\Psi}{dt} \cos\theta = \frac{P}{C} \cos\theta \tag{E-9}$$

For the V-2 condition that B = A, Equations (E-7) and (E-8) can both be true only if $d\theta/dt = 0$; therefore there should be no nutational motion, and the axis of figure should describe a cone about the P

vector. Therefore, also from Equation (E-7)

$$\frac{d\Psi}{dt} = \frac{P}{A} \tag{E-10}$$

and on using this in Equation (E-9)

$$\frac{d\phi}{dt} = \left(\frac{1}{C} - \frac{1}{A}\right) P \cos\theta \tag{E-11}$$

The relation between $d\phi/dt$ and $d\Psi/dt$ is (from Equations (E-10 and (E-11))

$$\frac{d\phi}{dt} = \frac{d\Psi}{dt} \left(\frac{A - C}{C}\right) \cos\theta \tag{E-12}$$

From the above relations, used in Equation (E-1), etc., the W components can be written

$$\sqrt{W_A^2 + W_B^2} = \frac{P}{A} \sin\theta \tag{E-13}$$

$$W_C = \frac{P}{C} \cos\theta \tag{E-14}$$

The total kinetic energy E of rotation of a free rigid body, as well as the angular momentum, must remain constant. E is the sum of the kinetic energies associated with the three principal axes of rotation; written for 2E rather than for E it is

$$2E = AW_A^2 + BW_B^2 + CW_C^2 \tag{E-15}$$

An Equation for cosine θ in the symmetric case can be obtained by using in Equation (E-15) the fact that B = A and by using Equations (E-13) and (E-14) for the W's. The result is

$$\cos\theta = \sqrt{\left(\frac{C}{A-C}\right)\left(\frac{2AE - P^2}{P^2}\right)} \tag{E-16}$$

If $A >> C$, this becomes

$$\cos\theta \cong \sqrt{\frac{2EC}{P^2} - \frac{C}{A}} \tag{E-17}$$

Equation (E-15) can be expressed as follows:

$$\frac{W_A^2}{\left(\sqrt{\frac{2E}{A}}\right)^2} + \frac{W_B^2}{\left(\sqrt{\frac{2E}{B}}\right)^2} + \frac{W_C^2}{\left(\sqrt{\frac{2E}{C}}\right)^2} = 1 \tag{E-18}$$

This form, together with Equation (E-4) makes it apparent that W can be thought of as the radius vector of an ellipsoid, the principal axes of the ellipsoid being the radicals in the denominators. Since B = A in a V-2, we are dealing with an ellipsoid of revolution, illustrated in section in Figure E-3. The major axis of the ellipsoid in this figure is $\sqrt{2E/A}$, and the minor axis $\sqrt{2E/C}$.

It is, of course, also true that

$$P = \sqrt{A^2W_A^2 + B^2W_B^2 + C^2W_C^2} \tag{E-19}$$

and that the direction cosines of the P vector relative to the principal axes are

$$\frac{AW_A}{P}, \qquad \frac{BW_B}{P}, \qquad \frac{CW_C}{P} \tag{E-20}$$

Thus the angular position of the ellipsoid relative to P is established.

It can be shown, starting with the above relationships, that the angular momentum vector will always be perpendicular to a plane placed tangent to the ellipsoid at the terminus of the vector W. Thus the vector W, the axis of figure, the tangent plane and the momentum vector are related to one another as illustrated in Figure E-3.

The direction cosines of both the W and P vectors relative to the principal axes have been stated; therefore the angle between P and W can be determined by the usual relationship involving the sum of the products of the respective direction cosines. The result is

$$\cos\,(<PW) = \frac{W_A}{W} \cdot \frac{AW_A}{P} + \frac{W_B}{W} \cdot \frac{BW_B}{P} + \frac{W_C}{W} \cdot \frac{CW_C}{P} \tag{E-21}$$

$$\cos\,(<PW) = \frac{2E}{PW}$$

This demonstrates that

$$2E = PW \cos\,(<PW) \tag{E-22}$$

Equation (E-22) permits us to point out that the scalar product of the P and W vectors is twice the kinetic energy. But this scalar product is the product of P by the projection of W on P. Since both P and 2E are constant, the projection W cos (<PW) must also be constant. But this projection is the distance from the origin to the tangent plane, therefore we have established that the distance of the tangent plane from the origin remains fixed.

E-3. Rolling Ellipsoid and Rolling Cone Visualization of Possible Angular Motions.

With the tangent plane at a fixed distance from the origin, as just stated, the overall motion can be visualized as corresponding to a rolling of the ellipsoid on the tangent plane. Thus the tangent plane is space-fixed, while the ellipsoid is a body-fixed configuration. The ellipsoid "Rolls" about its own axis of figure, coinciding with that of the rocket, with a velocity $d\phi/dt$ given by Equation (E-11) while the rolling of the ellipsoid causes the axis of figure to precess about the P vector with the velocity $d\Psi/dt$ given by Equation (E-10).

The fundamental basis of the rolling ellipsoid representation, Equation (E-3), is three-dimensional, therefore capable of indicating motions for the non-symmetric case, $A \neq B$. In this case the ellipsoid is not an ellipsoid of revolution, and θ will vary periodically, that is, there will be nutation. It should be noted that the cyclic period of nutation will not in general coincide with the precessional period. That is, the point of contact on the tangent plane will in general not trace the same identical path over and over again, although the path will be periodic with Ψ.

The rolling ellipsoid diagram indicates that a rocket that is long and thin corresponds to an ellipsoid long and thin in the same direction. Thus a long rocket has its least moment of inertia about the long axis, but since the principal axes of the ellipsoid are inversely proportional to the moments, the major axis of the ellipsoid will coincide with the long axis of the rocket.

For the symmetric case, θ not varying, a visualization at least as useful as the rolling ellipsoid is arrived at by recognizing that the identical motion results from rolling a body-fixed cone on a space-fixed cone. The P vector is the axis of the space-fixed cone, the axis of figure being the axis of the body-fixed cone. The total angular velocity vector W is the element common to the two cones. Figure E-4 shows two rolling-cone diagrams for contrasting conditions.

The rolling-cone diagram probably gives a somewhat more vivid conception of the motion than does the ellipsoid diagram. However, the ellipsoid diagram displays very well, by means of the tangent plane, how the sizes of the cones must be related to the shape of the ellipsoid and to the angle θ.

E-4. Discussion of Possible V-2 Angular Motions: Initial Conditions.

On the basis of the preceding discussion it appears that the angular motions of a V-2 rocket in flight depend on its two principal moments of inertia, and on the initial conditions that exist just after the moment the rocket motor exerts its last dying thrust. Thus one may say that just after fuel cut-off the rocket will possess a certain direction of the axis of figure, a certain direction of the axis of angular momentum, and a certain energy of angular motion, thus specifying:

1. The direction of the angular momentum P relative to the earth.

2. The angle θ.

3. The position of the plane initially containing the axis of figure and P; that is, the initial common cone element.

4. The energy of the motion.

5. By means of Equation (E-16) and the items just stated, the value of the angular momentum vector P.

Of course it would be equally valid to say that the initial conditions determine the magnitude of P, and therefore of E from Equation (E-16). Thus the initial conditions determine the orientation of the motion (by orienting P), the division of energy as between rotation and precession (by establishing θ), the violence of the motion (by establishing E and P), and the initial starting-point of the motion.

According to German Archive No. 84/17 the pitch moment of inertia (A) of the V-2 after complete burn-out is 8300 kilogram meters squared and the roll moment of inertia (C) is 120 kilogram meters squared. Thus, the ratio of A to C is 69.7 to 1 and Equation (E-17) is sufficiently accurate. Table E-1 presents relative values for $d\phi/dt$ and $d\Psi/dt$ corresponding to selected values of θ which might conceivably exist in a V-2 just after fuel cut-off.

It is impossible to prepare a drawing which will represent in readable fashion the cones corresponding to the A/C ratio of 69.7 to 1 used in preparing Table E-1. However, the general types of motions toward each extreme can be illustrated qualitatively. Figure E-4(A) shows a motion in which the angle θ is slightly less than 90^0, and the A/C ratio of the order of 10. The motion would be interpreted by a casual observer as being chiefly tumbling. Figure E-4(B) illustrates a condition in which the angle θ is moderately small and the ratio A/C perhaps 4 or 5, the most important motion being rotation.

For reasons given below, it is believed that the November 21 rocket behaved in a way that would be represented by making θ in Figure E-4 have a value much closer to 90^0, and by using a ratio of cone diameters of the order of 50.

The important lesson from Table I, in fact from this whole discussion, is that except when the angle θ is extremely close to 90^0 the precession of a V-2 will occur very much more slowly than the spin. But if the angle θ is very close to 90^0, the casual observer will describe the precessional motion as "tumbling."

With any reasonably attainable spin rates, an angle θ appreciably different from 90^0 would result in precession so slow as not to cause an observable change in axis of figure during flight, so the casual observer would say there is no procession. With values of the angle θ near enough 90^0 to make the precession observable during a flight, the precession would be so "flat," as in Figure E-4(A), as to make the observer call it tumbling. Practically speaking, the motion of the V-2 as observed should then consist of various combinations of spin and tumbling. Thus it is not to be expected at any time that the axis of figure will describe a cone of small to moderate angle during flight. It will only describe a cone whose half-apex-angle is very close to 90^0.

In summary, it is probably correct to say that the rocket should be considered as having two quite independent "degrees of freedom" of angular motion. It can spin about the axis of figure, and it can tumble, each nearly independent of the other, providing adequate energy of each type of motion exists in the initial state.

APPENDIX E

TABLE E-1

A = 69.7 C

θ, angle between axis of figure and angular momentum vector. Constant during free flight.	Approximate ratio $\frac{d\phi/dt}{d\Psi/dt}$ between spin rate and precessional rate.	Remarks
0^0	68.2	ϕ and Ψ have a common axis. The only motion is spin about the axis of figure, which is fixed in space.
30^0	59.0	
60^0	34.1	
89.16^0	1.0	Similar to Figure E-4(A)
90^0	0	Pure tumbling; no spin about axis of figure.

Relative values of rocket spin and precession during free momentum flight, for various values of the constant angle between the axis of figure and the angular momentum axis, based on the assumption that the ratio A/C of maximum to minimum moments of inertia is 69.7.

E-5. Causes of Deviation from Rigid-Body Free Flight Angular Motions.

There are various possible causes of deviation from the principles of motion described above, as follows:

1. Effects due to aerodynamic forces.

2. The axis of least moment of inertia may fail to coincide with the axis of symmetry, due to lateral unbalance in loading, or to structural distortion (elastic or permanent) in flight. In this case, the rocket, although still considered a rigid body, would no longer be a symmetric rigid body, and there would be nutation, probably of relatively small total angular change in θ.

3. The rocket in flight may in fact not be a rigid body because of the inertial motions of unburned fuel present in substantial amounts. If at the moment of fuel cut-off the unburned fuel has no relative motion with respect to the tanks, it is reasonable to suppose no relative motion will come into being, as gravitational forces do not set up internal movements in free flight. If, however, at fuel cut-off the unburned fuel has substantial motion relative to the tanks containing it, there will be an effect on rocket angular motion of a nature and extent extremely difficult to predict.

4. The rocket in flight may fail to be a completely rigid body of the ordinary type, due to elastic distortions. For example, if the loading is unbalanced, the rotational motion may cause elastic distortion of such a nature as to cause the axis of rotation not to pass through either the tip of the nose or the center of the tail structure. In this case the overall dynamics might be just the same as for a symmetric rigid body, but instrument response would betray a lack of agreement between actual angular motions and predicted possible motions.

The point of view of the last paragraph suggests that, when instruments are used for aspect determination, the instrument readings must be interpreted in the light of possible elastic distortions of the rocket structure.

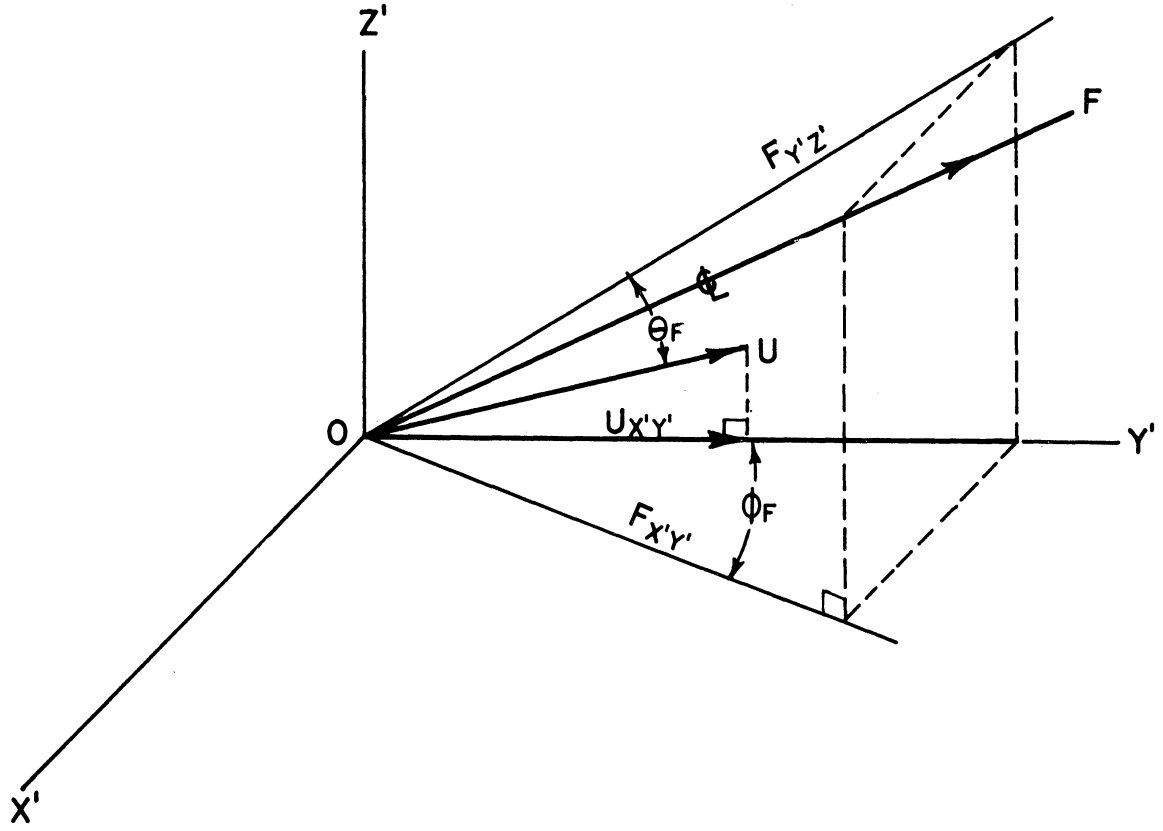

FIG. NO. E-1

THE GEOMETRY OF PITCH AND YAW ANGLES IN A SPACE FIXED COORDINATE SYSTEM

Θ_F = PITCH ANGLE
Φ_F = YAW ANGLE
U = LINEAR VELOCITY VECTOR
F = AXIS OF FIGURE OF ROCKET
Y'Z' = PLANE OF TRAJECTORY CONTAINING U
Z' = VERTICAL AXIS
O = CENTER OF GRAVITY

SUBSCRIPTS DENOTE PROJECTIONS ON THE REFERENCE PLANES

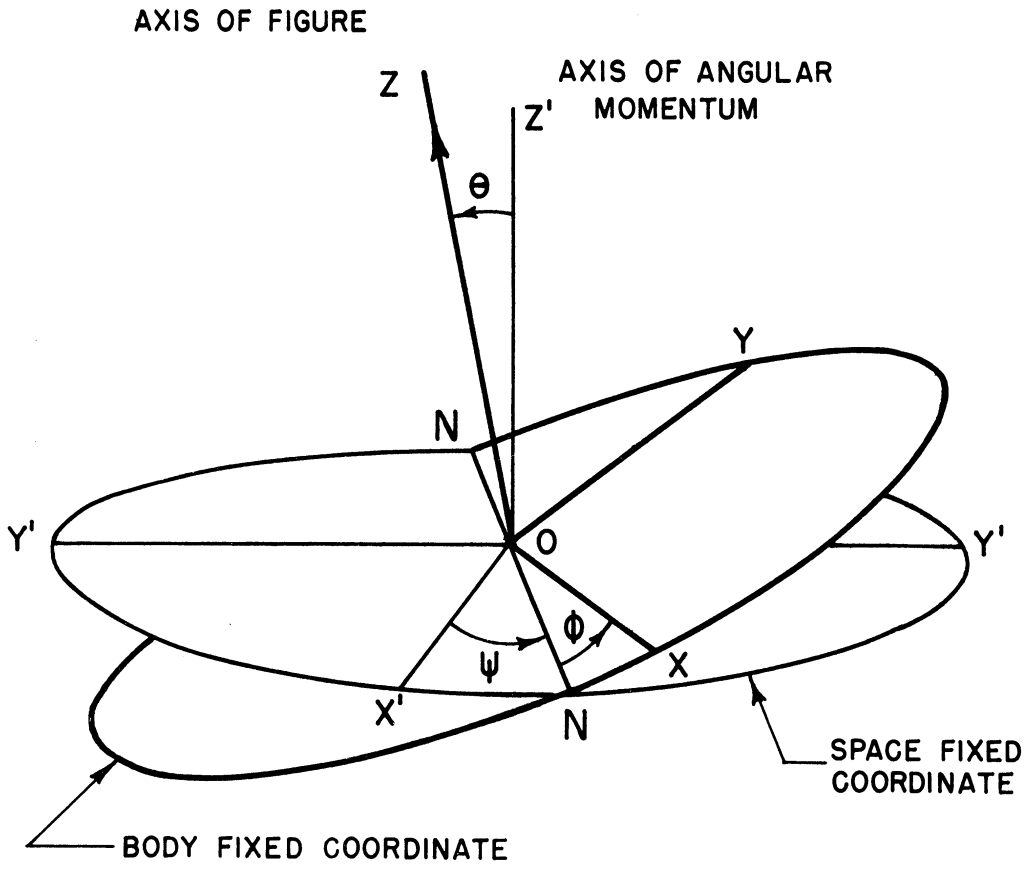

FIG. NO. E-2
COORDINATE SYSTEM TO ILLUSTRATE
FREE MOTION OF A SYMMETRIC BODY.

X,Y,Z ARE BODY FIXED COORDINATES. X',Y',Z' ARE SPACE FIXED COORDINATES. THE FUNCTIONS OF θ,φ AND ψ ARE DESCRIBED IN THE TEXT.

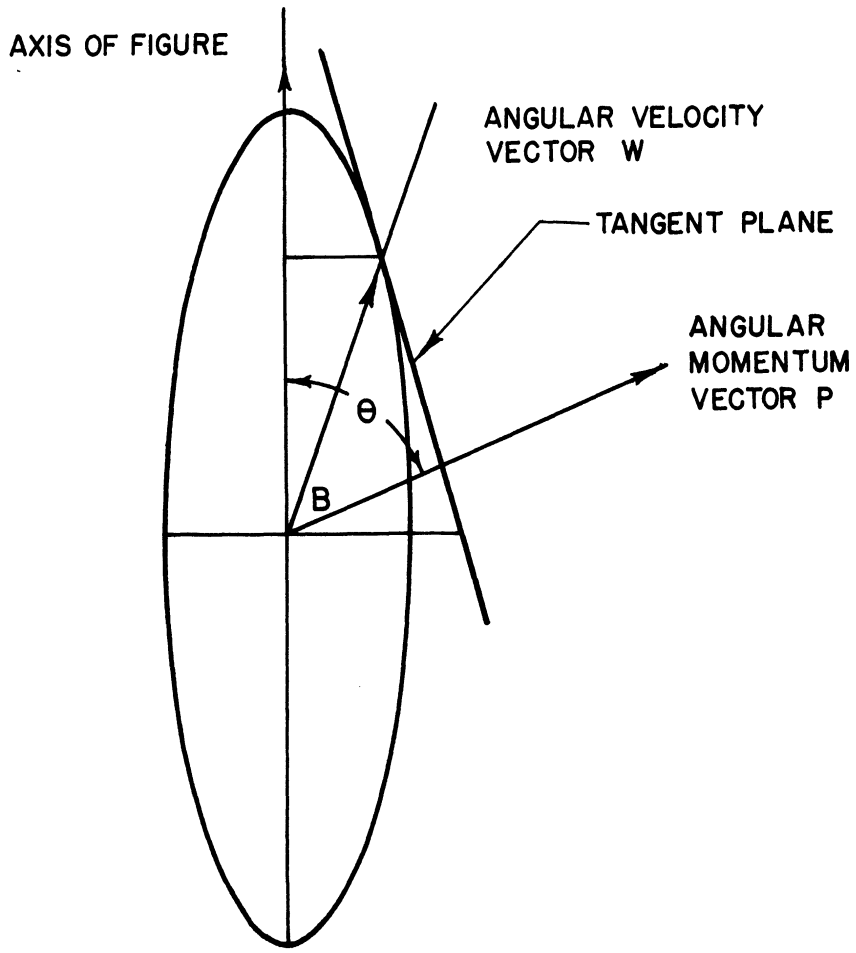

FIG. NO. E-3

ELLIPSOID OF REVOLUTION FOR A SYMMETRICAL BODY

THE BODY-FIXED ELLIPSOID OF REVOLUTION ROLLS ON THE TANGENT PLANE. THE ANGULAR VELOCITY VECTOR W IS IDENTICAL WITH THE ELEMENT OF CONTACT OF THE ROLLING CONES IN FIG. NO. E-4

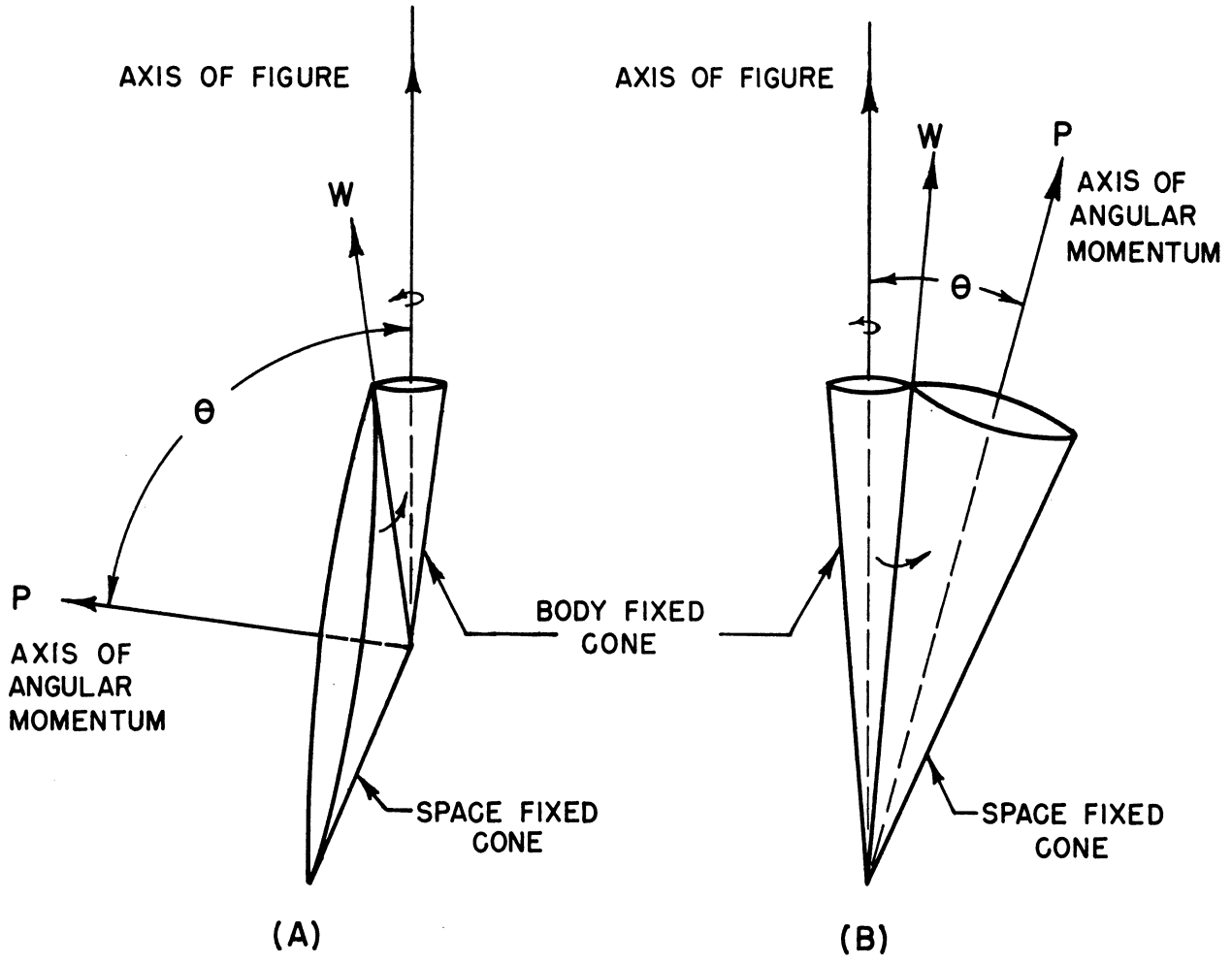

FIG. NO. E-4
ROLLING-CONE REPRESENTATION
OF ANGULAR MOTION OF ROCKET

NATURE OF THE FREE MOTION OF A SYMMETRIC BODY MAY BE VISUALIZED BY CONSIDERING ONE CONE ROLLING UPON ANOTHER. THE SMALL CONE IN EACH FIGURE REPRESENTS THE BODY; (A) WHEN MOTION APPEARS TO BE LARGELY TUMBLING, (B) WHEN MOTION APPEARS TO BE LARGELY SPIN ABOUT THE MAJOR AXIS OF THE BODY.

APPENDIX F

PROCEDURE OF REDUCING PRESSURE DATA FROM TELEMETERING RECORDS, AND DISCUSSION OF PROBABLE ACCURACY OF DATA

F-1. Introduction.

This appendix consists of two parts: first, a discussion of the method used for obtaining the pressure from the telemetering records, and second, an analysis of the probable error of the pressure data thus obtained. These two, somewhat distinct, subjects are discussed in a single appendix because a knowledge of the details of reducing the data from the records is necessary to an understanding of the calculation of the probable error of the results.

F-2. Reduction of Pressure Data from Telemetering Records.

F-2.1. Pertinent Facts Concerning the Telemetering System in Use at the White Sands Proving Ground.

Some knowledge concerning the telemetering system which is used to relay the information from the rocket to the ground and to put it into a useful form from which the data may be obtained, is helpful in understanding the following description of the reduction of these data. The telemetering system which was designed and built by the Naval Research Laboratory, employs 23 channels, is pulse-time modulated and operates at a carrier frequency of 1,000 megacycles. The transmitter is installed in the instrument chamber of the rocket, just aft of the warhead. A coaxial cable feeds the crossed dipole antenna which is mounted on one of the tail fins of the rocket. The transmitter has a multichannel input, that may be supplied with a crystal-limiter in the input circuit of each channel if desired, which limits the input voltage to a range of from 0 to 6 volts. This means, of course, that the output voltage of any equipment feeding into the telemetering system must be held to these limits, if the limiter is used.

The 23 telemetering input channels are sampled in rotation by the pulse-time modulator of the telemetering transmitter. The time for one complete cycle of sampling is .0052 seconds, thus each of the 23 channels is sampled at a rate of 192 times per second. Since data voltages which are fed into the telemetering channels are sampled at the rate of 192 times per second, any data voltage which is commutated prior to being fed to the telemetering system should be switched at a rate considerably slower than 192 times per second in order to insure that a record be obtained.

There are two complete ground stations housed in a concrete block structure which is located 6 miles north of the launching site. Each station is made up of a receiver, a decoder and a recorder. The recorder is a Hathaway string oscillograph which records the data from each channel on a continuous strip of film. The film is developed and printed at the New Mexico College of Agriculture and Mechanic Arts and prints are then sent to all of the participating agencies. A sample of the telemetering record for the V-2 rocket fired February 20, 1947 is shown in Figure F-1. In Figure F-2 is shown a sample of the record for the rocket fired December 8, 1947.

Just prior to the rocket firing the entire telemetering system is calibrated. A series of known voltages, in steps of 0.5 volt, is fed into the input of each channel at the transmitter, and these voltages are recorded on an oscillogram by the Hathaway recorders in the ground station. During the actual flight, two known voltages (zero, and 3.5 volts) are periodically and alternately applied to the input of each channel, thus providing two known points on the calibration curve, and a basis for the continuous calibration of each channel. Samples of the pre-flight calibrations are shown in Figures F-3 and F-4.

F-2.2. Discussion of Telemetering Records Obtained on Three V-2 Flights Involving University of Michigan Instruments.

The telemetering record obtained from the V-2 rocket No. 15, flown on November 21, 1946, was reduced by the New Mexico College of Agriculture and Mechanic Arts. The records obtained from the

two subsequent firings in which the University of Michigan participated were reduced at the University of Michigan. Samples of the latter two records, one for February 20, 1947 and one for December 8, 1947 are shown in Figures F-1 and F-2.

In the following table are listed the channel numbers, and the information carried on each channel, for each of the three rockets. This information is included for the November 21, 1946 flight for the sake of completeness, although it was not possible to obtain a sample of the record for this report.

INFORMATION ON TELEMETERING RECORDS

Rocket Number Date of Flight	Channel Number*	Information
No. 15 November 21, 1946	1	Ionization gauge grid current
	2	Ionization gauge plate current
	3	Gauge wall thermometer voltage
	4	Variable voltage probe current
	5	Nose-opening pulse
	6	Operation of nose-opening mechanism
No. 20 February 20, 1947	1	Ionization gauge grid current
	2	Ionization gauge plate current
	3	Gauge wall thermometer voltage
	4	Variable voltage probe current
	5	Nose-opening pulse
No. 28 December 8, 1947	5	Pirani gauge output voltages
	4	Variable voltage probe current
	3	Gauge wall thermometer voltage and calibration voltages
	2	Ionization gauge plate current
	1	Ionization gauge grid current

*Channel numbers are listed reading from bottom to top of each record.

It seems advisable to discuss one of these records in further detail, explaining the pulses that appear in each channel. The sample of the December 8, 1947 record is the one which has been chosen for this purpose, since it is the most recent record and the space available for each channel is greater than on the other records. Also, an understanding of this record leads at once to an understanding of the records for the earlier flights. Channel No. 1 shows the ionization gauge grid currents. Positions 1 to 5 of the channel show the grid current of each of the 5 ionization gauges, position 5 being for the nose gauge. The sixth position presents a calibration voltage of 1.94 volts.

The positions in telemetering channel No. 2 correspond directly to those in channel No. 1, except that position 6 is the zero plate current pulse, corresponding to a telemetering voltage of 0.49 volts. (Positions in channels Nos. 1 and 2 for February 20, 1947 are completely analogous except that positions 6, calibration plate and grid current pulses, have different voltage values.) The positions in channel No. 3 (the calibration channel) are as follows:

1. Gauge wall thermometer voltage.
2. Variable voltage probe current.
3. 3.1-volt calibration voltage.
4. Ground.
5. Cross-connection to position 5 of channel No. 2.
6. Cross-connection to position 6 of channel No. 1.

The circuitry by which this was achieved is discussed in Appendix B.

The variable voltage probe current is shown in channel No. 4. A complete discussion of the probe will be given in a later report.

The positions in channel No. 5 which show the Pirani gauges, are:

1. Ground.
2. Tail gauge battery voltage.
3. Calibration voltage, 4.26 volts.
4. Nose gauge output voltage.
5. Tail gauge output voltage.
6. Nose gauge output voltage.
7. Tail gauge output voltage.
8. Nose gauge output voltage.

In both the November 21, 1946 and the February 20, 1947 firings there was a channel with information on the opening of the nose. This consisted of the latch motor current which dropped to zero when the nose opened. A voltage proportional to the position of the latch was included on the record for the rocket fired November 21, 1946 (channel No. 6). (The operation of the nose opening mechanism is described in Appendix B.)

At regular intervals on all three telemetering records, zero- and 3.5-volt calibration pulses appear, as mentioned above. Two of the zero-volt calibration pulses are labelled in Figure F-1.

F-2.3. Details of Data Reduction.

The details of the data reduction process can best be explained by giving a sample calculation of pressure. For this example data have been taken from the February 20, 1947 record, at 165.6 seconds after rocket take-off. This occurred during the ascent portion of the trajectory, at an altitude of 106.2 kilometers.

The telemetering calibration records for receiver No. 3 will be considered. This is the record which was actually used in the pressure data reduction process. The calibration records for channels Nos. 1 and 2, the ionization gauge grid current and plate current channels, respectively, are shown in Figures F-3 and F-4. The calibration of channel No. 1 (Figure F-3) starts with a zero-volt pulse followed by voltages increasing in steps of 1/2-volt, up to 5 volts. A 3 1/2-volt calibration pulse (for purposes of further checking of the calibration) occurs between the 1 1/2-volt and the 2-volt pulses. Figure F-4 shows the corresponding calibration for channel No. 2. The distance from the zero-volt pulse to each of the other pulses was measured (in hundredths of an inch) for both channels and graphs were plotted from the data, Figures F-5 and F-6. It should be noted that the reproductions of the telemetering records (Figures F-1 and F-2) are reduced in size as compared to the originals. Therefore the spacings between the pulses cannot be read directly from these two figures.

It was necessary to adopt some convention in measuring the distances on the telemetering records which indicate telemetering voltages. Hence, measurements were made from the center of the reference line to the center of the pulses in channel No. 2 and to the center of the denser portions of the pulses in channel No. 1. Readings were taken at each end of each pulse and the average value was used. A magnifying glass was used in order to obtain greater accuracy.

Figure F-1 is a sample of the telemetering record for receiver No. 3 showing the ionization gauge grid current and plate current information necessary for computing the pressure. (A description of Figure F-1 is included in paragraph F-2.2.) The same convention for measuring distances was adopted as for the calibration record for each channel.

In order to show a sample calculation of pressure, it will be convenient to assign the following symbols to the quantities involved:

t = time in seconds after the launching of the rocket.

q_1 = vertical distance from the pulse under consideration (calibration, grid current or plate current pulse) to the reference line, in inches. This quantity is illustrated in Figure F-1 for a pulse which is not the pulse under consideration in the sample calculation.

q_1 is taken as positive when the pulse is below the reference line, negative when it is above the reference line.

q_2 = vertical distance from the pulse under consideration to the zero-volt level, in inches. This quantity also is illustrated in Figure F-1 for the same pulse for which q_1 is shown.

K = scale correction factor, necessary because the scales of the telemetering and calibrating records are not the same.

Q = distance q_2 corrected to the scale of the calibrating record: $Q = q_2 K$.

E_T = Telemetering voltage of the pulse under consideration. E_{T_1} refers to channel No. 1, E_{T_2}, to channel No. 2.

For the purposes of this calculation, the pulses for ionization gauge No. 1 appearing at 165.6 seconds in Figure F-1 were chosen. The calculation of grid current (I_g) for this gauge will be described in detail and summarized in a table. Since the calculation of plate current (I_p) is entirely similar, it will be summarized in a table only. From the values of grid and plate current obtained, the calculation of pressure will then be carried out.

The pulses chosen at the time 165.6 seconds fall between two zero-volt calibration pulses. The average of the distances q_1 for these two pulses will be used as the zero-volt level in the calculations for 165.6 seconds.

Channel No. 1:

Pulse	t	q_1
zero calibration	163	1.988
zero calibration	177	1.983
calculated zero-volt level	165.6	1.985

The average value of q_1 for the two nearest 3.5-volt calibration pulses will be used as the q_1 for 3.5 volts at 165.6 seconds. This value is 0.941 inch.

By subtracting q_1 for 3.5 volts at t = 165.6 seconds from q_1 for zero volts at that time, q_2 for 3.5 volts at t = 165.6 seconds is obtained.

Channel No. 1:

1.985 - 0.941 = 1.044 inches

From Figure F-5 (the calibration curve of channel No. 1) the Q corresponding to 3.5 volts may be read. This value of Q is found to be 0.81 inch. Then, the scale correction factor K for channel No. 1 at t = 165.6 seconds may be calculated:

Channel No. 1:

$$K = \frac{Q}{q_2} = \frac{0.81}{1.044} = 0.775$$

Next, q_1 for the pulse under consideration is measured and q_2 for this pulse is calculated from it, as done above for the 3.5-volt calibration pulse:

Channel No. 1, gauge No. 1 at t = 165.6 seconds:

q_1 = 0.677 inch

q_2 = 1.985 - 0.677 = 1.308 inches

Then the corresponding Q is calculated:

$Q = q_2 K = 1.308 \times 0.775 = 1.012$ inches.

By reference again to Figure F-5, the corresponding telemetering voltage E_{T_1} is found (using the above value of 1.012 inches for Q):

Channel No. 1	t	Q	E_{T_1}
Gauge No. 1	165.6	1.012	4.50

The calibration curve of grid current as a function of telemetering voltage was made before rocket launching. This is shown in Figure F-7. Thus, from this curve, once the telemetering voltage E_{T_1} of a pulse is known, the corresponding grid current may be obtained.

Channel No. 1	t	E_{T_1}	I_g(ma)
Gauge No. 1	165.6	4.50	0.70

This calculation of grid current and the completely analogous one of the plate current are summarized in the following tables:

SUMMARY OF CALCULATION - CHANNEL NO. 1

Pulse	t	q_1	q_2	$Q = q_2 K$	E_{T_1}	I_g(ma)
Zero-volt calibration	163	1.988			0	
Zero-volt calibration	177	1.983			0	
Calculated zero-volt	165.6	1.985			0	
Calculated 3.5-volt	165.6	0.94	1.045	0.81	3.5	
Gauge No. 1	165.6	0.68	1.305	1.01	4.50	0.70

$$K = \frac{0.81}{1.045} = 0.775$$

SUMMARY OF CALCULATION - CHANNEL NO. 2

Pulse	t	q_1	q_2	Q	E_{T_2}	$I_p(\mu a)$
Zero-volt calibration	163.5	0.64			0	
Zero-volt calibration	177.5	0.65			0	
Calculated zero-volt	165.6	0.645			0	
Calculated 3.5-volt	165.6	-0.50	1.145	0.882	3.5	
Gauge No. 1	165.6	0.04	0.602	0.465	1.88	1.80

$$K = \frac{0.882}{1.145} = 0.771$$

A calibration curve for each ionization gauge was also made in the laboratory at the University of Michigan. These curves relate the plate current in microamperes, for a grid current of 5 milliamperes, to the pressure in millimeters of mercury. This calibration curve for gauge No. 1 is reproduced in Figure F-9. Thus, in order to use the calibration curve, the plate current (I_p) obtained directly from the telemetering record, must be corrected to a value I_{pc} which is the plate current for a grid current of 5 milliamperes. Since the curve of I_p versus I_g, when all other variables are held constant, approximates a straight line, this correction may be made as follows:

$$I_{pc} = \frac{5}{I_g} \; I_p$$

$$I_{pc} = \frac{5}{0.70} \times 1.80 = 12.9 \text{ microamperes}$$

From Figure F-9, the pressure in millimeters of mercury corresponding to this value of I_{pc} is found:

$$P = 1.69 \times 10^{-4} \text{ millimeter of mercury}$$

The following is a summary of these results:

Gauge No. 1

t	E_{T_1}	E_{T_2}	I_g(ma)	I_p(μ a)	I_{pc}(μ a)	P(mmHg)
165.6	4.50	1.88	0.70	1.80	12.9	1.69×10^{-4}

Thus, the pressure at t = 165.6 seconds (an altitude of 106.2 kilometers) as recorded on the ascent by gauge No. 1, has been found.

The procedure used in reducing the telemetering data for the November 21, 1946 firing was almost identical to the sample shown for the February 20, 1947 firing. The telemetering voltages, however, for the former firing were calculated at the Physical Science Laboratory at the New Mexico College of Agriculture and Mechanic Arts. At the University of Michigan the remainder of the calculation of pressure was carried out as described above.

For the December 8, 1947 firing, the calibration was done in a different manner, as described in Appendix C. However, as before, the telemetering voltages were translated into ionization gauge grid and plate currents by means of calibration curves taken before the firing. No correction of plate current to a constant value of grid current was necessary, as the calibration of plate current versus pressure was taken for various grid currents. To facilitate the process of obtaining the pressure from the values of grid and plate currents, a nomogram was plotted for each ionization gauge. The method of reading the telemetering record was greatly improved, as far as ease and speed of reading were concerned, by using a glass plate on which were ruled 100 divisions per inch. Again, a magnifying glass was used to aid in taking the readings.

F-3. Random Errors Occurring in Data.

The random errors which occurred in the overall procedure of system calibration and of reducing the pressure data have been investigated and the results are summarized in this section. The details are omitted since the procedure used for calculating the resultant probable error curves was the standard method used in such cases.

The sources of error occurring in the ionization gauge pressure reduction which have been considered are these:

1. Overall telemetering system.
2. Use of linear scales to read telemetering records.
3. McLeod gauge used to calibrate ionization gauges.
4. Meters used in calibration of ionization gauges.
5. Reading of ionization gauge calibration curves.
6. Reading of curves showing telemetering voltage plotted against deflection on telemetering charts.
7. Determination of position of pulse on telemetering chart.

APPENDIX F

The curves of probable error versus the pressure readings of the ionization gauges are shown in Figures F-10, F-11 and F-12. The largest of these random errors were those introduced by the McLeod gauge and those arising from reading ionization gauge grid currents of considerably less than five milliamperes and then correcting the plate currents to those which would have existed if the grid currents had been five milliamperes. The McLeod gauge error was greatest in the low pressure range and this fact caused the overall error curves to rise at the low pressure end. This error will be reduced considerably in all future firings by the use of a more accurate McLeod gauge, which has been obtained. The random error curve for the February 20, 1947 rocket is higher than those for the other two rockets because the ionization gauge grid currents were much lower on the February flight than on the other two flights. This made the percentage error in reading the grid currents much higher than normal. Also, this error was greatest at the higher pressures and this caused the overall error curve to rise at the high pressure end.

A rough check of the random error curves (shown in Figures F-10, F-11 and F-12) may be made by noting the deviations of the pressure versus altitude curves, of Section V of this report, from a mean curve. This has been done and the correlation is satisfactory.

The sources of error occurring in the obtaining of the Pirani gauge pressure curves were of the same general nature as those listed previously for the ionization gauges. The largest error arose in reading the calibration curves for the gauges, which curves are shown in Figures C-21 and C-22. It is evident that the error in reading these calibration curves becomes very large where the curves are very flat, and this is borne out by the plots of error versus pressure. The only Pirani gauge pressure data used in Figure i-1 are those lying in the region of operation of minimum error (less than about 20 per cent).

FIG. NO. F-1

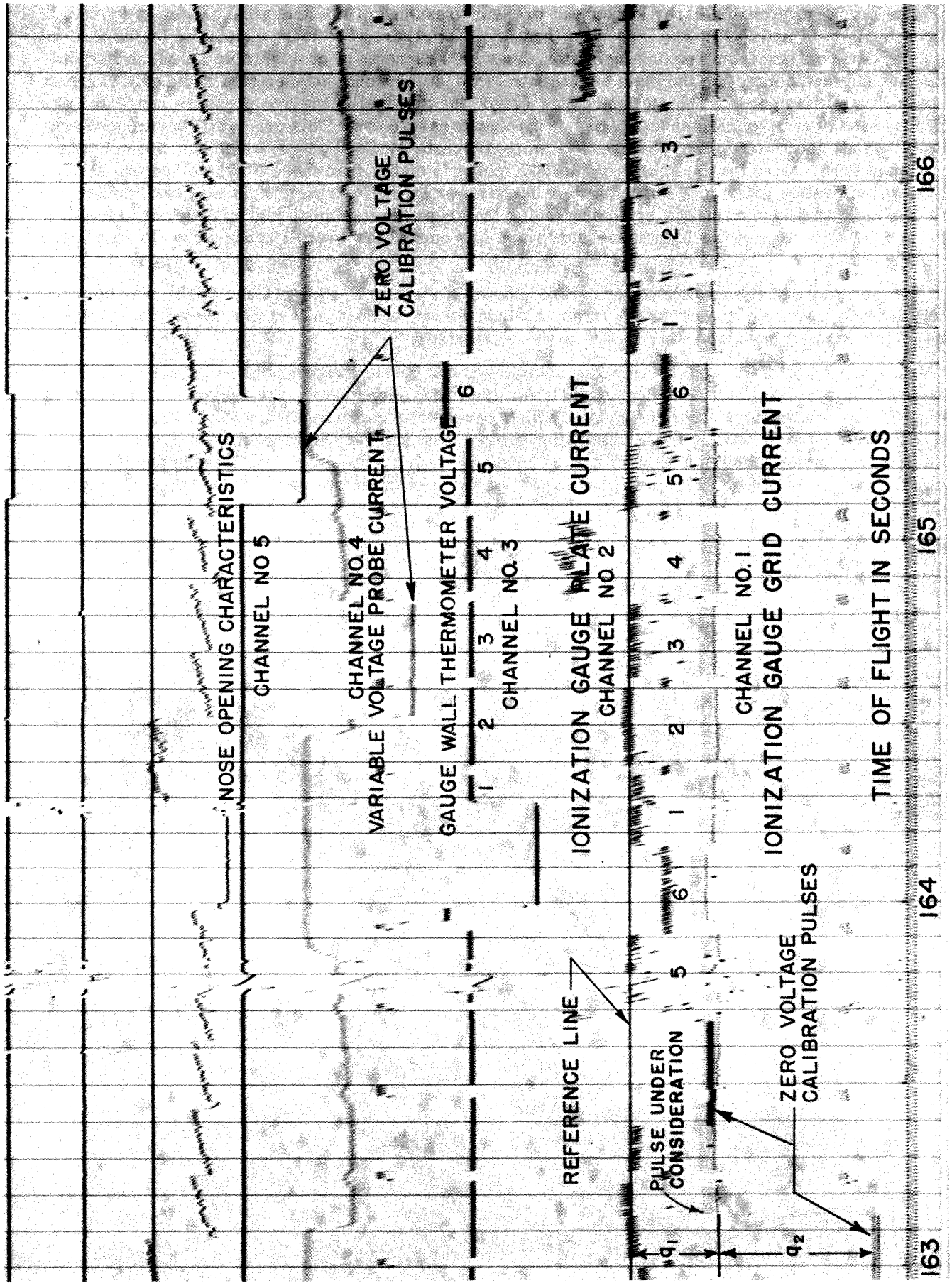

FIG. NO. F-1
SAMPLE OF TELEMETERING RECORD OF FEB. 20, 1947

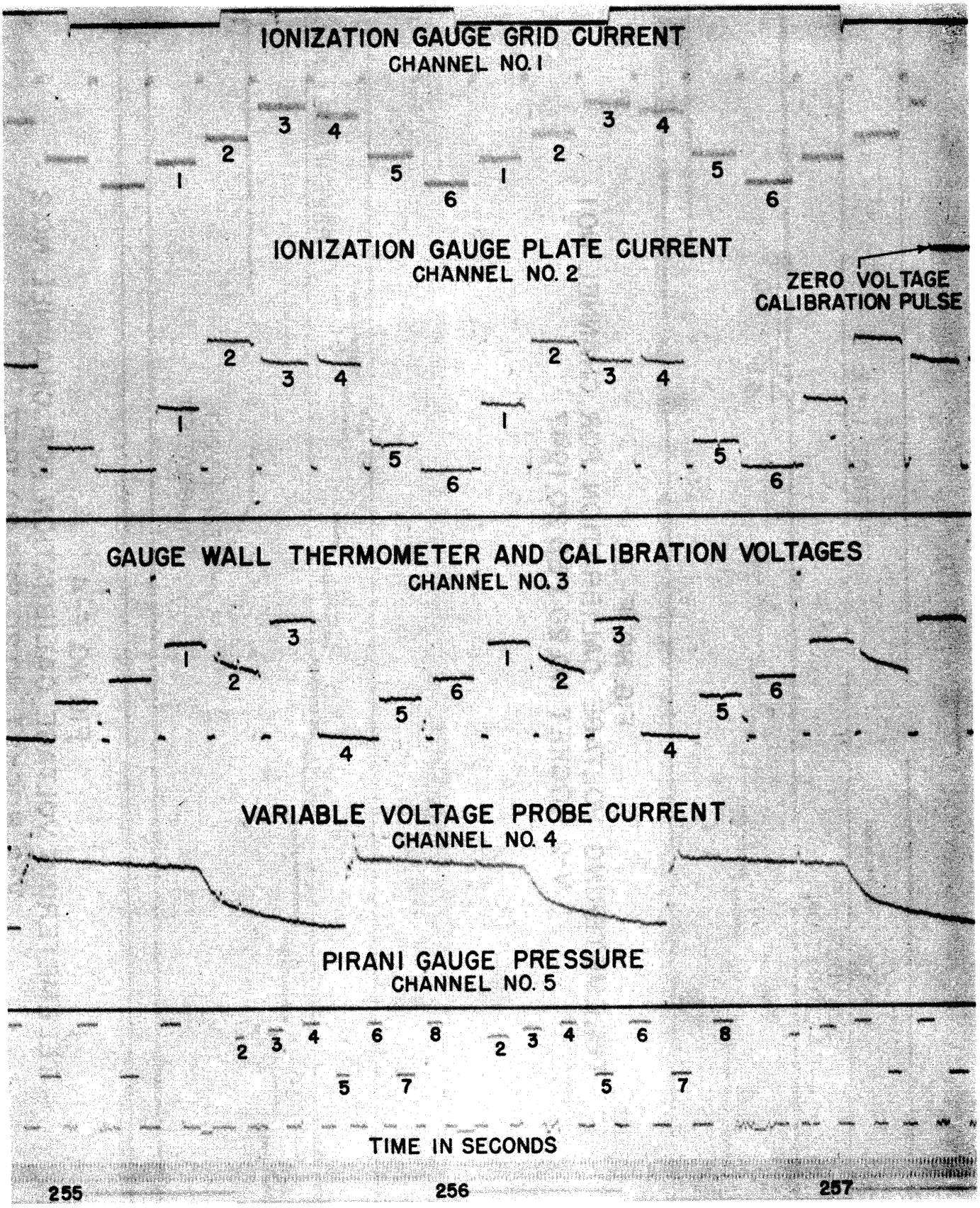

FIG. NO. F-2
SAMPLE OF TELEMETERING RECORD OF DEC. 8, 1947

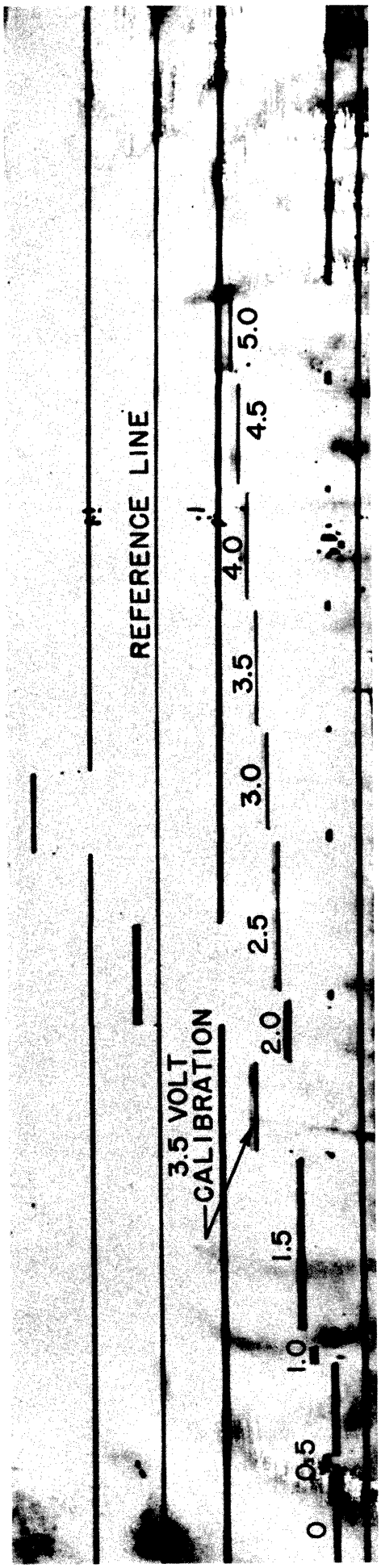

FIG. NO. F-3
TELEMETERING VOLTAGE CALIBRATION FOR CHANNEL NO.1
V-2 ROCKET NO. 20 FEB 20, 1947

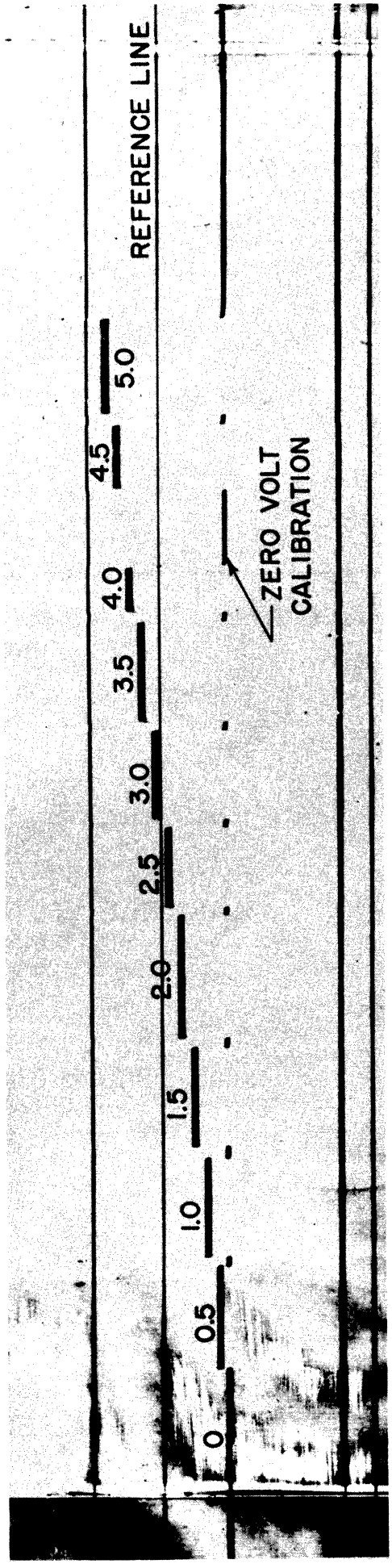

FIG. NO. F-4
TELEMETERING VOLTAGE CALIBRATION FOR CHANNEL NO.2
V-2 ROCKET NO.20 FEB. 20, 1947

FIG. NO. F-5

TELEMETERING VOLTAGE VS DISTANCE FROM ZERO VOLT LEVEL
FROM CALIBRATION RECORD FOR RECEIVER NO. 3 - CHANNEL NO. 1
V-2 ROCKET NO. 20 FEB. 20, 1947

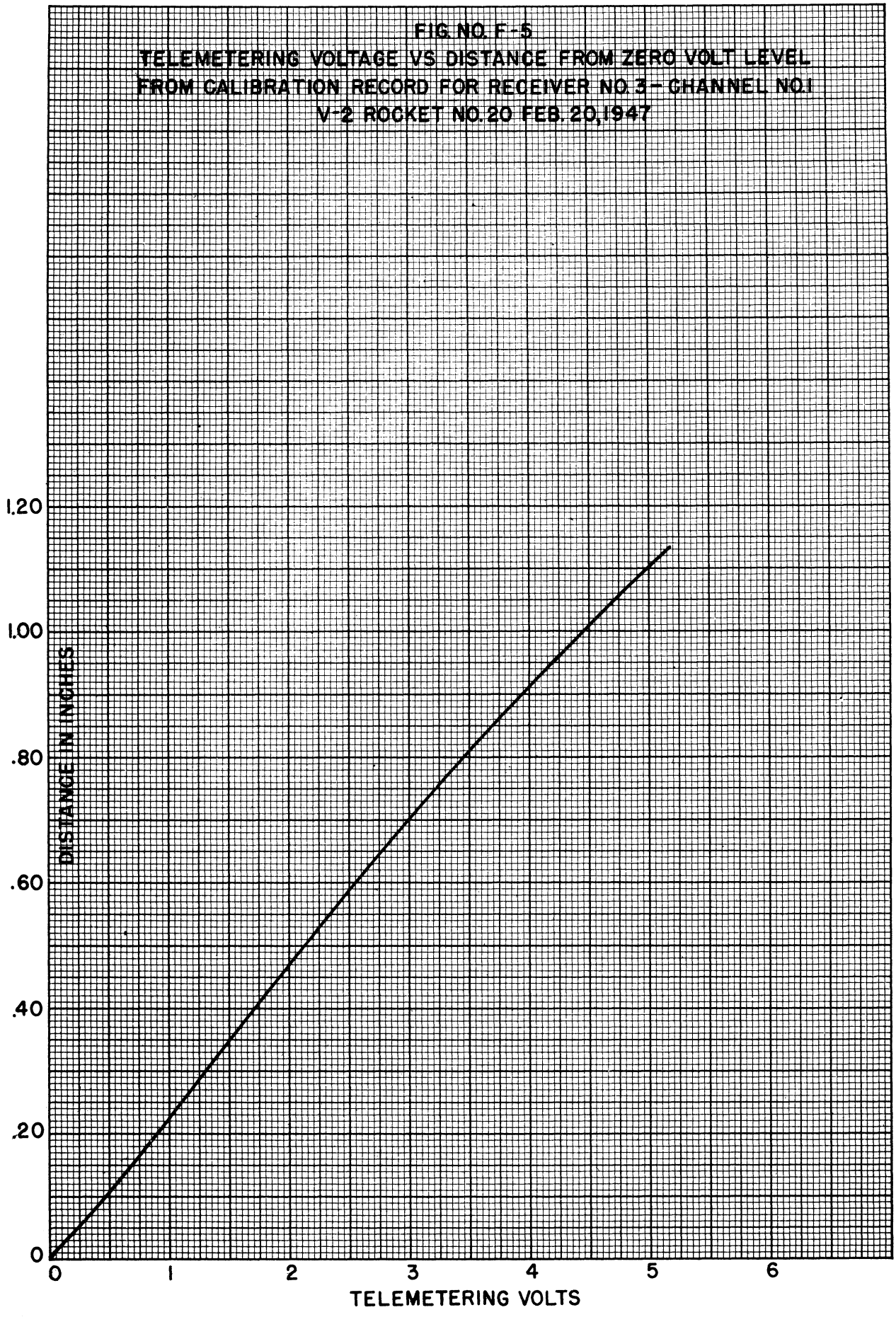

FIG.NO. F-6

TELEMETERING VOLTAGE VS DISTANCE FROM ZERO VOLT LEVEL

FROM CALIBRATION RECORD FOR RECEIVER NO.3-CHANNEL NO.2

V-2 ROCKET NO. 20 FEB. 20, 1947

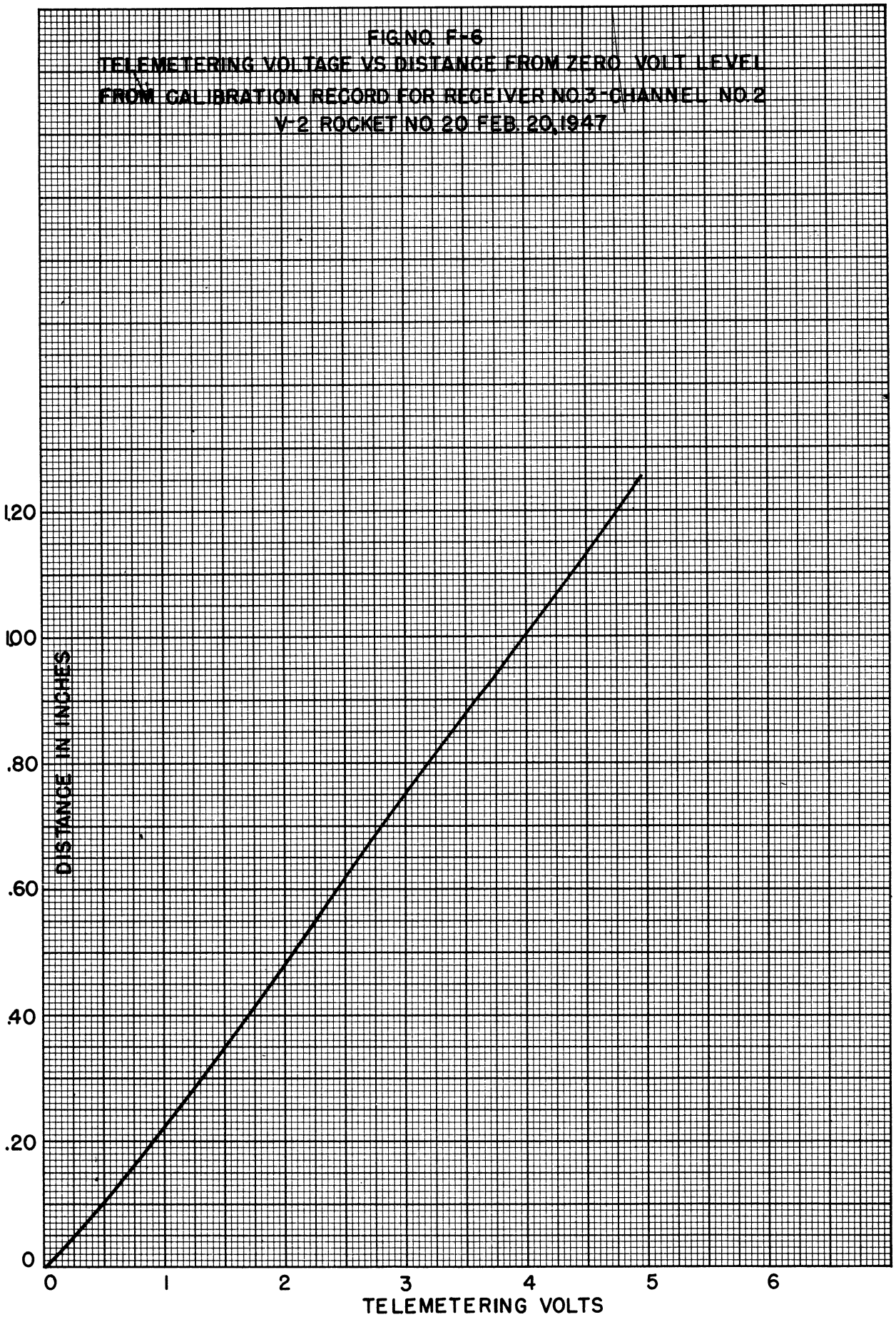

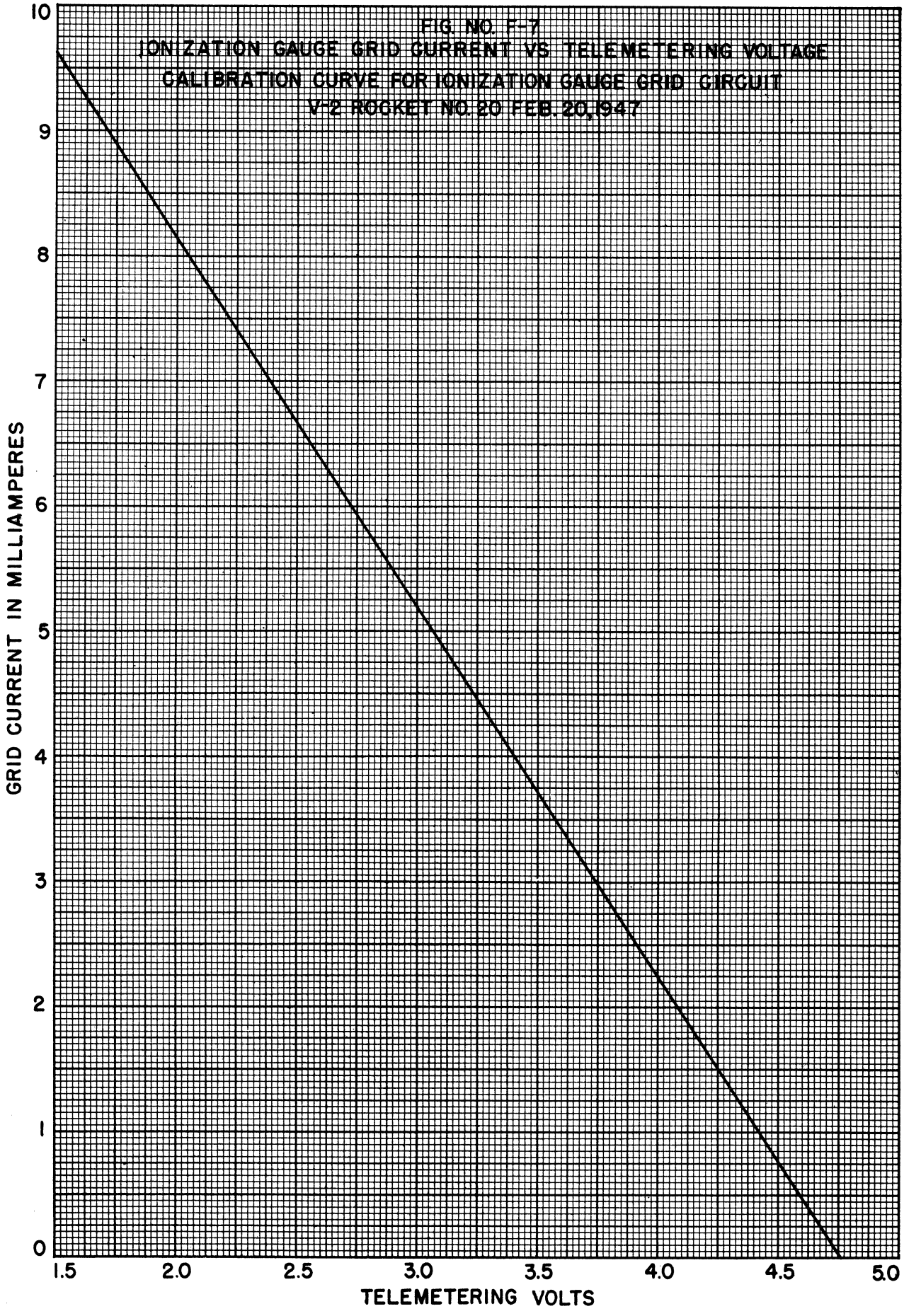
FIG. NO. F-7
IONIZATION GAUGE GRID CURRENT VS TELEMETERING VOLTAGE
CALIBRATION CURVE FOR IONIZATION GAUGE GRID CIRCUIT
V-2 ROCKET NO. 20 FEB. 20, 1947
GRID CURRENT IN MILLIAMPERES
0
1
2
3
4
5
6
7
8
9
10
1.5
2.0
2.5
3.0
3.5
4.0
4.5
5.0
TELEMETERING VOLTS

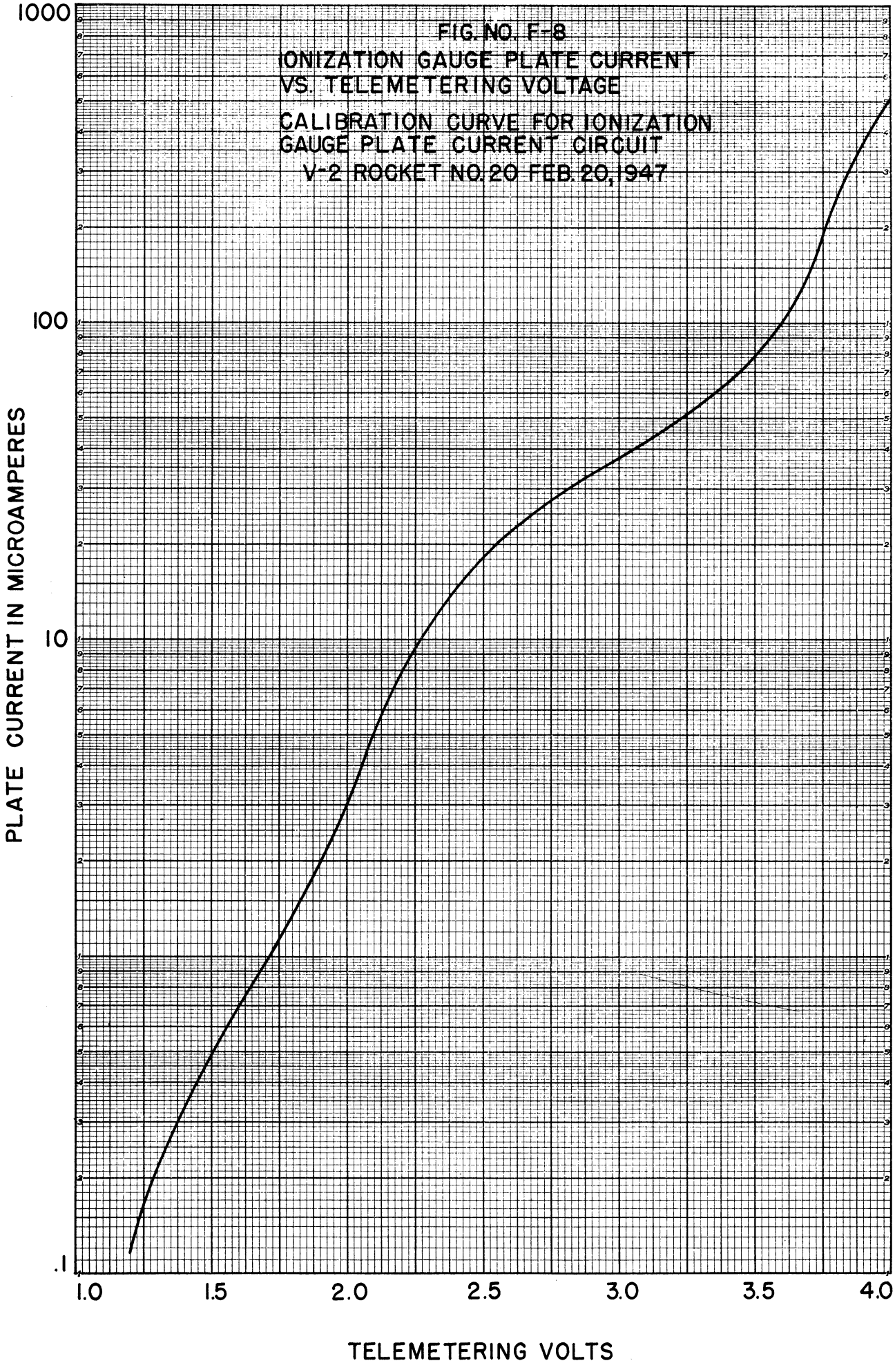
FIG. NO. F-8
IONIZATION GAUGE PLATE CURRENT
VS. TELEMETERING VOLTAGE
CALIBRATION CURVE FOR IONIZATION
GAUGE PLATE CURRENT CIRCUIT
V-2 ROCKET NO. 20 FEB. 20, 1947
PLATE CURRENT IN MICROAMPERES
1000
100
10
.1
1.0
1.5
2.0
2.5
3.0
3.5
4.0
TELEMETERING VOLTS

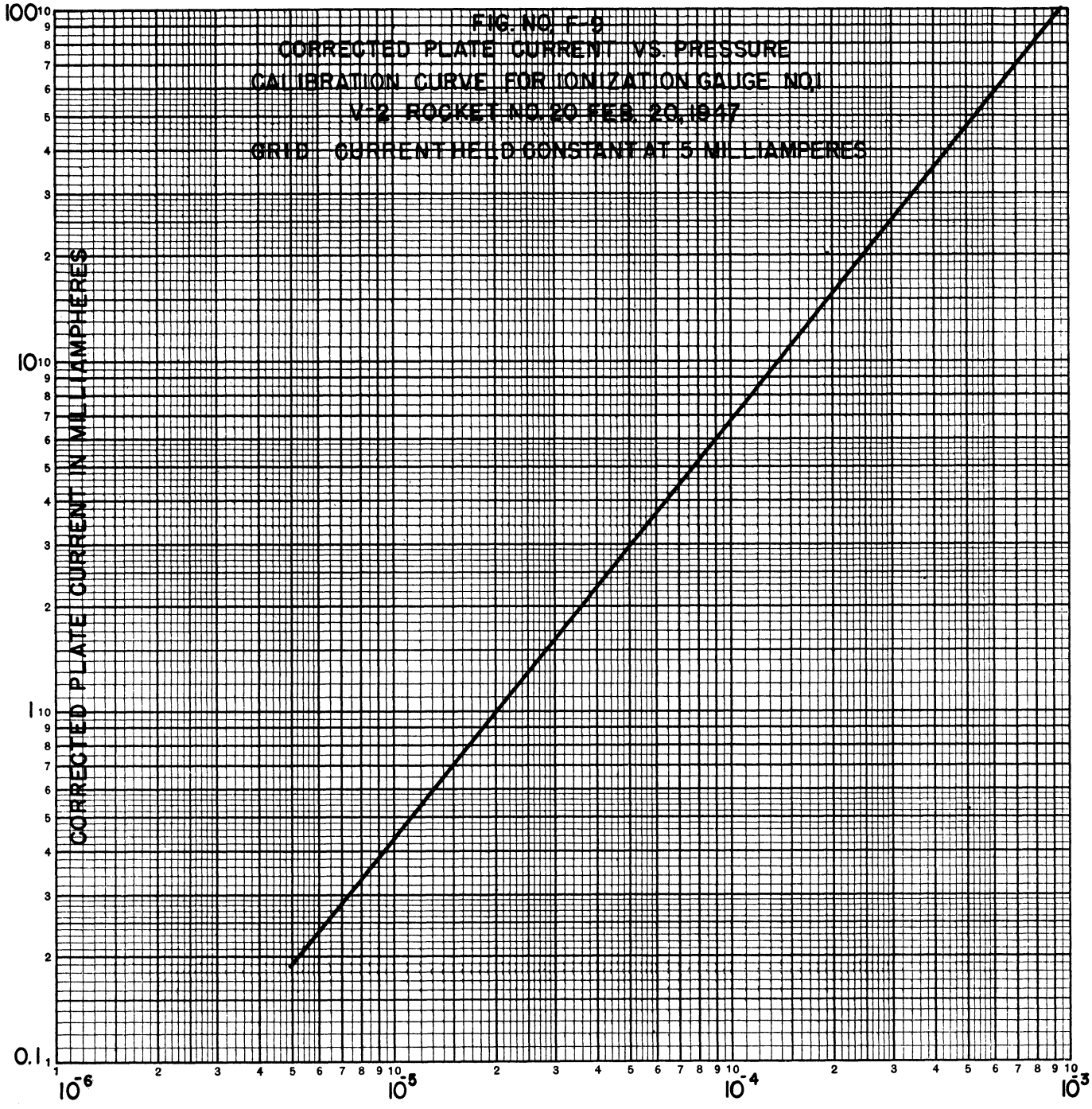
FIG. NO. F-9
CORRECTED PLATE CURRENT VS. PRESSURE
CALIBRATION CURVE FOR IONIZATION GAUGE NO.1
V-2 ROCKET NO. 20 FEB. 20, 1947
GRID CURRENT HELD CONSTANT AT .5 MILLIAMPERES
CORRECTED PLATE CURRENT IN MILLIAMPHERES
100
10
1
0.1
10^{-6}
10^{-5}
10^{-4}
10^{-3}
PRESSURE IN MILLIMETERS OF MERCURY

FIG. NO. F-10

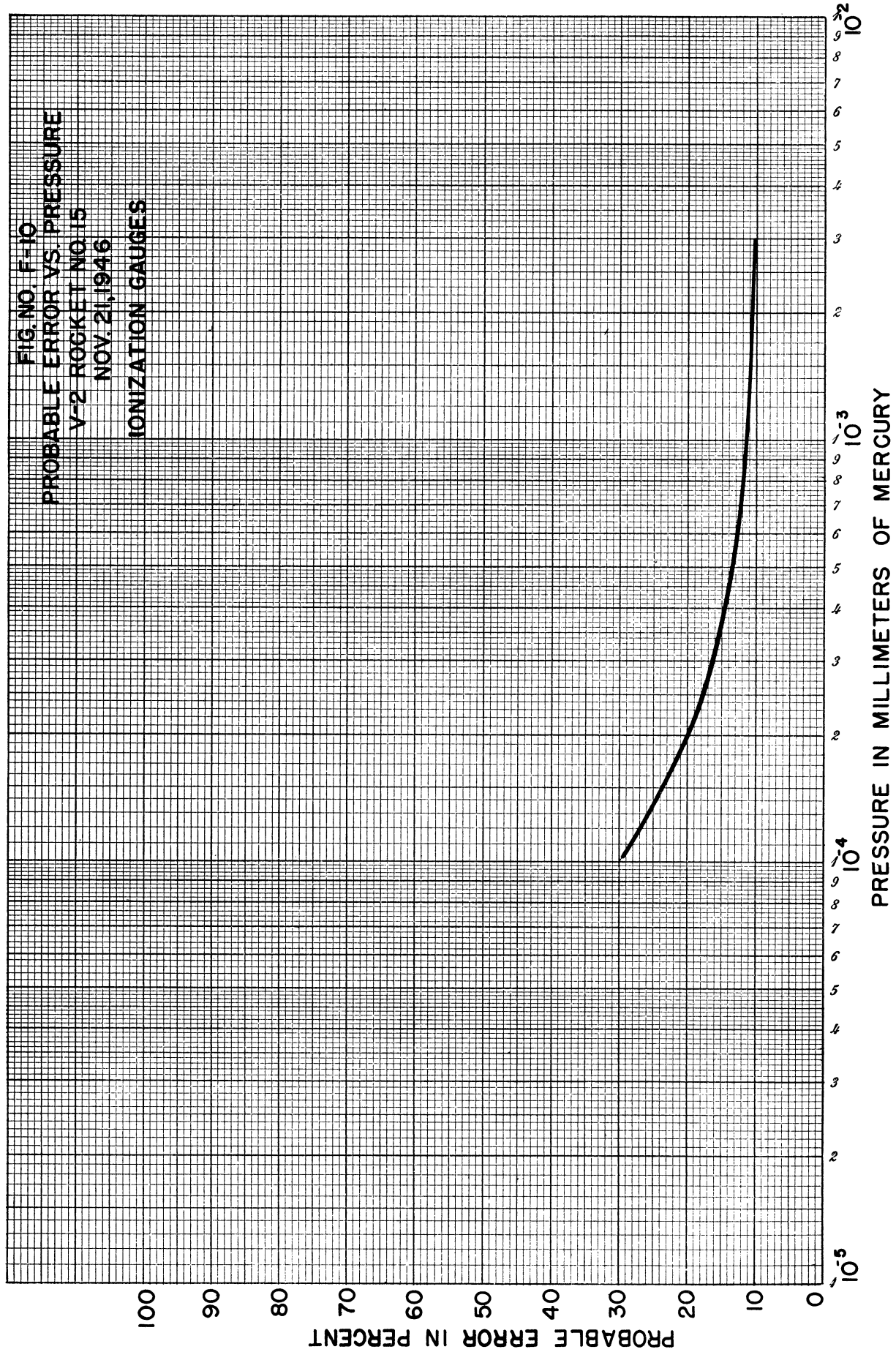
FIG. NO. F-10
PROBABLE ERROR VS. PRESSURE
V-2 ROCKET NO. 15
NOV. 21, 1946
IONIZATION GAUGES
PROBABLE ERROR IN PERCENT
100
90
80
70
60
50
40
30
20
10
0
PRESSURE IN MILLIMETERS OF MERCURY
10^{-2}
10^{-3}
10^{-4}
10^{-5}

FIG. NO. F-11

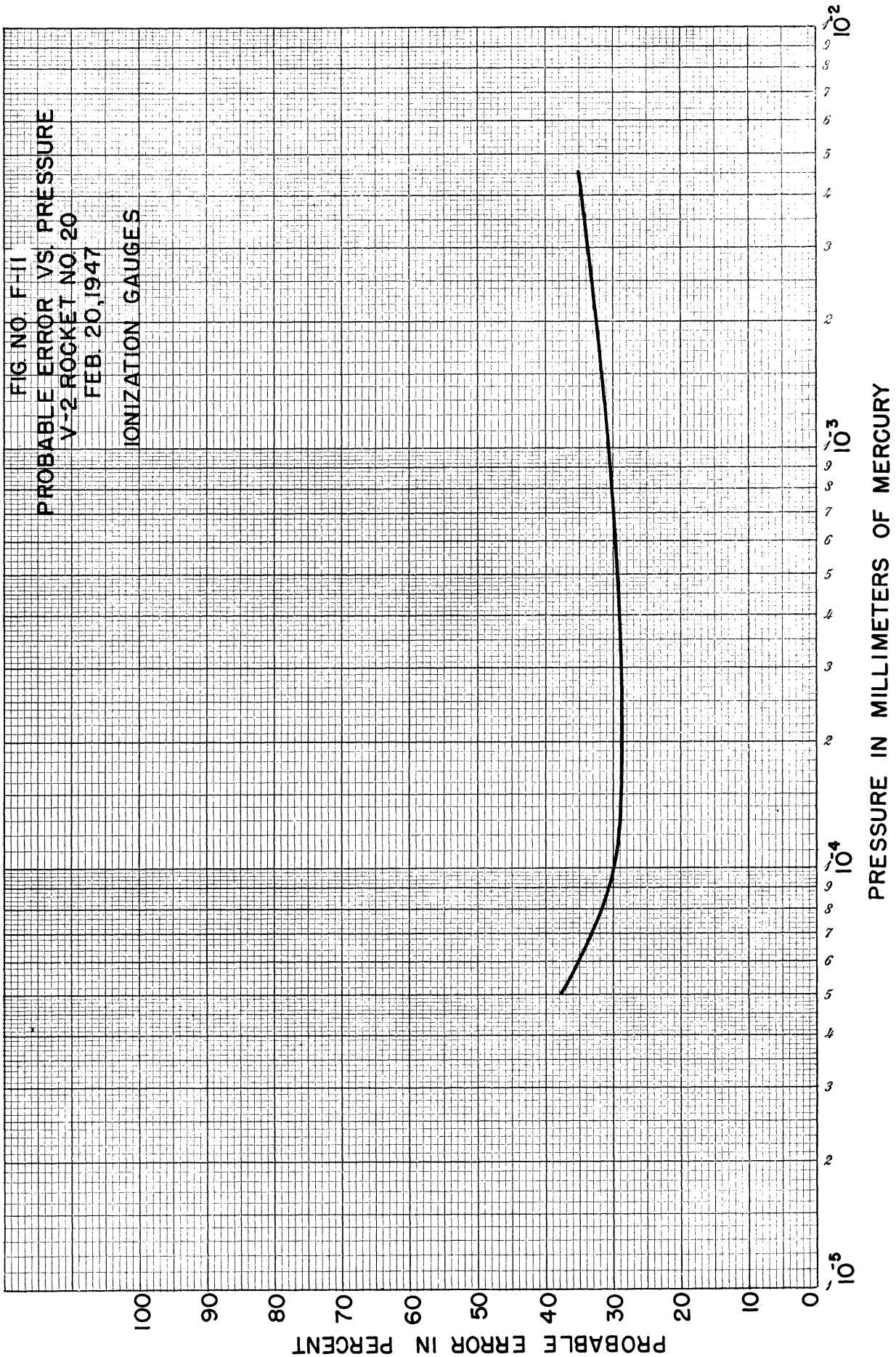
FIG. NO. F-11
PROBABLE ERROR VS. PRESSURE
V-2 ROCKET NO. 20
FEB. 20, 1947
IONIZATION GAUGES
PROBABLE ERROR IN PERCENT
0
10
20
30
40
50
60
70
80
90
100
PRESSURE IN MILLIMETERS OF MERCURY
10^{-2}
10^{-3}
10^{-4}
10^{-5}

FIG. NO. F-12

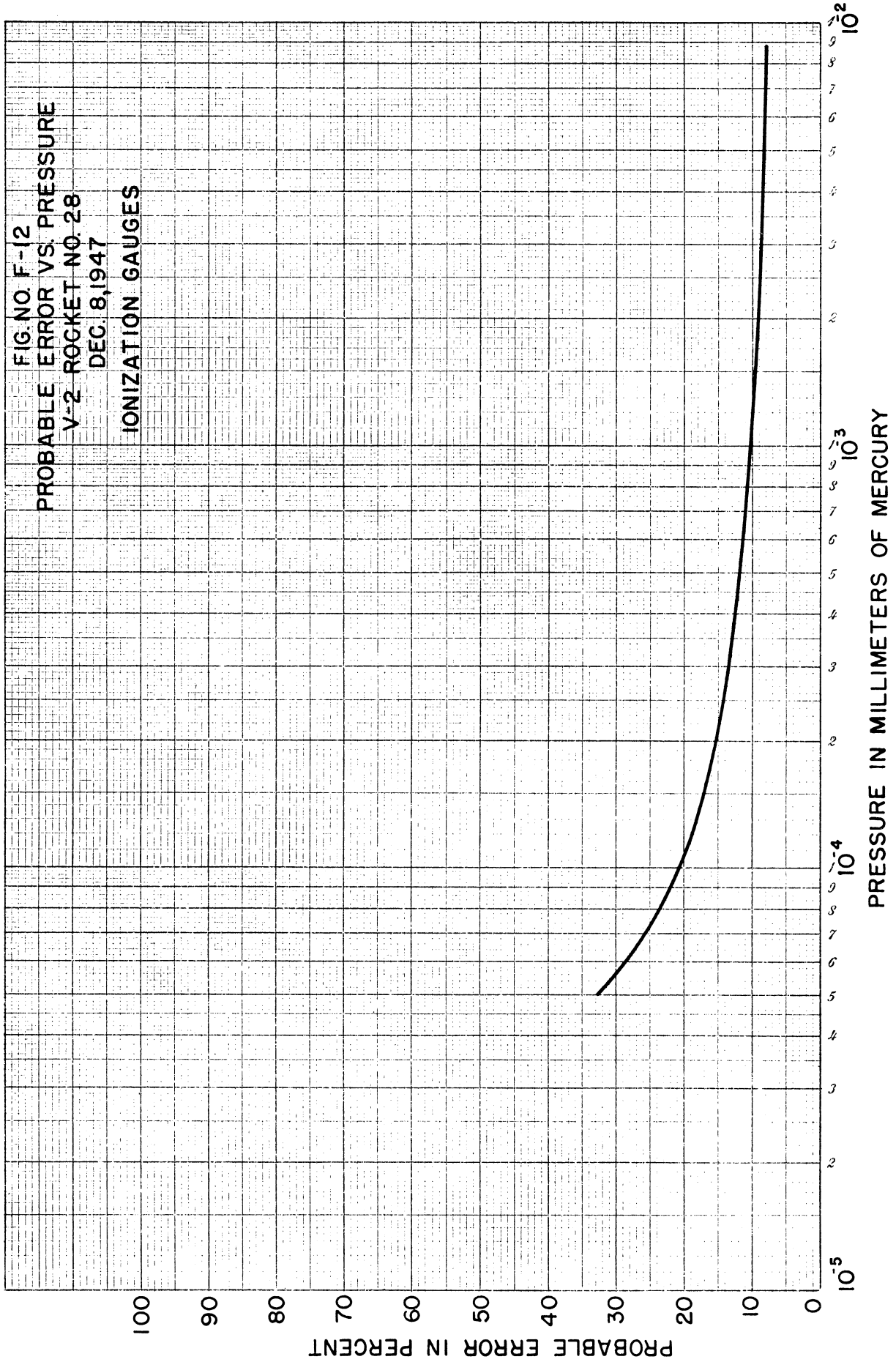
FIG. NO. F-12
PROBABLE ERROR VS. PRESSURE
V-2 ROCKET NO. 28
DEC. 8, 1947
IONIZATION GAUGES
PROBABLE ERROR IN PERCENT
0
10
20
30
40
50
60
70
80
90
100
PRESSURE IN MILLIMETERS OF MERCURY
10^{-5}
10^{-4}
10^{-3}
10^{-2}

FIG. NO. F-13

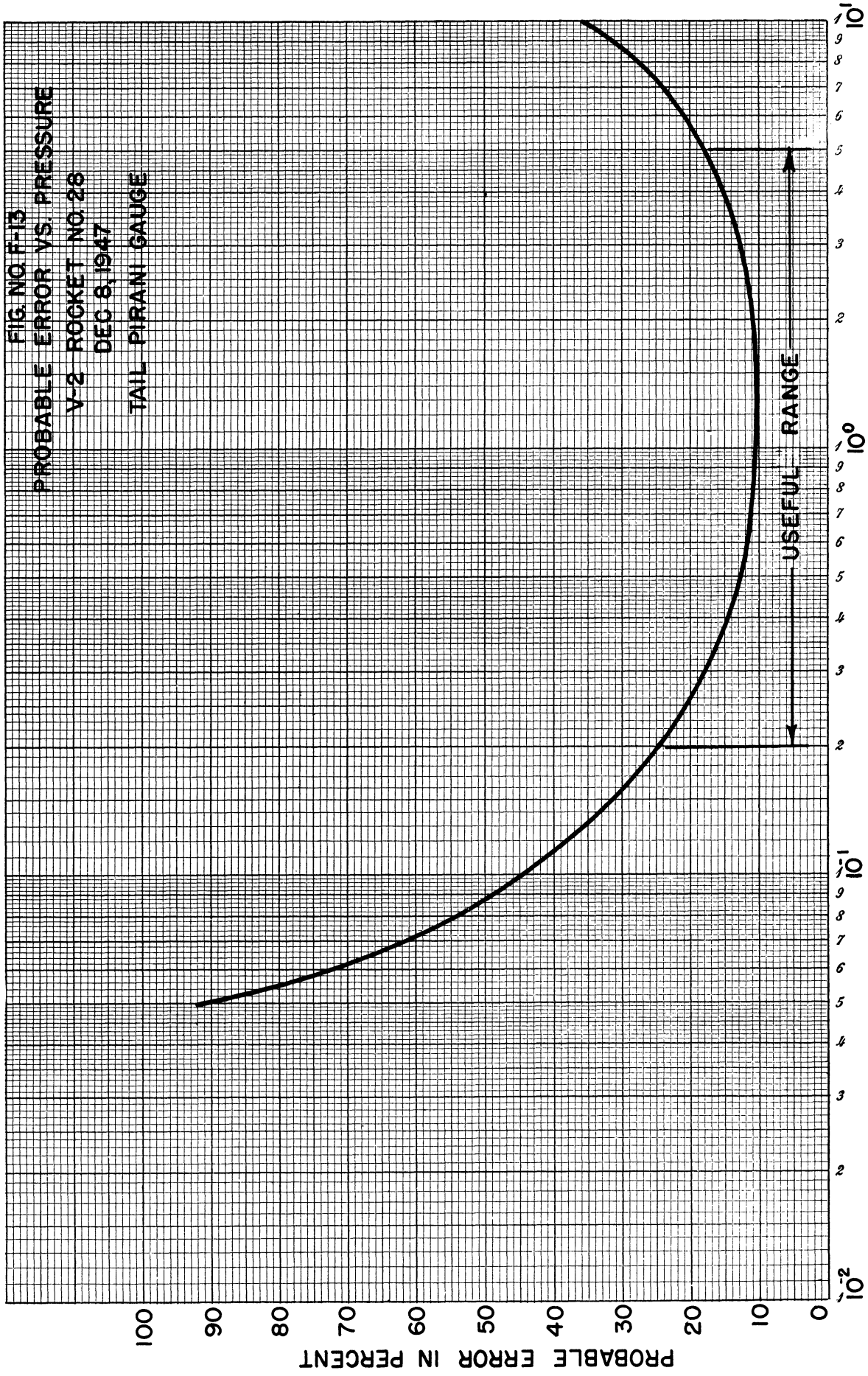
FIG. NO. F-13
PROBABLE ERROR VS. PRESSURE
V-2 ROCKET NO. 28
DEC. 8, 1947
TAIL PIRANI GAUGE
USEFUL RANGE
PROBABLE ERROR IN PERCENT
100
90
80
70
60
50
40
30
20
10
0
PRESSURE IN MILLIMETERS OF MERCURY
10^{1}
10^{0}
10^{-1}
10^{-2}

FIG. NO. F-14

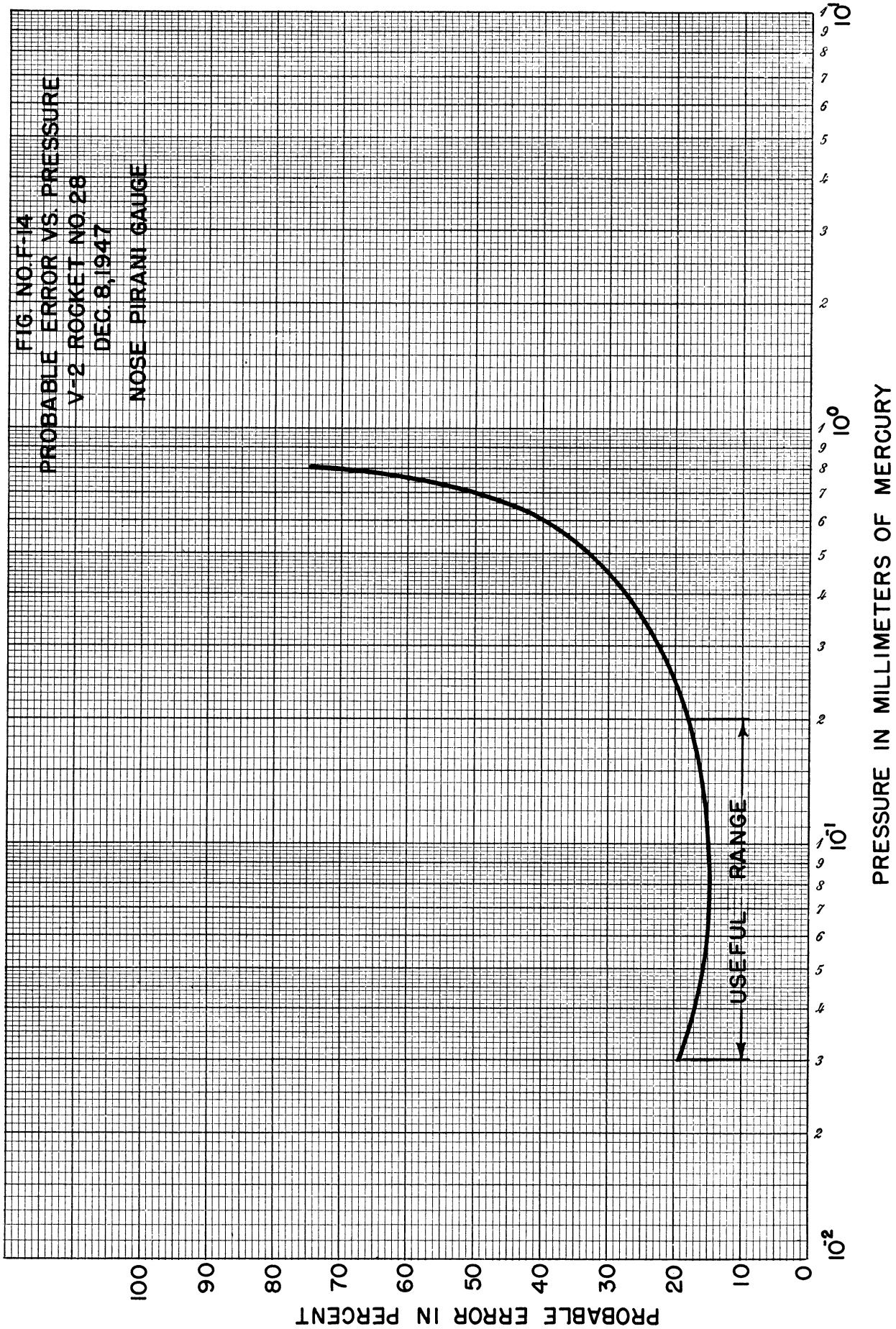
FIG. NO. F-14
PROBABLE ERROR VS. PRESSURE
V-2 ROCKET NO. 28
DEC. 8, 1947
NOSE PIRANI GAUGE
USEFUL RANGE
PROBABLE ERROR IN PERCENT
0
10
20
30
40
50
60
70
80
90
100
PRESSURE IN MILLIMETERS OF MERCURY
10^{1}
10^{0}
10^{-1}
10^{-2}

BIBLIOGRAPHY

1. Warfield, C. N., Tentative Tables for the Properties of the Upper Atmosphere, National Advisory Committee for Aeronautics, Technical Note No. 1200 (1947).
2. Dow, W. G., and Reifman, A., Technical Report on the Measurement of Temperature and Pressure in the Ionosphere, Report No. 1, University of Michigan, July 25, 1946.
3. Whipple, F. L., Meteors and the Earth's Upper Atmosphere. Reviews of Modern Physics, Vol. 15, No. 4, October (1943).
4. Air Materiel Command, Cambridge Field Station, Upper Air Research Program, Report No. 1, 1 September 1947.
5. Joos, Georg, Theoretical Physics, Hafner Publishing Company, Inc. (1934).
6. Kennard, E. H., Kinetic Theory of Gases, McGraw-Hill Book Company, Inc. (1938).
7. Prandtl, L. and Tietjens, O. G., Applied Hydro- and Aero-mechanics, McGraw-Hill Book Company, Inc. (1934).
8. Dow, W. G., Fundamentals of Engineering Electronics, John Wiley and Sons, Inc. (1937).
9. General Electric Company Report No. 45779, Report of A-4 Trajectory Calculations Preliminary to A-4 Missile Tests at White Sands, New Mexico, Aero and Marine Engineering Division, May 28, 1946.
10. Knudsen, M., Laws of Molecular Flow and Internal Viscosity Flow of Gases through Tubes, Annalen der Physik, Vol. 28, 75 (1908).
11. Knudsen, M., Thermo-molecular Pressures in Tubes, Annalen der Physik, Vol. 83, 797 (1927).
12. Maxwell, J. C., Scientific Papers, Vol. 2, p. 708 (1879).
13. Chapman and Cowling, The Mathematical Theory of Non-Uniform Gases, Cambridge University Press (1939).
14. Tsien, H., Superaerodynamics, Journal of the Aeronautical Sciences, Vol. 13, Number 12, December (1946).
15. Lees, L., The Stability of the Laminar Boundary Layer in a Compressible Fluid, N.A.C.A. Technical Note No. 1360, July (1947).
16. Durand, W. F., Aerodynamic Theory, Vol. III, Div. G, The Mechanics of Viscous Fluids (1943).
17. Taylor, G. I., and Maccoll, J. W., The Air Pressure on a Cone Moving at High Speeds, I and II, Proceedings Royal Society, A. Vol. 139, pp. 278-311 (1933).
18. Kopal, Tables of Supersonic Flow around Cones, Murray Printing Company, Cambridge, Mass. (1947).
19. Newell, H. E., and Siry, J. W., Upper Atmosphere Research Report No. III, Naval Research Laboratory, Report No. R-3120 (1947).
20. Klein, F., and Sommerfeld, A., Uber Die Theorie Des Kreisels, R. G. Teubner, Leipzig (1910).